Hydrological Assessment of LULC and Climate Change within the Water Resource Development Scenarios of Omo Gibe Basin, Ethiopia

Dissertation

By: Shiferaw Eromo Chaemiso

ROLL No: ***166104046***

Programme: ***Ph.D.***

Supervisor: ***Suresh A. Kartha, Ph.D.***

INDIAN INSTITUTE OF TECHNOLOGY GUWAHATI DEPARTMENT OF CIVIL ENGINEERING

Nov / 2021

Self Declaration

I declare that the thesis entitled "Hydrological Assessment of LULC and Climate Change within the Water Resource Development Scenarios of Omo Gibe Basin, Ethiopia" submitted by me is a presentation of my original research work done under the guidance of Dr. Suresh A. Kartha, Professor, Department of Civil Engineering, Indian Institute of Technology Guwahati. This work is original and has not been submitted elsewhere for the award of any degree, diploma, associateship, fellowship, titles in this institute or any other university or institution of higher learning. I also undertake the responsibility of the contents that are inscribed in the thesis.

Oct-2021

Shiferaw Eromo Chaemiso,

Roll No. 166104046,

Department of Civil Engineering,

Indian Institute of Technology Guwahati,

Assam - 781039, India

Certificate

It is hereby certified that the work contained in this thesis entitled **"Hydrological Assessment of LULC and Climate Change within the Water Resource Development Scenarios of Omo Gibe Basin, Ethiopia"** submitted by **Shiferaw Eromo Chaemiso** (Roll No. 166104046) for the award of the degree of Doctor of Philosophy, has been carried out in the Department of Civil Engineering, Indian Institute of Technology Guwahati under my supervision and this work has not been submitted elsewhere for the award of any other degree or diploma.

This thesis in my opinion, has reached the standard fulfilling the requirements for the award of the degree of Doctor of Philosophy in accordance with the regulations of the institute.

15-Nov-2021

20/04/2022

Dr. Suresh A. Kartha
Professor
Department of Civil Engineering
IIT Guwahati, India-781039

Abstract

The hydrological functions of river catchments are affected by numerous natural and man-made changes. Climate change is also one among them that has a complex effect on river basins. The river basins are vulnerable to natural and anthropogenic disruptions, changes in land use and land cover, and changes in hydrological characteristics because of water resources developments. The present study utilized hydrological modelling and remote sensing methods to determine the catchment response due to LULC changes at spatial and temporal scales for a river basin in Ethiopia. The study envisages hydrological assessment of LULC and climate change within the water resources development scenarios of the Omo Gibe Basin in Ethiopia.

Soil and Water Assessment Tool (SWAT) software was provided with inputs related to precipitation, topography, elevations, and soil types for hydrological modelling of the basin. Surface runoff, streamflow, and groundwater yield are some of the important outputs from SWAT for the basin. The precipitation inputs were provided with forecasts from climate models using different Representative Concentration Pathway (RCP) emission scenarios. The seasonal variation of precipitation in Gibe III dam site catchment during the summer precipitation season forecasted an increasing trend from 12.63 % in the midterm (during 2050s) to 13.95 % in the long-term (during 2080s) using RCP2.6. A similar trend exists for the RCP8.5 scenarios as well. However, the RCP4.5 scenario shows a decreasing trend from 3.61% in the midterm to 3.11% in the long-term prediction for this catchment. These trend analyses have shown the future shift of precipitations from summer to the winter and from the winter to spring seasons. The mean annual maximum temperatures in the mid-term are projected to increase by 1.34°C, 1.58°C, and 1.47°C for the RCP2.6, RCP4.5, and RCP8.5 scenarios, respectively, whereas the mean annual minimum temperatures in future long-term increase by 0.98°C, 1.03°C, and 1.35°C, respectively.

Further, SWAT was calibrated using the basin data from 1995 to 2007 and validated from 2008 to 2015 with 3 year's warm-up period. As there is an increase in percentage change in the future for precipitation in the basin, the corresponding increase in runoff is also witnessed. However, the evapotranspiration rates decreased in the futuristic scenarios for the basin. The mean annual maximum temperatures in the mid-term year (i.e., the 2050s) are projected to increase by 1.34°C, 1.58°C, and 1.47°C for the RCP2.6, RCP4.5, and RCP8.5 scenarios, respectively, whereas the mean annual minimum temperatures in future long-term 2080s increase by 0.98°C, 1.03°C, and 1.35°C, respectively. In this portion on temperature forecasts, the geo-statistical analysis

shows that Root Mean Square Standardized Error (RMSSE) is nearly 0.98 for both the ordinary kriging and Inverse Distance Weighted (IDW) interpolation method.

The statistical parameters Nash and Sutcliffe efficiency (NSE) criteria, the coefficient of determination (R^2), and Percent Bias (PBIAS) for both SWAT simulated and measured streamflow were estimated during calibration as 0.83, 0.76, and −3.37, and during validation as 0.856, 0.825, and −11.42, respectively. This shows that simulations have a very good correlation with the monthly observed and simulated streamflow in the lower Omo-Gibe basin. Climatic situations that influence evapotranspiration and precipitation processes, directly affect the basin's surface runoff, and soil moisture. Precipitation, evapotranspiration, and streamflow indicated increasing trends. The analysis revealed the impact of climate change on future annual streamflow to be directly correlated with an annual change of precipitation and indirectly correlated with evaporation.

The Land-use/Land-cover (LULC) classifications are some major inputs in SWAT model. The LULC classifications of Omo-Gibe for different periods were deduced from satellite images using the normalized difference indices on areas on vegetation, water bodies, and built-ups. The results indicate that LULC changes from 1987 to 2017 are significant for the region. The land-cover changes revealed an increase in the proportion of agricultural land and human settlement. The SWAT model assessed the impact of LULC dynamics on hydrological components. The calibrated and validated SWAT model simulations reveal that the percentage differences in surface runoffs show increasing trends while comparing the LULC changes between 1987, 2002, and 2017. Similarly, evapotranspiration values also increased from 1987 to 2017. However, other processes like groundwater flow, soil moisture, lateral flow, and water yield decreased in the basin from 1987 to 2017. Satisfactory comparison between the observed sediment yield from the basin and SWAT output justified the model's capability to use in different land-use scenarios.

Best management practices (BMPs) like – filter strips, terracing, and reforestation were artificially introduced in SWAT simulations of relevant sub-basins of Omo-Gibe. The simulations revealed reforestation as the BMP in reducing the sediment yield. Reforestation scenario simulation suggested a decrease in sediment output by 49.25%, 34.55%, and 40.84% for the years 1987, 2002, and 2017, respectively. The revelation is essential for stakeholders and policymakers in managing surface-water projects using the LULC scenario.

Key words: Climate Change, LULC, SRES RCPs, Hydrological Model, GIS and RS, BMPs.

Acknowledgements

First and above all, I thank my almighty GOD for giving me this chance. Without his help, I would never and ever have travelled to this far.

This research work is financially supported mainly by the Ethiopian Ministry of Science and Higher education and Arbaminch Water Technology Institute in Water Resource Research Center (WRRC) Arba Minch University, Ethiopia. I would like to express my great gratitude to all of them for making the fund offered and that made this research possible through financing for my stay in Indian Institute of Technology Guwahati, India and during filed work time in Ethiopia.

I would like to thank my advisor Suresh A. Kartha (Ph.D.) for his supervision, encouragement and all rounded support he has provided me throughout my study and I Thanks Doctoral Committee (Sreeja Pekkat (Assos Prof.), Subashisa Dutta (Prof.), Anamika Barua (Prof.)) for introducing me new, interesting and thoughtful ideas throughout my study and His critical and frequent advice me to explore many ideas and thoughts. His keen supervision and frequent advises made my study feasible. For this I very much appreciate from my heart.

My special thankfulness to the Indian Institute of Guwahati, Department of Civil Engineering for this wonderful opportunity to support and help in all directions of academic issues. I would like to thank my colleague at AMU particularly, Dr. Nagash. W.A, Dr. Santosh. P. M and so on for their cooperation whenever I need any support from AMU and Individuals.

My special appreciation goes to Ethiopian National Meteorological Service, Ministry of Water and Energy of Ethiopia, Ethiopian Mapping Agency, and Ethiopian Electric Power Cooperation for providing me the necessary input data and kind cooperation throughout my study. Last but not least, I am grateful to all my colleagues at IITG (Indian Institute Technology Guwahati, for the continuous support that you made during my stay in India. And it was a pleasure for me to work with you.

I would like to thank my beloved families; Nitsu K.L and Zatseat .SH. E. (Wife and kids), Eromo Chaemiso and Ayelech Gichamo (Father and Mother), all my Brothers, sisters, and all my family. Their love, support, and encouragement made the success of this effort feasible. Especially the effort and encouragement from all my brothers made me very strong and courageous to finish my study. I ‘m very proud to be part of such a beautiful family.

Shiferaw Eromo Chaemiso

Table of Contents

List of Figures

List of Tables

List of Abbreviations

ALPHA_BF	Base Flow Alpha Factor
ARS	USDA Agricultural Research Service
ASE	Average Standard Error
BCM	Billion Cubic Metres
BMPs	Best Management Practice Scenario
CH_K2	Effective Hydraulic Conductivity of Main Channel (Mm/Hr.)
CMhyd	Climate Model data for hydrologic modelling
CMIP3	Coupled Model Inter comparison Project Phase 3
CMIP5	Coupled Model Inter comparison Project Phase 5
CN	Curve Number
CN_2	SCS Runoff Curve Number
CORDEX	Coordinated Regional Downscaling Experiment
CSA	Central Statistical Authority
CV	Coefficient of variation
DDM	Dynamic downscaling Method
DEM	Digital Elevation Model
DOI	Digital Object Identifiers
DRS	Data Reference Syntax
EEPCO	Ethiopian Electric Power Corporation
ERDAS	industry leading geospatial data production software
ESCO	Soil Evaporation Compensation Factor
ESGF	Earth System Grid Federation
ET	Evapotranspiration
ETM^+	Enhanced Thematic Mappers Plus and
ET_o	Evapotranspiration
FAO	Food and Agricultural Organization
FDREPCC	Federal Democratic Republic of Ethiopia Population Census Commission
GCM	General Circulation Model
GIS	Geographical Information System
GO-ESSP	Global Organisation for Earth System Science Portals
GW_DELAY	Ground Water Delay (Days)

GW_REVAP	Threshold Depth Of Water in the Shallow Aquifer Required for Return Flow (Mm)
GWQMN	Shallow Aquifer Required For Return Flow To Occur
HadCM	Hadley Centre Climate Prediction Models
HadGEM1	Hadley Centre New Global Environmental Model 1
HRU	Hydrological Response Unit
IDW	Inverse Distance Weighted
IPCC	Intergovernmental Panel on Climate Change
ITCZ	Inter-Tropical Convergence Zone
IWMI	International Water Management Institute
LULCC	Land Use Land Cover Change
ME	Mean Error
MLM	maximum likelihood Method
MOM	Method of Moments
MoWRIE	Ministry of Water Resource Irrigation and Electricity
MR	method of regression
MSE	Mean Standardised Error
MSL	Mean Sea Level
NDBI	Normalized Difference Built-up Index
NDVI	Normalized Difference Vegetation Index
NDWI	Normalized Difference Water Index
NIR	Near Infrared
NMA	National Meteorology Agency
NSE	Nash- Sutcliff Efficiency
OLI	Operational land image
PBIAS	Percent difference Bias
PCP	Precipitation or Rain fall
PET	Potential Evapotranspiration
PWM	Probability weight method
R^2	determination coefficient
RCM	Regional climate Model
RCPs	Representative Concentration Pathways Scenario
RMSE	Root Mean Square Error

RMSSE	Root Mean Square Standardised Error
RS	Remote sensing
RVE	Relative volume error
SAT	CORDEX Science Advisory Team
SDSM	Statistical Downscaling Model
SEE	Standard Error of Estimate
SNNP	South nation Nationality and People
SOL_AWC	Soil Available Water Capacity (Water/Mm Soil)
SOL_Z	Total Soil Depth (Mm)
SRES	Special Report on Emission Scenario
SRTM	Space Shuttle Radar Topography Mission
SURLAG	Surface Lag
SURQ	Surface Water Runoff
SWAT	Soil Water Assessment Tools
SWAT-CUP	SWAT calibration and Uncertainty Parameter
SWIR	Short-Wave Infrared
T ^{o}C	Temperature in Degree Centigrade
TIRS	Thermal Infrared Sensor
USDA	United States Department of Agriculture
USGS	United State Geological Survey

List of Nomenclatures

$aq_{sh,j-1}$	the amount of water stored in the shallow aquifer on day i-1
$aq_{sih,j}$	The amount of water stored in the shallow aquifer day i.
e_a	Actual vapor pressure (KP_a)
e_s	Saturation vapor pressure (KP_a)
ET_0	Reference evapotranspiration (mm/day)
l_v	Latent heat of vaporization MJ kg-1
Q_{gw}	Groundwater flow
R_n	Net radiation at the top of crop surface (MJm^2day^{-1})
$SW_{ly,excess}$	The volume of water in soil
TT_{perc}	The travel time for percolation (hrs)
$W_{perc,jy}$	The amount of water percolating to soil,
$w_{pump,sh}$	The amount of water removed from shallow aquifer by pumping on day i.
$w_{rchrg.sh}$	Recharge entering the shallow aquifer on day
w_{revap}	The soil zone in response to water deficiencies.
$-\Delta t$	The length of the time step (hrs)
A	Drainage area (km^2)
C_V	Coefficient of variation of the rainfall values at the existing m stations (%)
Ea	Amount of evapotranspiration on day i (mm),
elev	Ground elevation (m)
G	Soil neat flux density (MJm^2day^{-1})
Gsc	Solar constant (0.082 $MJm^{-2}min^{-1}$)
J	mean daily air temperature at 2 m height (ms^{-1})
k	Growth rate (%)
L	River reach length / Flow length (m)
N	optimal number of stations(no)
n	Decade or years
p / r	Precipitation (mm) / Rainfall (mm)
PET	Potential evapotranspiration (mm)
P_n	Population at n decades or years
Q	Surface runoff / Daily surface runoff (mm)

Q_{gw}	Amount of return flow on day i (mm)
Q_{gwj}	Groundwater flow into the main channel on day j
q_{lat}	Lateral flow (mm/ day)
Q_{obs}	Observed discharge (m^3/s)
Q_{sim}	Simulated discharge (m^3/s)
Ra	water equivalent of extra-terrestrial radiation (mm day^{-1})
R_{day}	Amount of precipitation on day i (mm),
REVAP	Water flow from the shallow aquifer back to the soil profile (mm day^{-1})
R_I	Rainfall intensity (mm/hr)
Rn	Net radiation (MJ m^{-2} day^{-1})
R_{nl}	Net outgoing long wave radiation (MJ m^{-2} day^{-1})
R_{ns}	Net incoming short wave radiation (MJ m^{-2} day^{-1})
S	Drainable volume of soil water per unit area of saturated thickness (mm/day)
SC	Saturated hydraulic conductivity (mm/h)
SW(t)	Soil water content in the day t (mm)
S_{wo}	Initial soil water content on day i (mm)
S_{wt}	Final soil water content (mm)
T_{max}	daily Maximum temperature (°C)
T_{mean}	mean air temperature
T_{min}	daily Minimum temperature (°C)
V	slope vapor pressure
W_{seep}	Amount of water entering the vodose zone from soil profile on day i (mm)
α	Slope of the land / Albedo
α_{gw}	Base flow recession constant
β	Slope of the saturation vapour pressure curve (Kpa C^{-1})
γ	psychometric constant
Δt	Time step
ε	allowable degree of (percentage) error in the estimate of the mean rainfall
σ	Stefan-Boltzmann constant (MJ K^{-4} m^{-2} day^{-1})
ϕ	Latitude of the climate station (rad)
ωs	Sunset hour angle (rad)
θ_d	Drainable porosity

Chapter 1 Introduction and Background

1.1 General

Global warming will raise existing challenges and create new risks for both the natural and human systems (*Pachauri et al., 2014; Nordhaus et al., 2019; Seddon et al., 2020; Rasul et al., 2020; Islam et al., 2020)*. According to climate model predictors, the global mean temperature probably will increase from 1.1 to 6.4 ^{o}C in the next 100 years (*Islam et al., 2020; IPCC, 2001*) using several scenarios of greenhouse gas emissions. Precipitation is an important component in the hydrologic cycle (*Trenberth 2011*) that controls the mass balance of water in a catchment to cater water supplies and demands under various water stresses (*Seddon et al., 2020; Lacombe et al., 2016*). The knowledge of flow and appearances of rainfall are useful to predict its effect on hydrological cycles in a basin. In addition, the effects of evapotranspiration are also important to address catchment hydrological issues. The effects of climate change on the water resources system as well as on the water infrastructures have to be assessed through hydrological impact studies and thereafter devise suitable management practices (*Nordhaus et al., 2019; Tatsumi et al., 2011*). As precipitation is the major input of water in a basin, in general, its increase provides more available water and vice versa. In a similar way, the influence of temperature on water availability is also ascertained by the change in rates of evapotranspiration that causes variability in available water (*McCain, 2007; Zhao et al 2005*). This is one of the difficult challenges faced by water managers, as the available land and water resource in the basin are not utilized effectively to improve the livelihood and socio-economic conditions of the inhabitants.

The climate change impact on water availability causes demographic and economic deviations in a region. The land use/land cover of a region changes due to the anthropogenic socio-economic developments and, in addition to climate change, also influences the watershed hydrological responses (*Mango et al., 2011, Nie et al., 2011; Berihun et al, 2019*). The effect of land degradation in most catchments has reduced the infiltration rates and caused increased runoff generation from the catchment (*Borrelli et al., 2021; Altobelli et al., 2020; van Roosmalen et al, 2009*). Hydrologic modelling, in such circumstances, aids in estimating water availability as well as assist the water resources management of a basin (*Jain et al., 2021; Dwarakish and Ganasri, 2015; Wang et al., 2013*). Climate change and hydrological impact assessment at a spatial scale are essential to know water resource potential as well as to study the impact of human interference on the watershed. The natural climate variability and anthropogenic change have a great influence on the surface and subsurface water resource availability and its distribution. The spatio-temporal hydrological modelling helps to visualize and strategize different environmentally sustainable

management scenarios in a basin. Henceforth, climate change effects on surface and sub-surface water resources must be utilized in integrated planning for a sustainable supply of water and its support to food security. The maximum and minimum temperatures in Ethiopia, in the last few years, have increased at about 0.37 °C and 0.28 °C per decades (*NMA, 2007; Mc Sweeney et al, 2008; Chaemiso et al, 2016*). In Ethiopia, the vulnerability to climate change is different from place to place. The vulnerability of the region to climate change indicated that the net effect of sensitivity, exposure, and adaptive capacity are different across the region (*Temesgen et al, 2006*). Therefore, an increasing occurrence of late rains and droughts is consistent with scientific assessments on the impacts of climate change in the basin. Droughts can be associated with higher temperatures and consequential higher evaporation rates. Increased variability of rains is consistent with changes in local rainfall patterns. Predictions of future temperatures rise and ever-increasing rainfall variability indicated that both droughts and late rains would probably become more pronounced in the coming decades (*Marius, 2009*). The ecosystems and biodiversity are affected because of climate change.

This means there will be an increase of extreme weather events as well as change in precipitation and atmospheric circulation patterns. Climate change will have an important impact on the hydrological cycle and in the magnitude and quality of water resource potentials (*Watson et al, 1998*). These variations can promote limitless changes in the availability of water resources at regional and national level. Ethiopia depends on agriculture (*Davis and Amudavi, 2009; White et al., 2001*), as it is the backbone of the country's economy. Besides, the agricultural yield and productivity depends on the availability of water resources in the region or country. Hydrological extremes and the increased pollution will affect the country's economy (*Easterling et al, 2000*), causing far reaching transformations in the economies that are dependent on the availability and demand for water resources (*Altobelli et al., 2020; Rasul et al., 2020; Islam et al., 2020; Tundisi 2008*). The extremes in hydrological events can affect human society through floods, landslides, low and high flows, increase in semi-arid and dry regions (*Tundisi 2008*). Urban areas can be extremely vulnerable to these hydrological extremes. Erosion, flooding, sedimentation, and other damaging actions of water are a part of the water resource problem that must be given major attention in human settlement areas. Climate change can affect the function and operation of existing water infrastructures (B*ates and Wu 2008; Altobelli et al., 2020; Rasul et al., 2020*) like hydropower, flood protection structures, drainage and irrigation systems as well as water management practices.

Estimating the possible hydrological impact due to the effect of climate change on water resources is important for sustenance of the society on river basins. Precipitation, in particular, greatly influences the amount of water flowing through the water cycle and the availability of water in a basin. In general, higher precipitations lead to more water availability and similarly, lower

precipitations lead to reduced water supply. The change in temperatures due to climate change influences the water availability of the region (*Liu et al, 2009*).

A river basin is a dynamic and complex system involving a number of natural or anthropogenic physical processes (*Tilmant et al., 2020*; *Deshmukh et al, 2013*) that can function at the same time and have various spatial and temporal effects. Remote sensing data (*Butt et al, 2015*) is the primary source data for evaluating land use and land cover (LULC) and environmental processes in the local or global spatial scale. LULC changes alter the watershed hydrological responses like surface runoff, evaporation, transpiration, infiltration, subsurface interflow, percolation to groundwater aquifers, and base flow to the rivers, etc. (*Mengistu 2009*). The uncertainty of land-use resulting from population growth, urbanization sector expansion, and climate change (*Tan et al, 2015*) is increasing at an alarming rate. Agricultural expansion (*Lee 2005*) and intensification, urban growth, and other natural resources are expected to intensify in the coming decades to meet the demands of a cumulative population. Urban land-use change is mostly influenced by the activities of human beings due to growing population pressures (*Smith et al, 2016*) and the rise in economic levels of the region (*Rajan and Ryosuke, 2001*).

The rapidly growing population and climate impact in the basin, particularly in the developing world (*De Sherbinin et al., 2008*) resulted in forest destruction. The influence of human activities on the land has increased exponentially over the past two centuries (*Ellis et al., 2013; Boivin et al., 2016)* due to population growth and technological progress, thereby, altering the entire ecosystems, and increasingly affecting both the biodiversity, nutrient and hydrological cycles of the environment (Tilmant et al., 2020; *De Sherbinin, 2002*). These changes in LULC systems have important environmental consequences through their impacts on soil and water, biodiversity, and microclimate (*Lambin et al., 2003*). The types of LULC will affect both the infiltration and the amount of runoff by falling precipitation (*Hougton, 1995*). Types of land cover significantly affect both surface and sub-surface flow. Surface runoff is mostly contributed directly from precipitation, whereas groundwater flow is contributed from infiltrated or percolated water. However, the source of streamflow during the dry and wet month is primarily from the surface runoff and the groundwater (*Abebe, 2005*). In addition, deforestation also has its own effects on hydrological cycles, leading to reductions in precipitation and faster post-precipitation runoff (*Legesse et al., 2003*). Understanding watershed hydrology is very important to assess the potential impact of LULC change on catchment hydrology under land-use dynamics.

LULC changes are highly influenced by man-made actions and natural events that happened. Therefore, the LULC dynamics are the product of complex interactions between environmental and ecological conditions that can occur at different temporal and spatial scales (*Reid et al., 2000*). The

main driving forces of LULC dynamics are: Population Growth, Economic Growth, Demographic conditions, and Technology (agricultural chemical) (*Mather and Needle, 2000; Noe et al., 2017*). According to (*Lambin et al., 2003*), evaluating the impact of LULC change on water resource management and formulating policies are very important in monitoring future basin-level water resource potential. LULC change will alter the hydrological cycle by increasing or reducing flow and storage (*Wang, 2014*). Long-term reduction in the evapotranspiration and recycling of water activates changes in climate and weather patterns of the region.

Omo-Gibe basin is one of the main source of water for Ethiopia's economy. Effective use and management of LULC under consideration of water resources projects (*Mango et al., 2011*) is very important when considering the effect of catchment hydrology on the development of the basin. It requires optimizing these potential resources of water with increasing population growth. Analysing sensitive parameters affecting the basin and understanding how LULC influences streamflow will allow planners to formulate policies to minimize the unwanted effects of future land-use changes on the pattern of catchment streamflow. Furthermore, by changing the future LULC and developing different LULC scenarios will have major impacts on basin water resources (*Zhang et al., 2015*). However, to predict the future effects of LULC, it is important to accept the effects of historic LULCs on its flow. Land use planning and land management are inter related to the available water resources in the region. The land degradations in most catchments have reduced the infiltration rates and detention storages that have increased the surface runoffs (*van Roosmalen et al., 2009; Carmona et al., 2013*).

The application of climate change model and hydrological model in the basin at spatial and temporal scale along with the LULC changes are essential to estimate the water resource potential as well as to study the impact of natural and human interference on the watershed. Such studies help to set different management scenarios that will lead to sustainable water resources and eco-systems. As climate change affect precipitations and its intensities, the hydrological response studies should accommodate climate change projections for optimal water allocation in the basin for comfort of the current and future human generation and ecosystems.

1.2 Statement of problem

The IPCC findings indicate that developing countries, such as Ethiopia, will be more vulnerable to climate change (*Abdo et al., 2009 Evangelista et al., 2013: Matewos 2020: Daba and You 2020*). The climate change may have far-reaching implications to Ethiopia for various reasons. The country is planning to boost its economy significantly by increasing water-related projects like hydropower,

irrigation, and water supply, etc. (*Sirte et al.,2008*). The effects of climate change can significantly impact the hydropower production as the river flows may get affected by change in temperature, precipitation, and evaporation (*Arnell 1999a*). This change in stream flow has a direct pronounced effect on the water-related project capacity. In order to predict the future effects of land use and land cover on basin flow, it is important to have an understanding of the effects of historic land use land cover scenario on the river flow. The impact assessment and planning of water resource development based on hydrological analyses under the land use land cover dynamics are essential (*Chang et al., 2015*). The hydrological responses of a basin due to water resource development as well as climate changes have to be integrated in planning and sustainable management of the resources. These studies can point out the sensitive areas in the basin that might be affected by natural and anthropogenic effects as well as climate changes and water resources developments. The agricultural activities in arid and semi-arid parts of the basin are highly dependable on rainfall and the systems are affected by hydro-meteorological changes as a result of climate change. Since water and food security are closely related and also reliable access to water increases agricultural yields; lack of this can be a major cause of drought, famine, and malnutrition for arid and semi-arid areas. Therefore, proper planning of water resource management is crucial to assess climate impacts that alter the precipitation, temperature, runoff, and evaporation.

In Omo Gibe basin, there are three existing hydropower projects and further two under construction and in planning stages. The project in planning stage includes irrigation project in the downstream as the basin has much potential for multi-purpose water resource development. Such projects may affect the natural flow regime and the amount of water flow into downstream ecology and the main inflow for Turkana Lake (*Avery and Eng, 2012*). There is a cascade hydropower project, which is under construction and in the planning stage in the basin. The change in water availability in the basin due to climate change may affect the performances of the water resources project planned at the site. Hence, climate change assessment is a vital step for optimal water allocation in the basin for the well-being of the human being and ecosystems. Considering the present challenge in the Omo-Gibe basin in Ethiopia, it is essential to understand the climate change effects on the basin hydrology in the present and future scenarios. The Gibe III dam is located within the Omo Gibe River basin in the middle part of the basin of the Omo River around 450 km by road South of Addis Ababa. The Gibe III dam is on the Omo River and the reservoir stretches to its tributaries - the Gibe and Gojeb Rivers. It is having 243 m high roller-compacted concrete dam with an associated hydroelectric power plant on the Omo River, which is largest hydroelectric plant in Africa with a power output of with a total installed capacity of 1870 MW. Besides the Gibe III dam, Gibe I dam (184 MW) and Gibe II power station (420 MW) are also located in the upstream part of

GIII. After Gibe III dam major tributaries of Omo Gibe basin downstream like Guma, Zigna, Mensa, and Denchiya join at the right side, while Deme, Zage and Irgene join to the system at the left side.

1.3 Research Motivation

Climatic change affects the natural system and disturbs hydro-ecological flow based on high and low streamflow. The basin streamflow depends on climatic parameters like evaporation, precipitation, temperature, and so on. The impact of upstream strong precipitation has the effect on downstream flooding and sedimentation. This ensures that the increasing year-to-year variability of rainfall increases both in droughts and heavy precipitation events, which decreases agricultural production (*Gornall et al., 2010*; *J Tigabu et al., 2021*) with associated negative effects on food security. Due to the increased evaporation and variability of rainfall events, the qualitative and quantitative availability of freshwater all over the country is likely to decline. Ecosystems and biodiversity are affected as a result of climate change and eventually, heavy rainfall and landslides would destroy the infrastructure (*Marius, 2009; Amin et al., 2018*; *Miller et al., 2020*) and disturb human settlement.

LULC data at different spatial resolutions have also shown the changes that affect hydrologic model outputs (*Wegehenkel et al., 2006; Shrestha et al., 2016*). Upper Omo Gibe basin is located in high land and have rugged topography. Because of this complex catchment structure, there is a need to study how to sustain the basin hydro climatological parameter based on futuristic scenarios. The basin's downstream portion is lowland, with arid and semi-arid climate characteristics that are frequently affected by flooding and sedimentation (Miller et al., 2020; Tigabu et al., 2021; *Ayalew, 2009*) (for example, August 2006 flooding and destruction). This necessitates the development of futuristic climate scenarios based on past and current hydro-climatic characteristics.

1.4 Research Question

The following research questions are pertinent to the region:

- What are the expected physical impacts of climate change land use cover dynamics and hydrologic and climate-based surface water potential?
- What effect does precipitation and evaporation have on the flow of streams under a climate change scenario and what are the general climate trends compared to the present situation?
- What are the potential impacts of climate change on future hydrological and the basin's potential water resource?

- What are the potential effects of land-use land-cover changes on seasonal flow?
- What is the current and future water resource management scenario for Omo-Gibe basin?

1.5 Objective of the study

The general objective of this study is Hydrological Assessment of Impact of LULC and Climate Change within the Water Resource Development Scenarios of Omo Gibe Basin, Ethiopia.

1.5.1 Specific Objectives**:**

- To develop future scenarios on climate change using spatial report emission scenario (SRES) and RCPs approach.
- To assess the influence of precipitation and evaporation on stream flow using RCP and RCM scenario.
- Forecasting hydrological events based on rainfall magnitude and flood frequency with in different return period using frequency model Under RCP scenario.
- Assessment of the possible effects of climate change on future hydrological events.
- Verification of suitability of SWAT hydrological model for the Omo-Gibe and its sub-basins.
- Effect of land use/land cover changes on surface water availability using Best Management Practices (BMPs).
- To simulate the water balances of the catchment and to identify sensitive parameters' effect on surface water potential.

1.5.2 Organization of the thesis

Chapter 1 Covers the introductory and background information including significance of the study and its objectives

Chapter 2, Gives a description of the study area, including the main characteristics of the Omo Gibe river basin including the location, rainfall characteristics or rainfall pattern, land use, topography and drainage sub basins.

Chapter 3, The literature review and talks about methods how to manage water resources at a river basin scale. The chapter reviews the available simulation models and describes the GCMs output, RCMs, RCPs, dynamical Downscaling, GIS and RS, ERDAS Imagine, LULCC, SWAT and SWAT-CUP model, it characteristics and applications. Besides, the general condition and previous studies conducted in the basin are broadly discussed in the chapter.

Chapter 4, Describes methods and materials taken to achieve the objectives of the thesis. The chapter focuses on hydrological, meteorology, operational and physical data collection and analysis.

Chapter 5 This Chapter assessment of the Impact of LULC Change on Surface water potential under different time based land use classification 1987, 2002 and 2017 image analysis, NDVI, NDWI, NDBI, hydrological model simulation results and discussion, sediment analysis and surface water impact analysis with conclusion and recommendation

Chapter 6 Describes Water Management Scenario and best Management Practice scenario (BMPs) development, runoff mapping and including discussion and conclusion.

Chapter 7 Deals with how GCMs output, RCM, RCPs analysis, SWAT, SWAT-CUP model was built for Omo Gibe river basin and how information was used and analyzed. The chapter that follows this presents simulation results and discussion and conclusion.

Chapter 8 Analysis the impact of Climate change assessment in South Omo Gibe, GCM out pout RCPs, Evaporation, Precipitation and Streamflow, Geostatistical analysis, IDW interpolation, ordinary Kriging interpolation, Using Hydrological Model SWAT calibration and validation under analyzing downstream stream flow predication.

Chapter 9 the thesis including the summary of overall dissertation conclusion and recommendation chapters, reference and the appendix sections.

1.6 Significance of the study

The aim of this study is to understand the complexity of the hydrological response of Omo Gibe basin at sub catchment level, on different timescales, and the roles of various controlling factors under homogeneity and heterogeneity identification (*Siderius et al., 2018; Gebremicael et al., 2019; Miller et al., 2020; Jain et al., 2021*). The study will contribute for local community and concerned bodies for devising appropriate management measures to minimize the undesirable effects of runoff and sedimentation. It can also aid in planning appropriate future land use/cover change developments without hampering the ecosystem. The effects of future midterm and longterm climate change on the catchment can be forecasted and its effect on the response of stream flow can be determined (*Tigabu et al., 2021; Miller et al., 2020; Jain et al., 2021*).

Chapter 2 Study Area

2.1 Introduction and Background

Ethiopia is located in The Horn of Africa. It has 12 river basins. The total mean flow is approximately 122 BCM (billion cubic meters) from these 12 river basins (*MoWR, 1999, Awulachew et al., 2007*). The Omo Gibe River Basin is geographically located between 34°55'50" and 38°25'42" East longitudes and between 4°25'40" and 9°2'48" North longitudes. The total area of the basin is about 79500 km^2 (Fig 2.1).

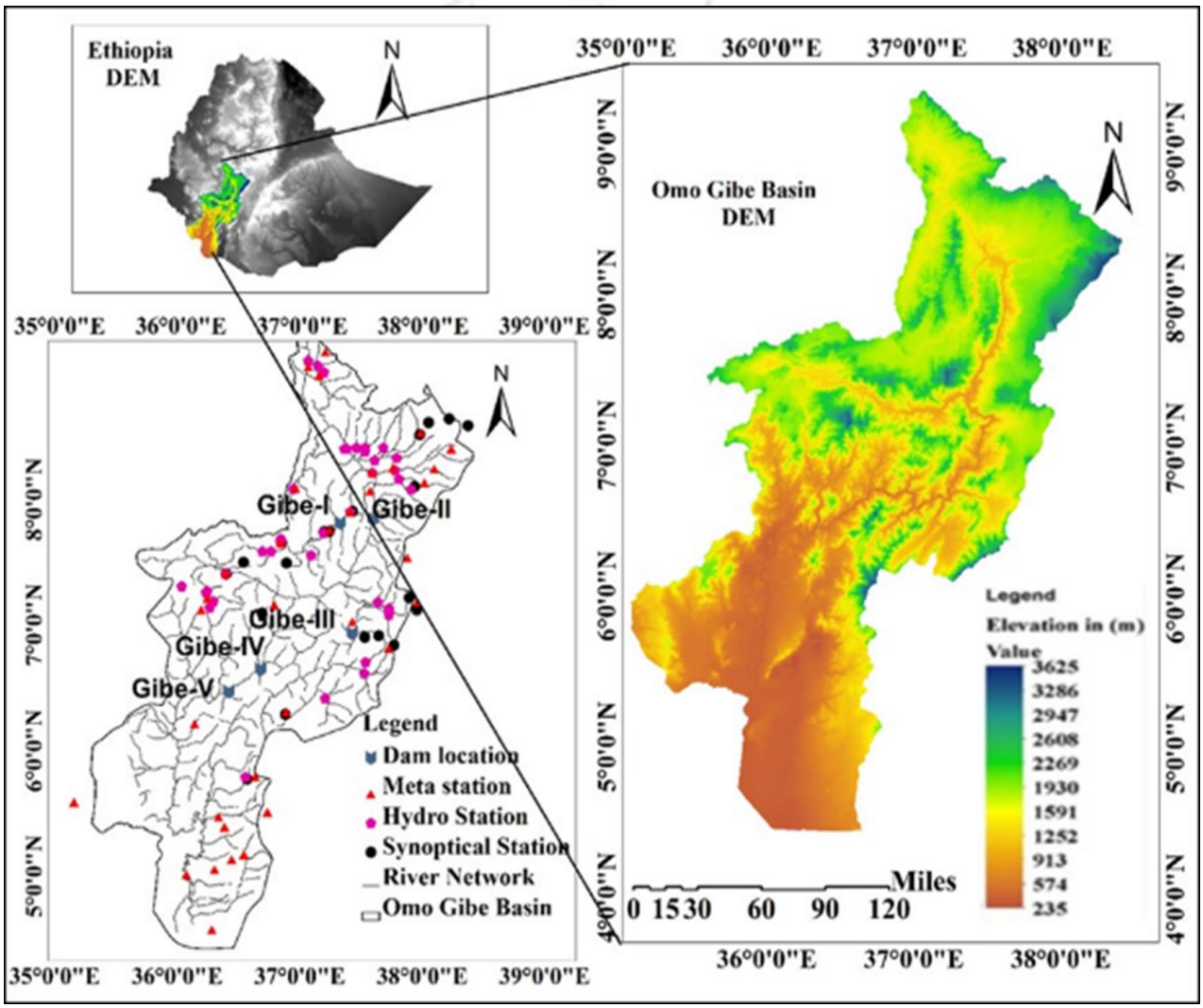

Figure 2. 1 Location of study area, Hydro-Climatological Station

The maximum elevation of the Omo Gibe basin is 3625 m above mean sea level (amsl) at the upstream edge and the lowest is 235 m amsl at the downstream side of the basin flood plain. Gilgel Gibe and Gojeb Rivers are major tributaries to the main river of the basin. Omo-Gibe river basin has low rainfall during Belg (spring) season from February to May; followed by the main rainy season Kiremt (summer) from June to September; and the Bega (winter) season from October

to January. The basin's average annual precipitation and evapotranspiration is 1640 mm and 1400 mm, respectively, and the basin's average air temperature varies from 15 to 29^{o}C. It has a varied LULC including forestry, grassland, woodland, bare land, and water bodies. The amount of rainfall decreases throughout the Omo-Gibe catchments with a decrease in elevation (*EEPCO, 2009*). Due to rapid growth of population, demographic changes, and the interference of human beings, the forests and vegetation covers are reduced and consequently, runoff has become more variable, with much more rapid response to rainfall in the last 20 years (*Avery, 2012*). These rapid responses resulted in increased flooding that are accompanied by accelerated sediment transport in downstream areas.

The basin is bounded by Baro-Akobo Basin in the western side; Blue Nile Basin in the north and northwest side; Awash Basin in the small area in the northeast; and Rift Valley Lakes Basin on the whole of the eastern side. The total length of the Omo Gibe River is approximately 1257 km. It has two main tributaries – Gojeb (230 km) and Great Gibe (170 km), respectively. Figure 2.2 and Table 2.1 shows the length of the main tributary and dam location of Omo Gibe basin.

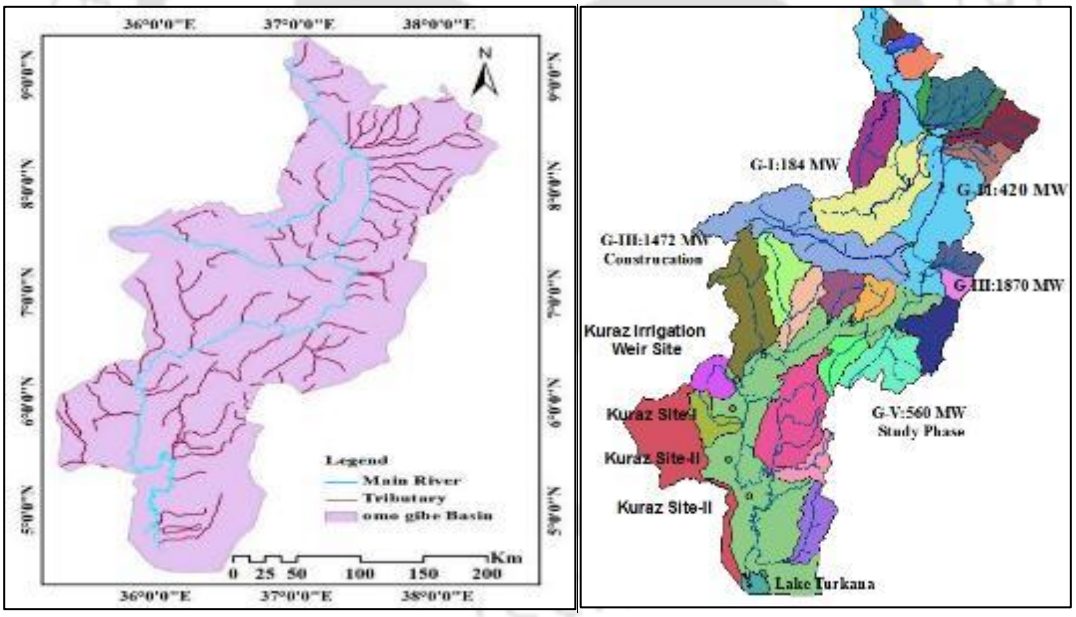

Figure 2.2 Length of the Main River and Dam locations in Omo Gibe basin

Table 2. 1 The total length of Omo Gibe Basin Main River

Omo Gibe Basin Main Tributary Length			
1	Gibe	107.3	Main River
2	Gojeb	230	Main River
3	G.Gibe	170	Main River
4	Omo	750	Main River
Total	Basin	1257.3 km	Omo Gibe River

2.2 Climate and Annual rainfall pattern in Omo Gibe Basin

Annual rainfall varies from 1900 mm/annum in the north-central areas of the Omo-Gibe Basin, to less than 300 mm/annum in the south of the basin. The annual rainfall generally diminishes through the basin as the river drains from the highlands in the north to Lake Turkana in the south. The mean monthly rainfall pattern over the basin varies distinctly (Figure 2.3 and Figure 2.4). The figures show the distribution of rainfall and in the north part of the basin the rainfall pattern is uni-modal, whereas further downstream to the south of the basin the pattern becomes bi-modal.

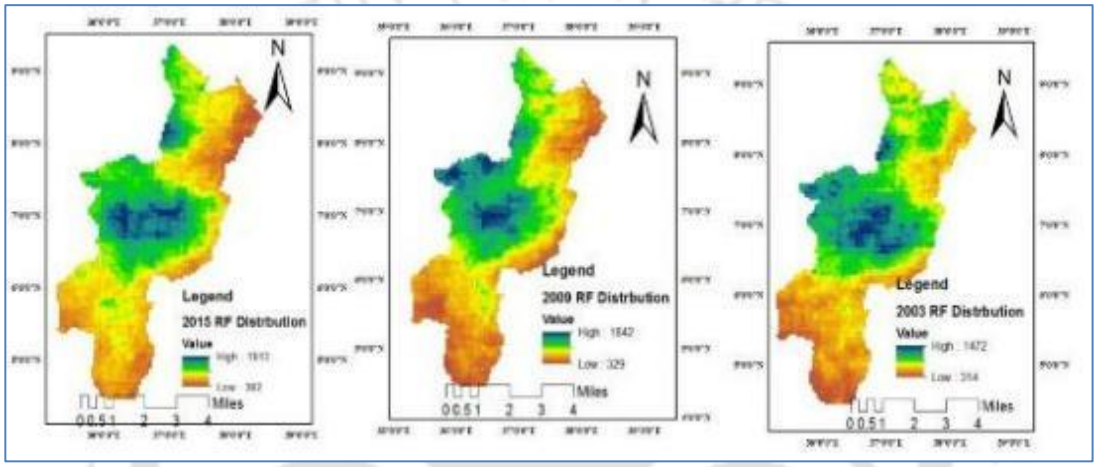

Figure 2.3 Past three years (2015, 2009, and 2003) Omo Gibe basin annual rainfall distribution

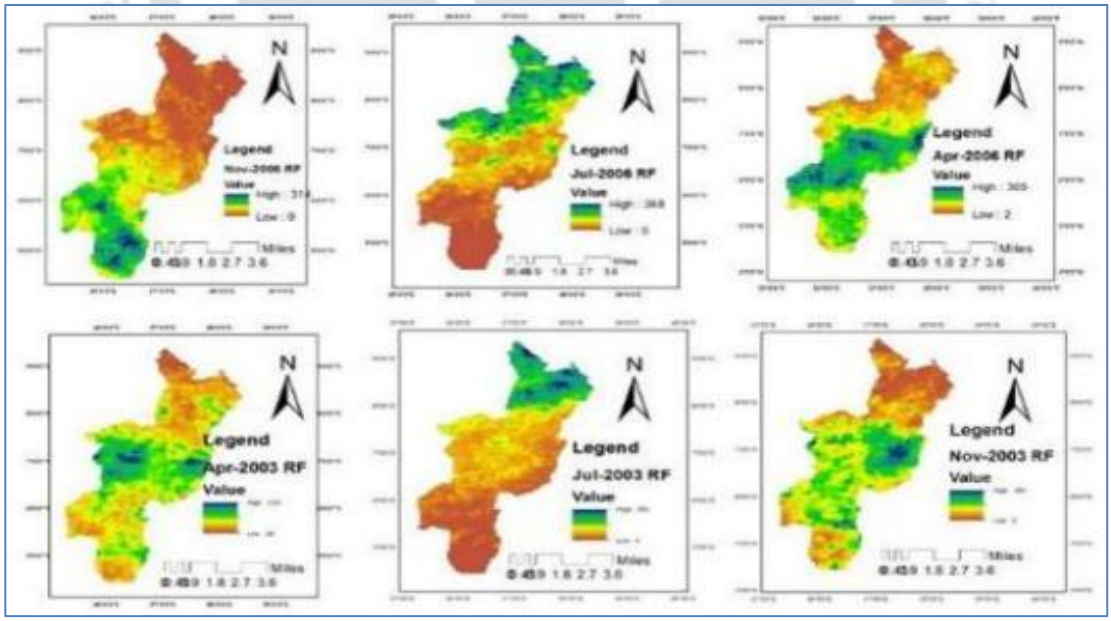

Figure2.4 In 2003 and 2006 Year seasonal rainfall distribution in Omo Gibe basin.

Climate of Ethiopia is classified into five zones based on the altitude and temperature. Namely, Wurch (cold climate and the altitude is more than 3000 m), Dega (temperate like climate

of high land and the altitude is between 2500-3000 m), Woina-Dega (warm climate and the altitude is between 1500-2500 m), Kola (hot and arid type of climate the altitude is less than 1500 m) and Bereha (hot and hyper arid type of climate) (NMA, 2001; Araya, et al., 2010). Since the elevation of the Omo-Gibe basin is lying between 235 to 3625 m above MSL, the study area is characterized by all kinds of the above mentioned climate zones.

The climate of Omo river valley varies from tropical humid in the highlands to the hot arid climate in the southern parts of the flood plain. Intermediate between these extremes and for greater part of the basin the climate is tropical sub-humid. The seasonal variation in climate is associated with the oscillation of the Inter-Tropical Convergence Zone (ITCZ), a low-pressure area of convergence (Cheung et al., 2008; Araya et al., 2010; Taye et al., 2019). Between June and September, the ITCZ is located north of Ethiopia and the project area is under the influence of Atlantic equatorial westerlies and southerly winds from the Indian Ocean. These south-westerlies ascend over the south-western highlands of Ethiopia to produce the main rainy season. The ITCZ shifts northwards across southern Ethiopia from September to November and southwards from March to May. Some moist air from the Gulf of Aden and the Indian Ocean reaches parts of southern Ethiopia during the period, causing little rains.

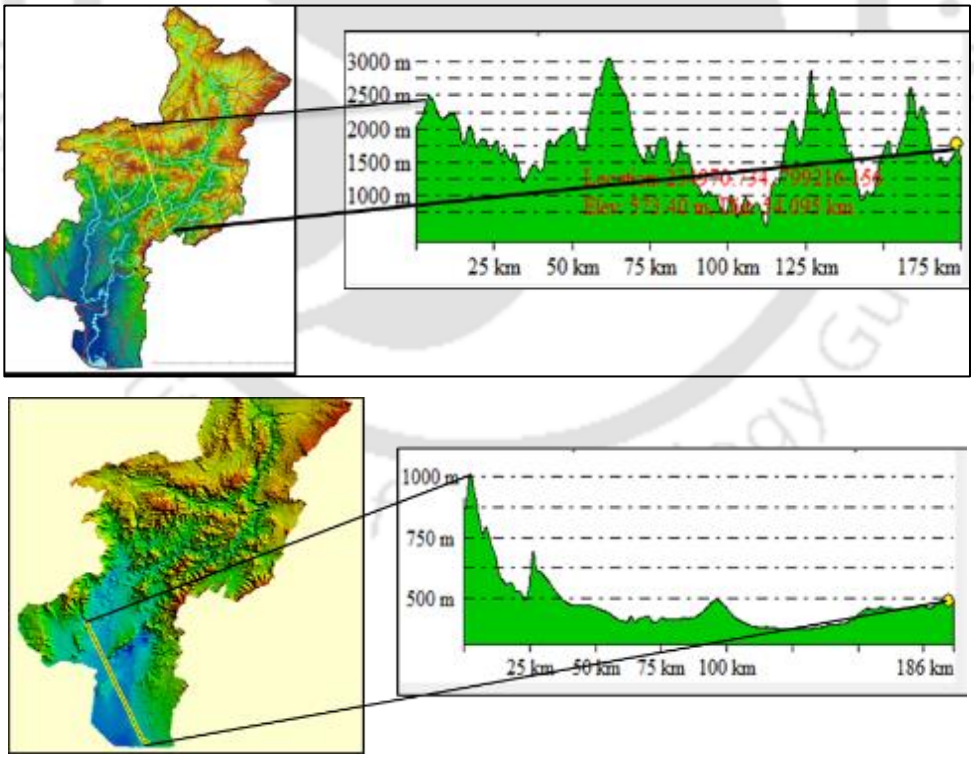

Figure 2.5 Topographic variation of Omo Gibe Basin

In Ethiopia, the “Dega” or “cool zone”, is witnessed in the central sections of the western and eastern parts of the north-western plateau that has elevation mostly above 2400 m and having daily temperatures ranging from near freezing to 16^{o}C. The “Weina Dega” or “temperate zone” is

observed in some parts of the central plateau and ranging in altitude between 1500 m and 2400 m. The “Kolla” or “hot zone” has areas below 1500 m altitude like the Danakil Depression and tropical valleys of the Blue Nile. Within each climate zone, seasonal variations and atmospheric pressure systems contribute to the creation of three seasons – Kiremt (main rainy) season, usually lasting from June to September, covering all of Ethiopia except the southern and south-eastern parts; Belg Season, the light rainy season, usually from March to May and is the main source of rain in the south and south-eastern parts of Ethiopia; and Bega Season, the dry season, from October to February, during which the whole country is dry (Araya et al.,2010; Taye et al., 2019), with the exception of occasional rainfall in the central sections. The difference in cross sectional elevations at upstream and downstream of the basin is illustrated (Figure 2.5). This large standard deviation in the elevation and the cross-sectional profile in area show the basin has rugged topography. The change of rainfall pattern and the altering stream flow on different timescales is the result of this complex system of catchment.

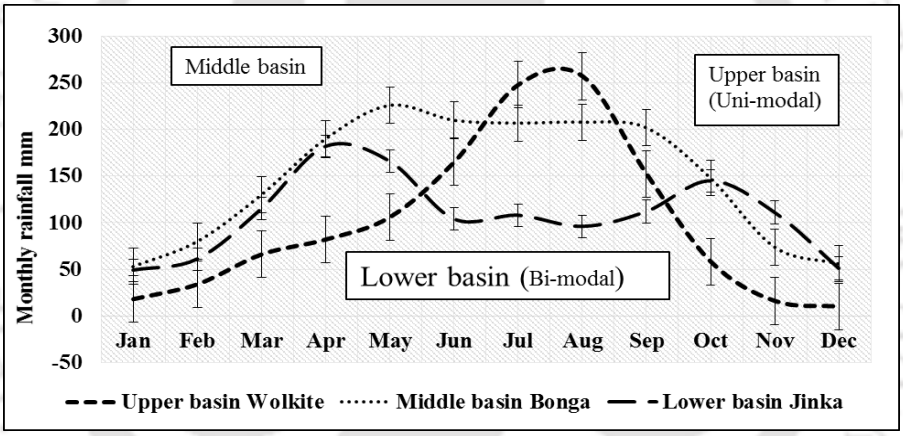

Figure2.6 Rainfall pattern of the Omo-Gibe river basin

Annual rainfall varies from 1900 mm/annum in the north/central areas of the Omo-Gibe Basin, to less than 300 mm/annum in the south of the basin. The annual rainfall generally diminishes through the basin as the river drains from the highlands in the north to Lake Turkana in the south. The mean monthly rainfall pattern over the basin varies distinctly (Figure 2.5). The means in the north part of the basin is uni-modal, but further downstream to the south of the basin the pattern becomes bi-modal.

The study area mean monthly rainfall has been established from the synoptic rainfall station data of these identified more than 10 stations - Jinka, Assendabo, Bonga, Chida, Gibe farm, Hossana, Jimma, Keyafer, Konso, Teppi, Sekoru, Wolta Sodo, Wolikite, Woliso (Figure 2.6). The temporal distribution of the mean monthly rainfall at the area is shown as uni-modal upper basin and bi-modal lower basin in Figure 2.6 and the seasonal rainfall pattern for this station were defend in Figure 2.6.

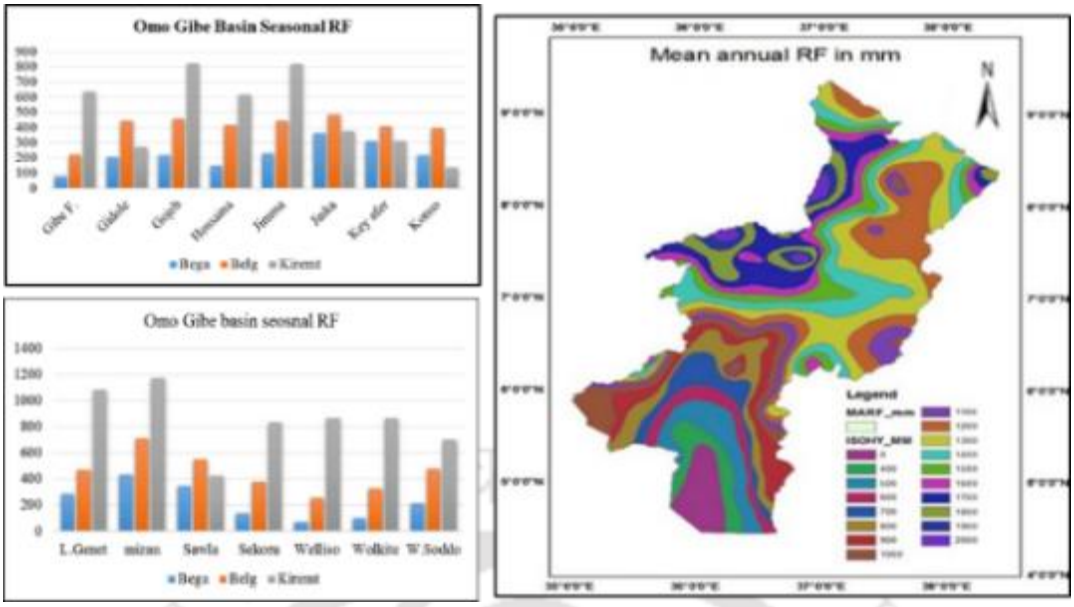

Figure 2.7 Mean annual precipitation in Omo Gibe basin at different station.

2.3 Optimum number of rain gauge stations

Based up on the statistical principle the following statisical analysis is used to fix optimum number of stations for the basin. The assumption *(Chen et al., 2008; Patel et al., 2016; Shahidi and Abedini 2018)* help to obtain number of gauges for a given basin optimally based on an assigned percentage of error estimatinig for mean aerial rainfall. The optimum number of station for Omo Gibe basin was evaluated using Equation 2.1.

$$N = \left(\frac{Cv}{\epsilon}\right)^2 \qquad (2.1)$$

where N = optimal number of stations, ε = allowable degree of (percentage) error in the estimate of the mean rainfall, and C_V = coefficient of variation of the rainfall values at the existing 'n' stations (%). The allowable perecentage of error ε is normally taken as 10% (Chen et al., 2008; Patel et al., 2016). While computing the value of C_v, if it comes less than 10%, we can assume the existing stations are sufficient for the basin. Based on the above analysis in Omo Gibe basin, there are thirteen class one stations, three class two stations, eleven class three stations, and eighteen class four stations. In the basin the existing station is less than the optimal number of stations (N>n). Therefore, it needs thirty additional estimations for stations under consideration of 10% of error.

2.4 Stream Flow

The river is originating from the upper escarpments located in the north-west bordering with Abbay Basin. Main Gibe River, which is the water source of project is passing along the fault and flows in

north-south direction forming Omo River system and then flows to Lake Turkana. Gibe River is not gauged for most of its lower portion, which is inconvenient for proper quantitative estimation of flow. Five or more major gauging stations are present in the upper area (Figure 2.7) that are useful for indirectly assessing lower catchment flow. Stream flow of the rivers highly depends on climate variables such as rainfall, temperature, and potential evapotranspiration of a basin. These climate variables directly influence the stream flow and therefore affects the amount of water available for supply, irrigation, and hydropower generation.

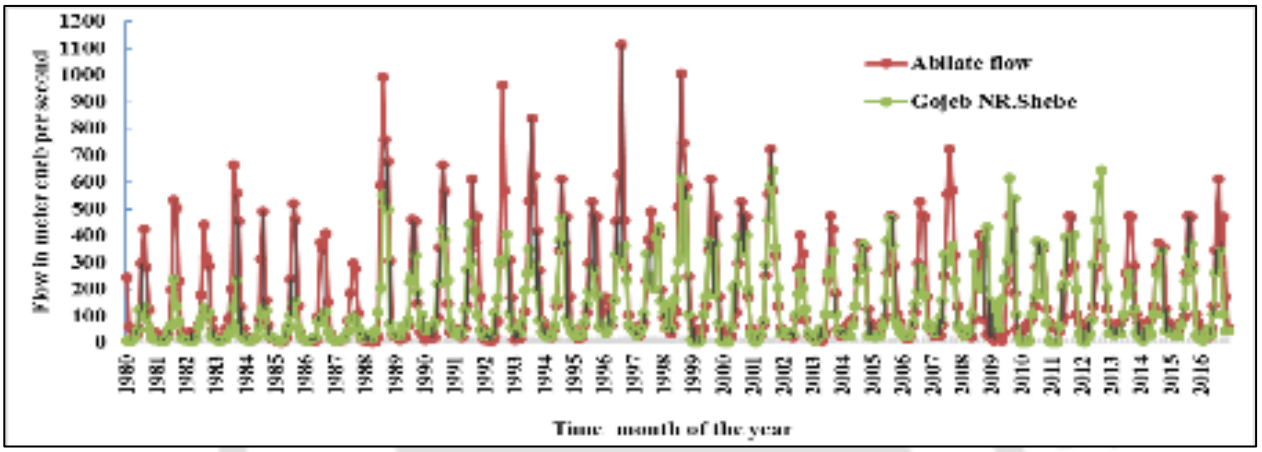

Figure2.8 Mean monthly stream flow data in Asandabo, Abilate and Gojeb in Omo-Gibe basin.

2.5 Maximum and Minimum Temperature in Basin

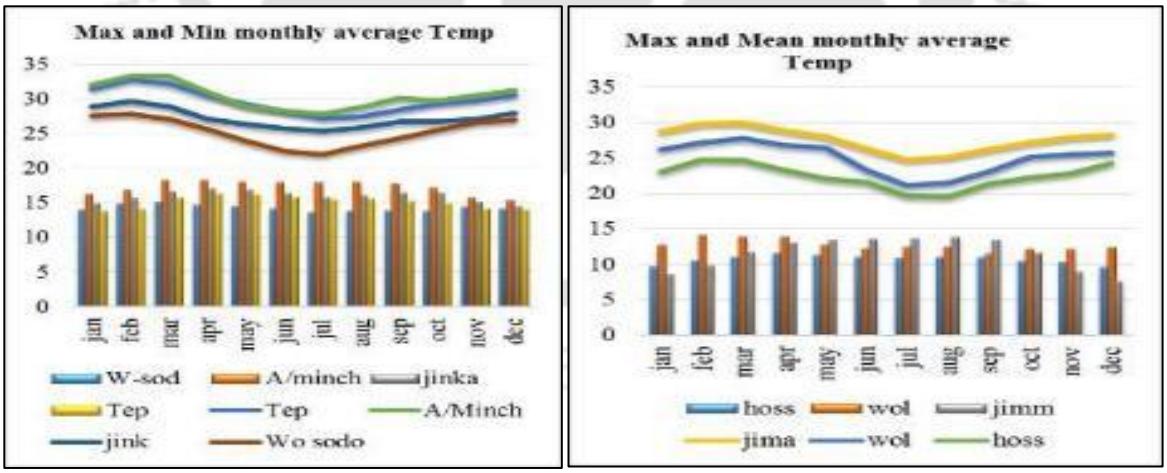

Figure 2.9 Mean monthly maximum and minimum temperature in different station in basin

The mean annual temperature of the entire basin varies from 16°C in the highlands in the north to over 29°C in the south (Figure 2.8). The monthly average temperature rises slightly as of January to May, however, declines afterwards in the months June to August. This is attributed to the fact that months June to August are the wet season of the area when peak rainfall activity is experienced (*EEPCO, 2008)*.

2.6 Estimation of Potential Evapotranspiration

2.6.1 Penman-Monteith Method of Evapotranspiration

Potential evapotranspiration represents the evaporation rate from a reference surface, not short of water. A large uniform grass field is considered worldwide as the reference surface. The reference crop completely covers the soil, is kept short, well-watered and is actively growing under optimal agronomic conditions. Food and Agricultureal (FAO) ET_O calculator software is used to calculate potential evaporation in this study. The software assess ET_O from meteorological data by means of the FAO Penman-Monteith equation. This method has been selected by the FAO as the reference because it closely approximates grass. ET_O at the location evaluated, is physically based, and explicitly incorporates both physiological and aerodynamic parameters and is given by (equation 2.2 and in Figure 2.9).

$$ET_0 = \frac{0.408(R_n - G) + \gamma \frac{900}{T+273} U_2 (e_s - e_a)}{V + \gamma(1 + 0.34U_2)} \qquad (2.2)$$

where, ET_0: Reference evapotranspiration (mm/day); R_n : Net radiation at the top of crop surface (MJm^2day^{-1}); G: Soil heat flux density (MJm^2day^{-1}); U_2: wind speed at 2 m height (ms^{-1}); e_s: saturation vapor pressure (KP_a); e_a is actual vapor pressure (KP_a); $(e_s - e_a)$: saturation vapor pressure deficit (KP_a); V slope vapor pressure (KP_a/c°); γ: psychometric constant (KP_a/c°).

2.6.2 Hargreaves Method of Evapotranspiration

Hargreaves and Samani model equation is an empirical radiation-based method, which is extensively used in the conditions of limited weather data (*Hargreaves and Samani, 1985*). It is expressed as in (equation 2.3)

$$ET_o = 0.0023 \times Ra \times (T_{mean} + 17.8) \times (T_{max} - T_{min})^{0.5} \qquad (2.3)$$

where, Ra=water equivalent of extra-terrestrial radiation (mm/day); T_{mean} = mean air temperature; T_{max} = daily maximum air temperature (°C); T_{min}= daily minimum air temperature.

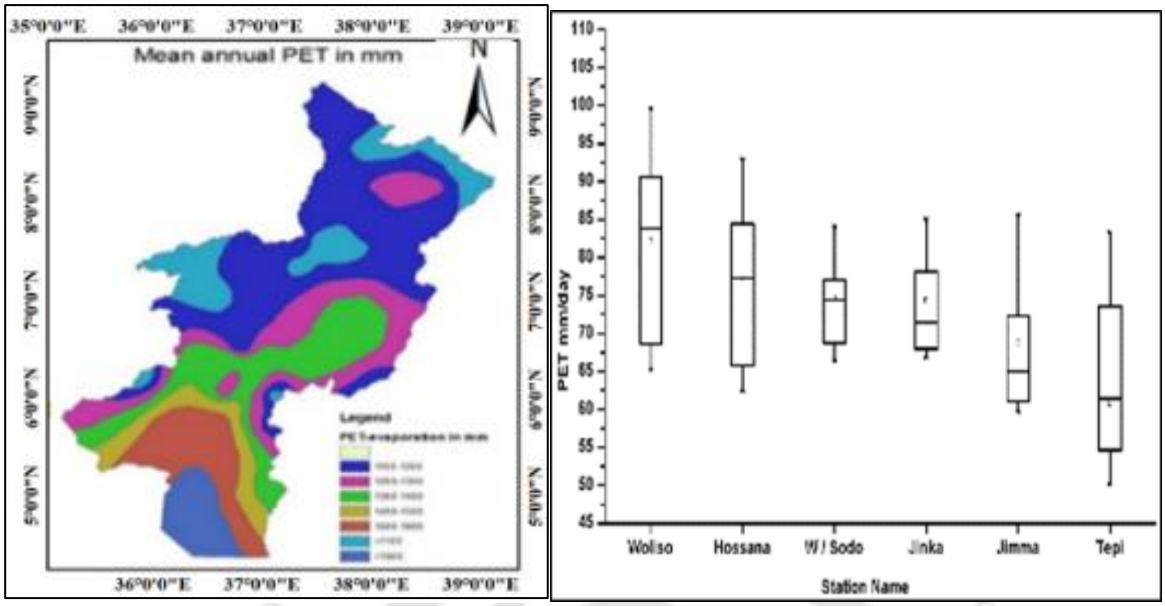

Figure 2.10 Mean monthly Potential evaporation in Omo Gibe basin at different station

2.6.3 Priestley-Taylor Method of Evapotranspiration

The using Priestley-Taylor equation according to Priestly-Taylor 1972 methods is defined as:

$$ET_o = \alpha \frac{\Delta}{\Delta+\gamma}\left(\frac{Rn-G}{l_v}\right) \qquad (2.4)$$

where ET_o evapotranspiration mm day^{-1}; α constant and equal to 1.26; and l_v latent heat of vaporization MJ kg^{-1} and it varies slightly with temperature according to 2.501×10^{-6}–2370T (J/kg) (*Chow, 2010*). Net radiation, the latent heat of vaporization, the psychometric constant, and the slope of the vapour pressure-temperature curve were calculated using the FAO-56 procedure and the daily soil heat flux G was assumed to be 0 based on the FAO-56 recommendation for daily ET calculation (Allen et al. 1998). In semiarid or arid areas where the advection component of the energy balance is significant, the Priestley-Taylor equation will underestimate potential evapotranspiration.

2.7 Geology and Topography

Ethiopia is situated in the northern corner of the African plateau, on the southwestern edge of the Red Sea (*Abdel-Gawad et al., 1970*), close to the present location of the triple junction between the Red Sea, and the Gulf of Aden. The Omo Gibe basin is situated on the southwestern plateau very close to the main Ethiopian rift valley and the area's geology consisted of rocks ranging from Precambrian to Quaternary in ages (*Foerster et al., 2012; Abbate & Sagri 2015*). The master plan report revealed that this rock is the hardest and most weathering-resistant than other volcanic rocks.

In general, very large blocks, boulders and cobbles, trace sand, and gravel deposits are concentrated on the river channel at the planned diversion weir site, both of alluvial and colluvial origin. The bedrock, which is very sound one, is estimated to be round at a shallow depth beneath the river channel from close site inspection. The area's topography can be grouped into different morphology-based geomorphic units (*Abbate & Sagri, 2015*). The region's major geomorphic genes are concave hills, higher chain of undulating hills, plateau, long, very steep slopes, and valley bottoms.

2.8 Population

The Omo-Gibe basin includes parts of the federal states of Oromia and SNNP. It is the second most populous basin in Ethiopia and the most densely populated basin in Ethiopia. Population is a major element in the nature of basin water resources.

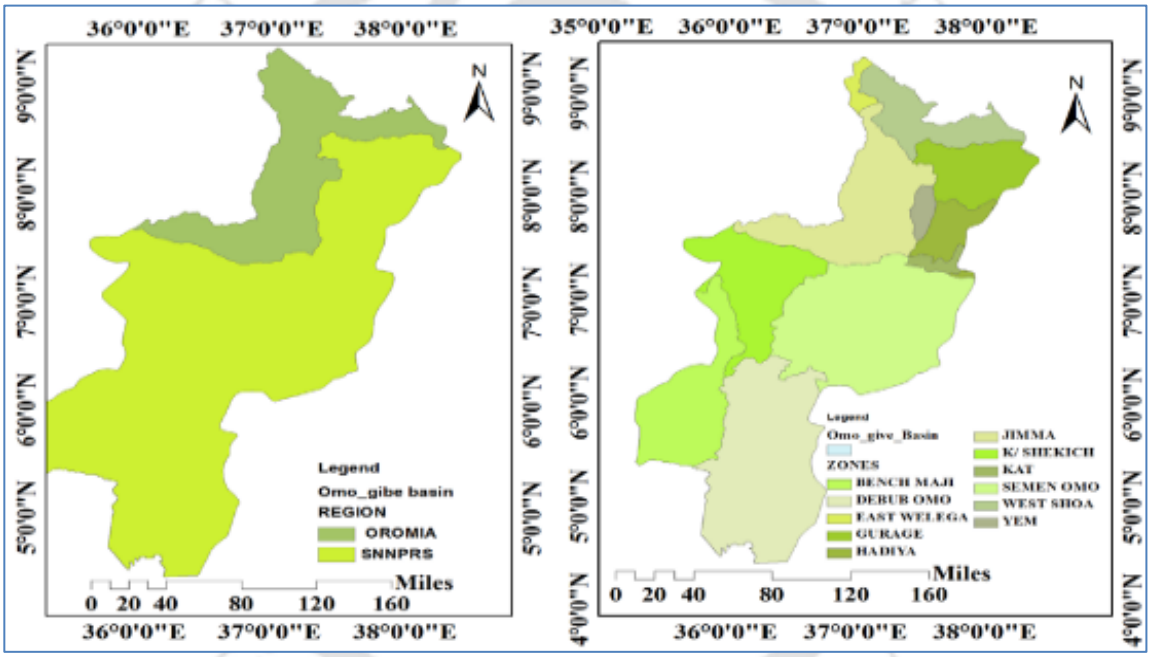

Figure 2.11 Regional state and zonal administration map in Omo-Gibe basin.

Population forecast in different periods is a relevant factor for estimating potential water demands. In Figure 2.11, the regional and zonal population distribution is depicted.

2.8.1 Factors affecting population growth

A great many factors affect population growth. Natural disasters like big fires, epidemics, floods, earthquakes, and anthropogenic influences like war, change in education, politics, recreation, economic change, sudden increase in religions importance of the city, political changes in the adjoining country, and nearness to the national borders, can affect the growth of population in the region.

2.8.2 Method of population projection estimation

The following are the common methods by which the projection of population is done. Arithmetic increase method, Geometric increase method, Incremental increase method, Decrease rate method, Logistic curve method, and Graphical method (*Mohammed, 2013; Gawatre et al., 2016; Isard, 1966*). The master plan method used by Ethiopian statistic authority. (Equation 2.5) is used to estimate futuristic population.

$$P_n = P_o \lambda^{kn} \qquad (2.5)$$

where P_n = population at n decades or years, n = Decade or years, k = Growth rate. Out of the population forcasting methods discussed, the exponential growth rate method is used population projection.

2.9 Hydropower development

The gross hydroelectric potential of Omo-Gibe basin is 36560 GWh a^{-1} (*Awulachew et al., 2007*), which is second largest potential next to Abay basin, accounting for 24% of the gross hydroelectric potential of the country. Currently a cascade of five hydroelectric power projects (Gibe I-V) is either planned or being developed along the Omo-Gibe River (Figure 2.12) (*Avery, 2010*). The basin has the highest potential of sedimentation of all basins of Ethiopia with the total suspended sediment load of 120 $\times 10^6$ t a^{-1} (*UNESCO-WWAP, 2004*).

2.10 Irrigated Agriculture

Large-scale and medium-scale irrigation potential are identified in the basin, with an estimated irrigable area of 57900 and 10028 hectares, respectively, and a total irrigable area of 67928 hectares (*Awulachew et al., 2007*). However, this figure could be much higher given the vast land area of lower Omo Gibe basin. The basin has 12% irrigable area of the country (*WAPCOS 1995 in Awulachew et al., 2007*).

2.11 Developments and their Positive and Negative Impacts in the Basin

The cascading dams in Omo-Gibe will have positive effects on generating hydroelectric power and regulating the flow there by reducing downstream flooding. Additionally, the downstream irrigation potential is also increased that can improve agro-economy. There are some adverse effects in the basin due to the cascading projects. Lake Turkana is almost entirely dependent on the Omo Gibe River for almost 80% of its inflow and its flow pattern modification in the upstream reduces the

lake level and associated biomass in the lake (*Avery, 2010*). If irrigation development takes place as planned in the Omo Basin, the lake will reduce, as will its biomass and fisheries (*Avery 2010*). Due to the interference of man-made impacts in the basin, forests and vegetation have been cleared and as a consequence, runoff has become more variable, with much more rapid response to rainfall in the last 20 years (*Avery, 2010*), resulting in increased flooding and sedimentation that are accompanied by accelerated sediment transport in downstream of the basin. Figure 2.12 indicates the various projects on Omo-Gibe that have commenced or under construction. Gibe I, II, and III have completed construction and are functioning. Gibe IV is under construction, and Gibe V is set in a planning stage projects including a downstream Kuraz site I and site II for irrigation development.

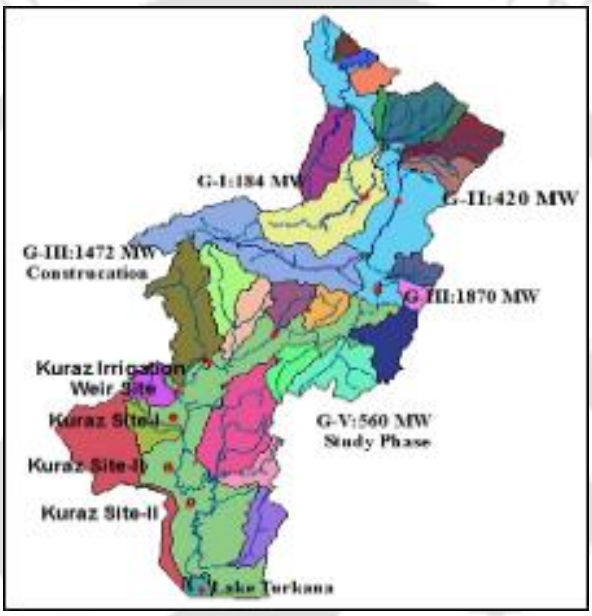

Figure 2.12 Location of water resource development struacture in Omo Gibe basin.

Flood disasters in Ethiopia are attributed to rivers that overflow or burst their banks and inundate downstream plain lands, for instance the flood that has recently assaulted Southern Omo Zone (*Gashaw and Legesse, 2011*). The development of integrated river basin management practise based on federal and regional level of the Omo-Gibe Basin is crucial to address the sustainable use of water resources of the basin and under considering downstream ecology and Lake Turkana.

2.12 Conclusion

The Change in Omo-Gibe river flow patterns has impacts in the flow regime in lower part of the basin as well as in the Lake Turkana ecology. Because of the natural and interference of human beings in the basin, forests and vegetation have been cleared and as a consequence, runoff has become more variable, with much more rapid response to rainfall in the last 20 years (Avery, 2010),

resulting in increased flooding, which are accompanied by accelerated sediment transport in downstream areas. Therefore, Integrated River Basin Management of the Omo Gibe Basin under the considering the impact of climate and land use land cover change is crucial to address the sustainable use of water resources of the basin. The majority of weather observation stations are located in the upstream section of the basin, with a poor distribution in the downstream part. Having access to hydrological and climatological data is essential when using any hydrological model. Without enough hydrological and climate data, using soil water assessment tools in the catchment was one of the most significant difficulties for accurate analysis.

Chapter 3 Literature Review

3.1 Climate Change and Modelling

Due to the dependence of the hydrological system on climate (*Nathan et al., 2019*; *McDowell et al., 2013*), changes in local and regional water availability would be among the most important and immediate effects of global warming (*Nathan et al., 2019*; *Hughes et al., 2003*). These effects may include the magnitude and timing of runoff, flood and drought frequency and intensity, rainfall patterns, extreme weather events, and water availability and quality (*Peterson et al., 2013*). These changes in hydrological features in turn, influence the water supply system, power generation, sediment transport and deposition, and ecosystem conservation. Some of these effects may not necessarily be negative, however due to the great socio-economic importance of water and other natural resources they need to be evaluated (*Andersen, 2007; Hussen et al., 2018*). Predicting water availability, water quality, and river sediment distribution, using models is crucial for the efforts to maintain food safety, water supply, human health and natural ecosystems (*Cosgrove & Loucks, 2015*).

Climate change analyses can provide the basis for significant impacts on water resources through changes in the hydrological cycle. Changes in temperature and precipitation may have a direct impact on the magnitude of the component of evaporation and surface runoff (Nathan et al., 2019; *Trenberth, 2011*). Changes in climate will intensify the existing challenges posed by tropical geography, a heavy dependency on agriculture, rapid growth, poverty, and a limited capacity to cope with an uncertain climate (*IPCC, 2007*).

3.2 Causes of Climate Change

Climate change is a long-term weather shift characterized by temperature variations, change in rainfall pattern, winds, and other measures (*Change 2020*; *Bouwer, 2011*). However, the balance between incoming and outgoing energy, which influences the energy balance of the Earth, governs its long-term state and average temperature (*Nordbo et al., 2011*). Factors that cause climate change can be divided into two categories: natural processes and human activity-related (*Change 2020*; *Karl et al., 2009*). Natural factors intrinsic to the climate system, such as changes in volcanic activity, solar output, and the Earth's orbit around the Sun will influence the Earth's climate (Palm et al., 2017; *Wuebbles & Jain 2001*). Differences in global temperature have led to climate patterns over the past century, but since the Industrial Revolution, greenhouse gas contributions to the atmosphere have had about ten times the effect of changes in the output of the sun (*Karl et al., 2009*). Human activities, like the burning of fossil fuels and the conversion of land for forestry and

agriculture, can also cause climate change (*Dale, 2011*). Such practices change the soil surface and emit various substances into the atmosphere in addition to other environmental impacts. Since the Industrial Revolution, the overall effect of human activities has been a warming trend, driven primarily by carbon dioxide emissions and intensified by other greenhouse gas emissions (*Palm et al., 2017*; *Houghton, 2009*). Such climate change could have far-reaching and/or predictable implications for the environment, society, and economy.

3.3 Climate change from Ethiopian situation

Climate change is already taking place today, thereby helping to reflect possible future changes in the past as well as the current. Over the last decades, Ethiopia's temperature has risen at around 0.37 °C and 0.28 °C per decade, as reported by the National Meteorological Agency (*NMA 2007; Mc Sweeney et al, 2008*). The increase in minimum temperatures is more pronounced with roughly 0.4 °C per decade. Precipitation, on the other hand, remained stable over the last 50 years, when averaged over the country.

However, large-scale patterns are the spatial and temporal variations of precipitation that do not necessarily reflect local conditions. In Ethiopia, the vulnerability to climate change is different from place to place (*Kundzewicz 2008; Kiesel et al., 2019*). The net impact of adaptation, exposure, and adaptive potential across the region is significant. Afar, Somali, Oromia, and Tigray are relatively more vulnerable to climate change than the other regions. The vulnerability of Afar and Somali is attributed to their low level of rural service provision and infrastructure development (*Palm et al., 2017*; *Temesgen et al., 2006*). Tigray and Oromia's vulnerability to climate change can be attributed to the regions' higher frequencies of droughts and floods, lower access to technology, fewer institutions, and lack of infrastructure. SNNPR's lower vulnerability is associated with the region's relatively greater access to technology and markets, larger irrigation potential, and higher literacy rate (*Temesgen et al., 2006; Hurni 1985*).

An increase in temperatures and increasingly variable rainfall in Ethiopia are affecting crops and livestocks in drought prone areas. Meanwhile, pastoralists are struggling to find enough water to keep their camels, cattle, goats, and sheeps alive (*CRS, 2009*). Therefore, a growing frequency of late rains and droughts is consistent with scientific assessments on the impacts of climate change in Ethiopia. Higher temperatures and its direct effect on higher evaporation levels can be correlated with the droughts. The increased rain variability is consistent with changes in the patterns of local rainfall. Future predictions of temperature rise and increasing variability in rainfall implies that both droughts and late rains are likely to become more pronounced in the coming years (*Elliott et al.,*

2014; Marius 2009). The disadvantageous and beneficial impacts of the current and expected climate change and instability are typically widespread in socio-economic as well as natural systems.

3.4 Climate models and model Scenario

There are commonly four components of a General Circulation Model (GCM): air, surface, ocean, and sea ice (*Popova, et al*., 2012; *Yongqiang et al., 2004*). As the four components are interactive, production runs must include all four model components. The atmospheric model was initially developed to a fair level of sophistication, while the land phase and ocean components were very simplistic. Runoff incorporates simulations of the new GCM model (*Popova, et al., 2012*; *Rowntree 1989; Kite et al., 1994*). Climate Models have demonstrated some of the problems associated with GCM modelling of the hydrological cycle, particularly the lack of adequate lateral transfer of water. Climate change has numerous impacts on an availability of basin inflows. It can change seasonal temperature and precipitation, shift the timing of stream flow and runoff, and reduce the capacity of existing sources to meet water needs. The only means available to quantify the non-linear climate response is by using numerical models of the climate system based on well-established physical, chemical, and biological principles, possibly combined with empirical and statistical methods. These are designed mainly for studying climate processes and natural climate variability, and for projecting the response of the climate to human-induced forces (*Baede et al., 2001*). The first models used to evaluate climate change examined the impacts of increased greenhouse gases on long-term weather patterns (*Van Lieshout et al., 2004; Adem et al., 2014*).

GCMs describe the global climate system, representing the complex dynamics of the atmosphere, oceans, and land with mathematical equations that balance mass and energy. By simulating interactions among sea ice, land surface, atmospheric chemistry, vegetation, and the oceans, they predict future climates characterized by temperature, air pressure, and wind speed. Because these models are so computationally intensive, they can only be run on supercomputers at large research institutes. However, the results are made available to the general scientific community and have so far been used for studies of climate change and its impacts on natural, social, and economic systems (*IPCC AR4, 2007; McCarthy et al., 2001*). GCMs results vary due to model attributes, including their components, resolution, flux-adjustment, and emission scenario forcing. Components refer to the individual processes modeled by smaller models with in a given GCM. Current GCMs are referred to as “coupled models” because they are comprised of linked components, which model physical processes such as the atmosphere, oceans, land surfaces, and

sea ice. Atmospheric and ocean components are represented as grid cells in all GCMs while the representation of land surfaces and sea ice vary more. “Couplers” integrate these domains into one unified model by routing the flow of data between components. GCMs may not accurately replicate the current climate and required correction factors (*IPCC, 1996*).

3.4.1 Climate Model Scenario

Climate Change Impact on Ethiopia was done using the A2 and B2 scenarios, where A2 is referred as the medium-high emissions scenario and B2 as the medium-low emissions scenario of Hadley Centre Climate Prediction Models (HadCM3) output (*Arsiso, et al., 2018*; *Abdo et al., 2009; Worqlul et al., 2018; Müller, 2009*). The temporal and spatial resolution disparity between the outputs of the GCM models and the data needed for such impact studies was adjusted using the most common approach called the statistical downscaling method. This method is advantageous as it is easy to implement, and generation of the downscaled values involve observed historic daily data. The latter advantage ensures the maintenance of local spatial and temporal variability in generating realistic time series data.

3.4.2 Types of climate scenario

Several types of climate scenario have been developed for impact studies (O’Neill et al., 2020; *Duinkerb and Greig, 2007; Den Elzen and Schaeffer 2002)*. These scenarios are generally classified into three main classes; synthetic scenarios, analog scenarios, and GCM output-based scenarios. Synthetic scenarios define methods where particular climate-related elements are altered by a realistic but arbitrary amount, often according to a region-specific qualitative interpretation of climate model simulations (*Duinkerb and Greig, 2007; Carter, et al., 2001; Midhuna and Dimri, 2019*). This means baseline temperature adjustment of + 1, 2, 3 and 4°C and baseline precipitation of ±5, 10, 15 and 20 % could represent different magnitudes of future changes. Analogous scenarios are constructed by assessing documented climate regimes that might be similar to the future climate in a given region. At present, these records can be obtained either from the past or from another region. Spatial analogues are regions that today have a climate close to that anticipated in future study regions (*Mearns et al, 2001*; O’Neill, et al., 2020). Whereas temporal analogs make use of past climate information as an analogous to potential future climate.

3.4.3 The SRES Emission Scenario

Global mean warming estimates by the year 2100 (*Levermann et al., 2013; Friedrich et al., 2016*; *Ford et al., 2018*) due to anthropogenic greenhouse gas emissions to the atmosphere vary from 1.8 ^{o}C to 4.5 ^{o}C rise with current climate (*Johns et al. 2003; IPCC, 2007a*; *Den Elzen and Schaeffer 2002*). The global change would be a sum of regional changes scattered over both sides of the global mean. Different climate change scenarios were constructed in the context of the IPCC assessments (*IPCC-TGICA, 2007; Deb et al., 2018*). This has to do with the global emissions scenarios, which are based on population and economic growth models. Climate scenario data is required to quantify the relative change of climatic variables between the current and future time horizon.

The projected or generated climate variables are used as input to hydrological model for assessment of hydrological impacts on water structure. Based on the available data, the scenario generated (RegCM3 forced by ECHAM5 GCM model output with A1B emission scenario) will be used in this study. RegCM3 forced by ECHAM5 model output with A1B emission scenario for study area can be obtained from International Water Management Institute (IWMI). RegCM3 forced by ECHAM5 model outputs future scenarios are in the period of three decades. The baselines period is considered from 1991 to 2000. The future scenarios will be developed by dividing the future time series into two periods of 10 years: 2031-2040 and 2091-2100. The period from 1991-2000 (or here called as "baselines period") will be taken as a base period with which the comparison are made.

It is difficult to know exactly how anthropogenic emissions will change in the future. However, the IPCC Special Report on Emission Scenario (SRES) has developed new emission scenarios, the so-called "SRES scenarios". Emission scenarios are plausible representations of future emissions of substances that are radioactively active (i.e. greenhouse gases). The IPCC attributes most of the global warming observed over the last 50 years to greenhouse gases released by human activities. To estimate future climate change, the IPCC (*SRES 2000; Pachauri et al., 2014; Myles, 2011; Im et al., 2012; Im et al., 2012*) prepared forty greenhouse gas and sulfate aerosol emission scenario for the 21st century that combine a variety of assumption about demographic, economic, and technological driving forces likely to influence such emissions in the future. Each scenario represents a variation within one of four storylines such as A1, A2, B1, and B2 *(Nakicenovic et al., 2000*). The experts who created the storyline were unable to arrive at a most likely scenario and probabilities were not assigned to the storylines. The storylines can be summarized as follows:

a) A1 scenario family: - reflects the world as very rapid economic growth, global population peaks in the mid-century and decline thereafter, and rapid introduction of new and more efficient technologies *(Nakicenovic et al., 2000)*

b) **B1 scenario family**: - reflects the world as a convergent world with the same global population as in the A1 storyline but with rapid changes in economic structures toward a service and information economy, with reductions in materials intensity, and the introduction of clean and resource efficient technologies *(Riahi 2007; Change IPOC 2001; Nakicenovic et al., 2000).*

c) **A2 scenario family:** - reflects the world as continuously increasing global population and regionally oriented economic growth that is more fragmented and slower than in other storylines *(Swart et al., 2003; Riahi 2007; Change IPOC 2001; Nakicenovic et al., 2000).*

d) **B2 scenario family:** - The world emphasis goes to local solutions to economic, social, and environmental sustainability, with continuously increasing population (lower than A2) and intermediate economic development.

3.4.4 Downscaling methods

Downscaling is the term given to the process of deriving finer resolution data (*Hewitson and Crane, 1996*) from coarser resolution GCM data. A relationship between location climate and large-scale (GCM grid box scale) climate can be established, which can then be used to derive more accurate values of the future climate on the site scale (*Sailor et al., 2000; Wilby et al., 1990; Wilby et al., 2002; Hewitson and Crane, 1996*).

a) *Dynamic Downscaling Method*

Dynamical downscaling method (DDM) is one of the significant methods to obtain fine-scale climate information using Regional climate model based on GCM output *(Xu., et al 2019*). DDM is a method for obtaining high-resolution climate or climate change information from relatively coarse-resolution GCMs (*Ramírez and Jarvis, 2010*). The correlation coefficient between the selected stations is carried out in order to find a single station for downscaling purpose that has high correlation with most of the other neighboring stations (*Pour et al., 2014; Huang et al., 2011*). In addition to the correlation coefficient, the quality and the available length of period of record also take into consideration during selection of stations for downscaling. GCM downscaled output for study area is used for this analysis as the daily precipitation, daily maximum and minimum temperature, solar radiation, and wind speeds. Statistical and dynamic downscaling outputs have been broadly used in the fields of climate change impact on annual water availability, seasonal water availability, and Extreme events (Floods and Droughts).

b) *Empirical (statistical) downscaling*

Empirical-statistical downscaling model (ESDM) models use statistical relationships to infer local climate information from large-scale climate information produced by global climate models

(GCMs) (*Hanssen-Bauer et al., 2005; Busuioc & Dumitrescu, 2018*). ESDM is able to simulate all except the extreme climatic events (*Huang et al., 2011*). The model underestimates the farthest values in both extremes and keeps more or less an average event (*Pour et al., 2014*). The ESDM model simulated maximum temperature more accurately than minimum temperature and precipitation (*Hassan et al., 2014; Mahmood and Babel 2013*). ESDM more accurately reproduced monthly and seasonal climatic variables averaged over years than individual monthly and seasonal values in a single year.

3.4.5 Regional climate model

A Regional Climate Model (RCM) is a tool to add accurate, small-scale information about future climate change to a GCM's large projections (*Rummukainen 2016; Teutschbein & Seibert 2013*). RCMs are complete climate models and as such are physically focused, describing most or all of the processes, interactions, and feedback between the components of the climate system represented in GCMs *(Richards et al., 2004; Steffen et al.,2006*). In these methods of obtaining of sub-grid scale estimates (sometimes down to 50 km resolution) are able to account for important local forcing factors such as surface type and elevation, which conventional GCMs (*Maraun et al., 2010*) are unable to resolve. For this reason, very few simulations have been made for a sufficient period of simulated years to allow meaningful climate change statistics to be extracted. Furthermore, the commonest approach, nesting, is still heavily reliant on specialized GCM outputs for its boundary conditions. The GCMs do not always provide accurate simulations of the large-scale flow, and there may be inconsistencies between the behavior of the driving model's physical parameterizations and the regional model's finer grid (*Prein et al., 2015; Maraun et al., 2010; Wang et al., 2004*).

3.4.6 Representative Concentration Pathways Scenarios

The Fifth Assessment Report (AR5) of Intergovernmental Panel on Climate Change (IPCC) has set scenarios that replace the Special Report on Emissions Scenarios (SRES). The new scenarios are called Representative Concentration Pathways (RCPs) (Wayne 2014; Egeru et al., 2019). There are four pathways: RCP8.5, RCP6, RCP4.5, and RCP2.6. RCPs are referred to as pathways in order to emphasize that their primary purpose is to provide time-dependent projections of atmospheric greenhouse gas (GHG) concentrations and emphasize that it is not only a specific long-term concentration or radiative forcing outcome, such as a stabilization level, that is of interest, but also the trajectory that is taken over time to reach that outcome. The RCPs are consistent with a wide range of possible changes in future anthropogenic (human) GHG emissions, and aim to represent their atmospheric concentrations. The four RCP scenarios used in CMIP5 lead to radiative forcing

values that span a range larger than that of the three SRES scenarios used in CMIP3 (*IPCC WGI AR5, 2011; Van Vuuren et al., 2011; Thomson et al., 2011).* IPCC WGI Fifth Assessment Report also projected the potential for temperature rises of up to 4.8°C and sea level rise of up to 0.82 m by 2100 (*Stocker, 2013*).

Global mean temperature changes projected range from 4.7°–8.6°F (2.6°–4.8°C) under the higher scenario (RCP8.5) to 0.5°–1.3°F (0.3°–1.7°C) under the lower scenario (RCP2.6) (*Hayhoe, K., J. et al., 2017*). Lower scenarios (RCP4.5 and RCP2.6) *(Tian et al 2017; You et al 2014; Jiang et al 2016)* is similar to SRES B1, but the RCP2.6 scenarios is much lower than any SRES scenario and A1B is similar to Higher scenario RCP8.5. RCP4.5 is close to SRES B1, RCP6.0 is in between SRES B1 and SRES A1B, and RCP8.5 is higher than SRES A2 and close to SRES A1FI. RCP2.6 is lower than any SRES scenario and very close to the ENSEMBLES E1 scenario (*Johns et al., 2011 Stocker et al., 2013*). Results obtained with one GCM confirm that the only two SRES and RCP scenarios that are close are RCP4.5 and SRES B1, and that the temperature increase with RCP8.5 is larger than that with SRES A2 (*Dufresne et al., 2011*).

The estimated global warming distribution through the RCP scenarios is much higher than with SRES scenarios. RCP scenarios (*Moss et al., 2010*) have been applied to prescribe future radiative forcing. In the RCP scenarios, the concentrations of greenhouse gas are expressed as equivalent CO_2 concentrations, and interpolated from year to year. Here we use three different RCP scenarios. RCP 2.6 (*Jiang et al 2016*) adopt strategies for reducing greenhouse gas emissions that cause radiative forcing to stabilise at 2.6 W/m² before the year 2100 (*IPCC, AR5*). RCP 4.5 adopt strategies for reducing greenhouse gas emissions that cause radiative forcing to stabilise at 4.5 W/m² before the year 2100 (*used by IPCC, AR5*). RCP 8.5 that have higher greenhouse gas emissions mean by the year 2100 (*IPCC, AR5*), in which radiative forcing would exceed 8.5 W/m^2 (*Gordon et al., 2000)*.

3.5 Bias Correction

The downscaled RCPs data can often not be used explicitly for impact assessment, since the measured variables vary systematically from those observed (*Field 2014; Ekström et al., 2015; Liang et al., 2008*). Therefore, bias correction is applied to counteract the propensity to overestimate or underestimate the mean of the downscaled variables. Factors for bias correction are determined from data on observed and simulated variables (*Leander and Buishand 2007*). Two bias correction methods were tried in this study. First, the nonlinear bias correction method proposed by (*Mangistu 2009*) and the second method called “delta approach”. The formulas used for the correction of

rainfall and temperature bias are shown in linear and power faction. Factors of correction for each month of climatic variable were calculated.

3.5.1 Bias Correction Using Delta Change Method

The Delta Change technique is generally used for future climate change forecast instead of directly using the RCM simulation (*Teutschbein and Seibert, 2012*). In this study, the Delta Change method was used for correct precipitation and temperature data in Lower Omo Gibe River Basin using (equation 3.1 and 3.2).

$$P_{corr}(d) = P_{obs}(d) \times \left[\frac{\mu_m(P_{corr}((d))}{\mu_m(P_{raw}(d))}\right] \quad (3.1)$$

$$T_{corr}(d) = T_{obs}(d) + \mu_m(T_{corr}(d)) - \mu_m(T_{raw}(d)) \quad (3.2)$$

where , $P_{obs,}$ P_{raw} and P_{corr} denote observed, uncorrected, and corrected precipitation, respecatively, while T_{obs} , T_{raw} and T_{corr} are observed, uncorrected and corrected temperature on the day (d^{th}) of the month (m) respectively, and μ_m denotes the mean.

3.5.2 Bias Correction Using Linear Scaling Method

A Linear Scaling technique was used to correct the monthly values depending on the long-term monthly average of observed and simulated. This system does not correct the bias in frequency and intensity distribution (*Ines and Hansen, 2006*). The rainfall and temperature data were adjusted using equation, respectively according to *(Teutschbein and Seibert, 2012, Fang et al., 2015, Smitha et al., 2018*).

$$P_{corr,m,d} = P_{raw,m,d} \times \left[\frac{\mu(P_{obs,m,})}{\mu(P_{raw,m})}\right] \quad (3.3)$$

$$T_{corr,m,d} = T_{raw,m,d} + \mu(T_{obs,m}) - \mu(T_{raw,m}) \quad (3.4)$$

where $P_{obs,m,}$and $T_{obs,m}$ denote the observed precipitation and temperature on a month (m), and, $P_{corr,m,d}$ $T_{corr,m,d}$ and $T_{raw,m,d}$ are corrected and uncorrected temperature and precipitation on the day (d^{th}) of the month (m) respectively. ($\mu(P_{obs,m,}$) ($\mu(P_{raw,m}$) denote the mean value of observed and uncorrected precipitation on the month (m) respectively.

3.5.3 Bias Correction Using Power Transformation Method

Using Power Transformation method further adjusts the bias in standard deviation and variance an exponential form (*Teutschbein and Seibert, 2012, Leander and Buishand, 2007*). The Power Transformation technique was used only for rainfall data due to the use of power function.

$$f(bm) = \left[\frac{\delta_m(P_{obs}((d))}{\mu_m(P_{obs}(d))} - \frac{\delta_m(p_{raw}^{bm}((d))}{\mu_m\left(P_{raw}^{bm}(d)\right)}\right] \quad (3.5)$$

$$P_{corr}(d) = p_{raw}^{bm}((d) \quad (3.6)$$

$$P_{corr}(d) = P_{corr}(d) \times \left[\frac{\mu_m(P_{obs}((d))}{\mu_m(P_{corr}(d))}\right] \quad (3.7)$$

where $P_{obs}(d)$ and P_{raw} are the observed and uncorrected daily RCM precipitations on the day (d) respectively. δ_m and μ_m denote the mean and standard deviation on a month (m), and is the exponent for the month.

3.6 Climate model and descriptions

Climate models are applied as an investigation tool to study and simulate the climate change, and for functioning resolutions, including monthly, seasonal, daily and inter annual climate forecasts *(Furevik et al, 2003; Auffhammer et al., 2013).* The dataset has a daily time based resolution and is available from 1979 to 2016. The data are interpolated to the Coordinated regional downscaling experiment—African Domain (CORDEX-Africa) grid (0.44°, ~50 km) of the projected model data for comparison. For historical and future projections (period 1979–2100) we used daily maximum and minim temperature, daily precipitation data from 13 regional climate model (RCM) simulations of the CORDEX-Africa multi-model scenario. In the set of simulations, 4 RCMs (Russo et al., 2016) are driven by 13 different general circulation models forced with two scenarios, RCP4.5 and RCP8.5 adopted by the Intergovernmental Panel on Climate Change (IPCC) for its fifth Assessment Report (AR5, Christensen et al 2013; Russo et al., 2016; Schaefer et al., 2014; Russo et al., 2014). Equivalent climate simulations using the other RCPs (RCP2.6 and RCP6.0) were not available. For the comparison with the reanalysis we use historical simulations (Taylor et al 2012) for the period 1979–2005. Therefore, for more information on RCM and driving GCM from the cordex Africa simulations found at

http://cordex.org/index.php? option=com_content & view=article &id=242&Itemid=769.

Table 3.1 Climate Model and description

Model ID	Institutions Name /centre	Resolution (lat/lon)	Reference
CGCM1	Canadian Centre for Climate Modelling and Analysis Canada	Atmospheric component: ~3.7° × 3.7°	*Flato et al., 2000*

HadCM2	Met Offce Hadley Centre, UK	2.5°× 3.75°	*Johns et al., 1997*
HadCM3	Met Offce Hadley Centre, UK	2.5°× 3.75°	*Gordon et al., 2000*
RegCM3	National Center for Atmospheric Research, USA	RegCM3 ~50 km	*Giorgi et al., 1993 a, b*
ECHAM4	the Deutsch Klimarechenzentrum (DKRZ), Germany	~2.8° × 2.8°	*Roeckner et al., 1996*

Climate projections are distinguished from climate predictions (*Auffhammer et al., 2013)* in order to emphasise that climate projections depend upon the emission/concentration/radiative forcing scenario used, which are based on assumptions concerning, for instance, future socioeconomic and technological developments that either or realised the uncertainty of the projection.

3.7 Hydrological Modelling

Modelling is defined as the process of organizing, synthesizing, and integrating component parts into a realistic representation of the prototype (*van Delden., 2011; Sass and Oxman, 2006*). Some of the benefits of modelling are:

- Models help sharpen the definition of hypotheses,
- Define and categorize the state of knowledge,
- Provide an analytical mechanism for studying the system of interest, and
- Can be used to simulate experiments instead of conducting the experiments on the watershed itself.

Hydrological models are characterizations of the real world system. Modelling of the rainfall runoff processes of hydrology is needed for many different reasons and one of the main reasons being the limited range of hydrological measurement techniques and limited range of measurements in space and time (*Beven, 1999*). Therefore, it is necessary to develop a means of extrapolating from those available measurements in space and time to ungauged catchments and into the future to assess the likely impact of future hydrological changes. The researchers use a wide range of hydrological models; however, the applications of those models are highly dependent on the purposes for which the modelling is made. *Beven (1999*), stated that many rainfall-runoff models are carried out purely for research purposes as a means of enhancing knowledge about hydrological systems. He also added that other types of models are developed and employed as tools for simulation and prediction aiming ultimately to allow decision makers to improve decision making about hydrological

problems. Before developing the hydrological models, it is very important to understand how the catchment responds to rainfall under different conditions.

Even though, estimates of sediment yield are required in a wide spectrum of practical studies for the planning, design, operation, and maintenance of water resources structures, the measurement and sampling of sediment transportation is very lengthy and costly. One of the options is usage of hydrological models. Most runoff - sediment modelling uses physically based models or/and empirical models (*Babovic and Keijzer, 2002; Vieira et al. 2018; Chang and Franczyk 2008*). The sediment yield from any drainage system is calculated by averaging the data collected over a period of years. It is, therefore, an average of the results of many different hydrologic events.

3.7.1 Types of Hydrological Models

Hydrological modelling can be defined as the characterization of real hydrologic features and system by the use of small-scale physical models, mathematical analogues, and computer simulations (*Allaby and Allaby, 1999*). There are two types of hydrological models - Lumped and Distributed. In lumped models, the parameters of hydrologic models do not vary spatially within the basin and thus, basin response is evaluated only at the outlet, without explicitly accounting for the response of individual sub basins *(Refsgaard and Knudsen 1996; Pechlivanidis et al., 2011)*. Parameters of lumped models often do not represent physical features of hydrologic processes and usually involve certain degree of empiricism. The impact of spatial variability of model parameters is evaluated by using certain procedures for calculating effective values for the entire basin. The most commonly employed procedure is an area-weighted average (*Haan 1982*). Lumped models are not usually applicable to event scale processes. If the interest is primarily in the discharge prediction only, then these models can provide just as good simulations as complex physically based models (*Beven 1999*).

a) Semi-distributed models

Parameters of semi-distributed (simplified distributed) models are partially allowed to vary in space by dividing the basin into a number of smaller sub basins. There are two main types of semi-distributed models: 1) kinematic wave theory models (KW models, such as HEC-HMS), and probability distributed models (PD models, such as TOPMODEL). The KW models are simplified versions of the surface and/or subsurface flow equations of physically based hydrologic models (*Beven 1999*). In the PD models, spatial resolution is accounted for by using probability distributions of input parameters across the basin.

b) Distributed models

Parameters of distributed models are fully allowed to vary in space at a resolution usually chosen by the user. Distributed modelling approach attempts to incorporate data concerning the spatial distribution of parameter variations together with computational algorithms to evaluate the influence of this distribution on simulated precipitation-runoff behaviour. Distributed models generally require large amounts of (often unavailable) data for parameterization in each grid cell. However, the governing physical processes are modelled in detail, and if properly applied, they can provide the highest degree of accuracy.

3.7.2 Selection of Hydrological Model

Every model type requires some application, and selecting an appropriate model structure depends heavily on the function the model needs to serve (*Asl-Rousta et al., 2018; Yuan et al., 2020; Cunderlik et al., 2003; Samadi et al., 2009*). There are various requirements that can be used to select the appropriate hydrological model for a particular problem. Such standards are always project based, since each plan has its own particular needs and requirements. Further, some criteria are also user-depended.

In this research, the physically based Soil and Water Assessment Tool (SWAT) model was used as the hydrological model. The model was selected by considering the criteria on inclusive of availability of data, level of application, purpose, required accuracy, space and time scale, catchment area, simplicity, previous trends (studies) in the surrounding area and Ethiopia as a whole. SWAT model is physically based, spatially distributed and belongs to the public domain. Rather than incorporating regression (*Asl-Rousta et al., 2018*) equations to describe the relationship between inputs and output variables, SWAT requires specific information about weather, soil properties, topography, vegetation, and land management practices occurring in the watershed. It has been tested (Yuan et al., 2020; Zhang, et al., 2018) that the model has obvious advantages as a hydrological modelling tool that includes modularity, computational efficiency, ability to predict long-term impacts as a continuous model, and ability to use readily available global datasets. The availability of a reliable user and developer support has contributed to its acceptance as one of the most widely adopted and applied hydrological models worldwide. It is computationally efficient for simulations of very large basins or a variety of management strategies. The SWAT models were also tested for prediction of runoff and sediment in basin with satisfying results and good performance.

3.7.3 Description of Selected SWAT Model

Jeff Arnold for the USDA Agricultural Research Service (ARS) developed the SWAT model. SWAT was developed to predict the effect of land management activities on water, sediment, and agricultural chemicals yields over long periods in large complex watersheds with varying soils, land use, and management conditions (*Neitsch et al., 2005*). In recent years, SWAT model *(Arnold et al., 1998*) has gained international acceptance as a robust interdisciplinary watershed modelling. SWAT is currently applied worldwide and considered as a versatile model that can be used to integrate multiple environmental processes, which support more effective watershed management and the development of better-informed policy decision.

The model is a physical based, semi-distributed, continuous time and operating on daily time step. As a physical based model, SWAT uses Hydrological Response Units (HRUs) to describe spatial heterogeneity in terms of land use, soil types and slope within a watershed. As SWAT simulates at catchment scale, the catchment is divided into hydrological response units (HRUs) based on soil type, land use, and slope classes that allows a high level of spatial detail simulation. The major model components include hydrology, weather, soil erosion, nutrients, soil temperature, crop growth, pesticides agricultural management, and stream routing. The model predicts the hydrology at each HRU using the water balance equation, which includes daily precipitation, runoff, evapotranspiration, and percolation and return flow components. In the model, the surface runoff is estimated using two options, Natural Resources Conservation Service Curve Number (CN) (*USDA-SCS, 1972*) and Green and Ampt (*Seyfried 1991*) methods. The percolation through each soil layer is using storage routing techniques combined with crack-flow model (*Arnold, 2001*). SWAT estimates evapotranspiration using three options: Priestley-Taylor (*Priestley 1972), Penman-Monteith (Monteith 1965*), and Hargreaves (*Hargreaves, 1985*). The flow routing in the river channels is computed using the variable storage coefficient method or Muskingum method (*Chow 2010*) SWAT is a basin-scale, continuous-time model that operates on a daily time step and is designed to predict the impact of management on water, sediment, and agricultural chemical yields in ungauged watersheds.

The model is physically based, computationally efficient, and capable of continuous simulation over long periods. Major model components include weather, hydrology, soil temperature and properties, plant growth, nutrients, pesticides, bacteria and pathogens, and land management. In SWAT, a watershed is divided into multiple sub watersheds, which are then further subdivided into HRUs that consist of homogeneous land use, management, and soil characteristics. The HRUs represent percentages of the sub watershed area and are not identified spatially within a SWAT simulation. Alternatively, a watershed can be subdivided into only sub watersheds that are characterized by dominant land use, soil type, and management. There are only few reported

applications of SWAT model to Ethiopian conditions and that too in relatively small watershed areas (*Dilnesaw, 2006; Haile et al., 2013*). Hence, the application of SWAT for the entire Omo-Gibe basin is highly relevant and informative.

3.8 Hydrological components of SWAT model

The simulation of a watershed hydrology is categorized into two categories (*Rahman et al., 2013*). One is the land phase of the hydrological cycle, which controls the amount of water, sediment, nutrient, and pesticide loading in each sub basin to the main channel. Hydrological components simulated in land phase of the hydrological cycle are canopy storage, infiltration, redistribution, evapotranspiration, lateral subsurface flow, surface runoff, ponds, tributary channels and return flow *(Neitsch et al., 2011*). The second is the routing phase of the hydrologic cycle that can be defined as the movement of water, sediments, nutrients and organic chemicals through the channel network of the watershed to the outlet *(Neitsch et al., 2011; Gleeson et al., 2012)*.

3.8.1 Hydrological process modeled by SWAT tools using water balance equation

$$S_{wt} = S_{wo} \sum_{i=1}^{t} (R_{day} - Q_{surf} - E_a - S_{seep} - Q_{gw}) \qquad (3.8)$$

where, Swt =final soil water content (mm), Swo = initial soil water content on day i (mm), Q_{surf} =Amount of surface runoff on day i (mm), R_{day} = Amount of precipitation on day i (mm), Ea = Amount of evapotranspiration on day i (mm), W_{seep} = Amount of water entering the vadose zone from soil profile on day i (mm), Q_{gw} = Amount of return flow on day i (mm). There are two methods available to estimate surface runoff. They are - the USDA Soil Conservation Service SCS curve number procedure, and the Green & Ampt method of infiltration. The SCS curve number method was used in this study to estimate infiltration of the surface runoff. FAO Penman-Monteith, Priestley−Taylor method and Hargreaves method was used to estimate potential evapotranspiration (PET). The SCS curve number is described by equation (3.9)

$$Q_{sur} = \frac{(R-0.2S)^2}{(R-0.8S)} \qquad (3.9)$$

For R > 0.2S,

Q = 0.0 for R < 0.2S,

$$S = 251\left(\frac{100}{CN} - 1\right)$$

$$CN1 = \frac{200(100-CN2)}{100-CN2+e^{2.553-.0636(100-CN2)}} \qquad (3.10)$$

$$CN3 = CN2 \times (e^{(0.00673(100-CN2)})$$

where, Q = daily surface runoff (mm): R = daily rainfall (mm), S = retention parameter (mm); CN = curve number. The SCS curve number is a function of the soil's permeability, land use, and antecedent soil water conditions. SCS defines three antecedent moisture conditions.1-dry (wilting point), 2–average moisture, and 3–wet (field capacity). CN1 and CN3 are found out as function of CN2.

3.8.2 SWAT model predicts lateral flux

$$Q_{lat} = \frac{0.024\,(2SSC \sin \alpha)}{\theta_d C} \qquad (3.11)$$

where, Q_{lat} = lateral flow (mm/ day); S = drainable volume of soil water per unit area of saturated thickness (mm/day), SC = saturated hydraulic conductivity (mm/h); L = flow length (m); α = slope of the land: θ_d= drainable porosity.

3.8.3 SWAT-model estimates the base flow

$$Q_{gw} = Q_{gwi} e^{(-\alpha_{gw} \times \Delta t)} + W_{rchg} \times (1 - e^{(-\alpha_{gw} \times \Delta t)}) \qquad (3.12)$$

where, Q_{gwj} = groundwater flow into the main channel on day j; α_{gw} = base flow recession constant; Δt = time step

3.8.4 Evapotranspiration

SWAT model calculated Evapotranspiration using different methods like Penman-Monteith, Hargreaves, and Priestley-Taylor (listed in section 2.5).

3.8.5 SWAT lateral flow is calculated

$$Q_{lat} = (Q'_{lat} + Q_{latstor,i-1}).[\,1 - \exp\left|\frac{-1}{TT_{lag}}\right|] \qquad (3.13)$$

where Q_{lat} is the amount of lateral discharged to the main channel on a given day (mmH_2O), Q'_{lat} is the amount of lateral flow, $Q_{latstor,i-1}$is the lateral flow, TT_{lag} is the lateral flow travel time(day).

3.8.6 SWAT model used to calculate the amount of water percolating to the ground

$$W_{perc,jy} = SW_{ly,excess} \times (1 - \exp\left|\frac{-\Delta t}{TT_{perc}}\right|) \qquad (3.14)$$

where $W_{perc,jy}$ is the amount of water percolating to soil, $SW_{ly,excess}$ the volume of water in soil layer. $-\Delta t$ is the length of the time step (hrs), TT_{perc} is the travel time for percolation (hrs).
SWAT water balance for the shallow aquifer is

$$aq_{sih,}j = +aq_{sh,j-1} - Q_{gw} - w_{revap} + w_{pump,sh} - w_{rchrg.sh} \qquad (3.15)$$

where $aq_{sih,j}$ is the amount of water stored in the shallow aquifer day i. $aq_{sh,j-1}$ is the amount of water stored in the shallow aquifer on day i^{-1}, Q_{gw} is groundwater flow, w_{revap} the soil zone in response to water deficiencies. $w_{pump,sh}$ is the amount of water removed from shallow aquifer by pumping on day i. $w_{rchrg.sh}$ recharge entering the shallow aquifer on day.

3.8.7 SWAT water balance for the deep aquifer

$$aq_{dp,i} = aq_{dp,j-1} + w_{dep} - w_{pump,dp} \qquad (3.16)$$

where $aq_{dp,i}$ the amount of water stored in deep aquifer on day i. $aq_{dp,j-1}$ the deep aquifer on dayi-1 w_{dep} water percolating from the shallow aquifer into deep aquifer on day i. $w_{pump,dp}$ water removed from the deep aquifer by pumping on day i.

3.8.8 SWAT Model Adaptation in Ethiopia

The model has been evaluated by few researches in different regions of the country. *Zerihun (2011*) used SWAT to estimate watershed's sediment yield to the Tendaho dam. The recommendations of this research emphasized that small sub-basins should be adjusted separately within the system to capture the processes effectively on a small scale. *Tensay (2011*) used SWAT model to predict the sediment yield to Ribb dam reservoir. His assessment indicates that the observed values show good agreement with simulated value for both flow and sediment. He also recommended that the calibrated model can be used for further analysis of the effect of climate and land use change as well as other different management scenarios on stream flows and soil erosion *Joel et al., (2010; Narsimlu et al, (2015);* and *Meng et al, (2018*). used SWAT model to assess the suitability of SWAT model as sediment yield modelling tool in the Nile river basin, with particular interest in the tropical regions. (*Yacob 2010*) used SWAT model to analyse and quantify the effect of land use change on sediment yield and runoff. Model predictions on monthly basis show a strong relation between water yield and land use change during the calibration and validation periods, as indicated by model performance parameters (Wolka and Zeleke 2016; Betrie et al. 2011; Choto and Fetene 2020).

The results of these studies on SWAT model application suggested that poor catchment representation of important hydrological features might lead to poor performance of the model. However, based on the review, SWAT model seems to perform satisfactorily in the catchments of Nilotic countries and there exist prospect for its wide applications in the region. Despite the basins being characterized by scarce data, the use of SWAT models allows some perception to the hydrological characteristics of the region.

3.8.9 Limitation of SWAT model

The popularity of the SWAT model is largely due to the multi-disciplinary coverage of processes representing the hydrology, soil science, erosion/sediment transport, crop growth, in-stream water quality and the agricultural management, but it has limitation on its low capacity to capture the spatial variability associated with precipitation within a large watershed and it does not simulate detailed event-based flood and sediment routing (F*rancesconi et al, 2016; Narsimlu et al, 2015; Meng et al, 2018*). Since SWAT is a process-based model, it intentionally incorporates simplified representations of most processes so that many parameters can be obtained from readily available geospatial coverage (*Francesconi et al, 2016; Narsimlu et al, 2015; Meng et al, 2018*). Another criticism on SWAT model is that the method of estimating runoff is by means of curve number method that applies universal soil loss equation that considers runoff caused when rainfall intensity rate is higher than infiltration capacity of the soil. In addition, when infiltration is higher than overland flow, the method of changing the algorithm of previous SWAT CN method to water balance method for estimating runoff entails the runoff.

3.9 Previous Studies in the Study Area

The Omo-Gibe River Basin Development Master Plan Study was carried out under the support of the government of Ethiopia between 1993 and 1996 with external assistance provided by the African Development Bank (*Stevenson 2018; Asefa 2011; Taye et al., 2018; Mereta et al., 2019; Dagnachew et al., 2020; Deribew et al., 2020*). The aim of the study was to prepare a master plan for the Omo-Gibe Basin that makes optimum use, both at a regional and national level, with the minimum possible adverse environmental impact (*Chaemiso et al., 2016; Estifanos 2014*). The research analysed basin surface water resource using a model of rainfall-runoff, preliminary hydropower, and large irrigation sites of the scheme. Under the guidance of the Ethiopian Electric Power Corporation and the research report (*Avery and Eng 2012; Merrick 2018; Adem et al., 2016*),

the hydrological analysis of the movement of sedimentation over the Gibe III Basin and the the sediment deposit distribution within the reservoir were estimated.

3.10 Runoff and Sedimentation

There are a variety of terms and phrases used to describe sediments such as mud, dirt, and sludge (*Owens 2008; IKHSAN 2010*) that are often used by the public or non-scientific community when referring to sediments. Mud is also a term used for organic and inorganic fine-grained material, which means clay and silt-sized material as opposed to coarse-grained sediment. Problems and issues of sediment management arise, that is, lack of understanding and consensus on what sediment is (*Morris and Fan, 1998*). Sediment yield (*Ran et al., 2013*) is the amount of sediment exported over a time by a river basin, which is also the amount that will enter a reservoir at the downstream limit of its tributary watershed. It is also the volume of eroded sediment at any given point drained by a stream (*Yang et al., 2014*).

The yield of the sediments is always lower than and often much lower than that of erosion within the same watershed (*Morris & Fan 1998*). Surface run off and reservoir sedimentation is a severe off-site consequence of soil erosion with significant environmental and economic consequences. However, on the other hand, runoff and reservoir sedimentation also provide valuable information in a drainage basin about erosion problems and sediment transport. Water erosion of the soil and man-made environmental changes (*Hooke 2006*) are one of the most important problems of land degradation. Long-term runoff and sediment yield estimates have been used for many decades to size the storage pool of sediments and to estimate the reservoir life. Thus, reservoirs accumulated sediments higher than originally planned. Most sediments are exported from catchments during a relatively short flood discharge period, and long-term sediment yield trends over decades may also have an impact on reservoir sediment management (*Ahmed et al., 2009*). Estimates of erosion and transport of sediments in major rivers reflects the difficulty of obtaining reliable sediment concentration and dumping values due to human activities such as deforestation, poor agricultural practices, road construction, and so on (*FAO 1998*). Many types of sediment-related problems can occur upstream as well as downstream of dams, and sediment interference (*Chandra et al, 2014*) may also interfere with the beneficial use of diverted water. Converting sedimentation reservoirs into sustainable resources that generate long-term benefits requires fundamental changes in the design and operation of reservoirs. This involves replacing the idea of a reservoir existence restricted by sedimentation with a concept of controlling both water and sediment in order to maintain reservoir function.

3.10.1 Runoff and Sediment Management Practice

Planning for soil and water conservation requires knowledge of the relationship between factors causing loss of soil, water, and those helping to reduce such losses. Soil and water conservation is a major part of watershed management intervention, which involves the creation of resource management and utilization systems for soil, water, and land use. Both conservation practices influence soil erosion rate, and are useful parameters to be considered in the modelling of runoff and erosion (*Chandra et al., 2014*). Sediment management strategies are the same for large reservoirs and small reservoirs, and sediment management practices for those two reservoir categories are often as different as their magnitudes.

In upstream watershed measures such as structural steps, land use land cover adjustments measures and tillage practices are generally taken to reduce the sediment load entering the reservoir / dam. Terraced fields, flood prevention and drainage works, gully head protection works, river protection works, check dams, and silt trapping dams are best management strategies (*Higaki et al., 205*). Vegetative measures include growing soil and water conservation forests, Filter striping, closing off hillsides, and reforestation (*Abbasi et al., 2019*). Contour farming, ridge and furrow cultivation, pit planting, grain and grass rotation, deep ploughing, intercropping and inter-planting, and no tillage farming (*Ranzi et al., 2012; Refsgaard & Knudsen, 1996*). For different watershed sizes, the effectiveness of soil conservation measures in reducing the sediment inflow to a reservoir varies. In the short term, soil conservation can hardly be effective for a large basin with poor natural conditions.

3.10.2 Sediment rating curve preparation

Data requirement for sediment is widely issued for assessing long-term sediment yield of the catchment (*Miller, 1951; Adib, & Tagavifar, 2010; Tabatabaei, & Salehpour 2017*), to know sediment capacity of the basin and to identify and undertake management scenario changes to minimize further reservoir sedimentation. Lack of available sediment data is experienced in the country as a whole and it is quite difficult to assess the watershed modelling with the scarce data. An option to solve this kind of scarcity is by generation of sediment rating curve (*Tabatabaei, and Salehpour 2017*), (developing exponential relationship between river discharge and sediment concentration for the existing data). However, such rating curves might increase uncertainty, which is not as equal as the real observed values. A supplementary analysis is carried out in this paragraph aimed to define the suspended sediment rating curve at the Gibe III dam section, that is the relationship $Q_s = aQ_w{}^n$ where Q_s is the suspended sediment transport in tons/day, Q_w is the

discharge in m^3/s, a and n are the coefficients of the correlation. This relationship will permit the calculation of the sediment load at a given flow rate and therefore it may represent a powerful tool to predict the suspended sediment transport in the Omo River especially if combined with the hydrometrical campaign currently in progress (*Tabatabaei, & Salehpour 2017*). Since no direct measurement exists at the dam site, a classical statistical procedure has been applied to the sediment data of the upstream gauged stations in order to assess the proper correspondence between liquid and solid flow. Data of the five main monitored catchments (Abelti, Wabe, Walga, Asendabo, and Shebe) within the Gibe III Catchment have been considered and specifically only official gauges of the 94 Omo Gibe basin Master plan (OGMP) sampling programme have been adopted. Suspended load and discharge have been both normalized by the median of the record and consequently all data have been homogenized and joined in a larger sample.

3.11 Water Management Scenarios

3.11.1 SWAT model based Best Management Practice (BMPs) Scenario

Scenarios will have to be built to investigate the impact on surface runoff and sediment loading in order to manage the various farming activities in the Omo Gibe basin taking into account segregated sub-basin using SWAT tools. The region is also witnessing population pressure and urbanization. The modelling incorporates alternative scenarios for possible outcomes for analysing possible future events (*Fazeli 2018; Mereta et al., 2019; Dagnachew et al., 2020; Deribew et al., 2020)*. The analysis is designed to encourage rational decision-making and evaluation by focusing more clearly on possible outcomes and their consequences (*de Vente et al., 2016*). Developing water resource planning and management strategies and assessing the impacts of potential environmental changes are often guided by an analysis of multiple possible future water management scenarios (*Chekol, 2006; Li et al., 2013*). For this purpose, the following catchment management scenarios were developed and in order to use the model as a tool for evaluating the effects of various management measures for runoff and sediment transport in the study area. This scenario involves the introduction of Best Management Practices (BMPs) (*Betrie et al., 2011*) and the parameters for these scenarios were incorporated in the management input data. Some of them are:

a) In Scenario 1, when the watershed existing conditions is considered.
b) In Scenario 2, If different filter strip widths have been imposed on all agricultural HRUs that are a combination of LULC, all soil types and slope groups since the filter strip has the function of filtering the runoff and trapping the sediment in a given plot (*Bracmort et al., 2006*). Therefore, this research used 5 m long filter strip for the analysis.

c) In Scenario 3, when parallel terraces with different slope length and stone bunds were placed on HRUs that are the combination of land use, all soil types, and slope classes. Thus for this study, 75% reduction of slope length was incorporated.

d) In Scenario 4, Reforestation. (*López-Ballesteros et al., 2019; Wu et al., 2021*). The actual land use database, a digital map of land use defined as the baseline land use (*Pandey et al., 2021*). The scenarios were used to evaluate the effect of reforestation on stream flow Omo Gibe Basin increase in population and the resulting need for farming, opening up the vegetation for various uses, and other infrastructure need accelerated land degradation. Since accelerated soil erosion is caused by the activities of man and is responsible for depleting soil productivity, destroying land and filling reservoirs with sediment, there is an intervention to implement the watershed management plan to protect the catchment water development. The reforestation has a function to reduce overland flow and rainfall erosivity (*Pandey et al., 2021*). The reforestation effect was simulated by introducing land use change, not by parameters changes.

4.12 Conclusion

The availability of published literature in the region is one of the major challenges in terms of climate change and land use land cover in Omo Gibe River Basin. This demonstrates that, Omo Gibe basin, very little work has been done to measure or estimate in detail the effects of climate variability or extremes at various levels. The lack of many literatures indicated that in the past and present on climate and climate change related problems in the basin had made the complex. Furthermore, based on the studied literatures for the entire country, they predicted that the maximum and minimum temperatures in Ethiopia will continue to rise, as well as a modest shift (increasing sign) in precipitation, but no one of them put any clear justification regarding to precipitation change, land use land cover dynamics and best managements practices scenario in the base for current and future case. As a result, this study will have a great input in filling of this missed gap in the area of climate change, land use land cover dynamics and water resource managements practice study in Omo Gibe Basin.

Chapter 4 Hydro-Climatological Data Analysis

4.1 Introduction to Analysis of Hydrological Time Series

According to the theories discussed below, there are two basic data sets (spatial and temporal) required for modelling and analysing the hydrological and climatic time series, which satisfy the hypotheses of homogeneity, randomness, non- periodic, and stationary (*Machiwal and Jha 2012*). As a result, for all water resources studies involving the use of data from hydrological time series, preliminary statistical analyses must be performed to validate whether the hydrological time series has all the required assumptions / characteristics (*Dahamsheh & Aksoy 2007*). Many analyses of the time series are performed using standard methods though. The method used in this research for testing independence and stationarity is the Wald-Wolfowitz (W-W) test (*Pohlert 2016*). The test for checking the homogeneity and stationarity used is Mann-Whitney (M-W) test (two sample of p and q, $p \leq q$) (*Hamed & Rao 1999*). The tests for trend analyses used are Mann-Kendall (non – parametric) and Spearman's Rho (non – parametric) (*Yue et al., 2002*). The Linear Regression (parametric) test procedures are checking the homogeneity, stationarity, and outliers (*Hamed & Rao 1999*). Hydrological data analysis is critical for testing the quality and consistency of the results. The objective of this study is to assess the possible effects of hydro-climatological time-series and analysis of hydrological events.

4.2 Statistical Methodology of the study

4.2.1 Filling Missing Data

Before using a runoff record of a station, it is necessary first to check the data for continuity. The integrity of a record may be disrupted with missing data due to numerous reasons such as: observer absence, and instrument malfunction or failure (Zakaria and Noor 2018; *Ibbitt, and Henderson 1998*). The missing data (*Kotsiantis et al 2016; Anjomshoa aand Salmanzadeh, 2019*) can be calculated using adjacent station data. There are various methods of filling missing data such as method of arithmetic average, method of normal ratio or other methods of approximation. All of the above approaches, however, require more than one local station and records at the same time. The missing data can be extrapolated /interpolated using the local or regional relationships between the dependant and the independent runoff (*Kotsiantis et al., 2016; Anjomshoaa & Salmanzadeh, 2019*).

4.2.1.1 Linear Regression

A suitable way adopted for this project is to fit a linear regression line between dependent and independent runoff (equation 4.1 and Figure 4.2). The linear regression is of good correlation, if the

correlation coefficients are in the range 0.6 < r < 1.0 (*Schober et al., 2018; Chok, 2010*). The correlation coefficient signifies the understanding of two variables, and how well the value of one can be used to predict the value of the other. The correlation coefficient r ranges between -1 and +1. A positive indicates that the variable allows perfect prediction of the other. A negative r values indicates that variable increases the other variable decreases and correlation coefficient of 0 indicates no relationship between the two variables. Abelti station is dependent in Assandabo because it is located upstream of the catchment, while Gojeb station is independent because it is located downstream of the catchment. (Figure 4.1) indicate that both gojeb and assandabo gauge station good correlation with Abelti gauge station

$$Y = aX + b \qquad (4.1)$$

$$a = \left(\frac{\sum_{i=1}^{N} XY - \sum_{i=1}^{N} X \times \sum_{i=1}^{N} Y}{\sum_{i=1}^{N} X^2 - (\sum_{i=1}^{N} Y)^2}\right)$$

$$b = \frac{\sum_{i=1}^{N} Y \sum_{i=1}^{N} Y^2 - \sum_{i=1}^{N} X \sum_{i=1}^{N} Y}{\sum_{i=1}^{N} X^2 - (\sum_{i=1}^{N} X)^2}$$

$$r = \frac{N \sum_{i=1}^{N} XY - \sum_{i=1}^{N} X \sum_{i=1}^{N} Y}{\sqrt{(N \sum_{i=1}^{N} X^2 - (\sum_{i=1}^{N} X)^2)\left(N \sum_{i=1}^{N} Y^2 - (\sum_{i=1}^{N} Y)^2\right)}}$$

where, a & b are constant, Y = dependent average runoff, X = independent average runoff, r = correlation coefficient. Using the above procedure, the regression coefficient between mean annual runoff and rainfall at station Ascendabo is found to be greater than 0.6 (Figure 4.1). Hence, the linear correlation between runoff in neighbor gauged catchment station is used to fill the missing data.

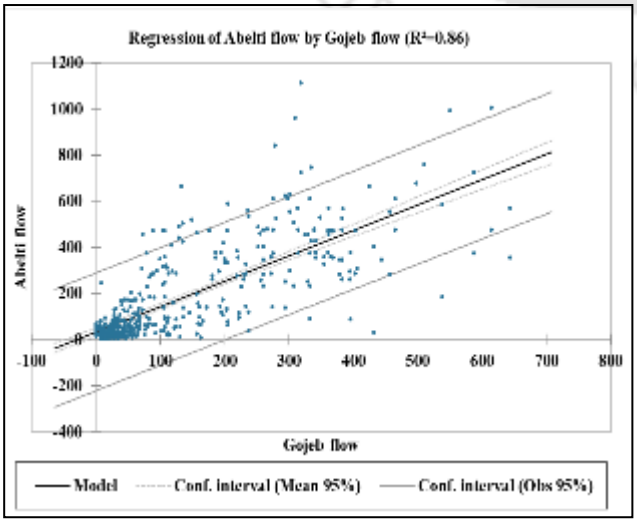

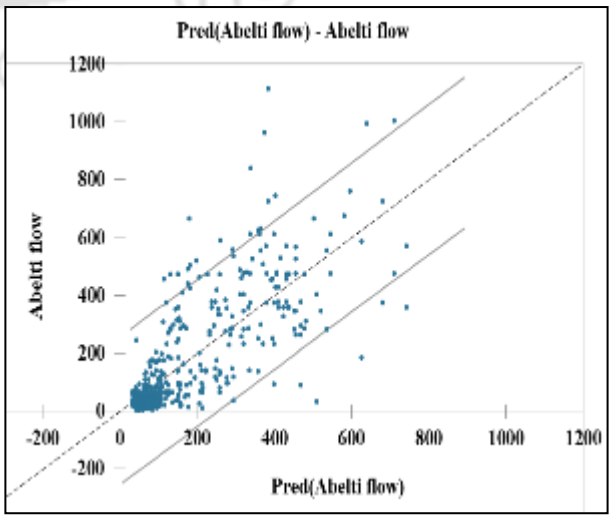

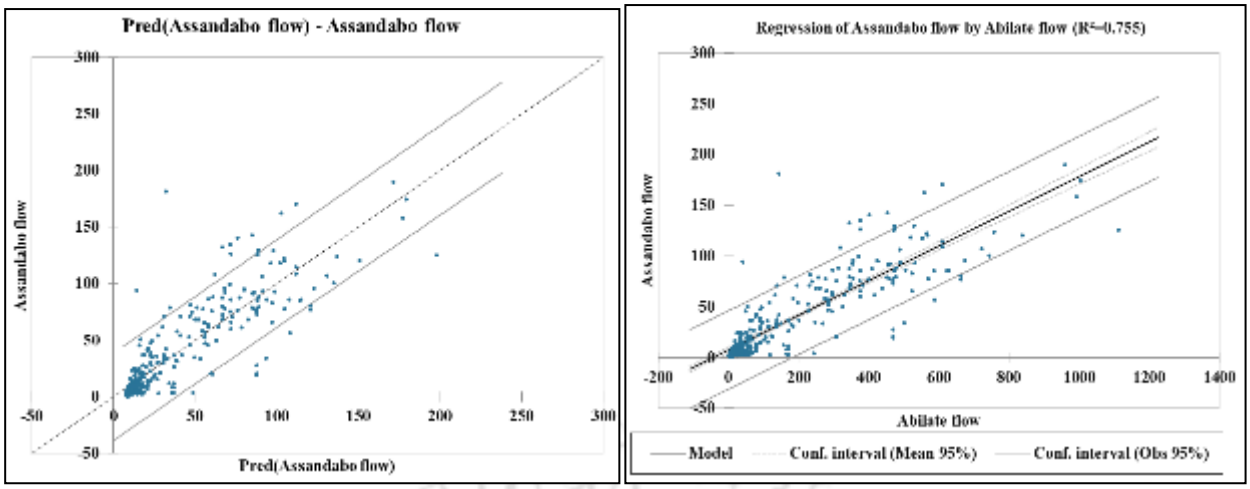

Figure 4. 1 Linear regression analysis.

A non-linear method of correlating a station's long -term runoff data to an adjacent known base station is by using Dicken's and Ryve's (*Chandramohan et al 2018; Jena and Nath, 2020*) formula (Equations 4.2).

$$Q_{sim} = Q_{obs}\left(\frac{A_X}{A_Y}\right)^{0.67} \qquad (4.2)$$

where Q_{sim} and Q_{obs} are discharge in m^3/sec of regressed and the station, A_x and A_y are the corresponding catchment areas in sq.km.

4.2.1.2 Extension of Flow Record

In many cases, a stream gauge in one site may have short period records (Y_i, i = 1, 2, 3…, n) and another gauging station may have long records (X_i, i =1, 2, 3, 4,...N). As per the statement, n <N and that records for both stations exists for the period i= 1, 2, 3… The correlation between X and Y may be explored to estimate the Y records, by estimating a set of N-n flows for the period during which there was an X record, but no Y record (Moog et al., 1999). The obvious approach to this problem is to use regression to estimate Y as the function of X. However, it is not the particular value of Y_i that is important, but the full collection of estimates of Y, which means a set of Y values those possess the correct statistical properties of Y. The simplest version MOVE 1, presents the variance and mean of Y using the (equation 4.3):

$$Y_i = a + bX_i \qquad (4.3)$$

where,

$$b = \sqrt{S_{yy}/S_{xx}} \times \mathrm{Sign}(r)$$

$$a = \bar{Y} - b\bar{X}$$

$$S_{xx} = \sum_{i=1}^{n} (X - \bar{X})^2$$

$$S_{yy} = \sum_{i=1}^{n} (Y - \bar{Y})^2$$

and Sign (r) = the sign of correlation coefficient , S_{xx} and S_{yy} the sample of covirance and $\bar{X}$ is the mean ot the sample. By using this method for this particular study, the flow recorded at different station has been observed for only for short years, but the other flow records at different station has been recorded for long time. Thus, the method of MOVE-1 technique (Moog et al., 1999) is to extend the short years recorded station data to long years of flow record using the known station data.

4.2.1.3 Thomas –Fiering Model

The model is used to produce dynamically the monthly and weekly or 10 daily volume of the discharge from a serially based sequence the Markov Model's extension (Harms and Campbell 1967; *West and Harrison 2006*) with the implies the monthly or regular variable depends only on the current one or two variable involving non-stationary mean and variance using equation 4.4.

$$Q_{j+1} = Q_{avj+1} + b_{j,i+1}(Q_i - Q_{av}) + Z_i S_{j+1}\sqrt{1 - R^2_{j,i+1}} \qquad (4.4)$$

where Q_{j+1} , Q_j are the discharge volume during $(j+1)^{th}$ and j^{th} month; $Q_{avj+1}$and Q_{avj} the mean monthly discharge volume for $(j+1)^{th}$ and j^{th} Months ; S_{j+1} and S_j stander deviation for $(j+1)^{th}$ and j^{th} Months; $R^2_{j,i+1}$ the correlation coefficient between the months j and (j+1); Z_j the random independentvariate with zero mean and unit variance ; $b_{j,i+1} = R^2_{j,i+1}\left(\frac{S_{j+1}}{S_j}\right)$.

4.2.2 Checking Homogeneity and Consistency of the Stations

4.2.2.1 Checking Homogeneity

Homogeneity or consistency implies that all the collected hydrologic time series data belong to the same statistical population having a time invariant mean (Feng and Qian, 2004; Agha et al 2017). So, the tests to check the homogeneity or consistency of data series are based on evaluating the significance of changes in the mean value. By checking consistency and homogeneity of individual stations, the data qualities regarding possible temporal and spatial variations or errors are investigated. Rainfall stations within each sub-basin is non-dimensionalised and plotted to compare the homogeneous stations (Feng and Qian, 2004; Agha et al 2017) within the watershed. This

procedure helps in filling missed values in the stations. The results of the homogeneity (non-dimensional) form data analyses are shown below (Figure 4.2 and equation 4.5). The non-dimensionalising of the month's value was calculated as;

$$P_i = 100\% \times \frac{(\overline{P_i})}{\overline{P}} \qquad (4.5)$$

where, P_i=is non-dimensional value of month rainfall for station i, $\overline{P_i}$ = Over year-averaged monthly rainfall at the station i, $\overline{P}$ = the over year -averaged yearly rainfall of the station.

4.2.2.2 Checking Consistency of the stations

If the conditions relevant to the recording of a rain gauge station have undergone a significant change during the period of record, inconsistency would arise in the rainfall data of that station. This inconsistency would be felt from the time the significant change took place.

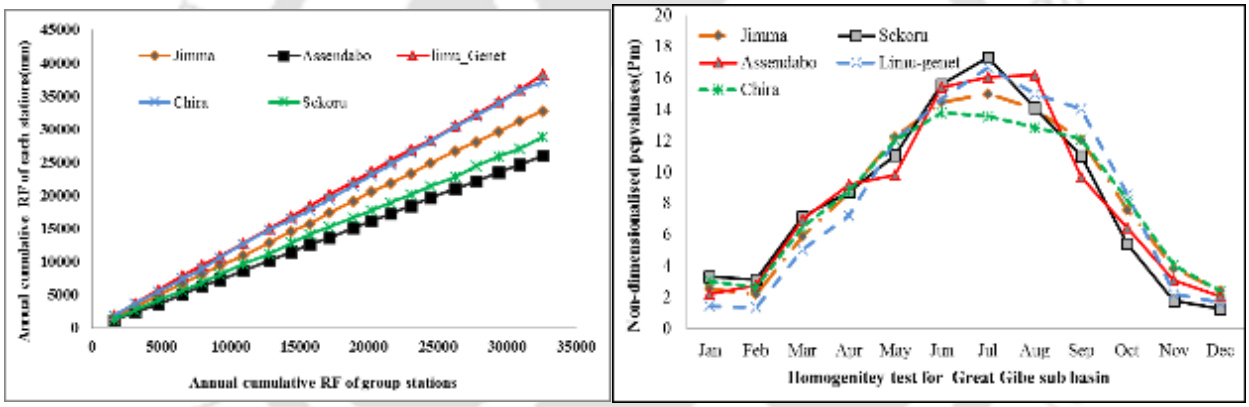

Figure 4. 2 Homogeneity and Consistency test in Upper Gibe catchments

The checking for inconsistency of a record is done by double mass curve technique (*Subramanya, 1998*). The above graphs showed all points set on or from almost the straight lines, which was plotted for checking of consistency of rainfall, all stations were consistent. Therefore, the stations did not need further adjustment.

4.2.3 Trend analysis for hydrologic data

Trend analysis of a time series consists of the magnitude of trend and its statistical significance. In general, the magnitude of trend in a time series is determined either using regression analysis (parametric test) or using Sen's estimator method (non-parametric method) *(Partal and Kahya 2006*). Both these methods assume a linear trend in the time series. Regression analysis is conducted with time as the independent variable and rainfall/temperature as the dependent variable. The

regression analysis can be carried out directly on the time series or on the anomalies (i.e. deviation from mean). A linear equation, Y = mX + B defined by B (the intercept) and trend m (the slope), can be fitted by regression (*Kahya & Kalayci 2004*). The linear trend value represented by the slope of the simple least-square regression line provided the rate of rise/fall in the variable. Sen's estimator has been widely used for determining the magnitude of trend in hydro meteorological time series. In this method, the slopes (T_i) of all data pairs are first calculated by equation 4.6.

$$T_i = \frac{X_j - X_k}{j-k} \qquad \text{for i=1, 2, 3....N} \qquad (4.6)$$

where X_j and X_k are data values at time j and k, where j > k always. The median of these N values of T_i is Sen's estimator of slope, which is calculated as

$$\beta = \begin{cases} T_{\frac{N+1}{2}} & \text{for odd N} \\ \frac{1}{2}\left(T_{\frac{N}{2}} + T_{\frac{N+2}{2}}\right) & \text{for even N} \end{cases} \qquad (4.7)$$

A positive value of β indicates an upward (increasing) trend and a negative value indicates a downward (decreasing) trend in the time series.

4.2.3.1 Significance of trend

Non-parametric Mann-Kendall (MK) test is used to assess the existence of statistically significant changes in hydrological climate variables, such as temperature and precipitation with respect to climate change (*Yue et al., 2002*). The MK test tests the null no-trend hypothesis against the alternative hypothesis of increasing or decreasing trend existence. The statistics (S) is defined as in equation 4.8

$$S = \sum_{i=1}^{N-1} \sum_{j=i+1}^{N} \mathrm{Sgn}(Xj - Xi) \qquad (4.8)$$

where N is the number of data points or the length of the sample, X_j and X_i are from k=1, 2, …, n-1 and j= k+1, …, Which is the number of positive differences minus the number of negative differences. If S is a positive number, observations obtained later in time tend to be larger than observations made earlier. If S is a negative number, then observations made later in time tend to be smaller than observations made earlier. Assuming (Xj – Xi) = θ, the value of sgn (θ) is computed as follows:

$$\mathrm{Sgn}\,(\theta) = \begin{cases} +1 & \text{if } \theta > 0 \\ 0 & \text{if } \theta = 0 \\ -1 & \text{if } \theta < 0 \end{cases} \qquad (4.9)$$

This statistics represents the number of positive differences minus the number of negative differences for all the differences considered. For large samples (N > 10), the test is conducted using a normal distribution, with the mean and the variance as follows:

$$E[S] = 0 = \text{Mean},$$

$$\text{Var}(s) = \frac{N(N-1)(2N+5) - \sum_{k-1}^{n} tk(tk-1)(2tk-5)}{18} \qquad (4.10)$$

where n is the number of tied (zero difference between compared values) groups and tk the number of data points in the k^{th} tied group. The standard normal deviate (Z-statistics) is then computed as:

$$Z_{MK} = \begin{cases} \frac{S-1}{\sqrt{\text{var}(s)}} & S > 0 \\ 0 & S = 0 \\ \frac{S+1}{\sqrt{\text{var}(S)}} & S < 0 \end{cases} \qquad (4.11)$$

A positive (negative) value of Z_{MK} indicates that the data tend to increase (decrease) with time. If the computed value of $|Z_{MK}| > z\alpha/2$, the null hypothesis (H_0) is rejected at α level of significance in a two-sided test. In this analysis, the null hypothesis was tested at 95% confidence level and Z_{MK} is accepted. Trends test of flow in upper Gibe Basin Using Mann-Kendall from 1985-2008.

Table 4. 1 Statistical analysis of flow for upper Omo-Gibe basin selected station.

Variable	Observations	Minimum	Maximum	Mean	Std. deviation
Gojeb_flow	50	110.016	255.008	153.29	36.94
Assandabo_flow	50	22.26	62.7596	39.59	10.65
Abelti_flow	50	88.189	372.95	200.72	76.61
Megecha_flow	50	15.319	45.275	27.035	7.0004

Table 4. 2 Mann-Kendall trend test for mean monthly flow of upper Omo-Gibe basin

	Gojeb_flow	Assandabo_flow	Abelti_flow	Megecha_flow
Kendall's tau	0.468037	0.106514	0.534618	0.043372
S	571	130	649	53
Var(S)	14281.6	14282.6	14266.3	14285.6
p-value	< 0.0001	0.28	< 0.0001	0.66
alpha	0.05	0.05	0.05	0.05

The Mann-Kendall trend test results for mean monthly flow indicates that a positive trend for the given data of stream flow with significant level at α = 0.05, or 95% confidence level because S value is greater than zero (S > 0) and p value is less than α (i.e., α = 0.05, p < α = 0.096 < 1.96 indicated in (table 4.2 and Figure 4.4). Therefore, the P-value is less than (or equal to) α, reject the null hypothesis we can chose the alternative hypothesis and the P-value is greater than α, do not reject the null hypothesis. This means that, the result of the mean monthly flow of the Mann-Kendall trend test analysis has revealed that the extreme values of flow have an increasing trend with a statistical significance. If the null hypothesis H_o is true, then S is approximately normally distributed with, $\mu = 0, \delta = \left(n\frac{(n-1)(2n+5)}{18}\right)$ $and\ Z = |Sx| / (\delta)^{0.5}$ /. The other Gojeb, Asandabo, and Megecha River stream flow time's series are defined in Appendix 3.

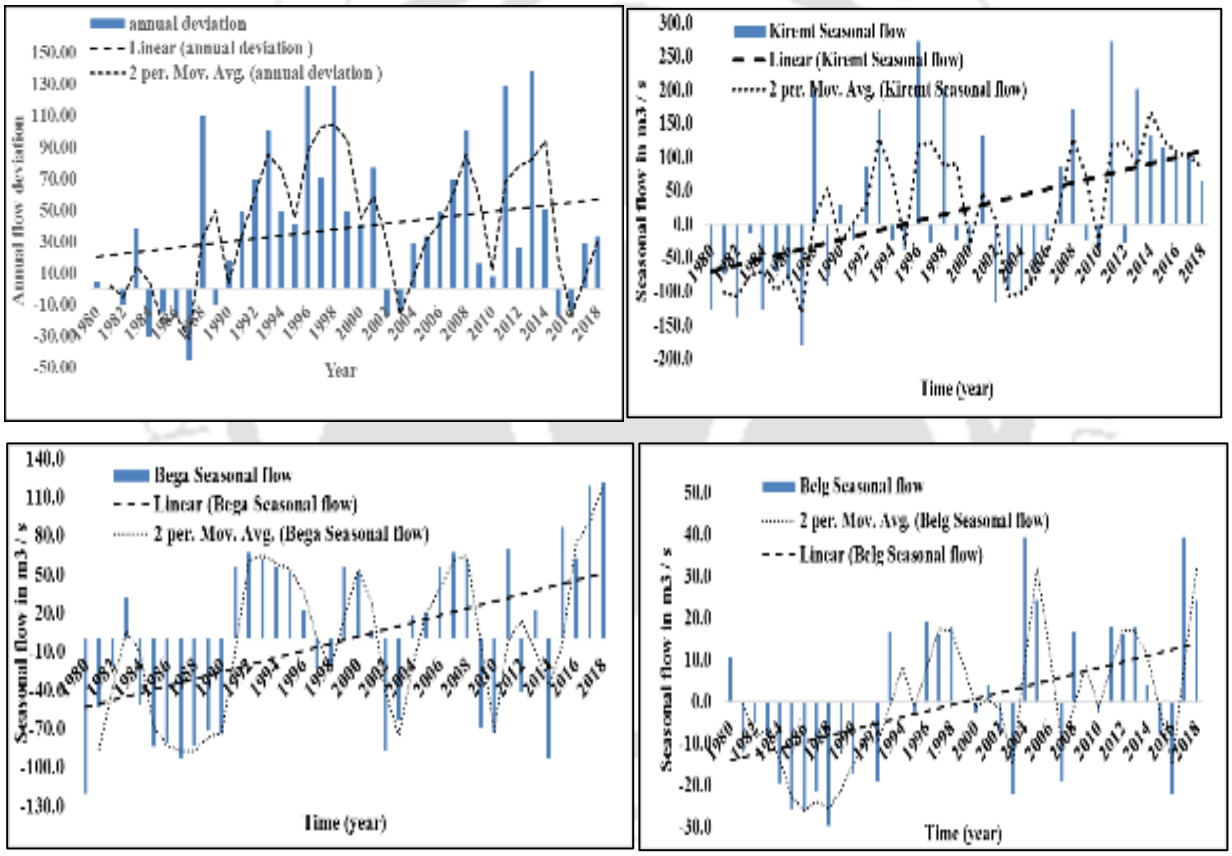

Figure 4.3 Trend of mean monthly flow of upper Omo-Gibe sub basin of selected stations Abelti

4.2.3.2 Spearman's Rho (Non parametric)

Two variables, where the value r = 1 means a perfect positive correlation and the value r = -1 means a perfect negative correlation. Spearman's Rho is a non-parametric test used to measure the strength of association between the two variable statistically significant. This is a rank based test that determines whether the correlation between two variables is significant.

$$\rho_s = \frac{S_{xy}}{(S_x S_{xy})^{0.5}} \qquad (4.12)$$

where, ρ_s = Spearman's rank correlation coefficient, $S_x = \sum(X_{obs} - \bar{X})^2$, $S_y = \sum(Y_{obs} - \bar{Y})^2$, and $S_{xy} = \sum(X_{obs} - \bar{X})(Y_{obs} - \bar{Y})$. By using Spearman's Rho (Non parametric) methods Abelti gauge station flow had been accepted because the value of R is 1 and the two tailed value of p is 0. By normal standards, the association between the two variables would be considered statistically significant with mean of 0 and variance 1.

4.2.4 Hydrological event analysis using Probability Distributions

Frequency analysis is the hydrological term used to describe the likelihood of a hydrological event such as rainfall, flooding, and drought occurrence (*Favre et al 2004; Field et al., 2014*). Evaluation of these extreme rainfall events is critical for hydrological risk analysis and water-related infrastructure design (*Biniyam and Kemal 2017*). Distribution of probability functions and statistical measurement of location, measurement of distribution, and measurement of skewness is important. Analysis of the frequency usually requires hydrological data recorded. Hydrological data either are recorded as a continuous record (water level or point, rainfall) or in a discrete series (mean daily / monthly / annual flow or rainfall, annual series, part series, etc.).

Probability distribution is a function representing the probability of occurrence of a random variable (*Chow 2010*). Some of the frequently used density functions in hydrological analysis are: Normal Distribution, Log-normal, Weibull, Gamma, Gumbel, Exponential, and Pareto. There are a lot of methods for estimating probability distributions like: Weibull, Hazen, and Californian (*Ewemoje ,& Ewemooje, 2011; Kang, & Ko,2018*). The Simulation & Probabilistic Analysis (SPA) Software Development Kit (SDK) supports over 50 continuous and discrete probability distributions. The SDK supports a number of continuous distributions divided into four categories (distribution types) like: Bounded; Unbounded; Non-negative; and Advanced Distributions. The following advanced distributions are robust and famous: Generalized Extreme Value, Generalized Logistic, Generalized Pareto, Log-Pearson3, and Wakeby. The Wakeby distribution is widely used for the modelling of extreme events. Each of the supported generalized distributions combines two or more simpler distributions. The generalized extreme value (GEV) distribution combines the Gumbel, Frechet, and Weibull families (*Ewemoje ,& Ewemooje, 2011; Kang, & Ko,2018*). The probability density function (PDF) is the probability that the variate has the value x:

$$f(x) = P(X = x) \qquad (4.13)$$

The cumulative distribution function (CDF) is the probability that the variate takes on a value less than or equal to x:

$$F(x) = P(X \leq x) \qquad (4.14)$$

Survival Function; the survival function (or reliability function) is the probability that the variate takes on a value greater than x: and is displayed similarly to the CDF.

$$S(x) = P(X > x) = 1 - F(x) \qquad (4.15)$$

The survival function is often used in reliability and related fields to denote the probability a unit survives beyond time (*Ewemoje, and Ewemooje, 2011; Kang, and Ko,2018*). Hazard Function (also known as the failure rate) is the ratio of the probability density function to the survival function. The hazard function is used in reliability applications to describe the instantaneous failure rate at any point in time.

$$h(x) = \frac{f(x)}{s(x)} = \frac{f(x)}{1-F(x)} \qquad (4.16)$$

4.2.4.1 Quantile-Quantile Plot

Quantile-Quantile (Q-Q) Plot *(Almeida et al., 2018; Yue and Jin-yang ,2021; Easton and McCulloch, 1990; Korkmaz, et al., 2014*) is a graph of the input (observed) data values plotted against the theoretical (fitted) distribution quantiles. Both axes of this graph are in units of the input data set. The quantile-quantile graphs are produced by plotting the observed data values x_i (i = 1... n) in the X-axis, and the following values in the Y-axis:

$$F^{-1}(F_n(x_i) - \frac{0.5}{n}) \qquad (4.17)$$

where: $F^{-1}(x)$ inverse cumulative distribution function (ICDF); Fn (x) empirical CDF; n-sample size. The Q-Q plot will be approximately linear if the specified theoretical distribution is the correct mode. (*Ewemoje ,& Ewemooje, 2011; Kang, & Ko,2018*)

4.2.4.2 Generalized Logistic distribution

Generalized Logistic distribution have three parameters that are continuous (shape (κ), scale (δ) and location (μ)) parameter and the scale parameter is greater than zero. The domain generalized Logistic Value $1 + \kappa\frac{X-\mu}{\delta} > 0$ for shape parameter is different from zero and the value of X is less than from positive infinitive and greater than negative for shape parameter is equal to zero *(Kang, & Ko, 2018)*. The probability density function (PDF) is

$$f(x) = \frac{(1+kz)^{-1-1/k}}{\sigma(1+(1+kz)^{-1/k})^2} \text{ for } k \neq 0 \qquad (4.18)$$

$$f(x) = \frac{\exp(-z)}{\delta(1+\exp(-z))^2} \text{ for } k = 0 \qquad (4.19)$$

Cumulative Distribution function (CDF) is

$$F(x) = \frac{1}{1+(1+kz)^{-\frac{1}{k}}} \text{ for } k \neq 0 \qquad (4.20)$$

$$F(x) = \frac{1}{1+\exp(-z)} \text{ for } k = 0 \qquad (4.21)$$

where, $Z = \frac{x-\mu}{\delta}$

4.2.4.3 Log-Pearson Type 3 Distribution

Log-Pearson Type 3 Distribution have three parameters α (α>0), β (β ≠ 0 and Y, which is a continuous parameter with in the domain $0 < x \leq e^y$ for $\beta < 0$ and $e^y \leq +\infty$ for $\beta > 0$.

The probability density function (PDF) is

$$f(x) = \frac{1}{x|\beta|\Gamma(\alpha)}\left(\frac{\ln(x)-\gamma}{\beta}\right)^{\alpha-1} \exp\left(-\frac{\ln(x)-\gamma}{\beta}\right) \qquad (4.22)$$

Cumulative Distribution function (CDF) is

$$F(x) = \frac{\Gamma(\ln(x)-\gamma)/\beta^{(\alpha)}}{\Gamma(\alpha)} \qquad (4.23)$$

4.2.4.4 Generalized Pareto Distribution

In Generalized Pareto Distribution there are a continuous (shape (κ), scale (δ) and location (μ)) parameter and the scale parameter is less than zero with a domain $\alpha \leq x < +\infty$ for $\kappa \geq 0$, and $\mu \leq x <\leq \mu - \frac{\delta}{\kappa}$ for $\kappa < 0$.

The probability density function (PDF) is

$$f(x) = \frac{1}{\delta}\left(1 + \frac{\kappa(x-\mu)}{\delta}\right)^{-1-\frac{1}{k}} \text{ for } k \neq 0 \qquad (4.24)$$

$$f(x) = \frac{1}{\delta}\exp\left(-\frac{x-\mu}{\delta}\right) \text{ for } k = 0 \qquad (4.25)$$

Cumulative Distribution function (CDF) is

$$F(x) = 1 - \left(1 + k\frac{(x-\mu)}{\delta}\right)^{-\frac{1}{k}} \text{ for } k \neq 0 \qquad (4.26)$$

$$F(x) = 1 - \exp\left(-\frac{x-\mu}{\delta}\right) \text{ for } k = 0 \qquad (4.27)$$

4.2.4.5 Wakeby Distribution

The Wakeby distribution is defined by quantile function with all continuous parameters α, β, γ, δ, ζ the following conditions are imposed. $\alpha \neq 0$ or $\gamma \neq 0, \beta + \delta >$ or $\beta = \gamma = \delta = 0$, if $\alpha = 0$, then $\beta = 0$, if $\gamma = 0$ then $\delta = 0, \gamma \geq 0$ and $\alpha + \gamma \geq 0$ With the domain of $\zeta \leq x < \infty$ if $\delta \geq 0$ and $\gamma > 0$, or $\zeta \leq x \leq \zeta + \frac{\delta}{\beta} - \frac{\gamma}{\delta}$ if $\delta < 0$ or $\gamma = 0$. Therefore, the Wakeby distribution (*Ewemoje, & Ewemooje, 2017*) is defined by quantile function.

$$x(F) = \zeta + \frac{\alpha}{\beta}\left(1 - (1 - F)^{\beta}\right) - \frac{\gamma}{\delta}(1 - (1 - F)^{-\delta} \qquad (4.28)$$

4.2.4.6 Extreme-Value Type I Distribution (Gumbel's Method)

Gumbel's Extreme Value Distribution is a model developed for predication of hydrological events such as flood peaks maximum rainfall maximum wind speed, etc. Extreme-Value Type I Distribution has continuous two parameters scale (δ) and location (μ)) parameter. The probability density function (pdf) and cumulative distribution function (cdf) (*Gumbel 1954; Kundzewicz et al., 2014*) are formulated for random variable X as follows.

The probability density function (PDF), is

$$f(x) = \frac{1}{\beta}\exp[-(z + \exp(-z))] \qquad (4.29)$$

where $Z = \frac{x - \mu}{\delta}; -\infty < x < \infty$

Cumulative Distribution Function (CDF) is

$$F(x) = \exp\left[-\exp\left(-\frac{x-\mu}{\delta}\right)\right] \qquad (4.30)$$

where μ location parameter and δ scale parameter with a range $-\infty<x<\infty$.

Extreme-Value Type I Distribution (*Kotz, & Nadarajah, 2000*) is also commonly known as Gumbel's distribution. It is one of the most widely used probability distribution functions for extreme values in hydrologic and meteorological studies for prediction of flood peaks, maximum rainfalls, and maximum wind speed (*Ewemoje, & Ewemooje, 2017*).

This extreme value theory of Gumbel is mostly applicable to annual extremes. In the Gumbel method the data are ranked in ascending order and it makes use of the probability of non-exceedance the probability that the annual maximum flow is less than a certain magnitude and with the return period. Therefore, the annual data series of extreme events such as floods and maximum rainfall depths are selected for this study

4.2.5 Parameter estimation

A number of methods can be used for parameter estimation. These include the maximum likelihood method (MLM), method of moments (MOM), method of regression (MR), and probability weight method (PWM) (*Shabri & Jemain 2013; Izinyon & Ehiorobo 2014*). The above four methods are considered here in the study. The method of moments is employed for those distributions whose moment estimates are available for all possible parameter values, and do not involve the use of iterative numerical methods. The MOM is a natural and relatively easy parameter estimation method (*Behr & Tente 2008; Spinoni et al., 2015*). MLM estimates are usually inferior in quality and generally are not as efficient as MR estimates, especially for distribution with large number of parameter (three or more) because higher order moments are more likely to be highly biased in relatively small samples.

However, according to *(Duhachek et al., 2000; Rukhin et al., 2000; Moore et al., 2008)* the maximum likelihood method (MLM) is considered the most efficient method since it provides the smallest sampling variance of the estimated parameters, and hence of the estimated quantiles compared to the other methods. For some particular cases such as Pearson type III distribution, the optimality of the ML method is only asymptotic and small sample estimates may lead to estimates of inferior quality *(Moore et al., 1991*).

The PWM method (*Shabri & Jemain 2013; Green wood et al., 1979; Hosking 1986a*) gives parameter estimates that are comparable to ML estimates. In some cases, the estimation procedures are much less complicated and the computations are simpler.

4.2.6 Quintile Estimation

If distribution parameters are determined, quintile estimates (X_T) may be calculated that correspond to the different return periods (*Ginos 2009*). The relation between return period and the probability of non-exceedance (F) is given by

$$F = 1 - \frac{1}{T} \qquad (4.31)$$

where $F = F(X_T)$ is the probability of having a flood of magnitude X_T or smaller.

The problem thus reduces to evaluate X_T for a given value of F. *Chow et al., (1988)* and *Izinyon and Ehiorobo (2014)* has shown that most frequency-distribution functions applicable in hydrologic studies can be expressed by the following equation known as the general equation of hydrologic frequency analysis: (*Han 2011*).

$$X_T = \mu + K_T\delta \qquad (4.32)$$

where, X_T = value of the variate X of a random hydrologic series with a return period T, μ = mean of the variate, σ = standard deviation of the variate, K_T = frequency factor that depends upon the return period T and the assumed frequency distribution.

4.2.7 Standard Error of Estimate (SEE)

It is clear that a point estimate of a certain quantile corresponding to a return period may be of no real significance unless there is an indication of the accuracy of the estimates (*Cunnane 1989*). A measure of the variability of the estimated value is the (SEE) S_T, which is defined as

$$S_T = \sqrt{E\{\ddot{X}_T - E(\ddot{X}_T)\}^2} \qquad (4.33)$$

The standard error of estimate accounts for the error due to small samples, but not the error due to the choice of inappropriate distribution. The standard error of estimate depends in general on the method of parameter estimation method (MOM, ML, PWM) (*Duhachek et al., 2000*). For example, the parameter estimation by using Method of Moments for Gojeb flow near to Shebe is given in Table-4.3:

Table 4. 3 Parameter estimation by using Method of Moments

Parameter estimation	μ	α	δ	κ	β	γ
Gamma	-	7.1153	-	-	20.24	-
Gamma(3p)	-	45.707	-	-	7.88	-216.4
GEV	122.72	-	52.67	-0.21		
Log-Pearson 3	-	5.29	-	-	-0.19	5.88
Lognormal	4.89	-	0.43	-	-	-
Weibull	2.67	-	-	-	159.35	-
Gen.Pareto	55.80	-	161.49	-0.83	-	-

4.2.8 Goodness of Fit Tests

Goodness of fit tests (GoF) measure a random sample's compatibility with a theoretical distribution of probability function (*Cirrone et al., 2004; Zeng et al., 2015*). These tests show how well the distribution have chosen fits in with the data and used to compare fitted distributions. The following GoF measures are commonly used in analysis: Kolmogorov-Smirnov, Anderson-Darling, and Chi-Square.

4.2.8.1 Kolmogorov-Smirnov Test

The Kolmogorov-Smirnov test (*Neter et al., 1988)* with significance correction (*Dallal & Wilkinson 1986)* is based on the greatest discrepancy between the sample cumulative distribution and the normal cumulative distribution. This test is used to decide if a sample comes from a hypothesized continuous distribution. It is based on the empirical cumulative distribution function (ECDF). The empirical CDF is denoted by

$$\mathrm{Fn}(x) = \frac{1}{n}\,[\text{Number of Observation } \leq x] \qquad (4.34)$$

The Kolmogorov-Smirnov statistic (D) is based on the largest vertical difference between the theoretical and the empirical cumulative distribution function:

$$D = \max_{1 \leq i \leq n} \left(F(xi) - \frac{i-1}{n}, \frac{i}{n} - F(xi) \right) \qquad (4.35)$$

The hypothesis regarding the distributional form is rejected at the chosen significance level (α) if the test statistic, D, is greater than the critical value obtained from a table. The fixed values of α (0.01, 0.05, etc.) are generally used to evaluate the null hypothesis (H_0) at various significance levels. The P-value, in contrast to fixed α values, is calculated based on the test statistic, and denotes the threshold value of the significance level in the sense that the null hypothesis (H_0) will be accepted for all values of α less than the P-value.

4.2.8.2 Chi-Square Test

The Chi-Square test is used to determine if a sample comes from a population with a specific distribution. The Chi-squared goodness-of-fit test is applied to binned data (*Snedecor & Cochran, 1989*) and requires a larger sample size than the other two tests**.** This test is applied to binned data, so the value of the test statistic depends on how the data is binned. Although there is no optimal choice for the number of bins (k), there are several formulas that can be used to calculate this number based on the sample size (N). SDK employs the following empirical formula:

$$K = 1 + \log_2 N \qquad (4.36)$$

The data can be grouped into intervals of equal probability or equal width. The Chi-Square statistic is defined as,

$$\chi 2 = \sum_{i=1}^{k} \frac{(O_i - E_i)^2}{Ei}, \qquad (4.37)$$

where O_i is the observed frequency for bin i, and E_i is the expected frequency for bin i calculated by $E_i = F(X_2) - F(X_1)$, where F is the CDF of the probability distribution being tested, and x_1, x_2 are the limits for bin i. The hypothesis regarding the distributional form is rejected at the chosen significance level (α) if the test statistic is greater than the critical value defined as $\chi 2_{1-\alpha,k-1,}$. Meaning the Chi-Squared inverse CDF with k-1 degrees of freedom and a significance level of (α). Though the number of degrees of freedom can be calculated as k-c-1 (where c is the number of estimated parameters), the SDK calculates it as k-1 since this kind of test is least likely to reject the fit in error *(Bagdonavicius & Nikulin, 2011; Goual, & Seddik-Ameur, 2014*). The P-value, in contrast to fixed α values, is calculated based on the test statistic, and denotes the threshold value of the significance level in the sense that the null hypothesis (H_0) will be accepted for all values of α less than the P-value. The SDK calculates the P-values based on the Chi-Square test statistics (χ^2) for each fitted distribution (*Bagdonavicius & Nikulin, 2011; Goual, & Seddik-Ameur, 2014*).

4.2.8.3 Anderson-Darling Test

The Anderson-Darling procedure is a general test to compare the fit of an observed cumulative distribution function to an expected cumulative distribution function (*Sinclair et al, 1990; Engmann, & Cousineau, 2011*). The Anderson-Darling statistic (A^2) (*Engmann, & Cousineau, 2011)* is defined as:

$$A^2 = -n - \frac{1}{n}\sum_{i=1}^{1}(2i-1)\left[\mathrm{LnF}(X_t) + \mathrm{Ln}\left(1 - \mathrm{F}(X_{n-t+1})\right)\right] \qquad (4.38)$$

where $F(X_t)$ is the assumed (Normal) distribution with the assumed or sample estimated parameters (μ, σ); X(t) is the tth sorted, standardized, sample value; "n" is the sample size; "ln" is the natural logarithm (base e) and subscript "i" runs from 1 to n

The hypothesis regarding the distributional form is rejected at the chosen significance level (α) if the test statistic, A^2, is greater than the critical value obtained from a table. In general, critical values of the Anderson-Darling test statistic depend on the specific distribution being tested. The Anderson-Darling test implemented in the SDK uses the same critical values for all distributions. These values are calculated using the approximation formula, and depend on the sample size only.

4.2.8.4 Goodness of fit by using easy fit for Abelti station flow data

Easy Fit software generates fitted distributions as well as evaluating the level of fit or goodness for certain models at various significance levels.

Table 4. 4 Goodness of fit result

critical Value(α)	0.2	0.1	0.05	0.02	0.01
Kolmogrov-Smirnov	0.18	0.2108	0.24	0.26	0.28
Anderson-Darling	1.37	1.93	2.51	3.28	3.90
Chi-Square	4.64	6.25	7.81	9.84	11.34

Assuming the flow distribution is normal, the Goodness of fit results in the Table 4.4 shows that α value at 80% and 99% of confidence interval should be accepted. The P-value and α based on critical value shows the null hypothesis is rejected or accepted at all predefined significance levels.

4.2.9 Med-Calc tools offers the following tests for Normal distribution

The D'Agostino-Pearson test (*Sheskin et al., 2011*; *Almeida et al., 2018; Yue and Jin-yang ,2021*) computes a single P-value for the combination of the coefficients of Skewness and Kurtosis. Using the histogram it can be evaluated visually whether the data are distributed symmetrically, normally or whether the distribution is asymmetrical or skewed. When the distribution is not Normal, it cannot accurately be described by mean and standard deviation, but instead the median, mode, quartiles, and percentiles have to be used (*Yue and Jin-yang ,2021; Korkmaz, et al., 2014*). Therefore, in this case, whether the data is distributed symmetrically is shown (Figure 4.5).

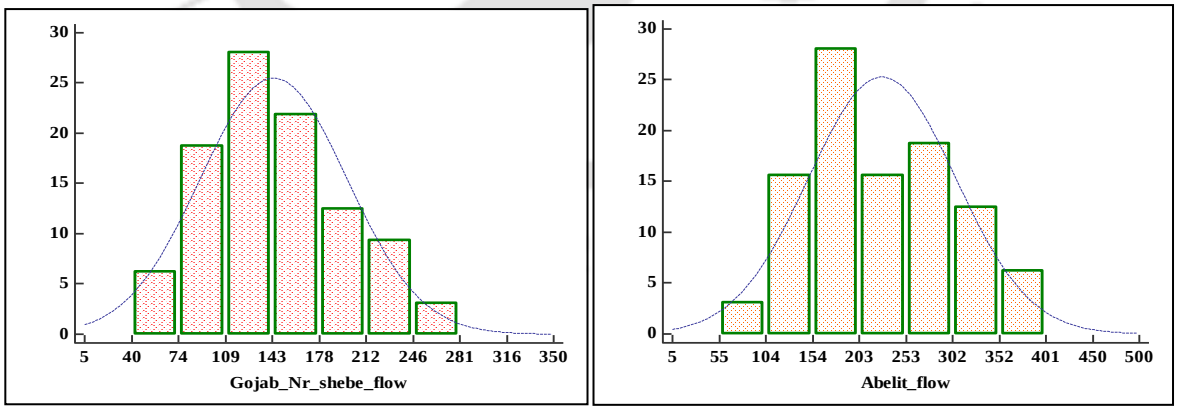

Figure 4.4 Histogram of Normal distribution

Cumulative Normal distribution curve displayed together with the cumulative distribution of the data (Easton and McCulloch, 1990; Korkmaz, et al., 2014) . The cumulative Normal distribution (with Mean and Standard Deviation of the data represented in the graph or curve is displayed as a

smooth line. When this option is selected the cumulative frequency distribution (Figure 4.6 Cumulative frequency polygon and/or Cumulative dot plot) (*Strahler. 1954;Almeida et al., 2018; Yue and Jin-yang ,2021; Easton and McCulloch, 1990; Korkmaz, et al., 2014)*) is plotted using a different algorithm, allowing better visual comparison of the observed frequency distribution with the theoretical Normal distribution.

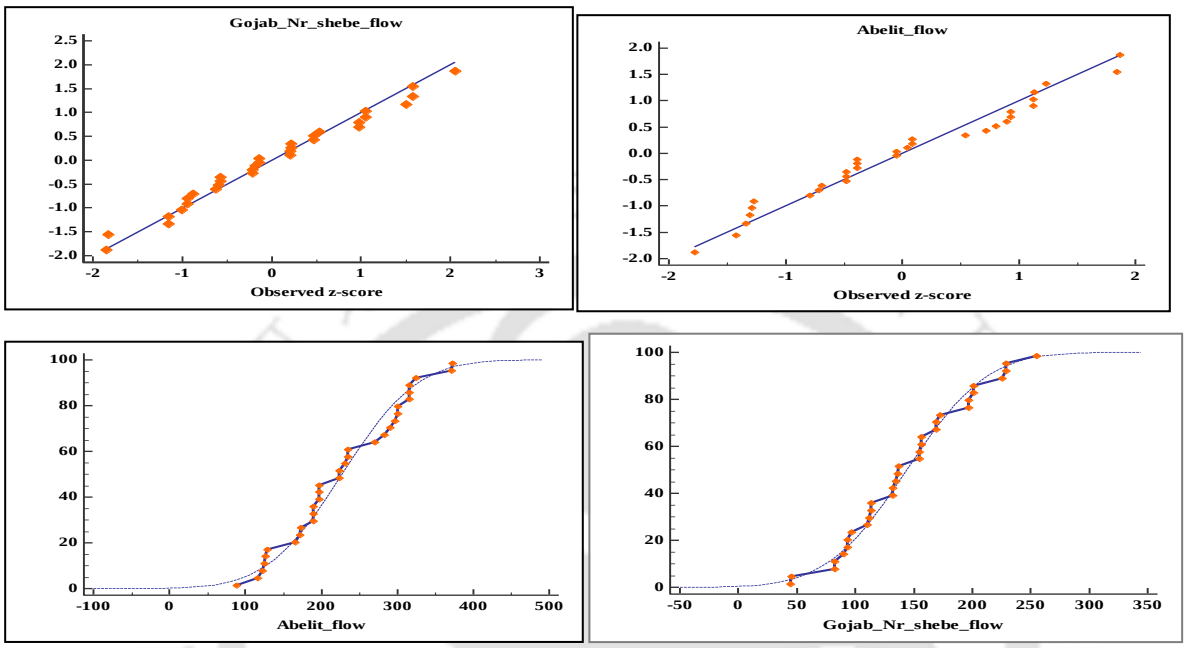

Figure 4.5 Cumulative Normal distribution curve and Normal plot graph.

The Normal plot is a graphical tool used to judge the Normality of the distribution of the sample data. A straight reference line represents the Normal distribution. If the sample data are near a Normal distribution, the data points will be near this straight line.

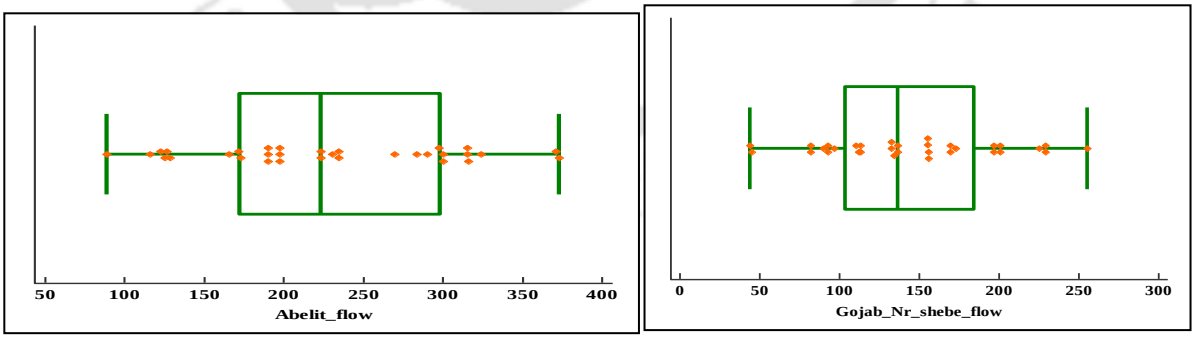

Figure 4.6 Box-and-whisker plot

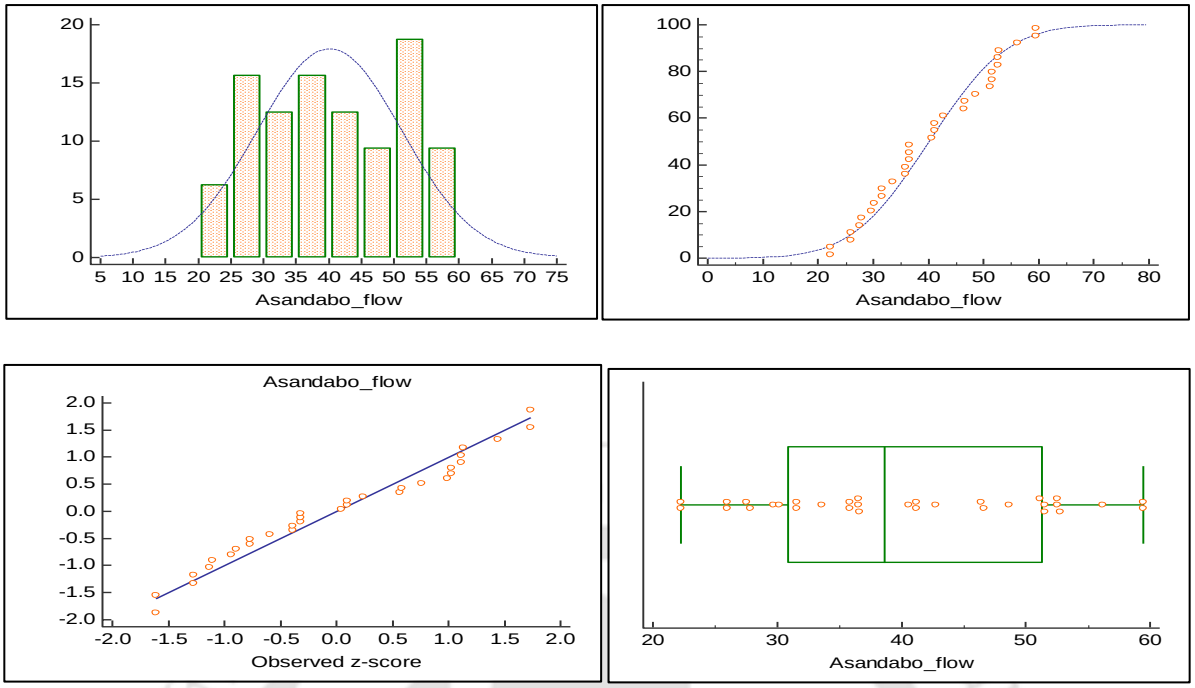

Figure 4.7 the expected and observed, Box plot, and Cumulative frequency of Asandabo flow

In the Box-and-Whisker plot in (Figure 4.7) (Spitzer et al, 2014), the central box represents the values from the lower to upper quartile (25 to 75 percentile) (*Tirumala et al., 2017*). The middle line represents the median. The horizontal line extends from the minimum to the maximum value, excluding outside and far out values, which are displayed as separate points.

4.3 GIS based Spatial Rainfall Interpolation techniques

The spatial interpolation techniques are used to produce daily rainfall data of a finer scale from regional climate modelling. (Yang et al., 2015) Common interpolation techniques were compared with ANUDEM, Spline, IDW, and Kriging and assessed against rainfall data from stations. For this research, two forms of interpolation method are used - IDW and Ordinary Kriging (*Mueller et al, 2004; Shahbeik et al, 2014*).

4.3.1 Inverse Distance Weighted Interpolation (IDW)

The IDW method predict the unknown value based on the neighbourhood measured value. It calculates the cell values by means of a weighted combination of sample points. The weight is an inversely distant function (*Yang et al., 2015*). The interpolated surface is that of a location dependent variable (*Tatalovich et al., 2015*). In the interpolation, nearby data will have the most effect, and the surface will have more detail.

Inverse distance weighted (IDW) interpolation explicitly implements the assumption that things that are close to one another are more alike than those that are farther apart. To predict a value for any unmeasured location, IDW uses the measured values surrounding the prediction location (*Mueller et al, 2004; Shahbeik et al, 2014*). The measured values closest to the prediction location have more influence on the predicted value than those farther away.

$$Y_p = \sum_{i=1}^{N} w_i Y_i,$$

$$w_i = \frac{d_i^{-a}}{\sum_{i=1}^{N} d_i^{-a}} \qquad (4.39)$$

where Y_p refers to the unknown rainfall data (mm); Y_i refers to the known rainfall data (mm), N is the amount of rainfall stations, w_i is the weighting of each rainfall stations, di is the distance from each rainfall stations to the unknown site, α refers to the power, and is also a control parameter.

4.3.2 Ordinary Kriging

The Kriging approach is a geostatistic method for generating and predicting unknown values from a set of points *(Gunarathna et al., 2016; Diggle and Ribeiro, 2002)*. It is a method of interpolation based on statistical relations and the distance among measured points (*Gotway et al., 1996; Yang et al., 2015*). The term "kriging" is derived from the name of D. G. Krieg who introduced the use of moving averages to avoid systematic overestimation of reserves (*Campozana, & Lake 2008*). Kriging is based on the regionalized variable theory, which assumes that the statistical surface to be interpolated has a certain degree of continuity. There are two types of Kriging interpolations - ordinary Kriging and universal Kriging. Ordinary kriging assumes the model:

$$Z(\mathbf{s}) = \mu + \varepsilon(\mathbf{s}) \qquad (4.40)$$

Where, μ is an unknown constant. One of the main issues concerning ordinary kriging is whether the assumption of a constant mean is reasonable. Sometimes there are good scientific reasons to reject this assumption. However, as a simple prediction method, it has remarkable flexibility.
Universal kriging assumes the model.

$$Z(\mathbf{s}) = \mu(\mathbf{s}) + \varepsilon(\mathbf{s}) \qquad (4.41)$$

where μ(**s**) is some deterministic function andwhich has the same data that was used for ordinary kriging concepts, the observed data is given by the solid circles.

4.4 ArcGIS Geo-Statistical Analyst

Geostatistics is a class of statistics used for the analysis and prediction of values associated with spatial-temporal occurrences (Johnston et al, 2001). It integrates the spatial and temporal coordinates of the data. Most geostatistic methods were originally developed as a practical means of representing spatial patterns and interpolating values for places, where measurements are not performed. Geostatistics is commonly used in many areas of science and technology, including temperature prediction, precipitation, and evaporation, as well as associated variables (*Johnston et al, 2001*). Geostatistical assessment has also been developed from univariate to multivariate and provides processes for incorporating secondary data sets that complement a primary interest variable, thus allowing interpolation that is more accurate and uncertainty models to be constructed. The extension of ArcGIS geostatistical analyst provides the surface modelling capability using deterministic and geostatistic methods (*Krivoruchko & Gotay, 2003*).

4.5 Prediction error statistics

The mean of the prediction errors should be near zero for unbiased predictions (*Cressie, N. 1990; Roy and Aher 2017*). However, this value depends on the scale of the data. In ordinary, and universal kriging (assuming the data is normally distributed), the quintile and probability maps depend on the kriging standard errors as much as the predictions themselves (*Papritz & Stein 1999*). If the average standard errors are close to the root mean squared prediction errors, the analyses are correctly assessing the variability in prediction. If the average standard errors are greater than the root mean square prediction errors, the analyses are overestimating the variability of predictions; and if the average standard errors are less than the root mean squared prediction errors, the analyses are underestimating the variability in predictions (*Papritz & Stein 1999*). The performances were assessed by the mean absolute error (MAE), mean relative error (MRE), root mean squared error (RMSE), and the spatial and temporal distributions.

Mean Error is the averaged difference between the measured and the predicted values.

$$ME = \sum_{i=1}^{n} \frac{Z(X_{obs}) - Z(X_{sim})}{n} \qquad (4.42)$$

RMSE indicates how closely the model predicts measured values. The smaller this error, the better.

$$RMSE = \sqrt{\sum_{i=1}^{n} \frac{Z(X_{obs}) - Z(X_{sim})^2}{n}} \qquad (4.43)$$

ASE—the average of the prediction standard errors.

$$ASE = \sqrt{\left(\sum_{i=1}^{n} \delta^2 \times (X_{sim})\right)} \qquad (4.44)$$

MSE- the mean of the standardized errors. This value should be close to 0.

$$MSE = \sum_{i=1}^{n} \left[\frac{Z(X_{obs}) - Z(X_{sim})}{\delta(X_{sim})}\right]^2 \quad (4.45)$$

RMSSE this should be close to one if the prediction standard errors are valid.

$$RMSSE = \sqrt{\sum_{i=1}^{n} \left[\frac{Z(X_{obs}) - Z(X_{sim})}{\delta(X_{sim})}\right]^2 / n} \quad (4.46)$$

where X_{obs} and X_{sim} is Observed and predicated valu respectively, δ^2 is Standard Deviation.

If the root-mean-squared standardized error is greater than one, the analyses are underestimating the variability in the model predictions. If the root mean square standardized error is less than one, it is overestimating the variability in the model predictions. Only the mean and root mean square error results are available for IDW, global polynomial interpolation, radial basis functions, diffusion interpolation with barriers, and kernel interpolation with barriers. Therefore, hydrological data are recorded either as a continuous record (water level or stage, rainfall, etc.) or in discrete series form (mean daily/monthly/annual flows or rainfall, annual series, partial series, etc.).

4.6 Conclusion

The main purpose of the downscaling technique is to provide error-free future climate and climate change data models. Because of the poor spatial resolution and simulations of GCM model outputs, RCM and RCP precipitation and temperature cannot be utilized directly as an input to hydrological models to analyze climate change consequences. A reliable and practical downscaling and bias correction method was applied to RCM and RCP outputs to solve this problem. The process can be described as a cumulative distribution mapping technique. Downscaling climate data has been done in a variety of ways, including Precipitation and temperatures are two significant variables to include in SWAT and SWAT CUP inputs. The model's performance was evaluated using simulated current climatic conditions and compared to observed climate data. Therefore, applying the methodology directly for simulating future temperature and precipitation data, it was calibrating and validated in a hydrological model by using control climate data from both observed and corrected climate data sets, the validation result showed that the bias correction method performs very well in maintaining the statistical.

Chapter 5 Assessment of the Impact of LULC Change on Surface water potential

5.1 Introduction / background

The river basin is a dynamic and complex system involving a number of natural or anthropogenic physical processes (*Deshmukh et al., 2013*) that can function at the same time and have various spatial and temporal effects. Remote sensing data (*Butt et al, 2015*) is the primary source data for evaluating land use and land cover (LULC) and environmental processes at local or global spatial scale. The uncertainty of land-use resulting from population growth, urbanisation sector expansion, and climate change (*Tan et al., 2015*) is increasing at an alarming rate. Agricultural expansion (*Lee 2005*) and intensification, urban growth, and other natural resources are expected to increase in the coming decades to meet the demands of a cumulative population.

Urban land-use change is mostly influenced by the activities of human beings due to increasing population pressures (Smith et al., 2016) and the rise in the economic levels of the region (*Rajan & Ryosuke 2001*). The influence of human activities on the land has increased exponentially over the past two centuries (*Ellis et al., 2013; Boivin et al., 2016*) due to population growth, technological progress altering entire ecosystems, and increasingly affecting both the biodiversity, nutrient and hydrological cycles and the environment (*de Sherbinin, 2002*). These changes in LULC systems have important environmental consequences through their impacts on soil and water, biodiversity, and microclimate (*Lambin et al., 2003*). Different LULC affect differently for both the infiltration and the amount of runoff from the falling precipitation (*Hougton, 1995*). Types of land cover significantly affect both surface and sub-surface flow. Surface runoff is mostly contributed directly from precipitation, whereas groundwater flow is contributed from infiltrated or percolated water. However, the source of streamflow during the dry and wet month is primarily from the surface runoff and the groundwater (*Alemseged & Tom, 2015; Abebe, 2005*).

In addition, deforestation also has its own effects on hydrological cycles, leading to reductions in precipitation and faster post-precipitation runoff (*Legesse et al., 2003*). Understanding watershed hydrology is very important to assess the water potential and impact of catchment hydrology under land-use dynamics. An increasing number of people and technology (*Noe et al., 2017*) are driving forces of LULC dynamics. The changes are highly influenced by man-made actions and natural events that happened. Therefore, the LULC dynamics are the product of complex interactions between environmental and ecological conditions that can occur at different temporal and spatial scales (*Reid et al., 2000*). The main driving forces of LULC dynamics are: Population

Growth, Economic Growth, Demographic conditions, and Technology (*Mather and Needle 2000; Liu et al., 2009)*. According to (*Lambin et al., 2003*), evaluating the impact of LULC change on water resource management and formulating policies, taking into account anthropological and computational modelling, are very important in monitoring future basin-level water resource potential. LULC change will alter the hydrological cycle either by increasing or reducing flow (*Wang et al., 2014*). Long-term reduction in the evapotranspiration and recycling of water activate changes in the climate and weather patterns of the region.

The Omo-Gibe basin is the main source of water for Ethiopia's economy and downstream ecosystems to develop or sustain. Effective use and management of LULC under consideration of water resources *(Mango et al., 2011*) is very important when considering the effect of catchment hydrology and water resources on the water for the development of the basin. It requires optimizing these potential resources of water with increasing population growth as the water demand will increase or decrease from the past and existing values. This change in water demand will effect the downstream ecology. Analysing the sensitive parameters affecting the basin and understanding how LULC influences the streamflow can allow planners to formulate policies to minimize the unwanted effects of future LULC changes on catchment streamflow patterns (Mango et al. 2011; Niraula et al. 2015; Setyorini et al. 2017). However, to predict the future effects of LULC, it is vital to have an acceptance of historic LULCs on its flow. The hydrological impact assessment of LULC dynamics using historic LULCs substantially assists in planning water resources developments. The LULC change impact from 1989 to 2013 on the Gojeb watershed, a sub-catchment of the Omo-Gibe basin, revealed the anthropogenic influence on the streamflow (Choto and Fetene 2019). Similarly, for the Winike watershed (Aneseyee et al. 2019, 2020), a sub-catchment of Omo-Gibe, the extensive soil losses, and changes in the ecosystem services were revealed due to wide LULC changes in the sub-basin. However, the past studies on the effect of LULC changes on streamflow in the entire Omo-Gibe river basin are rare. Moreover, the Omo-Gibe basin is anticipated to have rapid population growth from 2020 to 2035 (FDRE-PCC 2008), increasing future water demands and putting more stress on the water resources projects. Hence, studies on LULC changes' impact on water resources projects in the basin have importance regarding the futuristic demands.

5.2 Statement of the problem

Understanding watershed hydrology is very important to assess the potential impact on catchments under land use dynamics. Water mismanagement, increasing number of population and technology are some of the causes that effect the catchment hydrology. Omo Gibe basin is one of the main water

source of Ethiopia for development and sustainable economy. Effective utilization and management of land use land cover under the consideration of climate change is very important to cope up catchment hydrology and water resources. It requires optimizing these potential resources of water with increasing population growth. In order to predict the future effects of land use land cover on hydrology, it is prerogative to have an understanding of the effects of historic LULCs had on its flow. Therefore, proper planning of water resource development based on hydrological impact assessment of land use land cover dynamics under considering climate change is very essential.

5.3 Objectives

The general objective of this study is on assessment of the effect of LULC dynamics on surface water availability using remote sensing and mapping surface runoff in the case of Gibe-III hydropower dam catchment in Omo Gibe river basin.

The specific objectives of this study are:

- To analyse the impact of land use dynamics and climate change on surface water availability.
- Calibration and Validation of SWAT model using different land use land cover change.

5.4 Driving Forces of Land-Use Land Cover dynamics

Land use and land cover dynamics is highly affected by human-induced activities rather than natural events. Hence, Land Use and Land Cover dynamics are the result of complex interactions between several biophysical and socio-economic conditions that may occur at various temporal and spatial scales (*Reid et al., 2000*). *Mather and Needle (2000*) noted that high rates of deforestation in many developing countries are most commonly associated with population growth and poverty. Allen and Barnes, (1985) argue that most tropical deforestation occurred by the pressure from population growth and demand for more food resources. It is a significant driver of land-use and land cover change with other non-demographic factors, such as government policies, changes in consumption patterns, economic integration, and globalization. According to (*Lambin et al., 2003*), land-use policies and projections of the future role of land-use change must not only capture the complex socio-economic and biophysical drivers of land-use change but also account for the specific human-environment conditions under which the drivers of change operate. To explain land-use changes, it is also important to understand institutional setup (political, legal, economic, and traditional) and their interactions with individual decision-making (*Agrawal 2008*). Understanding the controlling parameters of various models thus may explain the management of resources, adaptive strategies,

compliance or resistance to policies, or social learning and social resilience in the face of land-use changes.

5.4.1 Interaction of Land Use Land Cover Change and Hydrology

Land-use Land cover changes and their associated effects are known to impact the hydrology of the catchment area (*Foley et al., 2005; Bronstert et al., 2002; Tang et al., 2005*). The effect of land-use and land cover change on low flows during dry periods depends on competing processes, most notably changes in evapotranspiration and infiltration capacity (*Calder, 1998; Piao et al., 2010*). Each combination of both the dominating natural processes and the anthropogenic impacts has a different effect on the low flow regime (*Smakhtin, 2001*). Therefore, the relatively quantitative impacts of various anthropogenic processes and factors on the low flow regimes vary substantially in different river sub-catchments (*Tu_Min, 2006*). However, vegetation cover plays an important role of increasing the capacity of catchments, conserving moisture, and increasing water yield (*Ngana 2002; Pereira 1989*). Land-use and land-cover change play a significant role in modifying the hydrological flow regime of the river basins. According to (*Namrata et al., 2004*) there are many connections between the land surface characteristics and the hydrologic cycle. Changes in the vegetation cover tend to affect the degree of infiltration, run-off, and evaporation rate and precipitation pattern (*Newson, 1995*). LULC changes may have both immediate and long-lasting impacts on terrestrial hydrology, altering the balance between precipitation, evapotranspiration (ET) and the resultant run-off (*Namrata et al., 2004*). In the short-term, LULC changes may alter the hydrological cycle either through increasing high flows or through diminishing the low flow. In the long-term, reduction in evapotranspiration and water recycling initiates a feedback mechanism that changes the climatic conditions of the area.

5.5 Earth Resources Data Analysis System (ERDAS) IMAGINE model

ERDAS IMAGINE is a remote sensing application with raster graphics editor abilities designed by ERDAS for geospatial applications (*George 2016; Chepkochei et al, 2011*). By manipulating imagery data values and positions, it is possible to see features that would not normally be visible and to locate geo-positions of features that would otherwise be graphical. The level of brightness or reflectance of light from the surfaces in the image can be helpful with vegetation analysis (*Thenkabail & Lyon 2016*), finding prospects for minerals (*Ustin et al., 2009*), etc. Other usage examples include linear feature extraction, generation of processing work flows ("spatial models"

in ERDAS IMAGINE), import/export of data for a wide variety of formats, orthorectification, mosaicking of imagery, and stereo and automatic feature extraction of map data from imagery.

5.5.1 Landsat Image Analysis

U.S. Geological Survey (USGS) Landsat imagery is acquired in a very precise manner, to better emphasize particular land cover aspects. Some of the parameters of this precision involve a scene's radiometry and providing distinct characteristics to components of the image scene. These measures help determine what the images are good for, from a science perspective. For example, Bands 1, 2, and 3 are used together to approximate how the real world appears. (*Schroeder et al., 2008*). Bands 4, 5 or 7 from ETM+ (*Baker et al., 2006*) are used in combination with 1, 2 or 3 to demonstrate vegetation conditions. It is sometimes necessary to convert the radiometric values from the initial at sensor measures, to compensate for atmospheric interference. Basic information that were used for image interpretation and band combinations for Landsat images as referred from GLCF site (*Ehsani, & Quiel 2010*) is provided in the (Table 5.2).

5.5.2 Image classification and accuracy assessment

Digital image classification is the popular and challenging approach of remotely sensed image analysis process (*Cavallaro et al., 2015; Li, et al., 2014*). In the process, pixels in the image are sorted to obtain meaningful information of the real world as derived in the thematic maps bearing the information such as land cover type; vegetation type, etc. (*Matinfar et al., 2007*). Image classification is the process of assigning of pixels of continuous raster image to the predefined land cover classes. The result of the classification is mostly affected by various factors such as classification methods. After the images were geo-referenced and geometrically rectified, image clipping was performed. This pre-process was performed using spatial analyst tool on a sub-scene from the full image based on a frame covering the watershed. These pre-processing tasks allowed us to export the satellite images to the ERDAS Imagine for classification and extracting land cover information.

5.5.3 Accuracy assessment

Accuracy assessment is an important step in the image classification process (*Rwanga, & Ndambuki, 2017*). The objective of this process is to quantitatively determine efficient pixels that were grouped in to the correct feature-classes in the area under investigation. It is a process used for estimating the accuracy of image classification by comparing the classified map with a reference map. The

most widely used classification accuracy is in the form of error matrix, which can be used to derive a series of descriptive and analytical statistics (*Manandhar et al., 2009*). The Land use and land cover change studies usually need the development and the definition of homogeneous land use and land cover units before the analysis is started. These have to be differentiated using the available data source such as ArcGIS techniques, any other relevant information, and the previous local knowledge. Accuracy assessment from ERDAS IMAGINE shows the users and producers accuracy and all numerical values (*Kumar et al., 2014; Aslami, and Ghorbani, 2018; Mesa-Mingorance, and Ariza-López, 2020*). The different accuracy definitions are provided in (equation 5.1 – 5.4)

$$UA = \frac{\mathrm{N} \times \mathrm{CCP}}{\mathrm{TN} \times \mathrm{CP} \times (\mathrm{RT})} \times 100 \qquad (5.1)$$

$$PA = \frac{\mathrm{N} \times \mathrm{CCP}}{\mathrm{TN} \times \mathrm{RP} \times (\mathrm{CT})} \times 100 \qquad (5.2)$$

$$OA = \frac{\mathrm{TN} \times \mathrm{CCP}}{\mathrm{TN} \times \mathrm{RP}} \times 100 \qquad (5.3)$$

$$KC = \frac{\mathrm{TA} - \mathrm{RA}}{(1 - \mathrm{RA})} \times 100 \qquad (5.4)$$

where: UA = Users Accuracy, PA = Producers Accuracy, OA = Overall Accuracy, KC = Kappa Coefficient, N = Number, TN = Total number, RT = Total row, CT = Total Column, CCP = Correct Classified Pixels, CP = classified pixels, RP = Reference Pixels, TA = Total Accuracy, RA = Random Accuracy.

5.6 Method of image classification

The method of the image classification is done as described in flow chart (Figure 5.1) for land use/land cover and change detection. The research here used Landsat TM images at three different time period i.e. 1987, 2002, and 2017 to prepare and analyse land cover change in a ten years' interval *(Kumar et al., 2014; Mesa-Mingorance and Ariza-López, 2020*). These images were downloaded from USGS web site and corrected using different image correction techniques like noise reduction, histogram equalization, and haze reduction in ERDAS IMAGINE 2014. After correcting imageries, a supervised image classification was employed to generate land cover map of the study area at different time. Finally, by using the classification results obtained in a different time the researcher analysed changes observed at different times and display it in the form of maps.

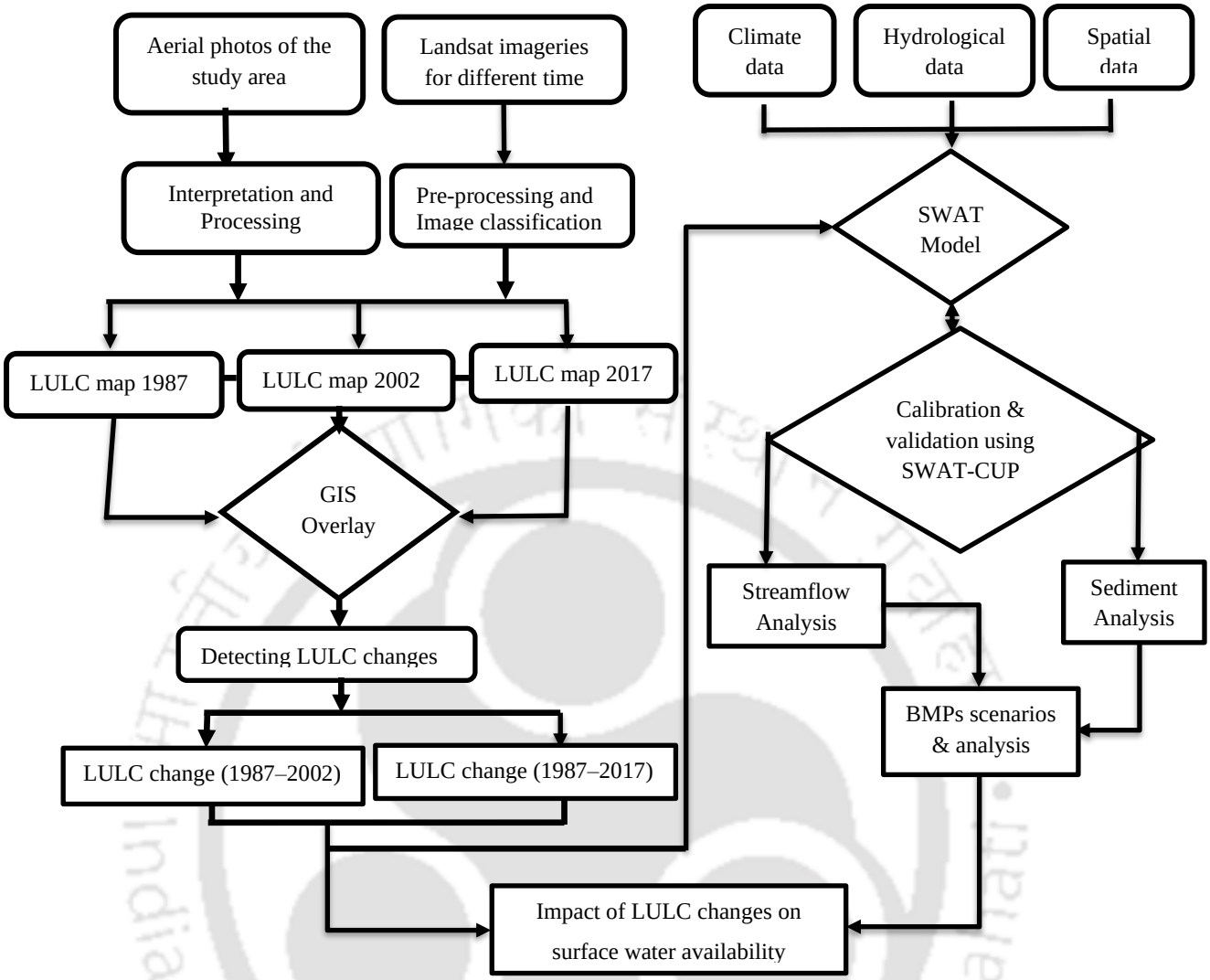

Figure 5. 1 Flow chart of methodology for land use/land cover and change detection.

5.7 Land Use Land Cover (LULC) classification

Land use land cover classification based on landsat images at three different time period i.e., 1987, 2002, and 2017 were used to prepare and analyse the LULC changes. The flow chart in (Figure 5.1) shows that the methodology used to evaluate the effect of land-use and the changes detection of land-use.

Remote sensing-based image classification is the common and challenging approach to the processes of image analysis (*Li et al., 2014; Cavallaro et al., 2015*). The pixel size in the images are sorted in the process to obtain meaningful information about the real world as obtained from thematic maps. The information provided are on type of land cover; type of vegetation, water bodies, urban locations, etc.(*Matinfar et al., 2007*). Image classification is the method by which pixels of a continuous raster image are allocated with ground truth to the predefined LULC groups. After the images were geo-referenced and geometrically rectified, the image clipping was done from the

whole image on the basis of a frame covering the watershed. Accuracy assessment is a significant step in the process of classification of satellite images (*Rwanga & Ndambuki 2017*). Studies of LULC change usually require their design and the description of homogeneous LULC units before the research begins. These must be distinguished using available data sources such as ArcGIS tools, any other relevant information, and relevant practical experience. Basic information that was used for image interpretation and band combinations for Landsat images as referred from GLCF site (*Ehsani, & Quiel, 2010*) Landsat 4-5 TM is given for Image 1987, Landsat 7 Enhanced Themetic Mappers Plus (ETM+) for Image 2002, and Landsat 8 Operational Land Imagers (OLI) and Thermal Infrared Sensor (TIRS) for Image 2017 with 30 meter resolution. Table 5.1 describes the details of Landsat 7 and Landsat 8 and their band combinations.

Table 5. 1 Landsat 7 and Landsat 8 description

Band	Landsat 8 OLI and TIRS			Landsat 7 ETM+		
No	Band Name	λ	R (m)	Band Name	λ	R (m)
Band 1	Ultra-Blue	0.435-0.451	30	Blue	0.45-0.52	30
Band 2	Blue	0.452-0.512	30	Red	0.52-0.60	30
Band 3	Red	0533-0.590	30	Green	0.63-0.69	30
Band 4	Green	0.636-0.673	30	NIR	0.77-0.90	30
Band 5	NIR	0.851-0.879	30	SWIR1	1.55-1.75	30
Band 6	SWIR1	1.566-1.651	30	Thermal	10.4-12.5	60*(30)
Band 7	SWIR2	2.107-2.294	30	SWIR1	2.09-2.35	30
Band 8	Panchromatic	0503-0.676	15	Panchromatic	0.52-0.90	15
Band 9	Cirrus	1.363-1.384	30			
Band 10	TIRS1	10.60-11.19	100*(30)			
Band 11	TIRS2	11.50-12.51	100*(30)			

NB: λ =Wavelength (Micro meters), R = Resolution (m), ETM+ (Enhanced Thematic Mappers Plus) OLI and TIRS (Operational land image and Thermal Infrared Sensor)

5.8 Normalized Difference Indices

5.8.1 Normalised Difference Vegetation Index (NDVI)

The NDVI is used to calculate the vegetation index and is very useful in defining good coverage of vegetation. Healthy plants with high Near Infrared (NIR) reflection range from 0.7 to 1.3 μm. Two

bands in the above wavelengths are used to measure NDVI for high reflectance in NIR and high absorption in the Red spectrum (*Dennison et al, 2005).*

$$\text{NDVI} = \frac{\text{NIR}-\text{RED}}{\text{NIR}+\text{RED}} \qquad (5.5)$$

The value of NDVI ranges from -1 to 1 (*Dennison et al, 2005*) increased the value of NDVI reflects high Near Infrared (NIR), The value between -1 to 0 represent water bodies, -0.1 to 0.1 barren rocks, sand or snow, 0.2 to 0.5 shrubs lands, grasslands or crops, and 0.6 to 1.0 Moderate and dense vegetation is shown in (Figure 5.2).

5.8.2 Normalized Difference Built-up Index (NDBI)

The NDBI is the most common index of the built-up areas for analysis. The build-up areas and bare land reflect higher SWIR than NIR (*Zhao & Chen 2005*). Landsat image classification technique is a complex process based on supervised classification and unsupervised classification and it is useful to use the built-up index to classify cover forms of land use (*Deng et al., 2008*). The value of the Normalized Build-up Difference Index also varies between -1 and + 1. The negative value of NDBI represents water bodies that view build-up areas as a higher value. The vegetation NDBI value is small.

$$\text{NDBI} = \frac{\text{SWIR}-\text{NIR}}{\text{SWIR}+\text{NIR}} \qquad (5.6)$$

where: SWIR = Short-Wave Infrared, NIR = Near-infrared

5.8.3 Normalized Difference Water Index (NDWI):

The NDWI can be used for estimating water bodies. The index uses green and near-infrared bands remote sensing images (*Li et al, 2013*). The NDWI will successfully develop water sensitivity in most situations. NDWI (*Gao 1996*) Low-reflective water bodies. There is no reflection in Near Infrared (NIR) and beyond to enhance the water-related features of the landscapes (*Li et al., 2013*). This index uses the Near-infrared (NIR) and Short-Wave Infrared (SWIR) bands, and the following formula can be used to calculate NDWI:

$$\text{NDWI} = \frac{\text{NIR}-\text{RED}}{\text{NIR}+\text{RED}} \qquad (5.7)$$

However, the result from the above formula may appear poor in quality. The pure water reflects neither NIR nor SWIR. Xu (2007) then modified the formula of NDWI. It uses a Green and SWIR band.

$$\text{MNDWI} = \frac{\text{Green}-\text{SWIR}}{\text{Green}+\text{SWIR}} \qquad (5.8)$$

Likewise, the value of NDWI varies between −1 and 1. In general, the NDWI value of the water bodies is greater than 0.5. The vegetation has much lower values that easily distinguish vegetation from water bodies for a large area (*Hansen and Loveland 2012; Kumar et al., 2014*).

Table 5. 2 Description of Spatial data sets used for Omo-Gibe basin

No	Image Type	Path/Row	Sensor	Date of Acquisition
1	Image 1986	170/(54-57) & 169(54-57)	Landsat 4-5 TM	31 / Jan / 87
2	Image 2002	170/(54-57) & 169/(54-57)	Landsat 7 ETM^{+}	05/ Feb /2002
3	Image 2017	170/(54-57) & 169/(54-57)	Landsat 8	05/ Jan /2017

The detail of the spatial data used in this research is tabulated in (Table 5.2 and Table 5.3). Topographic map in the scale of 1:50000 and global positioning system for ground verification were used (WGS_1984_UTM_Zone_37N).

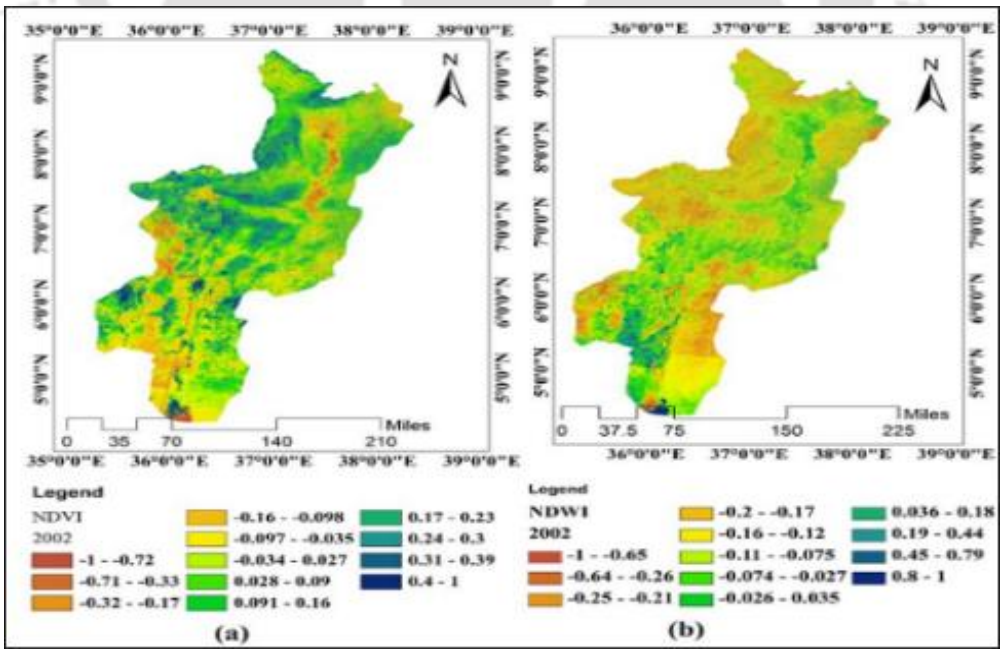

Figure 5. 2 Landsat 7 Image based difference index a) NDVI and b) NDWI for the year 2002

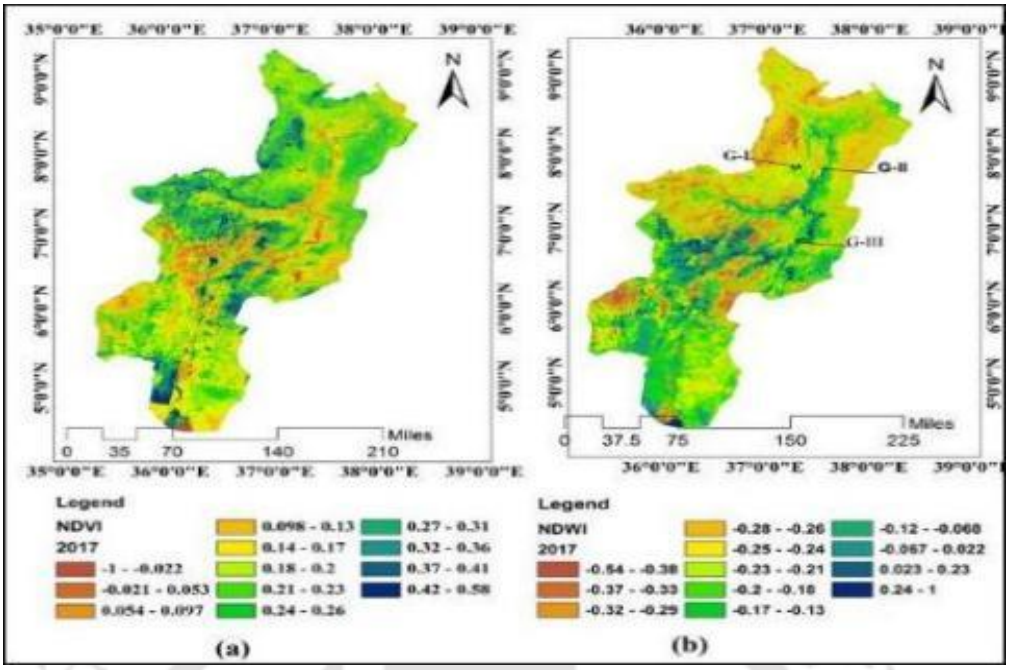

Figure 5. 3 a) Landsat 8 NDVI and b) NDWI for the year 2017

Table 5.3 Description of Spatial data sets used for Omo-Gibe basin

No	Spatial Data	Description	Source
1	DEM	30 × 30 grid resolution	SRTM of USGS , http:/strm.csi.cigar.org
2	LuLc	Land sat 8 , 11bands	USA_GS , http:/earthexpolorer.usgs.gov
3	Soil	From FAO	FAO digital map
4	Other data	Hydro-climatology	MoWRIE , EMA, and ENMA

5.9 LULC change, water resources, and population in the basin

Based on the fertility and mortality path to come (*Lutz, 2017*) and depending on the scale of mitigation initiatives, people will have to deal with the consequences of climate change, which may vary from 1.5° C to more than 3° C (*Lutz 2017; Tatalovich et al., 2006*) and its effects on environmental and eco-hydrological aspects of life. Policymakers and decision-makers need to tackle climate uncertainty and LULC change within an integrated assessment process that includes risk assessment, disaster reduction, and resilient community building (*Sweeney 2017*) at a watershed level. Assessing the hydrological effects of LULC, and population growth is of vital importance for land use planning and water resource management (*Ojeda Olivares et al., 2019*)

The 2007 Population and Housing Census results show that the population of Ethiopia grew at an average annual rate of 2.6 percent between 1994 and 2007. The population increase in the SNNP and Oromia states (through which Omo-Gibe flows) was 2.9 % in 2007 (Federal Democratic Republic of Ethiopia Population Census Commission, 2008). Population growth trends since projected to 2020, 2030, 2040 2050, and 2080, is important to estimate future water needs to balance supply and demand. Omo-Gibe basin is the second largest populated and the most densely populated basin of all Ethiopian basins. During the design of basin water resources, the population is a major element. The forecast of the population in various periods is a relevant factor to estimate future water demands. The Ethiopian statistic authority methods was used to estimate the futuristic population. Population projection in Omo Gibe basin is the 2006 population and housing census of Ethiopia as given in the results for SNNPR and Oromia region. Based on the statistical report on population size and characteristics published by the Central Statistical Authority (*CSA 2006*), the estimated population in the basin for the suceeding years was determined using the rates indicated by the CSA in their projections for urban and rural population size in SNNPRS and Oromiya. Figure 5.4 shows the approximate rural and urban population and population density in both SNNPRS and Oromiya area in the Omo Gibe basin, and (Figure 5.4) shows future population projection and population density projection. The figures reveal there is a rapid increase in population density up to 2035 and a slight increase up to 2050 in the Basin.

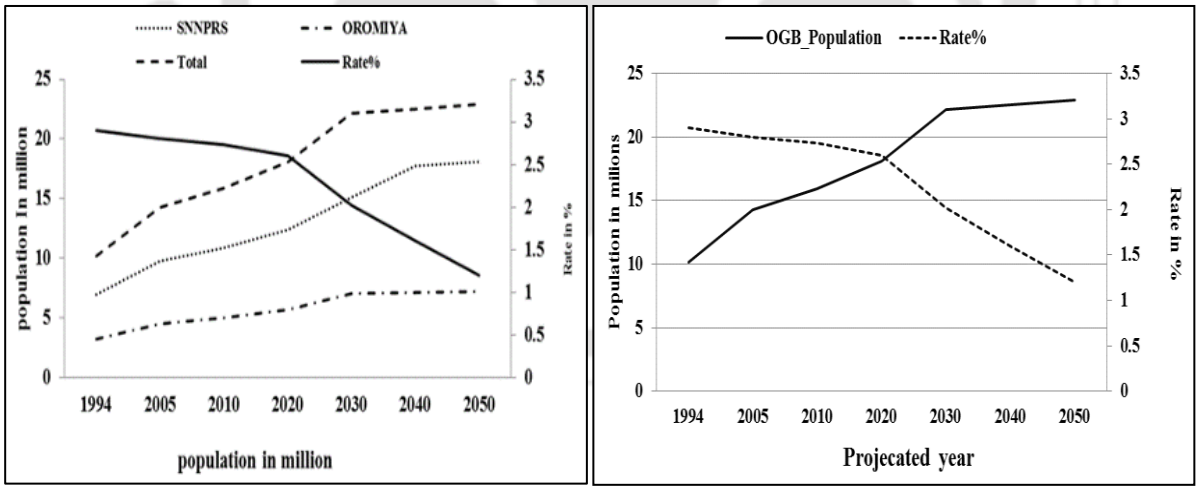

Figure 5. 4 Future Population projection and population densty projection

NB: - SNNPRS (South Nation Nationality People Region State), OGB (Omo Gibe Basin)

5.10 Results and Discussions

5.10.1 Impacts of LULC Dynamics

GIS and remote sensing technologies is an important tool for basin resource-wise planning and management. The spatial and temporal distribution of LULC is very important in understanding a wide variety of change phenomenon. The data from remote sensing helps us to monitor the variations of land use dynamics and used to estimate future changes in the area. As such, it is essential to have reliable information on the LULC and an understanding of the changes that happen within them. The (table 5.4) shows that overall completed accuracy of classification for image 2017 LULC was 83.45% and the overall Kappa Statistics for 2017 image was 78.33%. These statistics shows strong similarity between observed ground fact and classified image using ERDAS IMAGINE in Omo Gibe basin (Figure 5.5 and Table 5.4). Some of the major LULCs and their description in Omo Gibe basin are given in Table 5.4.

Table 5. 4 Omo Gibe Basin Land Cover Description

No	Type of LULC	Description
1	Annual Crop	The land that is mainly used for growing food crops such as maize, green grams, beans, mangos. Crops in this land are either grown by irrigation or rain-fed. Yearly (Rain fed; Cereal Land Cover System).
2	Perennial crop	The land that is mainly used for growing constant crops and this land are either grown by irrigation or rain-fed.
3	Dense Forest	The areas with evergreen trees mainly growing naturally in the reserved land, along the rivers and on the hills. Thick (Montane broadleaf; Dense (50-80% crown cover)
4	Moderate Forest	Lightly (Montane mixed; Open (20-50% crown cover)
5	Sparsely Forest	Thinly Evergreen trees
6	Woodland	Dense (>50% tree cover)
7	Open Grassland	This class of land cover defines grass as the main vegetation cover Unstacked (woody plant)
8	Closed Grassland	This class of land cover defines grass as the main vegetation cover moderately stocked
9	Open Shrubs land	Open (20-50% woody cover) Describes areas with sparse trees
10	Closed-Shrubs land	Dense (>50% woody cover) Describes areas with sparse
11	Bare land	This describes the land left without vegetation cover. This result from abandoned crop land, eroded land due to land degradation and weathered road surface.
12	Wetland	Open water

13	Water Body	The areas covered with water either along the river bed or man-made earth dams, Lake, River, Reservoir, and Dike
14	Settlement	The land covered with buildings in the rural and urban. It includes commercial, residential, industrial and transportation infrastructures.

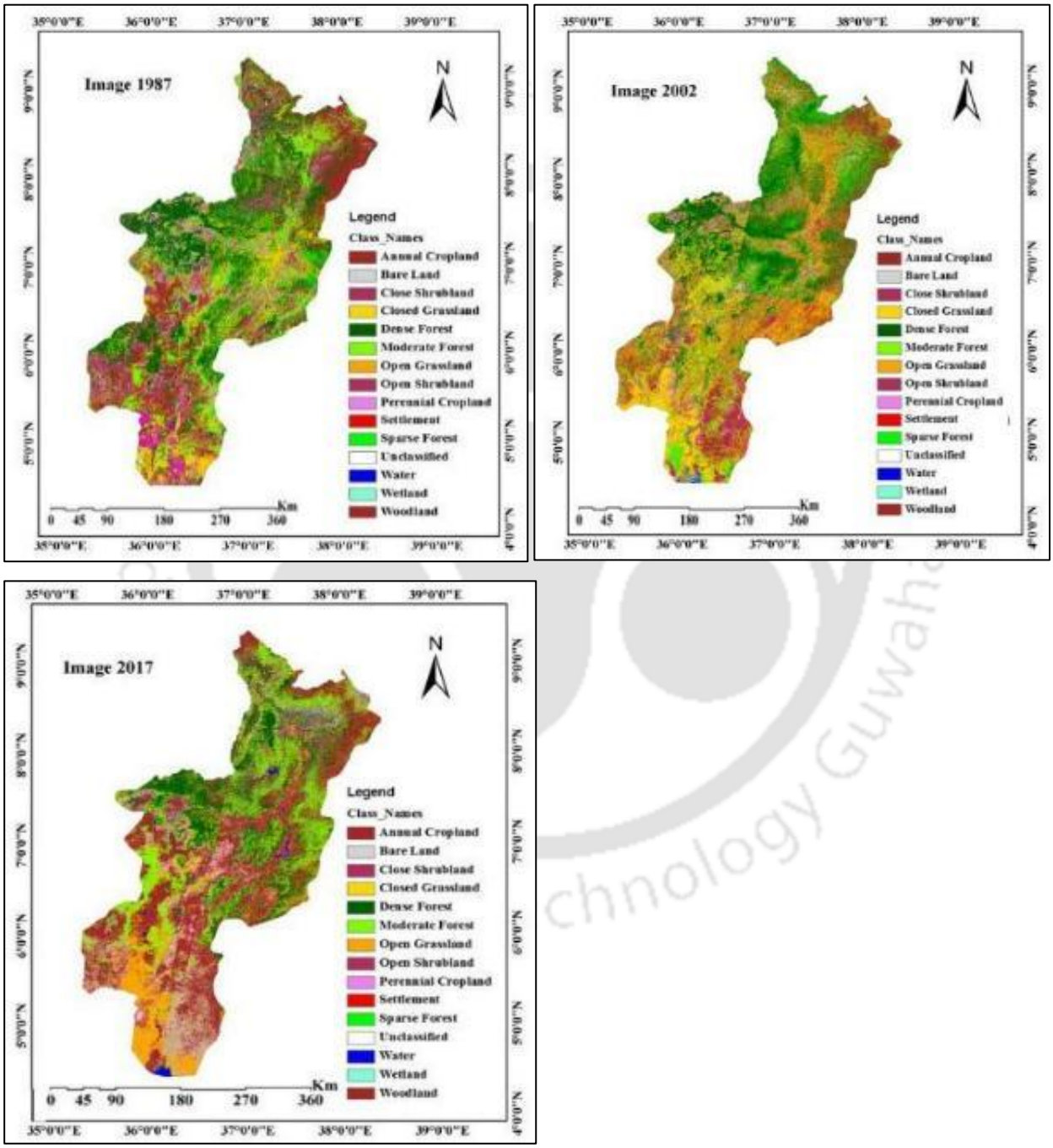

Figure 5. 5 Classified image for the year a) image 1987, b) image 2002, and c) image 2017

Table 5. 3 Accuracy assessment.

CN	WA	DF	MF	SF	WL	CG	OG	CS	OP	PC	AC	WL	SL	BL
PA	90.0	91.7	87.5	83.3	92.3	75.0	91.7	91.7	91.7	91.7	91.7	91.7	83.3	83.3
UA	75.0	73.3	70.0	76.7	80.0	60.0	73.3	73.3	73.3	91.7	91.7	73.3	76.7	76.7

NB: CN= Class Name, PA=Producers Accuracy, UA= Users Accuracy, WA=Water, DF= Deans Forest, MF=Moderate Forest, SF=Sparse Forest, WL=Woodland, OG=Open Grassland, CG = Closed Grassland, CS=Close Shrub land, OP=Open Shrubs land, PC=Perennial Cropland, AC= Annual Cropland, SL=Settlement, BL= Bare Land

5.10.2 Omo Gibe Basin Land Cover Description

The percentage of change between 2002 and 1987 is shown in (Figure 5.6). The figure indicates 3.23%, -3.55%, -11.3%, -1.07%, 0.133%, 2.29%, -10.5%, 21.41%, 17.5%, 0.605%, -8.35%, 1.24%, and -8.44% of land under Water, Dense Forest, Moderate Forest, Sparse Forest, Woodland, Closed Grassland, Open Grassland, Close Shrub, Open Shrubland, Perennial Cropland, Annual Cropland, Wetland, Settlement and Bare Land, respectively. The percentage of change between 2017 and 1987 for the respective classes is shown in Figure 5.6 and indicates 20.19%, -11.9%, -21.8%, 0.76%, 3.26%, 2.25%, -0.19%, -21.7%, -1.76%, 21.08%, 2.34%, 5.731%, 5.02% and -22.4% for Water, Dense Forest, Moderate Forest, Sparse Forest, Woodland, Closed Grassland, Open Grassland, Close Shrub, Open Shrubland, Perennial Cropland, Annual Cropland, Wetland, Settlement and Bare Land, respectively. Some area under evergreen forests in the upstream parts of the basin were converted to water bodies due to rivers/streams, tanks, and reservoirs and some downstream part of the basin is converted to cropland and built-up due to agro-industry. The evergreen forests, closed shrublands, and bare lands showed decreasing trends, in the LULC change analyses for both 2002 and 2017. The result of this study showed that built-up areas, water bodies, cropland, and bush-lands have increasing trends and the evergreen forest, closed shrubland, and bare land have decreasing trends respectively in both 2002 and 2017. In LULC change detecting scenario, it was found that the expansion of cultivated land took in place of forests. This study's results agree with other studies results (*Choto and Fetene 2019; Spera et al., 2016, Zeleke and Hurni 2001*). Similarly, recent research has shown that agricultural land growth has been at the detriment of natural vegetation lands.

5.10.3 Dominant LULC

The basin has a diverse LULC that includes forestry, grassland, woodland, and barren bodies of land and water. The basin based on the Master Plan of Omo Gibe Basin has a dominant land cover of approximately 28% forest/croplands and 40% forest and woodland. The 1987 land cover map

(Figure 5.6) shows the percentage of coverage forests, grasslands, shrubs, barren fields, and other features. Forestland dominantly covered most parts of the catchment; especially in the north-western and south-western catchment of the sub-basin around Gojeb and most upper part of the basin. In 1987, the dominant LULC in this sub-basin was forest and it was changed to mostly settlement and cultivated land in 2002 and 2017, respectively.

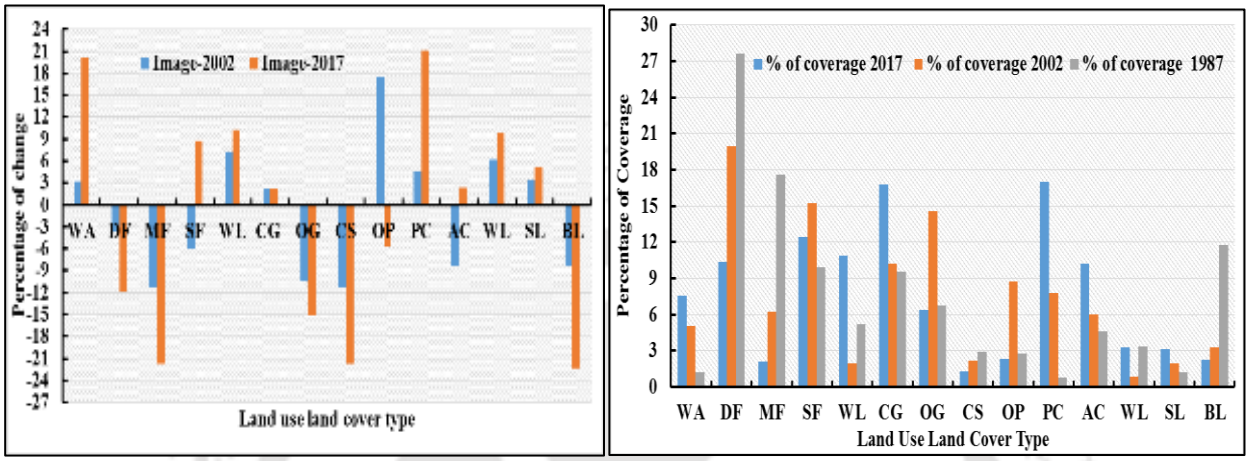

Figure 5. 6 Percentage of change and coverage comparison of LU/LC 1987, 2002 and 2017.

where: WA=Water, DF= Deans Forest, MF=Moderate Forest, SF=Sparse Forest, WL=Woodland, OG=Open Grassland, CG = Closed Grassland, CS=Close Shrub land, OP=Open Shrubs land, PC=Perennial Cropland, AC= Annual Cropland, SL=Settlement, BL= Bare Land.

The contribution of surface runoff to streamflow was used as the hydrological predictor to evaluate and address the sub-basin and basin-scale hydrological response to land-use change. Due to its rapid response and exposure to land surface cover, the generation of surface runoff was considered more prone to land-use transition. The analyses showed that sub-basins with decreased forestland cover responded with increased surface runoff generation. In addition, the deforestation affected the stability of the slopes resulting in soil erosion and easy flooding.

5.10.4 Impact of LULC scenario on past Streamflow

The farmlands got converted into settlements due to increasing urbanization and other development activities. Water spread region and natural water such as rivers/streams decreased to 80.12 km^2 in 2002 as compared to the 1987 satellite image and increased 309.81 km^2 in 2017, because of increasing water structure like dam, dike and so on. As the population has steadily increased in recent decades, there is increasing transfer of the water spread area into built-up areas or human development areas. The upper part of the basin is surrounded by dense forest with thick trees covering mainly wide-leaves and compact forest (50-80 % crown cover). Moderate forest land, which consists of mildly montane trees, covered nearly 17.5% of the land in 1987, decreasing in

2002 (6%) and 2017 (2%). The percentage of sparse forest increased from 10% in 1987 to 15% in 2002 and 12.5% in 2017. Bare lands, which occupied nearly 12% of the land cover in 1987, were significantly reduced to 3% in 2002 and even less in 2017 (Figures 5.5 and 5.6). The reduction in barren lands suggests the influence of human interventions in the basin. The agricultural lands that are perennial and annual cropland used for vegetables and other mixed varieties largely increased. The study observed that large quantities of agricultural lands are converted into settlements and developed into different types of water-related structure activities. Additionally, a large quantity of forest land shrubs transformed into farmland. Due to built-up rivers / streams and reservoir area, the water distribution area is increasing as population has increased significantly over the past decades. The hydrological processes rely on the types of LULC that have a significant impact on the availability of surface water. Figure 5.7 showed a change in mean annual surface water balance components and percentage of change in SWAT simulation for Lateral flow, Soil Water flow, percolation, total water yield, precipitation, potential evaporation groundwater flow, and surface water in the basin. The change could be explained as conversion of a forest land-use to another plantation increased the surface runoff and significantly increased lateral flow. Sub-surface flow and percolation decreased by 9.0% and 8.8%. Conversely, there was not much change in evapotranspiration, soil water content, and water yield. The main contributing reasons for those changes are deforestation and agricultural land expansion. Interception and infiltration rates are generally higher in forest areas compared to other types of land cover, so deforestation in the basin caused surface runoff to rise and water movement within the soil layer to decrease. The increase in deforestation resulted in a slight increase in the annual flow and a dip in the rate of evaporation.

5.10.5 Calibration and Validation SWAT Model Parameter

SWAT is used for the sensitivity analysis to classify specific parameters in the catchment. The result shows a flow parameter that is tabulated in (table5.5) that affects catchment flow. Model efficiency was evaluated using efficiency parameters like, determination coefficient (R^2) and Nash- Sutcliff Efficiency (NSE), (*Nash and Sutcliffe 1970*) used to calculate how well simulated results replicate patterns in the measured data over a specified period.

$$R^2 = \frac{\sum_{i=1}^{n}[(Q_{obs} - Q_{sim})\,(Q_{obs} - Q_{sim})]^{\,2}}{(\sum_{i=1}^{n}(Q_{obs} - Q_{mean}))^2\,(\sum_{i=1}^{n}(Q_{Sim} - Q_{mean}))^2} \qquad (5.8)$$

$$NSE = 1 - \frac{\sum_{i=1}^{n}(Q_{obs} - Q_{sim})^2}{\sum_{i=1}^{n}(Q_{obs} - Q_{mean})2} \qquad (5.9)$$

where: Q_{sim}: is the simulated value, Q_{obs}: - is the measured value, Q_{mean}: - is the average simulated value.

Relative volume error or PBIAS (% error) is being used to measure the volume errors. When the value zero is generated it does the best correlation between the simulated and the observed streamflow (*Janssen and Heuberger, 1995*).

$$\text{PBIAS} = \left(\frac{\sum_{i=1}^{n}(Q_{sim} - Q_{obs})}{\sum_{i=1}^{n} Q_{obs}}\right) \times 100 \qquad (5.10)$$

where: PBIAS (% error): Q_{Sim}: simulated flow and Q_{obs}: observed flow.

Table 5. 4 Sensitivity analysis result for SWAT-CUP flow parameter using the SUFI-2 algorithm to calculate the calibration and validation.

SWAT parameters used for the calibration of streamflow.

Parameter Ext	Description	Min	Max	FV
Parameters controlling surface water response				
r__CN2.mgt	Initial SCS Curve number	-0.2	0.2	**0.121**
v_SURLAG.bsn	Surface runoff lag coefficient	0.1	10	**0.93**
Parameters controlling subsurface water response				
v__ALPHA_BF.gw	Baseflow alpha factor (days)	0.0	1.0	**0.143**
v__GW_DELAY.gw	Groundwater delay time (days)	30.0	450.0	**93.3**
v_REVAPMN.gw	Depth of water for evaporation (mm)	0.01	250	**11.51**
v__GWQMN.gw	Depth of water for return flow (mm)	0.0	2.0	**1.16**
v__GW_REVAP.gw	Groundwater evaporation coefficient	0.0	1.0	**0.151**
v_RCHRG_DP.gw	Deep aquifer percolation fraction	0.01	1.0	**0.352**
Parameters controlling water balance				
v__ESCO.hru	Soil evaporation compensation factor	0.8	1.3	**1.03**
v__SFTMP.bsn	Snowfall temp	-5.0	5.0	**0.932**
v_CANMX.hru	Max canopy storage (mm of water storage)	0	10	**0.06**

v_EPCO.hru	Plant uptake compensation factor	0	1	**0.01**
	Parameters controlling channel's physical properties			
v__CH_N2.rte	Main channel manning	0.0	0.3	**0.045**
v__CH_K2.rte	Effective hydraulic conductivity (mm/h)	5.0	130.0	**96.6**
	Parameters controlling soil's physical properties			
r__SOL_AWC.sol	Available water capacity of the soil layer (mm water per mm soil)	-0.2	0.4	**0.064**
r__SOL_K.sol	Saturated hydraulic conductivity (mm/hr.)	-0.8	0.8	**0.101**
v__ALPHA_BNK.rte	Baseflow alpha factor for bank storage (days)	0.0	1.0	**0.06**
r__SOL_BD.sol	Moist bulk density (g/cm^3)	-0.5	0.6	**0.045**

where: - Ext: Extension, r: relative change (%) / Replace by value, v: value change by multiply by value, Min: Minimum value / lower bound, Max: maximum value /upper bound, FV: Fitted value

5.10.6 Sediment Yield Simulation

For all station-data, conventional rating curves $Q_s = aQ^b$ expressing daily sediment load (Q_s) as a function of daily streamflow (Q) were established by least- square method. Here, Q_s is sediment discharge, in tons per day; Q is water discharge in cubic meter per second; and *a* and *b* are constants. The rating curve established from the data collected is shown in equation.

$$Q_s = 12.54Q^{1.122} \qquad (5.11)$$

Sediment yield is the level of sediment that is moved from a sub-basin or watershed. This function is used to calibrate and validate the model because it can be matched with available data sources.

5.10.7 Sediment Sensitivity Analysis

Once the flow has been shown to be correctly defined by the model, the emphasis is changed to the model calibration for sediments. Analysis of sensitivity was performed for the sediment to define parameters that affect sediment yield and they are listed (table 5.6). Sediment flow parameters in the watershed included USLE support practice factor (USLE P), linear re-entraining parameter for channel sediment routing (SPCON), USLE cover or management factor (USLE C) and channel sediment routing exponential factor (SPEXP) that were found to be very high to highly sensitive to

sediment flows. Such sediment parameters are used to determine the amount of catchment and channel erosion.

Table 5. 5 Sensitivity analysis for sediment parameters.

Parameters	Description	L-bound	U-bound	Sensitivity index	sensitivity	Rank
USLE_P	USLE support practice factor	0	1	2.93	Very high	1
USLE_C	USLE cover factor	-25	25	0.596	High	2
USLE_C	Grass land (cover factor)	-25	25	0.43	High	3
USLE_C	Shrubs land (cover factor)	-25	25	0.112	Small	4
USLE_C	Crop land (cover factor)	-25	25	0.112	Small	5
Spcom	Linear factor for channel sediment routing	0.0001	0.01	0.00172	Small	6
Spexp	Exponential factor for sediment routing	1	2	0.003116	Small	7
Ch_cover	Channel cover factor	7	Def/t	0.00	Negligible	8
Ch_Erod	Channel erodibility factor	7	Def/t	0.00	negligible	9

5.10.8 SWAT model calibration and validation

The model was calibrated using flow data from Gibe-III catchment from 1985 to 1992 and validated using 1993 to 1995 for the land use image of 1987. Similarly, the flow data from 1996 to 2002 is used for calibration and from 2003 to 2006 for validation for the land use image of 2002 the data from 2006 to 2013 for calibration and 2014 to 2018 for validation for the land use image of 2017, respectively. The table 5.7 shows that Nash- Sutcliffe (NSE) value for LULC 1987, 2002, and 2017 land-use types in this catchment were 0.66, 0.77, and 0.81 for calibration and 0.88, 0.91 and 0.63 for the validation, respectively. The coefficients of determination (R^2) were 0.73, 0.82 and 0.86 for calibration and 0.79, 0.85 and 0.84 for validation, respectively. The significance of the LULC impact for the catchment analysed conclude that LULC impact assessment of the study area might be the most important to determine the catchment flow potential.

SWAT model were used to calculate the calibration and validation. Figure 5.7 provided the observed and simulated flow during calibration (1985-1992) and validation (1993-1995) for the 1987 LULC. Figure 5.8 provided observed and simulated flow during calibration (1996 to 2002)

and validation (2003 to 2005) for the 2002 LULC. Figure 5.9 provided observed and simulated flow during calibration (2006 to 2013) and validation (2014 to 2018) for the 2017 land use cover.

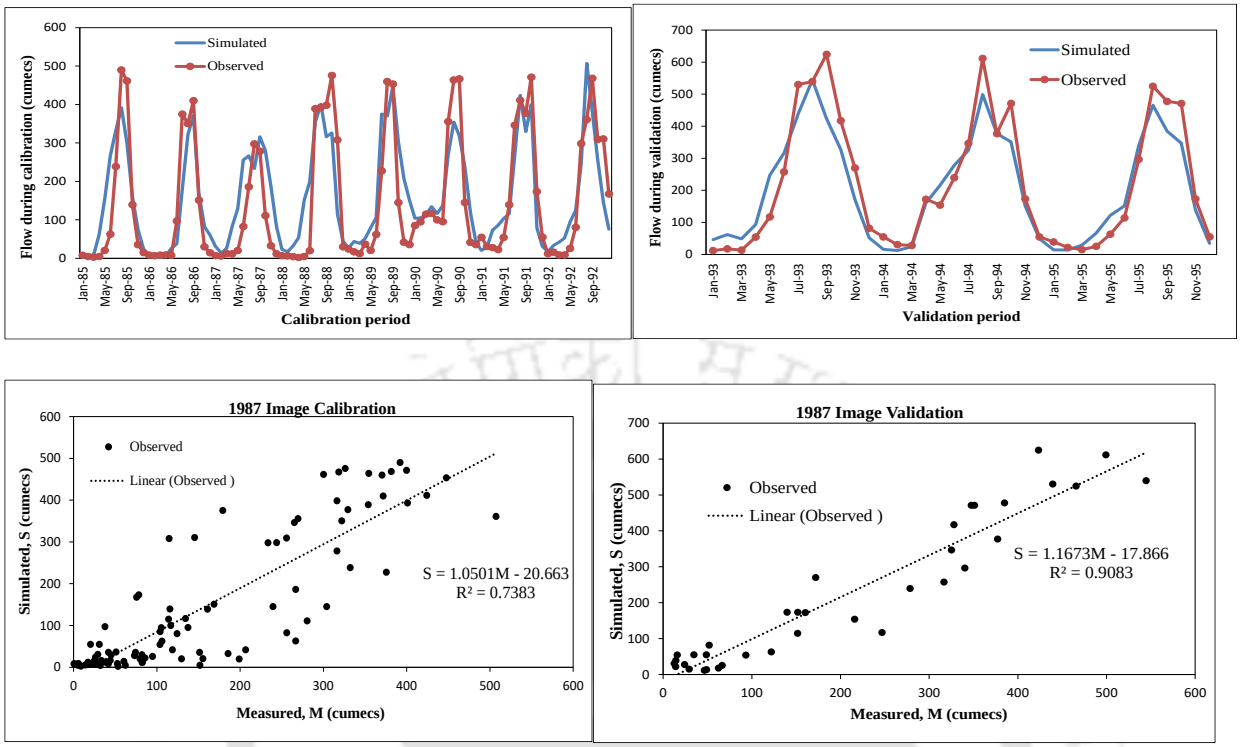

Figure 5. 7 Observed and simulated flow during calibration (1985 to 1992) and validation (1993 to 1995) period under 1987 LULC and regression fitted curves at Ableti gauging sataion.

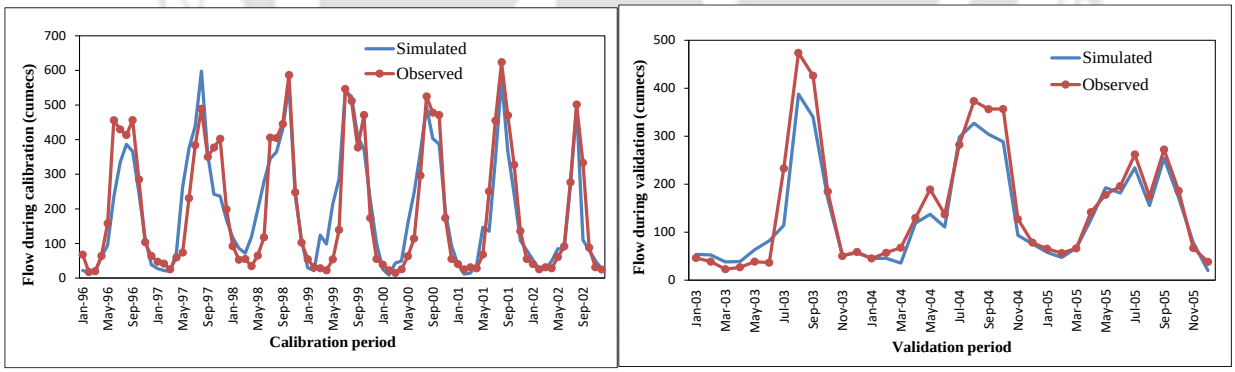

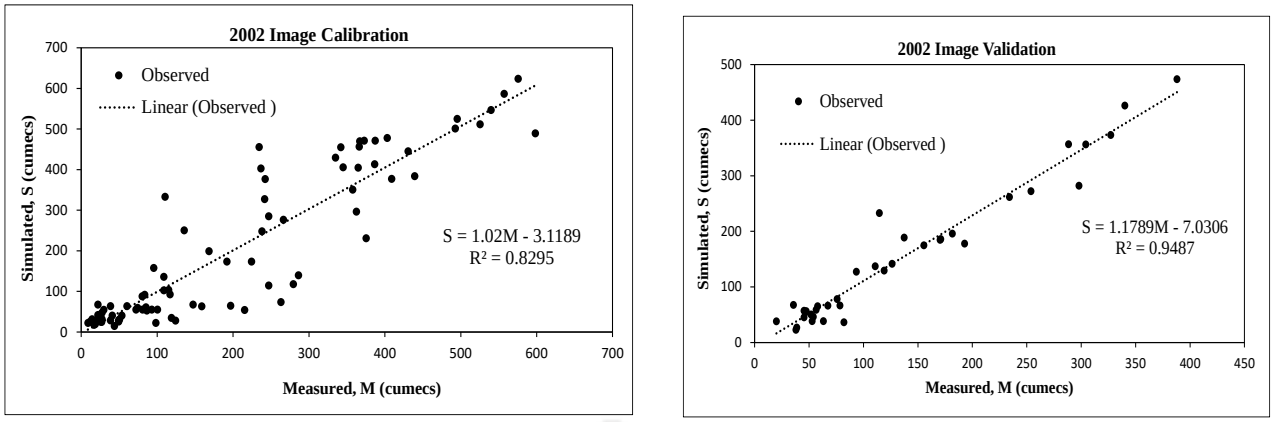

Figure 5. 8 Observed and Simulated flow during calibration (1996 to 2002) and validation (2003 to 2005) period under 2002 LULC and regression fitted curves

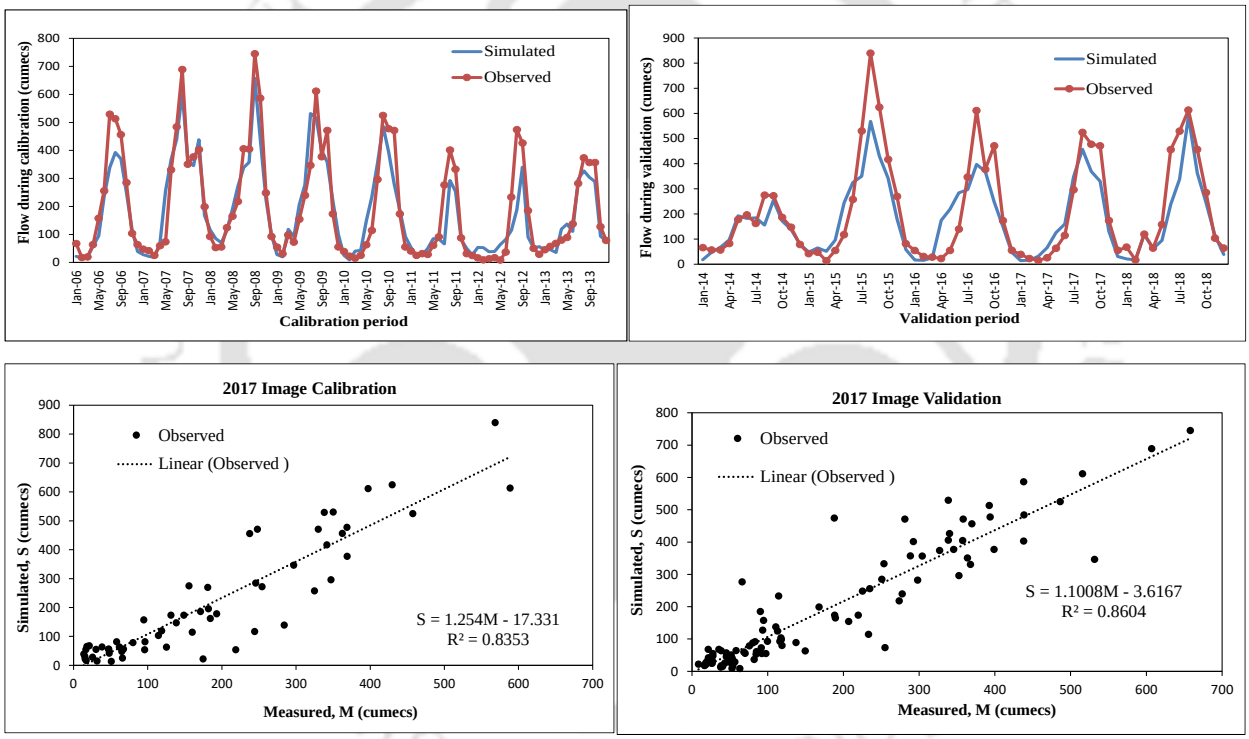

Figure 5. 9 Observed and simulated flow during calibration (2006 to 2013) and validation (2014 to 2018) period under 2017 LULC and regression fitted curves. The table 5.9 shows the suitability of SWAT model simulations for calibration and validation by comparing NSE, R2, and PBIAS.

Table 5. 6 SWAT statistical performance during calibration and validation Gibe-III Catchment.

	2017 LULC		2002 LULC		1987 LULC	
	Calibration	Validation	Calibration	Validation	Calibration	Validation
NSE	0.81	0.73	0.91	0.77	0.79	0.76

R^2	0.86	0.84	0.82	0.95	0.73	0.91
PBIAS	7.47	13.68	0.42	11.3	8.78	7.38

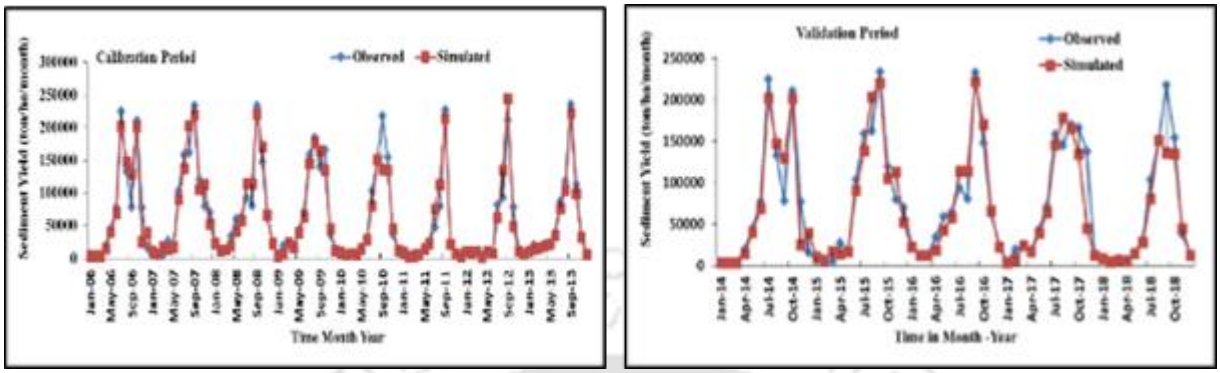

Figure 5. 10 Observed and simulated monthly sediment yield ton/ha/month data of Abelti Gauging Station during calibration (2006 to 2013) and validation (2014 to 2018) 2017 LULC.

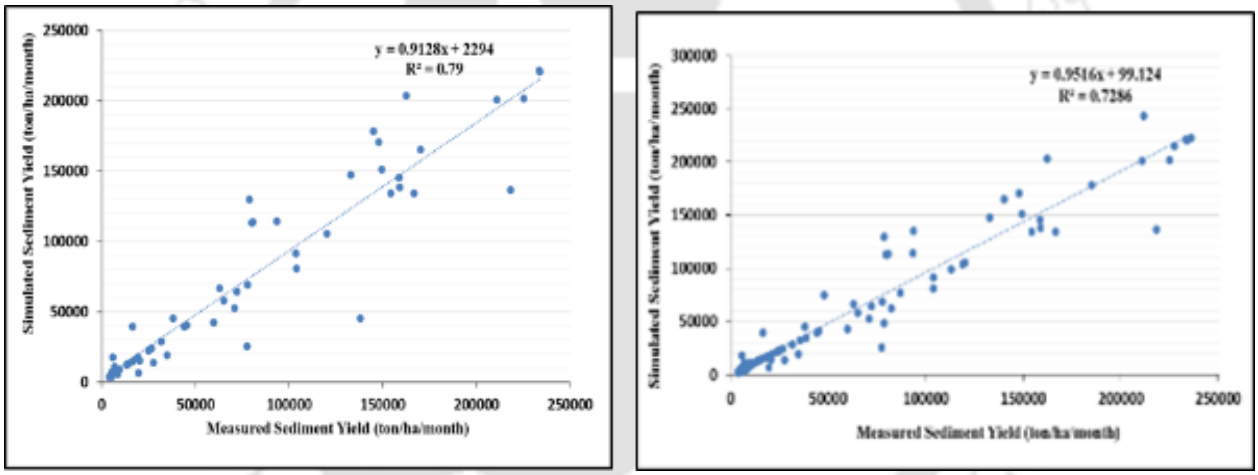

Figure 5. 11 Scatter plots of measured and simulated monthly sediment yield in calibration (2006 to 2013) and validation (2014 to 2018) period 2017 land use land cover

Figure 5.10, Figure 5.11 and Table 5.8 indicates statistical results estimated during sediment yield calibration and validation statistical parameters NSE, R^2, and PBIAS to evaluate SWAT performance with sediment data that shows 0.66, 0.79, and 3.78 in calibration and 0.78, 0.73, and 6.38 in LULC 2017 validation, respectively. The statistical variables imply a very good performance level for the SWAT model.

Table 5. 7 SWAT model statistical performance during Sediment yield calibration and validation gauging station

	2017 l LULC		2002 LULC		1987 LULC	
	Calibration	Validation	Calibration	Validation	Calibration	Validation
NSE	0.63	0.61	0.77	0.71	0.78	0.66
R^2	0.79	0.73	0.72	0.75	0.78	0.77
PBIAS	-4.7	15.38	-4.42	10.3	3.78	6.38

5.10.9 SWAT model output assessment

The SWAT model is used to assess the change in the contribution of the components of the streamflow due to LULC.

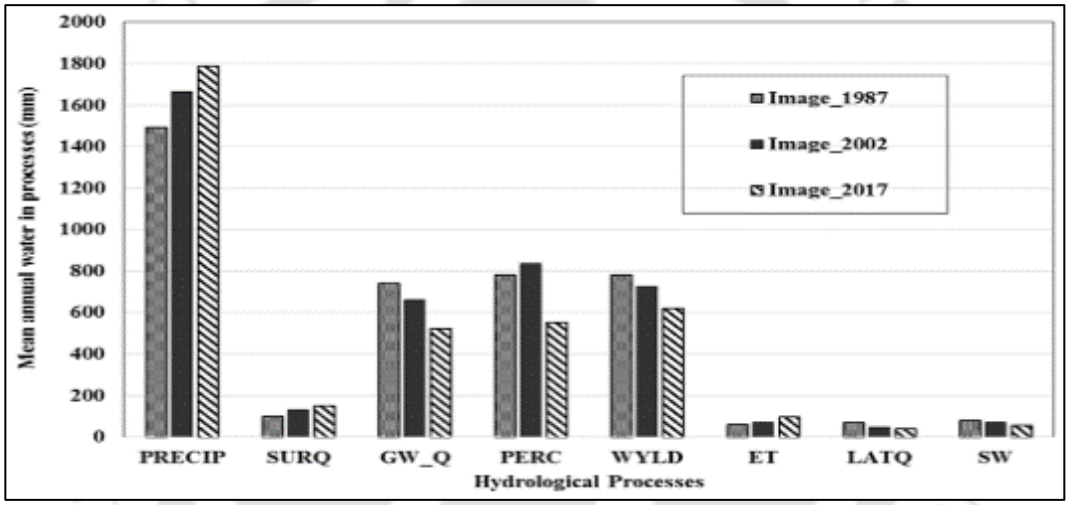

Figure 5. 12 Comparison of mean annual surface water balance (in mm)

where: In the Omo-Gibe basin for 1987, 2002, 2017 with respect to precipitation (PRECIP) using SWAT model outputs – surface runoff (SURQ), groundwater yield (GWQ), percolation (PERC), water yield (WYLD), evapo-transpiration (ET), lateral flow (LATQ), and soil water (SW)

In Figure 5.12, comparison of mean annual surface water balance based on SWAT model outputs is given. Figure 5.13 provides the comparison of percentage changes of the above processes in 2002 and 2017 from image of 1987. The results of precipitation and evaporation shows increasing trends, but total water yields have decreasing trends. In the Catchment of Gibe-III, annual percolation, groundwater, soil water, lateral flow and water yields have decreasing trends from 1987 to 2017 and surface runoff, evaporation, and precipitation have increasing trends. The decrease in Forest land and shrubs land and increase in agricultural lands affect surface runoff directly.

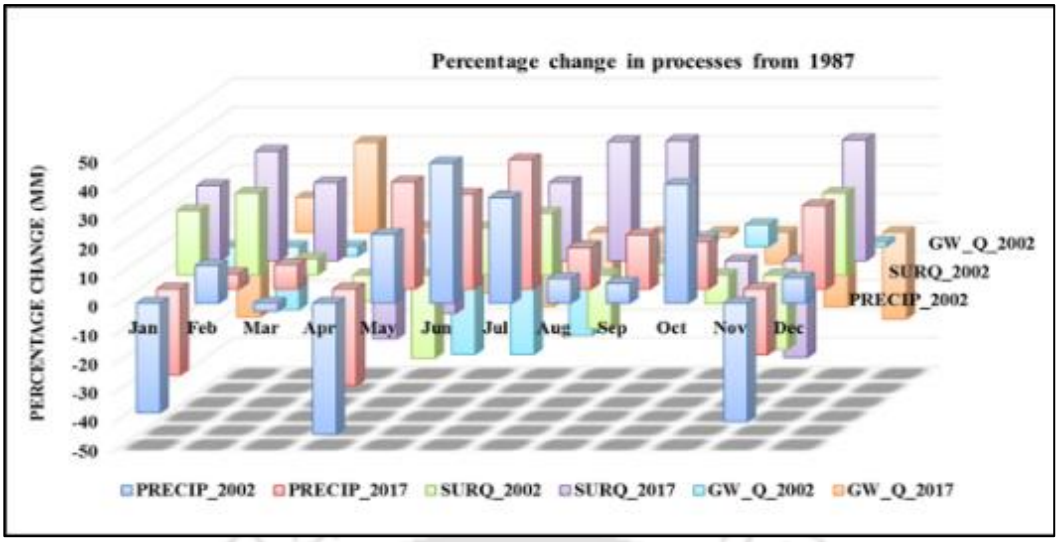

Figure 5. 13 Comparison of percentage changes for 2002 and 2017 from 1987

Percentage changes of the mean annual flow SURQ, ET, PET, and PCP, components comparing with the base time land use is 28.8%, 14.4%, and 11.43 for 2002s and 48.8%, 17.6%, and 13.9% for 2017s, respectively. The SW-Q LAT-Q, WYL, and GW-Q, components in each were -10.3%, -31.4%, -7.3%, and 10.5% in 2002s and -28.7%, -41.3%, -20.6%, and 29.9% in 2017s, respectively. Therefore, this assessment shows that urbanization has a high contribution to the increase in surface runoff, evaporation, and total water yield in the catchment.

Precipitation also shows increasing trend for 2002 image (11.41 %) and 2017 image (13.09%). Similarly, the percentage change for potential evaporation increased to 14.42% in 2002 image and 17.66% in 2017 image as compared to the 1987 image. The average annual water yield shows the percentage of change decreasing -7.11% in 2002 image and -8.66% in 2017 image while comparing with image of 1987.

The study also compared the surface runoff (SUR Q), groundwater flow (GW Q) and lateral flow (LAT Q) of the simulated flow using LULC map for period 1987, 2002, and 2017.The changes observed were 28 %, 39%, and 9%, respectively, for SUR Q, GW Q, and LAT Q while using the 2017 LULC data from that of 1987 image. The influence of surface runoff has increased from 28% to 39% due to the LULC change occurred between the period 1987 to 2017. For the 1987 and 2002 land cover average monthly streamflow was 4.3731 m^3/ s ,12.88 m^3 /s, while that of 2017 land cover data was between 36.796 m^3 /s. Monthly average stream flow for 1987 LULC, 2002 LULC and 2017 LULC was 11,081 m^3/s, 47,936 m^3/s, and 82,630 m^3/s respectively.

The result indicates that the mean wet monthly flow for 2002 land cover was increased by 6% than the 1987 land cover. Similarly, the 2002 land cover mean month flow increased by 7% than the 1987 land cover flow of wet months. On the other hand, dry average monthly flow decreased by

4% for the land cover of 2017 and by 2.6% for the land cover of 2002 than that of 1987 land cover. A comparison of daily catchment streamflow generated for the three land use land covers shows that the result obtained is different in daily peak flows between 1987, 2002, and 2017 land covers.

The hydrographs generated for 1987 land cover produced the highest peak flow of 11.081m^3/s, for 2002 land cover produced 47.934 m^3/s, whereas the 2017 land cover produced highest daily flow of 82.63 m^3/s. The majority of the peak flows occur during the month of August to December, which is the rainy season in the study area. The effect of land use management for surface and groundwater management or planning best for long-term and midterm policy formulation.

5.10.10 Mapping of Runoff & Sediment Source

SWAT measures the soil erosion and sediment yield within each sub basin's hydrological response units (HRU's). As a major factor contributing to soil erosion, the GIS method overlays the slope, land cover and soil in (Figure 5.14) shows the spatial distribution of surface runoff and production of sediments for the Omo-Gibe basin, as simulated by the model. Such figures identify sub catchments that produce high surface runoff and yield of sediments. The sediment yield in the watershed varies from HRU to HRU based on the spatial distribution of the model, depending on the type of soil, slope and land use in HRU. In this analysis, in the (Figure 5.16) indicate that sub-watersheds 1, 2, 4, 8, 10, 11, 13, 14, 17 and 20 provided the highest yield of sediments and the highest exposure to erosion. Thus, the aforementioned sub basin was chosen for the scenario of further management interference. It is also useful for catchment management planning to determine the spatial variation of Surface Runoff.

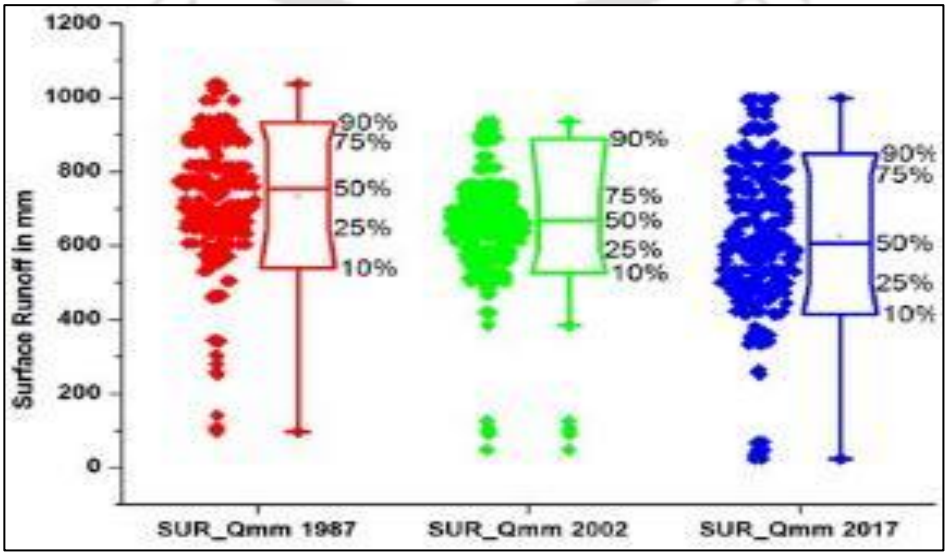

Figure 5. 14 Using Box plot Surface water runoff in the basin.

Figure 5.14 indicates the erosion/runoff prone areas in the basin. Most of the extreme erosion was observed in the cultivated land and low erosions in the grassland. High erosion was prevalent in sub-basins 1, 2, 4, 8, 10, 11, 13, 14, 17, and 20. Moderate erosion prevailed in sub basins 3, 5, 6 and 21; and low erosions occurred in sub basins 9, 12, 15, 16, 18, and 19. These surface runoff mapping is a better method to identify high surface runoff zones and sedimentation zones in the downstream of the basin.

5.11. Conclusions

GIS and remote sensing are important tools for resource-wise basin planning and management. When understanding a wide range of transition phenomena, the distribution of spatial and temporal LULC is very important. LULC data from remote sensing helps us to track changes in land-use trends and use them to predict possible changes in the environment. As such, reliable information on LULC and an understanding of the changes occurring within them is important. The purpose of this study was to determine the hydrological effect of LULC changes in the catchment using the hydrological model over the past years of 1987, 2002, and 2017. The LULC change observed in this catchment was established from collected satellite and ground truth data that provided useful information about land-use changes and allowed us to better understand the causes and effects of land-use change over time. In the past three 15-years interval data, the Omo Gibe basin had experienced a significant change over land use. It can be presumed that the rapid increase of the human population has created deforestation and the increase of farmland, and its annual crop production is not proportional in particular to this altered catchment area. Between 1987 and 2002, land-use changes are due to the reduction in forest land and grassland followed by the rise in agricultural and built-up areas, suggesting that the watershed region is under high population pressure. Forest and grasslands have been converted into farmland, and grasslands have been transformed into bare land, woodlands, and bush land. The surface runoff and sedimentation mapping allows identification of zones of high runoffs and sedimentations and the planners can earmark these zones to provid necessary protections.

Chapter 6 Water Management Scenario

6.1 Introduction

Omo Gibe basin has a complex and fragile landscapes and is one of the twelve river basins in Ethiopia. In this basin, there are twenty-one sub-watersheds covering the upstream and downstream part of the basin. Water resource management addressing land use and climate change at community-based ecosystem is essential for planning effective management strategies (*Voinov & Gaddis 2008*). Participatory water resources modelling at basin or watershed level is important to address water related issues by considering the global water management scenario (*Carmona et al., 2013*). However, in the recent decades, water has represented a growing crisis of both extremes: too much potential or too little potential at watershed and / or basin water-related resources and water-related development in a river basin level. There is a focus on the needs and requirements of society at large with regard to water at the present and in the future, thus aiming at maximum sustainability in all senses (*van Hofwegen & Jaspers, 1999*). One of the most critical issues to address at basin level water resource management is the development of dams to regulate flows to ensure availability of human water, irrigation, hydropower production, environmental control, water quality regulation, recreation and all other requirements. To address short-term and/or long-term watershed problems, and to ensure safe, successful and sustainable development of water resources is by using local leaders to make productive and reasonable use of water resource management. Frequent drought and flooding in the lowlands of Omo Gibe basin and at the mouth of the Turkana Lake have adversely affected the livelihoods of the surrounding communities. In addition to this the natural climate variability and anthropogenic change have also greatly influenced the water resource availability and its distribution. The dependence of the people on this river water is so high in this semi-arid to arid area and it has highly affected their life during drought and floods. The human interference of land use land cover change like deforestation, expansion of agricultural land, and excessive gazing have influenced the natural stream flow variability in which natural ecosystem pertain its existence. While the relative contribution of several causes is uncertain, reduced lake levels are believed to be primarily caused by land use change, increase in sediment inflow, decreased rainfall (*Carr, 1998*), increased upstream water diversion, and increased evaporation due to higher temperatures. The basin has much potential for the utility of multi-purpose water resources projects. These projects can have an effect on the natural flow regime and the amount of water flow in downstream ecosystem. Therefore, for the well-being of current and future generation and based on basin ecosystems, hydrological balance assessment of the surface and sub-surface catchment is a crucial step towards effective water management and distribution in the basin. It is very important

to map low and high rainfall areas that are seriously affected by flood and other water related problem like high soil erosion rate as result of steep slopes

6.2 Objective of the study

The main objective mapping surface water and apply the SWAT model Best management practices scenario, under different land use Lande cover change.

6.3 Methodology

The methodology of this study was (Figure 6. 2)

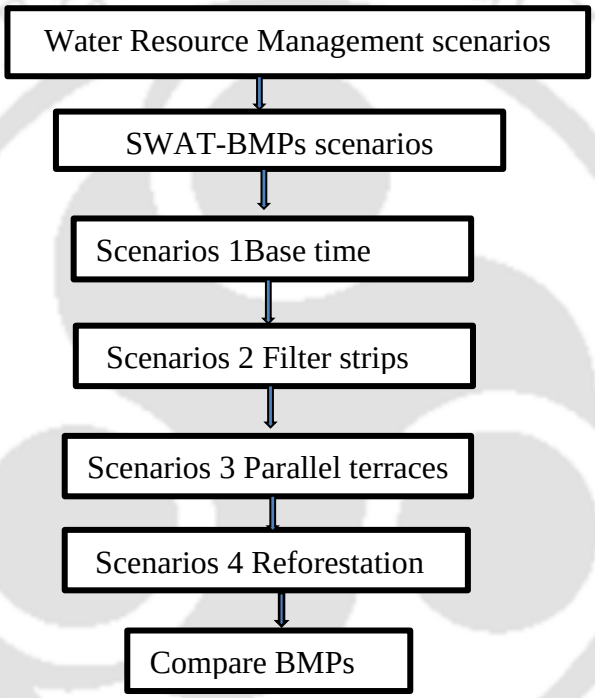

Figure 6 1 Flowchart for Water Resource Management Scenario

6.4 **Results and Discussions**

Watershed development is very important to secure water quality and quantity by using improved equity, efficiency, and sustainability. Good water management practice enhance water yield that can be used to expand irrigated areas and increase storage. Community based participatory watershed modelling and mapping can identify high surface water potential area from low surface water (Figure 6.2a). Community-based watershed management at sub watershed level (Figure 6.2b) can aid in planning recharge of subsurface water and to hold soil moisture for long time by harvesting rainwater, reforestation, and issues related toclimate change under considering LULC change in the region. This is very important in national and international level decision-making in

the water sector for policy maker and stakeholders. The water balance modelling exercise was made in order to check the capacity of Omo River in respect to satisfying the water requirement of water structure and maintain the channel flow downstream. The output of the assessment in the present research is (Figure 6.2a) - mapping high surface runoff (mm) under different LULC of 2017, 2002, and 1987. It also simulates discussion and debate in the management, planning and monitoring of watershed levels and facilitates visualization of the relationship and resources.

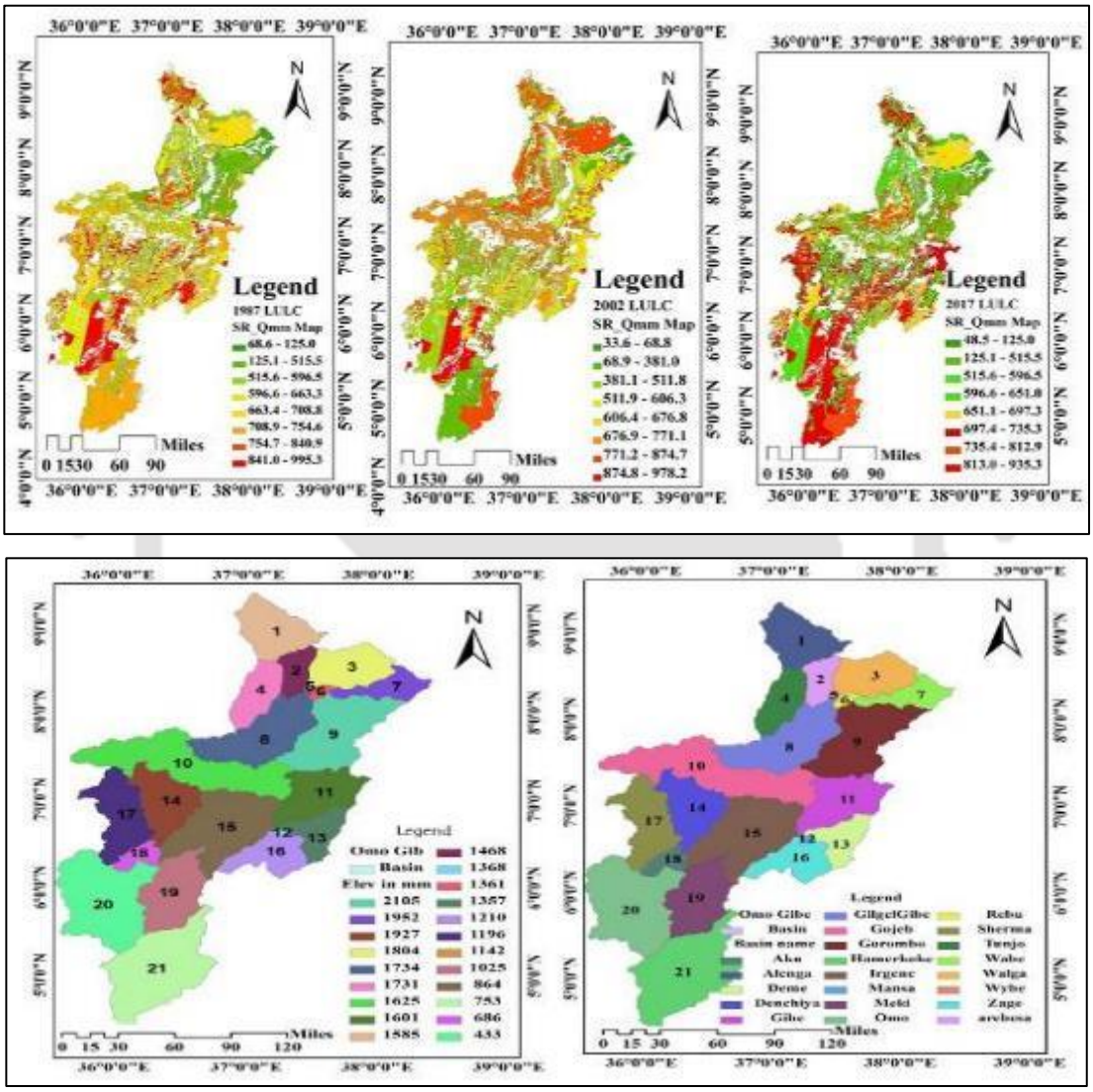

(b) (c)

Figure 6 2 a) Mapping high surface runoff (mm) using 2017, 2002 and 1987 LULCs, b) Mean elvations of sub catchments, and c) Sub-basin name

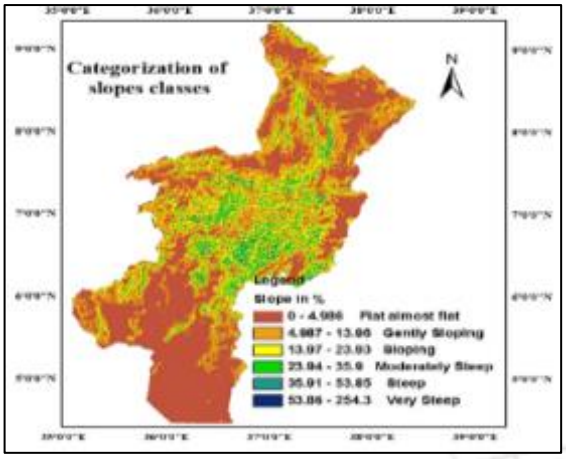

Categorization of slopes classes	
Slope Classes	Range (%)
Flat Or Almost Flat	0.0 - 4.986
Gently Sloping	4.986 - 13.97
Sloping	13.97 - 23.93
Moderately Steep	23.93 - 35.9
Steep	35.9 - 53.85
Very Steep	53.85

Figure 6 3 Slope class mapping and Percentages of Slope Class categorization

6.5 BMP Scenario developments

Table 6 1 SWAT parameters used to represent BMPs and Scenarios description

Scenarios	Description	Parameter name	input file	Calibration value	Modified Value
Scenario 1	Baseline - *	-	-	-	-
Scenario 2	Filterstrip	FILTERW.hru	5 m	0	17m
Scenario 3	Parallel	SLSUBBSN	Slope 0-5%	98	27m
	Terrace/ Stone	(.hru)	Slope 5-15%	71	17m
	Bund (75% SL		Slope 15-35%	34	13.2m
	Reduction)		Slope > 35%	19.1	19.1m
Scenario 4	Reforestation	CN2 (.mgt)		Default**	**Average
		USLE_P		0.78 *	**0.34
		(.mgt)		*	*

NB… * Assigned by SWAT Model

** The Extensions, .hru & .mgt are input files, where parameter value was edited

6.5.1 Scenario 1: Baseline Condition

A reference scenario was performed for the same simulation period described in Chapter-5 on impact of LULC on surface water availalbility for entire Omo-Gibe basin. In the simulations, provisions are made to to modify inputs according to the management strategies. Scenario-1 describes the baseline scenario of using the 1987 LULC, 2002 LULC, and 2017 LULC for Omo-

Gibe and estimating the corresponding sediment yields (Figure 6.5). This simulation represented the current conditions or baseline. The baseline scenario corresponds to the current land management practices without any conservation measures or without the use of best management practices for selected sub-basin as shown in Figure 6.5 and table 13 for different LULC.

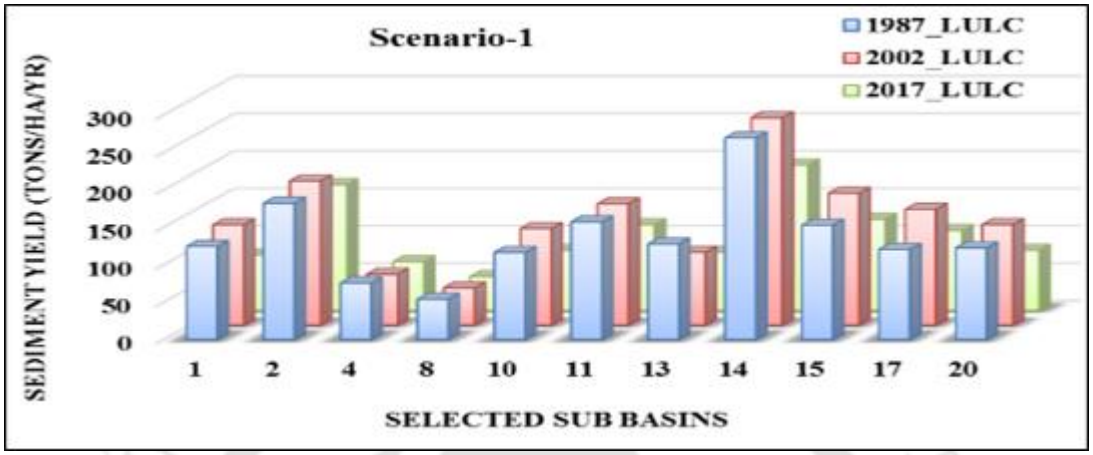

Figure 6 4 Sediment yield in selected sub basins in Baseline Condition (SYLD, ton / ha / year).

6.5.2 Scenario 2: Introducing different width of filter strips

In Scenario 2, hypothetical 5 m long filter strips were placed on all agricultural Hydrological Response Units (HRUs) of the above three years LULC (i.e., 1987, 2002, 2017), and the response from the SWAT model was observed. Filter strips, also known as vegetative filter strips or buffer strips, can filter the runoff and trap the sediments within a given plot (Bracmort et al. 2006). The model parameter representing the effects of filter strips is the width of the filter strip (FILTERW) in SWAT inputs. This value was modified by editing the HRU (.hru) input file of SWAT (Herweg and Ludi 1999; Choto and Fetene 2019). Such scenarios tested the efficacy of land reforms on soil erosion retardation and decreased sediment yields from the critical areas in the Omo-Gibe basin.

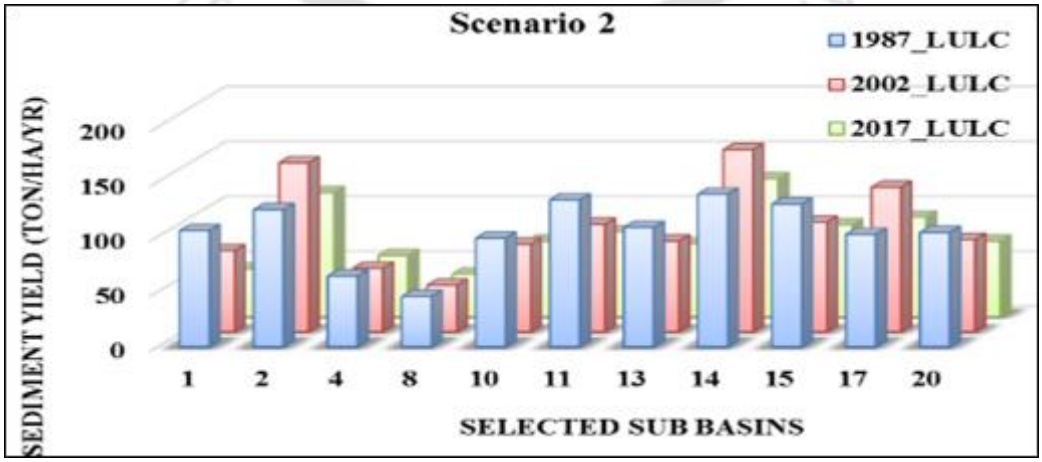

Figure 6 5 Sediment yield in selected sub basins in filter strips scenario (SYLD ton / ha / year).

During surface runoff, sediment, nutrients, contaminants and bacterial levels are decreased as the surface runoff moves through. The implementation of the filter strip scenario thus decreases the sediment yield by 24.15%, 14.97% and 15.13% respectively for 1987, 2002, and 2017 LULCs as compare to the baseline scenario in (Figure 6.5).

6.5.3 Scenario 3: Parallel Terraces with different Slope Length and Stone Bund

In Scenario 3, the agricultural HRUs were mounted on parallel terraces and stone bunds. This method decreases overland flow and soil erosion by reducing the length of the slope (Bracmort et al. 2006). Slope length and steepness have a significant impact on the surface runoff volume and velocity. In this scenario, the slope lengths of cropland HRUs are reduced by 75 % to assess the reduction in sediment yield. In the SWAT model, the parallel terraces and stone bunds are introduced by editing the ". hru" input file. The study incorporates Scenario-3 upstream of Gibe III dam to estimate the volume of sediments depositing in the reservoirs.

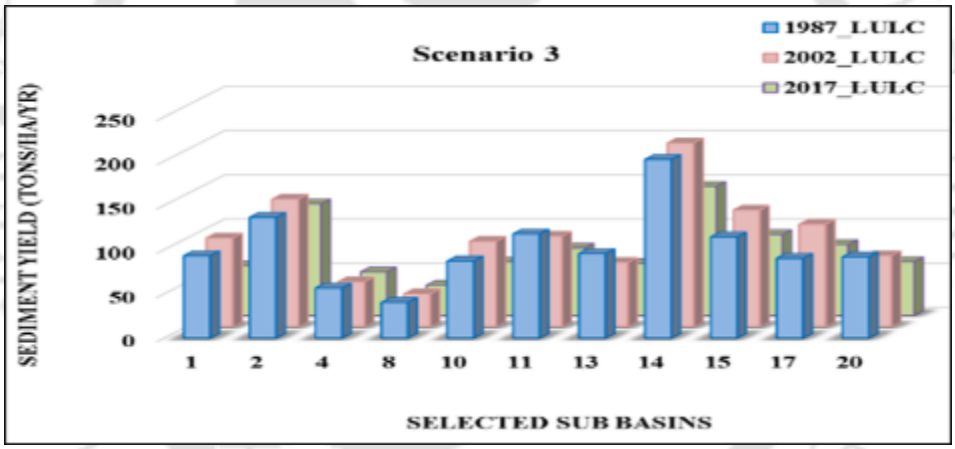

Figure 6 6 Sediment yield in selected sub basins in parallel terraces with different slope length and stone bund scenario (SYLD, ton / ha / year)

The reduction in sediment yield by 33.10 %, 16.84 %, and 22.90 % for LULC conditions of 1987, 2002, and 2017, respectively, from the baseline scenario, near the Gibe-III catchment proved the effectiveness of Scenario-3 (Fig 6.6)

6.5.4 Scenario 4: Reforestations

Omo Gibe Basin's increase in population and the resulting need for farming and other infrastructures have accelerated land degradation. Since accelerated soil erosion is caused by the activities of man and is responsible for depleting soil productivity, destroying land and filling reservoirs with sediment, there are interventions required to protect the catchment of the Gibe I, Gibe II, Gibe III,

and the downstream diversion dam. Reforestation has the component of reducing overland flow and erosivity of rainfall (Zorn and Komac 2013). In Scenario 4, reforestation of the land was proposed in sub-basins, where high sedimentation was observed in the actual situation described in Scenario-1. In this scenario, we replaced 30 % of the area occupied by Afro-alpine and cultivated lands into forest or woodlands

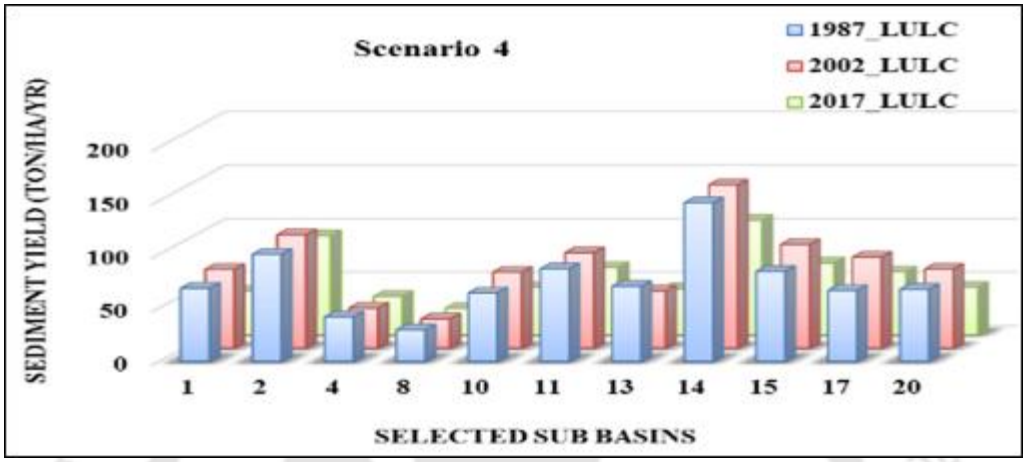

Figure 6 7 Sediment yield in selected sub basins in reforestation scenario (SYLD ton / ha / year)

The reforestation scenario's implementation reduced the sediment yield by 49.25 %, 34.55 %, and 40.84 % for LULC conditions of 1987, 2002, and 2017, respectively, proving its effectiveness in reducing sediment yield (Fig 6.7). However, the planning and development of forests and shrublands at various catchment levels should be coordinated with the respective agricultural services.

6.6 Comparison of the BMPs Scenario

On comparing the annual sediment yield generated from the basin using the LULC of 1987, Scenario-1 generated 160 t ha^{-1} $year^{-1}$, Scenario-2 120 t ha^{-1} $year^{-1}$, Scenario-3 90 t ha^{-1} $year^{-1}$, and Scenario-4 80 t ha^{-1} $year^{-1}$. Similarly, for the LULC data of 2017, the Scenario-1 generated 95 t ha^{-1} $year^{-1}$, Scenario-2 80 t ha^{-1} $year^{-1}$, Scenario-3 75 t ha^{-1} $year^{-1}$, and Scenario-4 60 t ha^{-1} $year^{-1}$ (Fig. 8.9a). The result indicates the effectiveness of BMPs in the basin lands to reduce the sediment yield. Among all the BMPs, Scenario-4 provided the maximum reduction in sediment yield for the LULC imageries of 1987, 2002, and 2017 LULC data (Fig. 6.8). This maximum reduction from Scenario-4 provides recommendations to the relevant agencies as the BMP for the Omo-Gibe basin.

Table 6 2 Total Mean annual reduced sediment yield for each scenario.

Scenario	2002_LULC	2002_LULC	2017_LULC

Scenario_1	161.9229	121.2625	97.43609
Scenario_2	115.9981	104.3459	82.0025
Scenario_3	88.35127	101.7651	76.25889
Scenario_4	78.6944	97.43609	56.58985

Table 6 3 Mean annual Percentage of reduction compare to baseline condition.

Scenario	1987_LULC_%	2002_LULC_%	2017_LULC_%
Scenario_2	24.18189	14.97746	15.83829
Scenario_3	33.10167	16.84948	22.90445
Scenario_4	49.25315	34.55543	40.8445

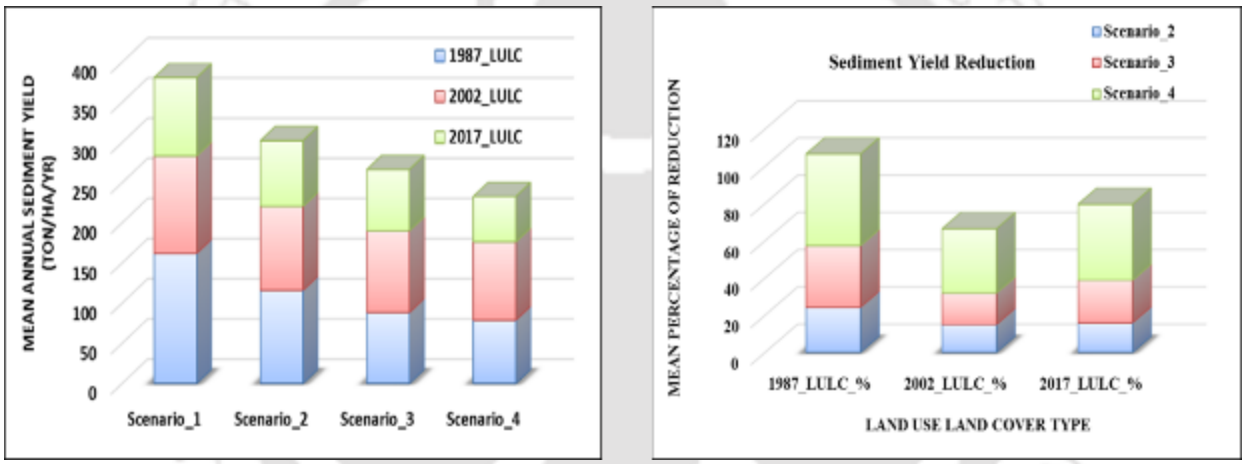

Figure 6 8 Mean Annual Sediment Yield under Different LULC Type in Ton / Ha / Yea

6.7 Conclusion

Hypothetical Best Management Practice scenarios was introduced in the basin to mitigate the hurdles from soil erosion. The BMPs that include the establishment of filter traps, incorporation of terraces in agricultural fields with a reduction in slopes, and reforestation, reduced the sediment yield from the basin. Reforestation is potentially the BMP that can reduce the sediment yield and safeguard the various hydro-projects in the basin. As a future scope, LULC changes along with climate changes and population explosion could be combined with hydrological models to predict the potential impacts on hydrological processes and availability of surface and subsurface water in the Omo-Gibe basin. It can help stakeholders and decision-makers make better adoptions for land use and climate change, to develop strategies for managing water resources.

Chapter 7 Climate Change Impact Assessment under Water Resource Development Scenario using RCP and SRES

7.1 Introduction / Background

Climate change is one of the main challenges in water resource sector (*Iglesias et al., 2007*). Stream flow of the rivers highly depends on climate variables such as rainfall, temperature, and potential evapotranspiration of a basin. These climate variables directly affect stream flow and therefore the amount of water availability and leading to river flow changes outside the margin of safety can have a negative impact on water structure, regardless of whether the flow rate increases or decreases (*IPCC, 2001*). The impacts of climate changes on hydrology is usually found on changes occurring to local weather conditions, such as temperature and precipitation in the catchment area. Moreover, *Seljom (2012*) indicated that increased inflow and climate change would result in a larger share of flooding, since it is not possible to utilise all the increased precipitation with the hydro- reservoirs. The flooding losses could increase due to climate change and affect normal trend. Climate processes can be represented in mathematical terms based on physical laws such as the conservation of mass, momentum, and energy. However, the complexity of the system means that the calculations from these mathematical equations can be performed in practice only by using computers. The mathematical formulation is therefore implemented in a computer program, which is referred to as a model. If the model includes enough of the components of the climate system to be useful for simulating the climate, it is commonly called a climate model (*IPCC, 2010; Adeniyi 2016*). Modern climate models consist of a system of interacting model components, each of which simulates a different part of the climate system (*Bader, 2008*). The atmospheric and ocean components are known as General Circulation Models (GCMs) because they explicitly simulate the large-scale global circulation of the atmosphere and ocean.

7.1.1 Problem statement

The water resources in the region depends on the hydrology of the region that includes the precipitation pattern, temperature, evaporation and geological locations, stratifications, etc. However, the climate change can affect the precipitation and its intensity that can affect the water resources. These climate changes can lead to extremes like intense water scarcity or floods and this change may be the natural climate variability and/or anthropogenic change have great influence on surface and ground water resource availability and distribution. The dependence of the people is so high in the semi-arid to arid area that highly affects their life during drought or flood. The human interference of LULC change like deforestation, expansion of agricultural land and excessive

grazing have influence on natural flow variability and reduce soil moisture. The cause of land use change can change surface water availability and increase the sediment inflow. The average annual outflow from the Omo Gibe basin into Lake Turkana was estimated about 16.6 Bm^3 although it is reported as 19 Bm^3 on GIWA 47 regional assessment report (*UNDEP, 2004*) and the inflow to lake from other sub basin catchment is also unknown. Hence, climate change assessment is a vital step for optimal water allocation in the basin for wellbeing of the current and future generation and ecosystems.

7.1.2 Objective of the study

The main objective of this study is to assess the possible effect of climate change impact on stream flow based on analysis of hydrological events in the case of GIII dam site catchment in upper Omo Gibe basin, Ethiopia.

7.1.2.1 Specific Objective

- To assess the influence of precipitation and evaporation on stream flow using RCP and RCM scenario.
- Forecasting hydrological events based on rainfall magnitude and flood frequency with in different return period using frequency model Under RCP scenario.
- To identify sensitive parameters and simulate the stream flow of the watershed after calibration and validation of SWAT model.

7.2 Study Area and Methodology

7.2.1 Study Area

The Upper Omo-Gibe river basin has an area of 33,000 Km^2 and it lies between 4° 30' to 9° 00' North Latitude and 35° 00' to 38° East longitude in (Figure 7.1). Gilgal Gibe and Gojeb Rivers are major tributaries to the main river that drains the western high lands. Upper Omo-Gibe river basin has low rainfall from March to May, preceded by the dry season from December to February and small rainy season from September to October. The amount of rainfall decreases throughout the catchments with a decrease in elevation (EEPCO 2008; Reis 2011). The mean annual temperature of the entire basin varies from 16 °C in the highlands to the north to over 22 °C to the south. The monthly average temperature rises slightly as of January to May, but declines afterwards in the months June to August. The mean annual rainfall of the catchment area is about 2280 mm. The mean monthly rainfall pattern over the basin varies distinctly in (Figure 2.6) shows that in the north

part of the basin the rainfall pattern is uni-modal, but further downstream to the south of the basin the pattern becomes bi-modal.

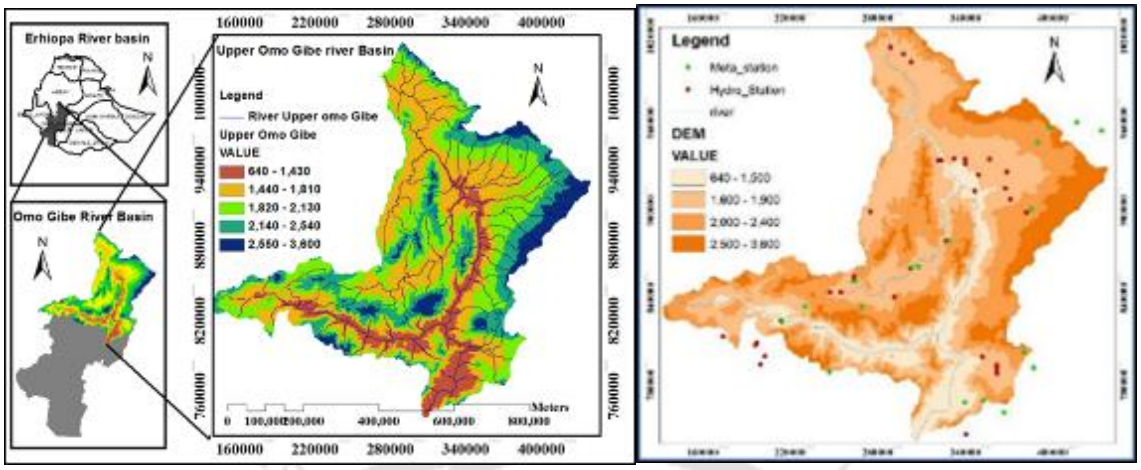

Figure 7.1 Digital Elevation Model location study area and hydro-meteorological station location

7.2.2 Digital Elevation Model (DEM)

The DEM resolution of 30 m by 30 m has been downloaded from the SRTM (Shuttle Radar Topography Mission) web site as seen in (Figure 7.1). The DEM was used to delineate the basin into various watersheds and to examine the patterns of drainage of the surface region of the basin.

7.2.3 Soil and Land Use Data.

The soil data were obtained mainly from the following sources: Soil and Terrain Database for north eastern Africa CD-ROM (Food and Agriculture Organization of the United Nations (FAO 1998), Major Soils of the world CD-ROM (FAO, 2002) as seen in (Figure 7.2), Digital Soil Map of the World and Derived Soil Properties CD-ROM (FAO 1995), Properties and Management of Soils of the Tropics CD-ROM, Omo Gibe River Basin Integrated Development Master Plan Project-Semi detailed Soil Survey. The major soil types in the Upper Omo Gibe river basin are as indicated in (Figure 7.2) Eutric Cambisols, Eutric Fluvisols, Eutric Vertisols, Haplic Luvisols, Eutric Leptosols, Chromic Luvisols, Haplic Nitisols, and Lithic Leptosols. The land use map of the study area was obtained from ministry of water resources and Electricity Ethiopia. We have reclassified the land use map of the area based on the available topographic map, aerial photographs and satellite images shown in (Figure 7.2).

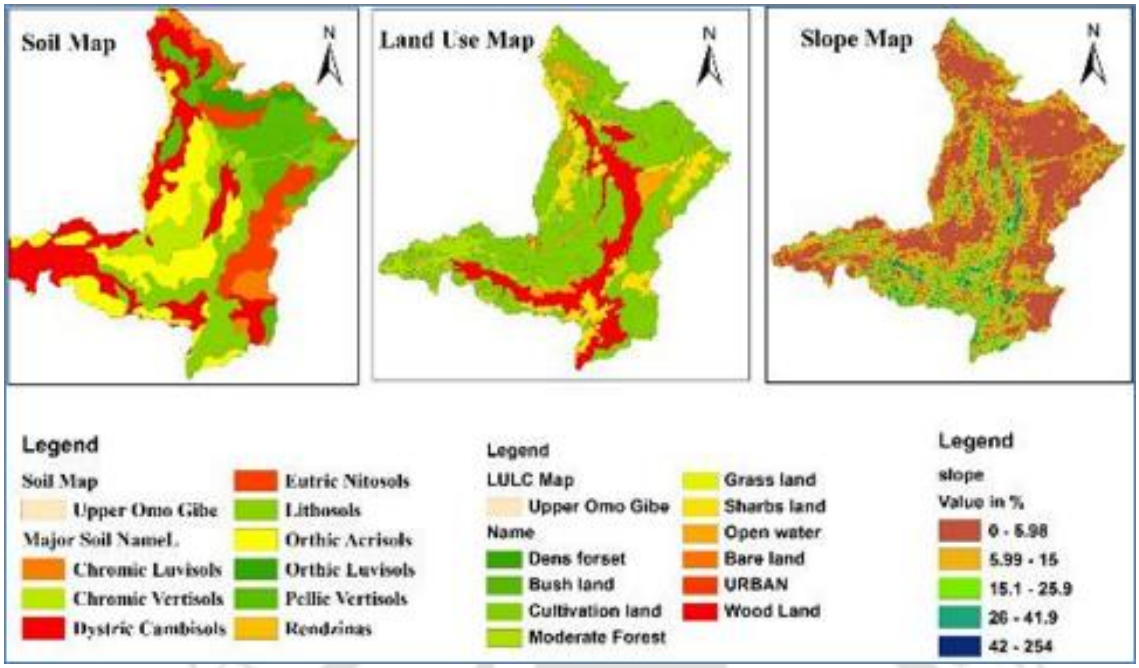

Figure 7.2 Soil Land Use and slope of Upper Omo Gibe basin

7.2.4 Weather data and Discharge

The weather data like daily precipitation, and minimum and maximum air temperatures are collected for the period 1981 – 2014. These data were obtained from Ethiopian National Meteorological Agency (NMA) for stations located within and around the watershed as seen in the spatial distribution in Fig 6.1. Daily river discharge or flow data were obtained from the Hydrology Department of the Ministry of Water Resources and Electricity of Ethiopia for the stations mentioned in Figure 7.1.

7.2.5 Model's statistical performance checking

The function of models and their results are compared with some necessary standards. Therefore, for this study, the observed and simulated hydrological data and RCM data were compared by using R^2, RMSE, and MAE. In these equations, X is data, μ is the mean of data, σ is the standard deviation and n is the number of data, o index and m index show observed (climatic variables) and model (GCM). R^2 shows a linear relationship between large-scale variables and downscaled data and its range is between 0–1. MAE cannot show stronger relationship between data, because there are many cases where large-scale data cannot simulate downscaled data behaviour pattern, in the event that there is many differences between large-scale and downscaled data.

$$r^2 = \left[\frac{\frac{1}{n}\sum_{m=1}^{o}(Xo-\mu_o)\times(Xm-\mu_o)}{\delta x_o \times \delta x_a}\right]^2 \qquad (7.1)$$

$$\text{RMSE} = \sqrt{\frac{\sum_{m=1}^{o}(X_o - X_m)^2}{\text{n}}} \quad (7.2)$$

$$MAE = \frac{(\sum_{m=1}^{o}|X_o - X_m|)}{\text{n}} \quad (7.3)$$

Also, other standards show the difference between large-scale and downscaled data. Hence, in this research, RMSE and MAE used as two creditable standards besides R^2, so if these standards are less it shows the strong relationship and there is not any specific description for their threshold (*Samadi et al., 2009*). The coefficient of determination R^2 is defined as the squared value of the coefficient of correlation. It is estimated as:

$$R^2 = \frac{\left[\sum_{i=1}^{n}(Q_s - \overline{Q_s})(Q_o - \overline{Q_o})\right]^2}{\left[\sum_{i=1}^{n}(Q_s - \overline{Q_s})\right]^2\left[\sum_{i=1}^{n}(Q_o - \overline{Q_o})\right]^2} \quad (7.4)$$

Where, Q_o= observed flow, Q_s= Simulated flow, $\overline{Q_O}$= Average of observed flow and $\overline{Q_s}$= Average of simulated flow (Moriasi et al, 2007) recommended for monthly time steps that NSE values between 0.75 and 1 is very good and NSE-value between 0.65 and 0.75 is good. Percent Difference ($PBIAS$), The percent difference for a quantity or the percent deviation of stream flows ($PBIAS$) over a specified period with total days calculated from measured and simulated values of the quantity in each model time step is determined using.

$$PBIAS = 100\% \times \left[\frac{\sum_{i=1}^{n} Q_o - \sum_{i=1}^{n} Q_s}{\sum_{i=1}^{n} Q_o}\right] \quad (7.5)$$

where, Q_o = Observed flow, Q_s = Simulated flow. A value close to 0 % is best simulation, negative value indicates model overestimation and a positive value indicate model underestimation.

7.3 Climate model and climate change Scenario

The temporal and spatial resolution disparity between the outputs of the GCM models and the data needed for such impact studies was adjusted using the most common approach called the statistical downscaling and dynamical downscaling method (*Houghton, 2009; Kharin 2007*) and The most appropriate technique for this case study is dynamical downscaling. This method is advantageous as it is easy to implement, and generation of the downscaled values involves observed historic daily data. The latter advantage ensures the maintenance of local spatial and temporal variability in generating realistic time series data. However, the method forces the future weather patterns to only those roughly similar to historic, which is its demerit. The correlation coefficient between the selected stations is carried out in order to find a single station for downscaling purpose that has high

correlation with most of the other neighbouring stations. In addition to the correlation coefficient, the quality, and the available length of period of record also taken into consideration during selection of stations for downscaling (*Field et al., 2012*).

7.3.1 Climate model and descriptions

Climate models are applied as an investigation tool to study and simulate the climate change, and for functioning resolutions, including monthly, seasonal, daily and inter annual climate forecasts. Climate projections are distinguished from climate predictions in order to emphasise that climate projections depend upon the emission/concentration/radiative forcing scenario used, which are based on assumptions concerning. For example, the future socioeconomic and technological developments that either or realised causes uncertainty of the projection. Daily maximum and minim temperature daily Precipitation data reanalysis from the European Centre for medium-range weather forecasts (Russo et al., 2016) are useful to assess the past, present and futuristic climate change impact analysis. The dataset has a daily time based resolution and is available from 1979 to 2016. The data are interpolated to the Coordinated regional downscaling experiment—African Domain (CORDEX-Africa) grid (0.44°, ~50 km) of the projected model data for comparison. For historical and future projections (period 1979–2100) we used daily maximum and minim temperature, daily precipitation data from 13 regional climate model (RCM) simulations of the CORDEX-Africa multi-model scenario. In the set of simulations, 4 RCMs (Russo et al., 2016) are driven by 13 different general circulation models forced with two scenarios, RCP4.5 and RCP8.5 adopted by the Intergovernmental Panel on Climate Change (IPCC) for its fifth Assessment Report (*AR5, Christensen et al 2013; Russo et al., 2016; Schaefer et al., 2014; Russo et al., 2014*). Equivalent climate simulations using the other RCPs (RCP2.6 and RCP6.0) were not available. For the comparison with the reanalysis we use historical simulations (Taylor et al 2012) for the period 1979–2005. Therefore, Swedish Meteorological and Hydrological Institute forced with eight global climate models (CCCma-CanESM2, CNRM-CERFACS-CNRM-CM5, ICHEC-EC-EARTH, IPSLIPSL-CM5A-MR, MIROC-MIROC5, MPI-M-MPIESM-LR, NCC-NorESM1-M, NOAA-GFDL-GFDLESM2M); three CCLM simulations (CLM Community) driven by lateral boundary conditions of three global climate models (CNRM-CM5, EC-EARTH and MPI-ESM-LR) (*Russo et al., 2016; Schaefer et al., 2014; Russo et al., 2014)*

7.3.2 Representative Concentration pathway (RCPs) Scenarios

Representative Concentration Pathways are new scenarios and the four RCP scenarios used in CMIP5 lead to radiative forcing values that span a range larger than that of the three SRES scenarios used in CMIP3 (*IPCC WGI AR5 2011; Mastrandrea et al., 2011*). IPCC WGI Fifth Assessment Report also projected the potential for temperature rises of up to 4.8 °C and sea level rise of up to 0.82 m by 2100 (Stocker, 2013; Metz et al., 2001). Global mean temperature projected changes range from 4.7°–8.6°F (2.6°–4.8°C) under the higher scenario (RCP8.5) to 0.5°–1.3°F (0.3°–1.7°C) under the much lower scenario (RCP2.6) (*Hayhoe et al., 2017*). The spread of projected global warming with the RCP scenarios is much larger than with SRES scenarios (IPCC, AR5). RCP scenarios (*Moss et al., 2010; Thomson et al., 2011*) have been applied to prescribe future radiative forcing. Greenhouse gas concentrations are expressed as equivalent CO_2 concentrations, following the RCP scenarios, and interpolated from one year to the next. Here we use three different RCP scenarios: RCP 2.6: Strategies for reducing greenhouse gas emissions cause radiative forcing to stabilise at 2.6 W/m² before the year 2100 (used by IPCC, AR5). RCP 4.5: Strategies for reducing greenhouse gas emissions cause radiative forcing to stabilise at 4.5 W/m² before the year 2100 (used by IPCC, AR5). RCP 8.5: Increased greenhouse gas emissions mean that radiative forcing will reach 8.5 W/m² by the year 2100 used by IPCC, AR5 (*Castillo et al., 2005; Riahi et al., 2011; Pachauri et al., 2014*).

7.3.3 Bias correction method of downscaled climate data

The downscaled RCPs data cannot be directly used for impact assessment as the computed variables may differ systematically from the observed ones. Bias correction is therefore applied to compensate for any tendency to overestimate or underestimate the mean of downscaled variables. Bias correction factors are computed from the statistics of observed and simulated variables (*Teutschbein and Seibert 2012; Leander and Buishand 2007*). Two bias correction methods were tried in this study. First, the nonlinear bias correction method proposed by (*Mangiestu 2009*) and the second method called “delta approach”. The formulas used for rainfall and temperature bias correction are indicated in Equations 7.13 and 7.14. The formulas used for the correction of rainfall and temperature bias are shown in linear and power function. Factors of correction for each month of climatic variable were calculated.

7.3.3.1 Bias Correction Using Delta Change Method

The Delta Change technique is generally used for future climate change forecast (*Maraun and Widmann, 2018; Maraun et al., 2018; Beyer et al., 2019*) instead of directly using the RCM

simulation (*Teutschbein and Seibert, 2012*). In this study, the Delta Change method was used for correct precipitation and temperature data in Upper Omo Gibe River Basin.

$$P_{corr}(d) = P_{obs}(d) \times \left[\frac{\mu_m(P_{corr}((d))}{\mu_m(P_{raw}(d))}\right] \quad (7.6)$$

$$T_{corr}(d) = T_{obs}(d) + \mu_m(T_{corr}(d)) - \mu_m(T_{raw}(d)) \quad (7.7)$$

where P_{corr}, $P_{obs,}$ and P_{raw} denote corrected observed, and uncorrected, precipitation, respectively, while T_{corr}, T_{obs}, and T_{raw}, are observed, uncorrected, and corrected temperature on the day (d^{th}) of the month (m) respectively, and μ_m denotes the mean.

7.3.3.2 Bias Correction Using Linear Scaling Method

Linear Scaling technique was used to correct the monthly values depending on the long term monthly average of observed and simulated. This system does not correct the bias in frequency and intensity distribution (*Ines and Hansen, 2006*). The rainfall and temperature data were adjusted using equation, respectively according to (*Teutschbein and Seibert, 2012, Fang et al., 2015, Smitha et al., 2018*).

$$P_{corr,m,d} = P_{raw,m,d} \times \left[\frac{\mu(P_{obs,m})}{\mu(P_{raw,m})}\right] \quad (7.8)$$

$$T_{corr,m,d} = T_{raw,m,d} + \mu(T_{obs,m}) - \mu(T_{raw,m}) \quad (7.9)$$

where, $P_{obs,m,}$and $T_{obs,m}$denote the observed precipitation and temperature on a month (m), and, $P_{corr,m,d}$ $T_{corr,m,d}$ and $T_{raw,m,d}$ are corrected and uncorrected temperature and precipitation on the day (d^{th}) of the month (m) respectively. ($\mu(P_{obs,m,}$) ($\mu(P_{raw,m}$) denote the mean value of observed and uncorrected precipitation on the month (m), respectively.

7.3.3.3 Bias Correction Using Power Transformation Method

Using Power Transformation method further adjusts the bias in standard deviation and variance using an exponential form (*Teutschbein and Seibert, 2012, Leander and Buishand, 2007*). The Power Transformation technique was used only for rainfall data due to the use of power function.

$$f(bm) = \left[\frac{\delta_m(P_{obs}((d))}{\mu_m(P_{obs}(d))} - \frac{\delta_m(p_{raw}^{bm}((d))}{\mu_m(P_{raw}^{bm}(d))}\right] \quad (7.10)$$

$$P_{corr}(d) = p_{raw}^{bm}((d) \quad (7.11)$$

$$P_{corr}(d) = P_{corr}(d) \times \left[\frac{\mu_m(P_{obs}((d))}{\mu_m(P_{corr}(d))}\right] \quad (7.12)$$

where $P_{obs}((d)$ andP_{raw} are the observed and uncorrected daily RCM precipitations on the day (d) respectively. δ_m and μ_m denote the mean and standard deviation on a month (m), and is the exponent for the month.

7.3.3.4 Precipitation Bias Correction

In the bias correction technique, nonlinear correction each daily precipitation amount P is transformed to a corrected P* a power transformation equation have been used.

$$P^* = aP^b \quad (7.13)$$

Where P* is the simulated data in the projection period, where 'a' and 'b' are the parameters obtained from calibration in the baseline period and subsequently applied to the projection period. They are determined by matching the mean and coefficient of variation (CV) of simulated data with that of observed data (*Mangiestu 2009; Leander & Buishand 2007)*).

7.3.3.5 Temperature Bias Correction

For temperature, monthly systematic biases were calculated for the baseline period by comparing RCPs outputs with the observations.

The monthly mean biases correction has been calculated according to the following Equation (*Ashley 2005*)

$$T_x = T_{om} + \frac{\delta t}{\delta i}(T_i - T_{im}) \quad (7.14)$$

where; T_x is bias corrected future temperature, T_{om} is mean of observed temperature in base period, T_{im} is mean of RCPs temperature in base period and T_i is RCPs temperature of base period δ_i and δ_t, represent the standard deviation of the daily RCPs output and observations in the reference period respectively.

The correction of precipitation and temperature leads to satisfactory result in hydrological impact studies. This includes the temporal extent and temporal resolution, but also on the spatial resolution of the observational data each of with have varying importance depending on the method and the main purpose of the bias correction (*Peter et al., 2010; Robbert and Adri 2006*). Therefore, bias corrections for maximum and minimum temperature and precipitations at each selected stations are studied in this research. The bias correction is done for selected stations for the RCM data. Thereafter, the bias corrected data is spatially interpolated for the study region (Figure 7.3).

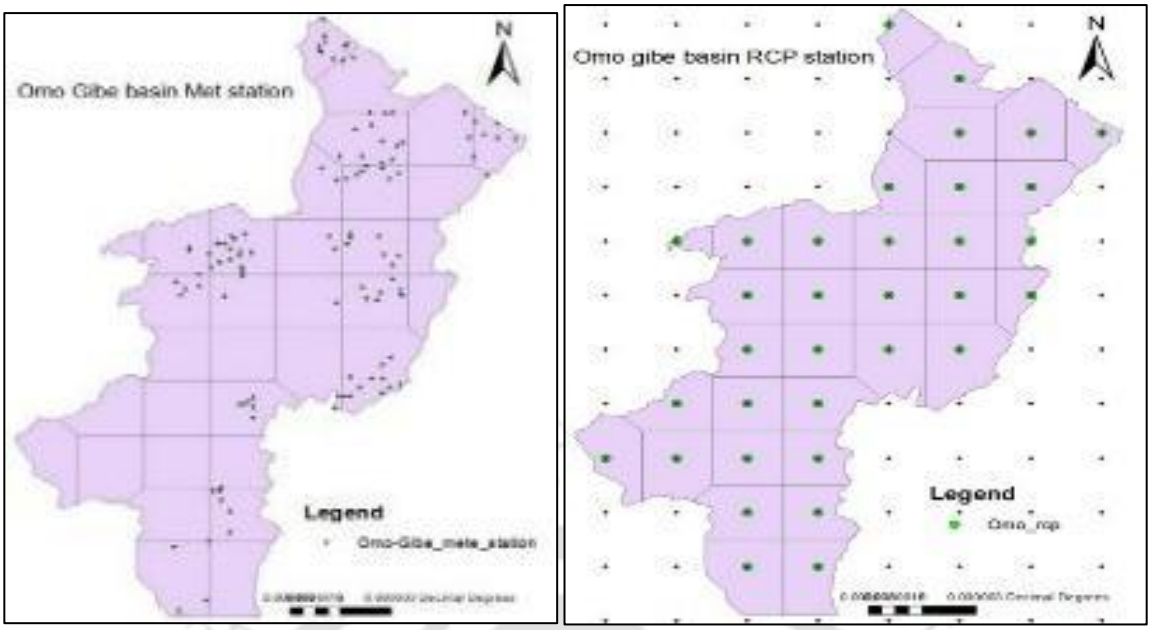

Figure 7.3 Omo Gibe basin both observed and RCP station location.

7.3.3.6 CMhyd (Climate Model data for hydrologic modelling) tools methods

Bias correction processes are used to minimize the inconsistency between observed and simulated climate variables on a daily time step or monthly time step. CMhyd is a tool that can be used to extract and bias-correct data obtained from global and regional climate models. Eight bias correction methods have been implemented into CMhyd.

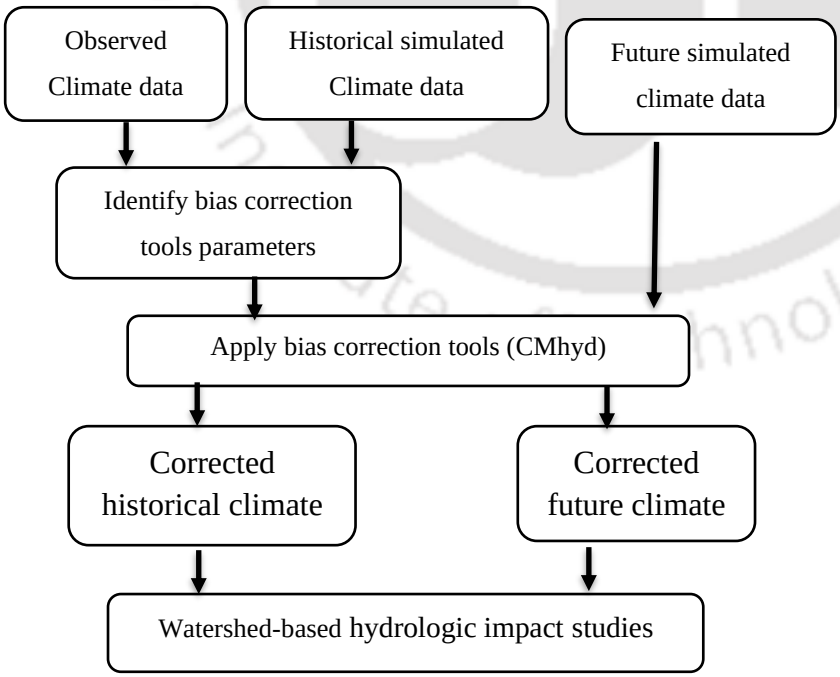

Figure 7. 4 Bias correction flowchart

7.4 Results and discussions

7.4.1 Using RCP Scenarios

RCP Scenarios is used to forecast temperature and rainfall time sequence data from regional climate outputs of Coordinated Regional Climate Downscaling Experiment (CORDEX)-Africa. For the three RCP scenarios (RCP2.6, RCP4.5, and RCP8.5), three periods are analysed - base or historical time (1985–2005), mid-term (2030–2050), and long-term (2070–2090) scenario.

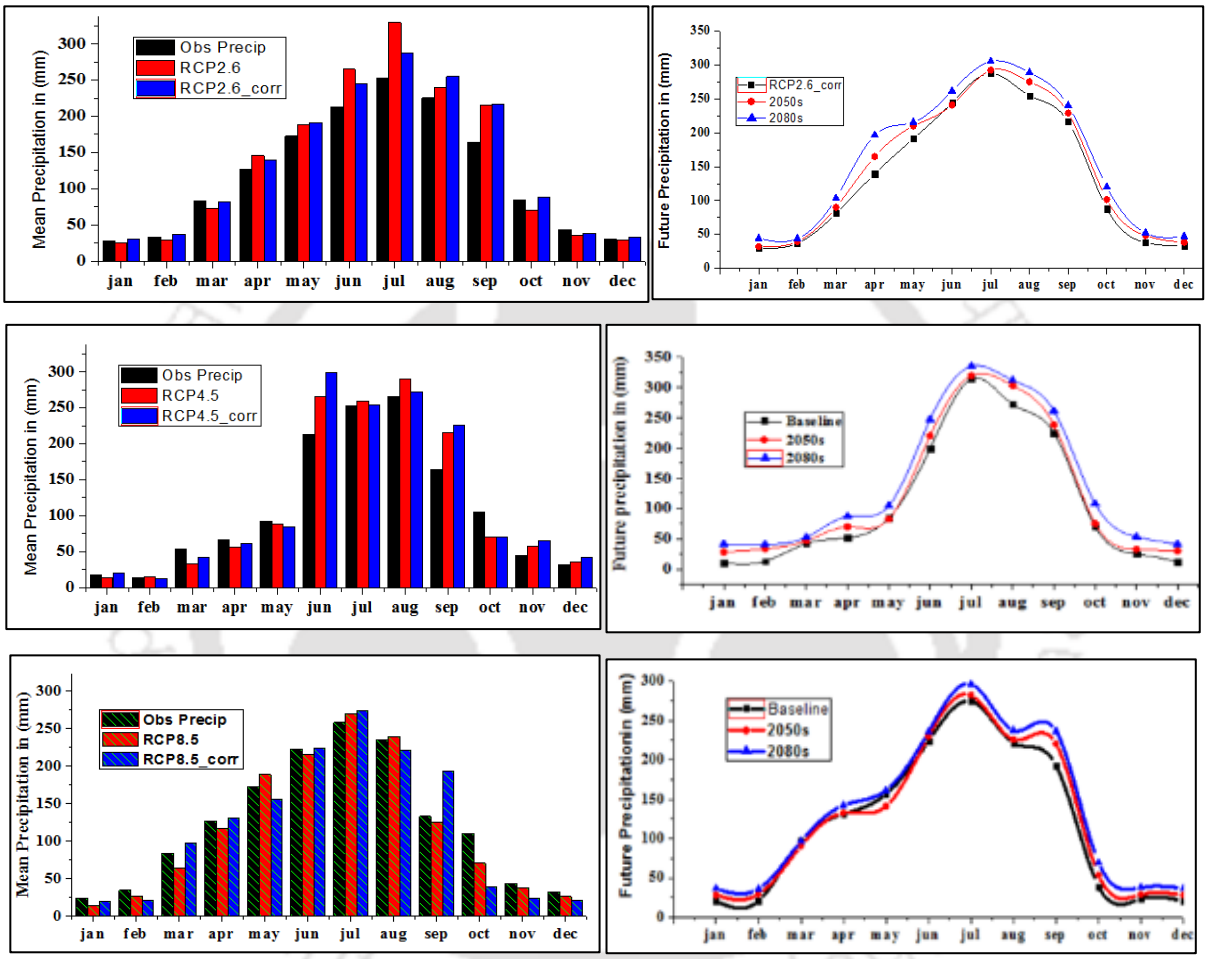

Figure 7.5 Bias corrected precipitation future 2050s and 2080s in Upper Gibe catchment.

Since the output of GCM is not directly used for climate change impact assessment on water resource, bias corrections have been done for the base period using the measured weather data at each selected stations. As seen in Figure 7.5, the estimate for precipitation for the base period using RCP 2.6, RCP4.5 and RCP8.5 data for each station was not good before the bias corrections are applied. Therefore, to adjust and minimize the variation in observed and estimated precipitation bias corrections are essential. On applying the monthly bias correction for the base period, the RCP and observed precipitation exactly match at the station (Figure 7.6). Note that, the power correction for

precipitation and linear correction for temperature were adopted for this study to correct the future precipitation and temperature.

7.4.2 Percentage Change in precipitation in Upper Gibe Basin.

Climate model output is used to simulate the future impacts of climate change on a stream flow. As precipitation is the main driving force for generating streamflow at catchment level, therefore the change in precipitations due to climate change affects the streamflow. Figure 7.6 shows long term (2080s) and midterm (2050s) predictions for precipitation using RCP2.6, RCP4.5, and RCP8.5. The percentage change of monthly precipitation shows an increasing trend during the 2050s and 2080s while using RCP8.5 scenarion. The same shows decreasing trends during the 2050s and 2080s while using RCP2.6 (Figure 7.6, 7.7, 7.8). The predictions using RCP2.6 and RCP4.5 shows increasing trend, while RCP8.5 summer season shows decreasing trend with increasing winter and spring season precipitation.

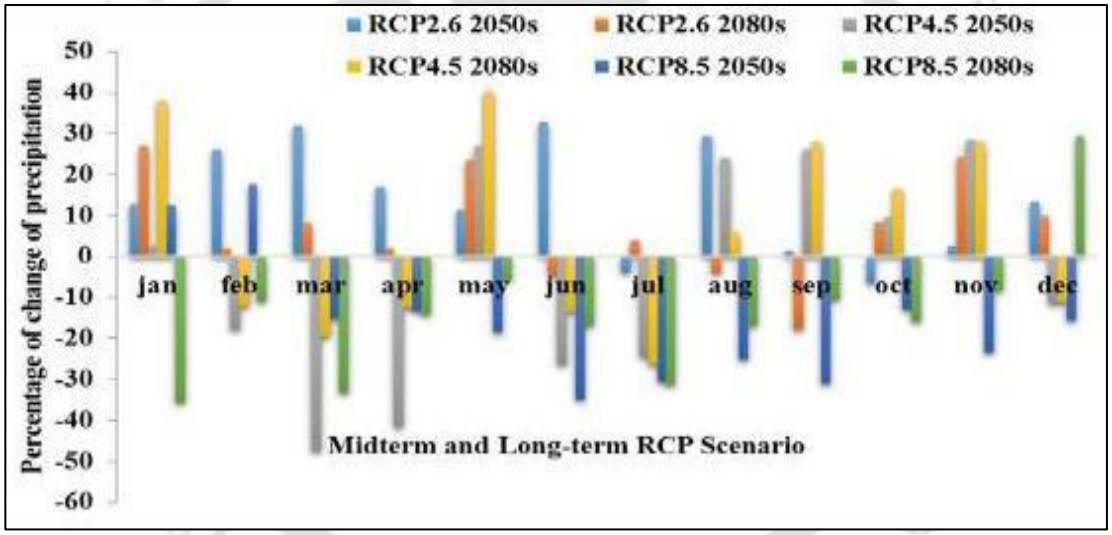

Figure 7.6 Percentage change of precipitation in Upper Gibe catchment.

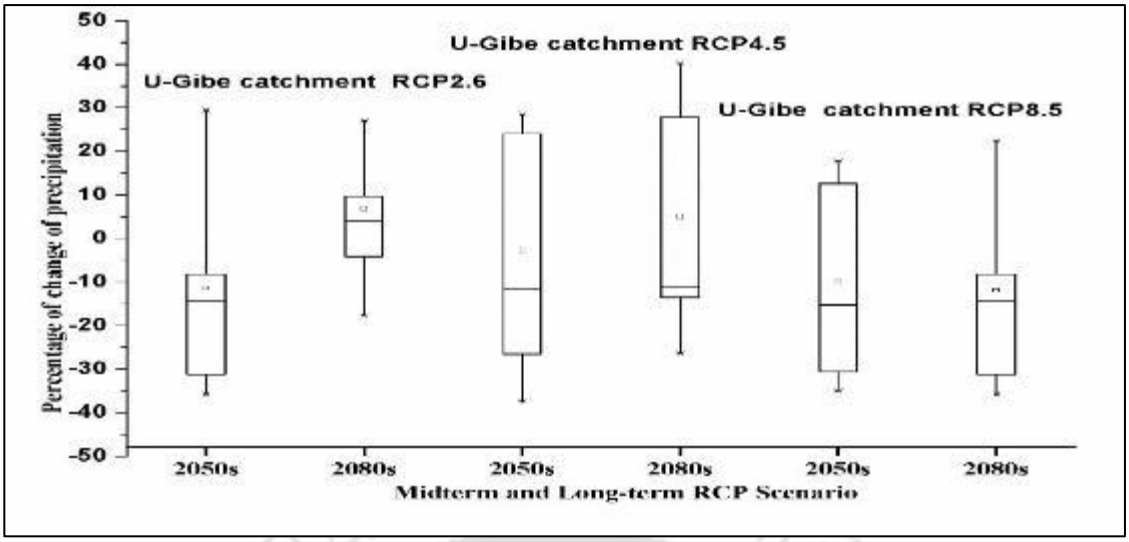

Figure 7. 7 Box plot Percentage of Change of Precipitation Comparing all Three Scenario

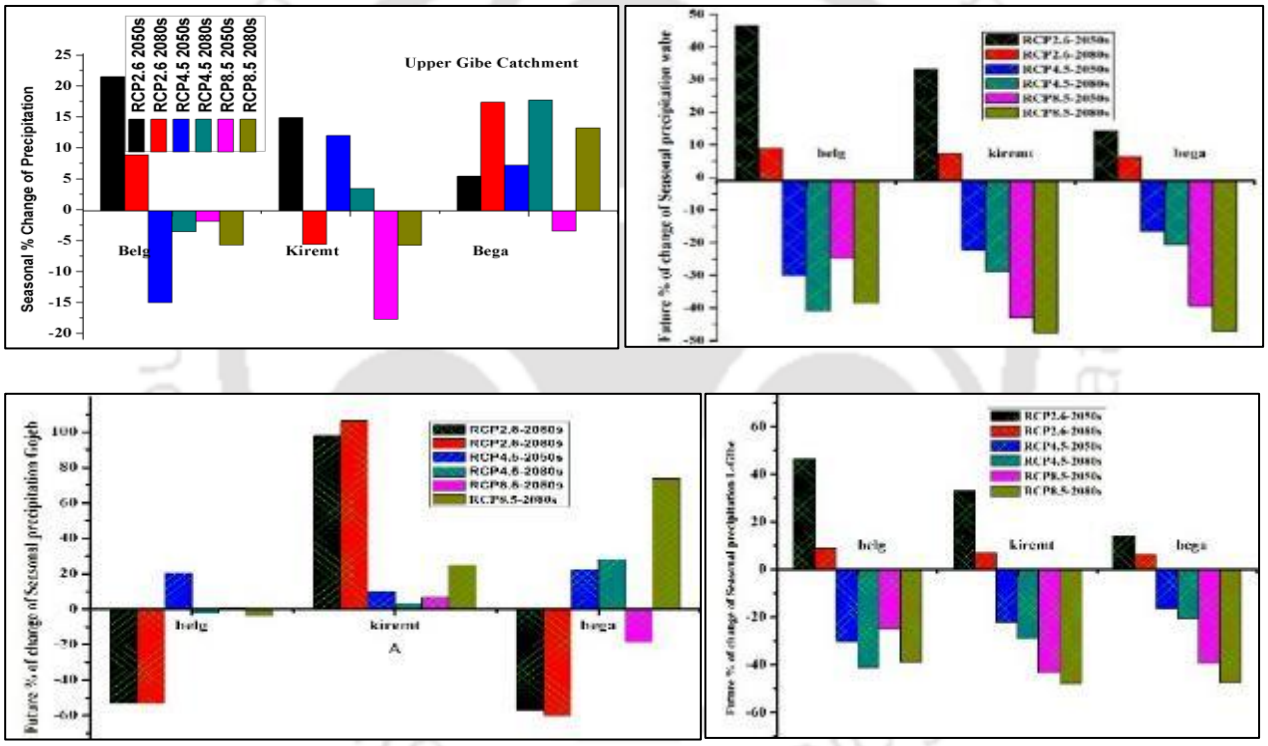

Figure 7.8 Seasonal variation of precipitation pattern in Upper Gibe, Lower Gibe Wabe and Gojeb. Catchments

Maximum and minimum Temperature after bias correction in (Figure 7.9 and Figure 7.10) shows that the RCP and observed precipitation exactly tie at the station. Note that, the linear correction were adopted for this study and the coefficient "a" and "b" were used to correct the future temperature.

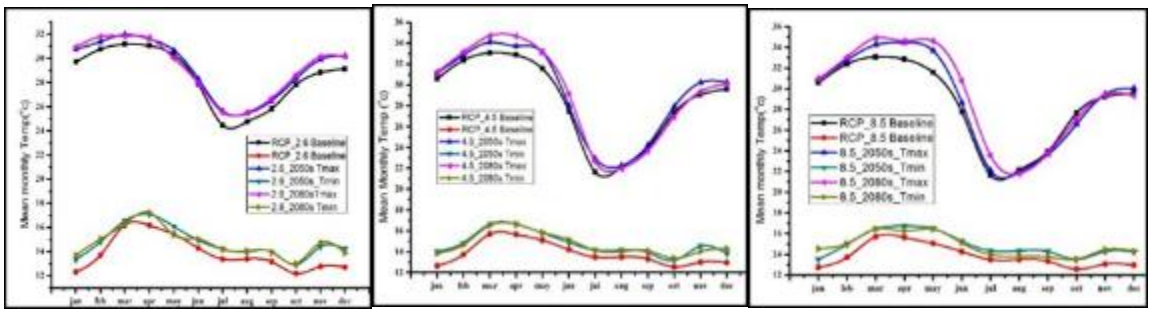

Figure 7. 9 Bias corrected average future temperature at Upper Gibe catchment

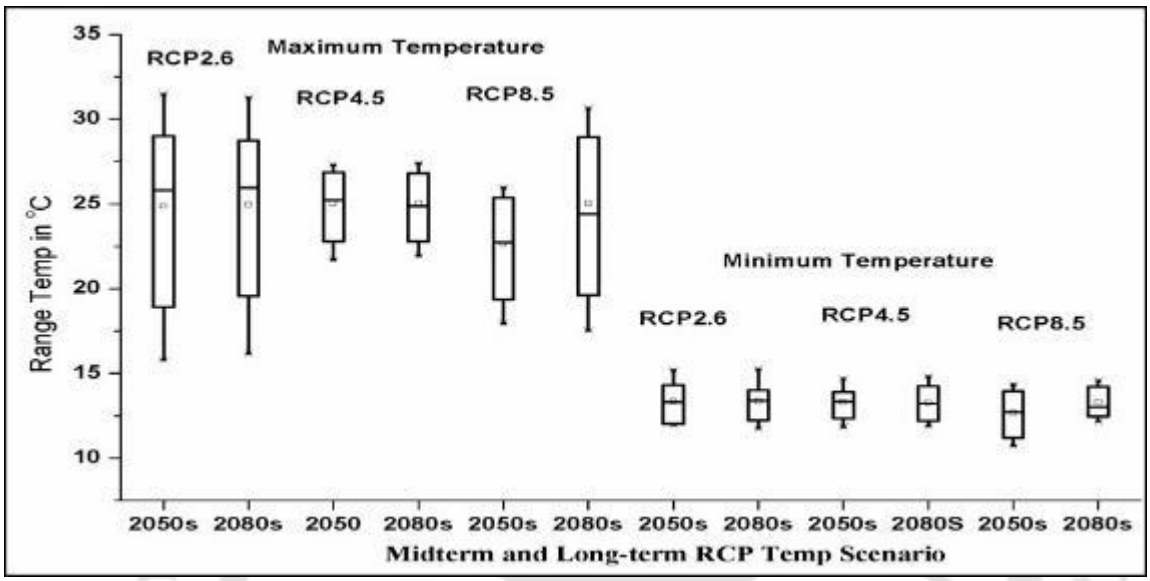

Figure 7. 10 Box plot future temperature comparing all three scenario in Upper Gibe catchments

7.4.3 Seasonal variation of maximum and minimum temperature in RCP scenario

Global surface temperature change for the end of the 21st century is projected to likely be in the ranges of 1.5–2.0 °C relative to 1850–1900 (IPCC, 2013; Sun, 2013).). The future projection of maximum and minimum temperature under RCPs indicate increasing trend for all months. An increase in the monthly mean temperatures in the warm and cold season in all areas of upper Omo Gibe based on RCP scenario approximately from the base time 2005s to the mid-term the 2050s and long-term 2080s as shown (Figure 7.10) discussed that Climate models are used for a variety of purposes from the study of under currents of the weather and climate system to forecasts of upcoming climate. RCPs assess the results of the historic or baseline data (1985-2005) relating with midterm and long-term future climate scenarios. It shows the future projection of maximum temperature under RCP 8.5 have increasing trend for all months and the average annual maximum temperature increased with the rate of 0.51°C to 0.95°C. However, for RCP 4.5 the rate of increase was from 0.75°C to 0.78°C and for RCP 2.6 it was 0.75°C to 0.79 °C in 2050s and 2080s, respectively. The future projection of minimum temperature show increasing trends for all months

in these three RCP scenarios. The average annual minimum temperature shows decreasing trends from 1.03°C to 0.97°C for RCP 8.5. However, it shows increasing trends for RCP 4.5 (from 0.90°C to 0.928°C) and RCP2.6 (0.92°C to 0.94°C) in 2050s and 2080s, respectively.

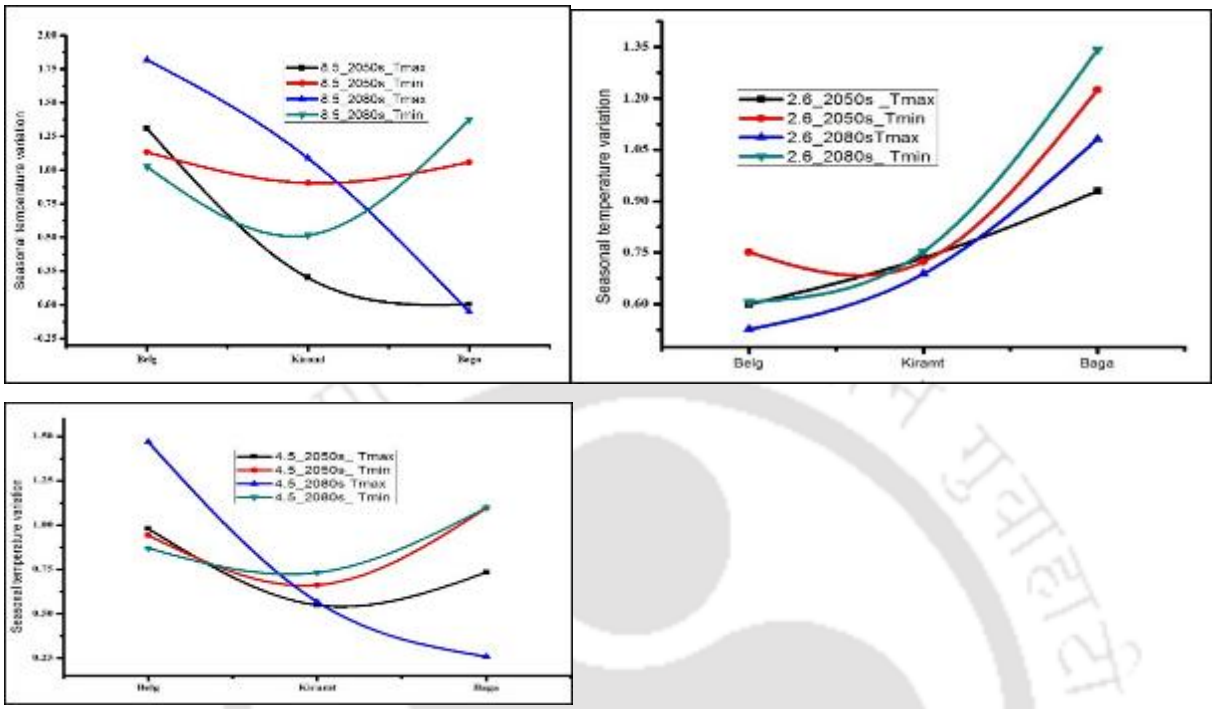

Figure 7.11 Average maximum and minimum future seasonal temperature scenario.

7.4.4 Temperature anomaly of Upper Omo Gibe Catchment

The mean maximum and minimum temperature for all scenarios can be found to have an increasing trend, but a higher degree of increase can be projected in the RCP8.5 scenarios for upper Omo Gibe catchment. The average annual maximum and minimum temperatures for the base time, mid-term, and long-term using RCP 2.6, RCP 4.5, and RCP 8.5 emission scenarios are plotted. Temperature anomaly is increasing as per the trend line in upper Omo Gibe catchment.

From the climate change scenarios in (Figure 7.11) shows that, the average annual maximum temperature increase in Belg and bage, decrease in Kiremt. This change indicates that seasonal change in the catchment is happening. The seasonal rainfall at Wabe catchment in (Figure 7.11) with three seasons' bega (dry season), kiremt (main rain season) and belg (small rain season) shows that increasing trend in mid-term 2050s to long term 2080s in RCP2.6 and the decreasing trends in both RCP4.5 and RCP8.5.

7.4.5 Percentage change of precipitation of some sub-catchments of Upper Omo Gibe

In the same way percentage change of precipitation is carried out in some sub-catchments of Upper Omo-Gibe (Upper Gibe, Lower Gibe, Upper Wabe, Lower Wabe, Great Gibe, and Gojeb). Great Gibe Catchment summer precipitation shows increasing and Gojeb catchment decreasing in winter and spring season for RCP2.6 and increasing trends in both RCP4.5 and RCP8.5 future scenario. This indicates that the pattern of precipitation change from historical and reflect seasonal shift might be observed in the catchment.

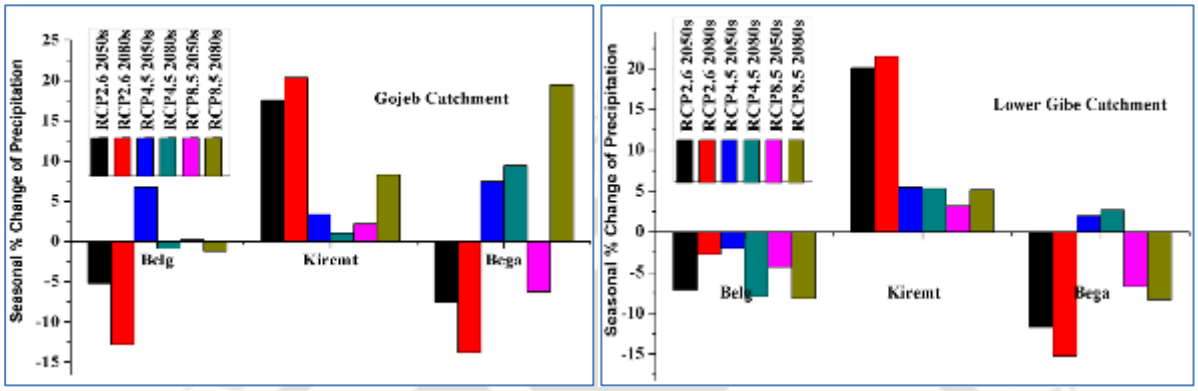

Figure 7.12 Future projection of seasonal variation of precipitation pattern in Gojbe and Lower Gibe Catchments by using RCP2.6 RCP4.5 and RCP8.5 scenario

Mean monthly percentage of change of future precipitation in (Figure 7.13) for RCP2.6, RCP4.5, and RCP8.5 scenarios in Lower Gibe and Gojeb catchments are increasing for summer main rainy season for short-term, mid-term, and long-term scenarios. However, the same is having decreasing trend in winter or spring dry season while using RCP2.6 and RCP8.5 at Lower Gibe catchment. Also, RCP4.5 in Gojeb catchment shows increasing trend in both long-term and mid-term scenarios.

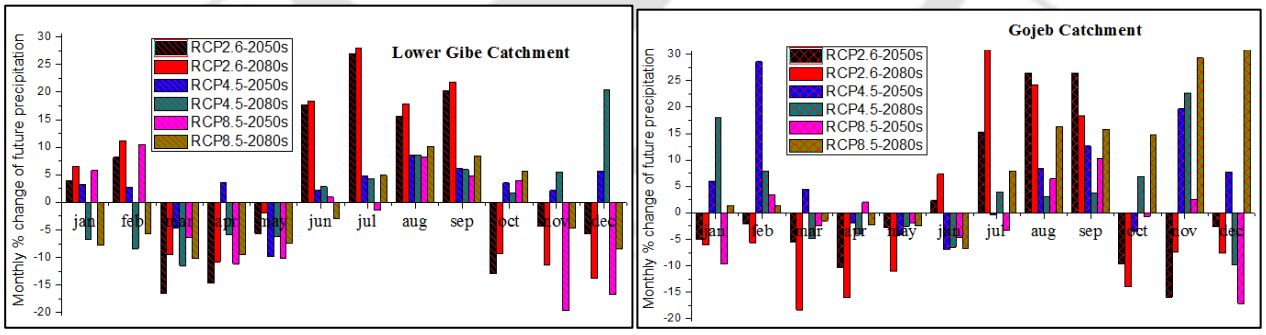

Figure 7.13 Percentage of change of future precipitation in Lower Gibe and Gojeb catchments

The future climate change projections for Gibe-III was assessed by RCPs for the midterm and long-term projections of precipitation and temperature. Seasonal variation of precipitation in Gibe-III dam site catchment in (Figure 7.14 and Figure 7.15) shows that summer precipitation has increasing trend from 12.63% (midterm) to 13.95% long-term in RCP2.6 and has the same trend in RCP8.5 but a decreasing trend in RCP4.5 from 3.61% midterm to 3.11% long-term in a dam site

catchment. This variation has shown the future pattern of precipitation shift from summer to winter and from winter to spring seasons.

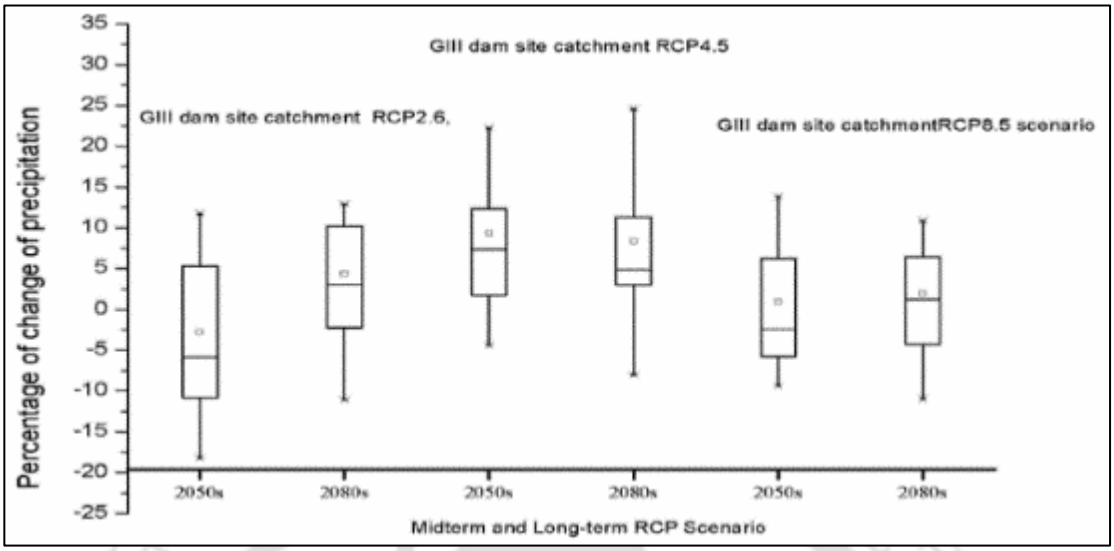

Figure 7.14 Box plots Percentage of change of future precipitation in GIII catchment

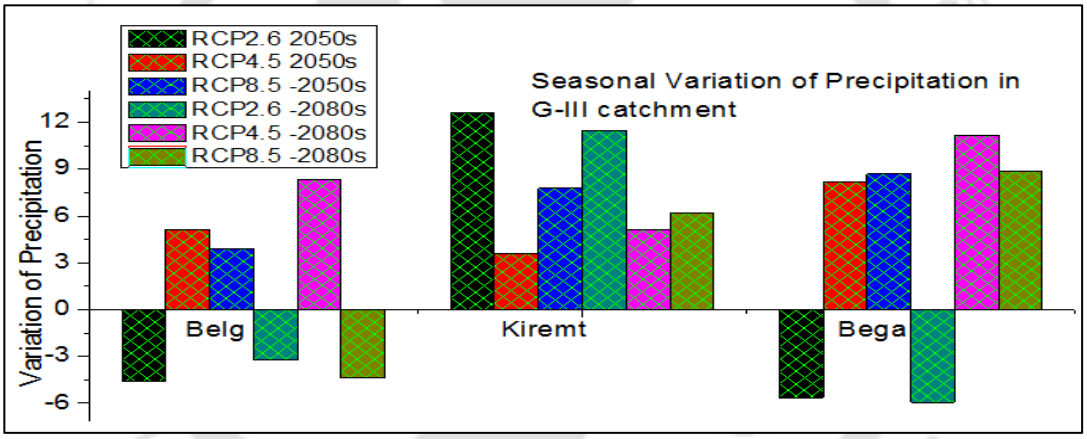

Figure 7. 15 Seasonal Variation of Precipitation in GIII dam site catchment

From the Table 7.1, it is obvious that G-III percentage change of precipitation for future long-term and midterm mean annual change is having increasing trend from 2.41 % to 16.88% while using RCP2.6. Similarly, the percentage change has increasing trend from 16.34 20.63% while using RCP4.5.

Table 7.1 percentage change of Seasonal Precipitation in Gibe-III dam catchment

Season/ RCP	% of change of Seasonal Precipitation in Gibe-III dam catchment					
	RCP2.6 2050s	RCP2.6 2080s	RCP4.5 2050s	RCP4.5 2080s	RCP8.5 2050s	RCP8.5 2080s
Belg	-4.58	5.11	3.89	3.23	8.29	-4.37
Kiremt	12.63	3.61	3.77	11.45	5.11	6.19
Bega	-5.64	8.16	8.69	5.94	11.18	8.89

Annual	2.41	16.88	16.34	20.63	24.57	10.71

7.4.6 Rainfall Frequency Analysis of sub-catchments of Omo Gibe Basin

Rainfall Distribution from 2003 to 2018 as defined on the map Figure 2.3 and Figure 2.4 (in Chapter-2) show that the upstream part of the basin is more intense, the downstream part is less intense, and middle parts of the basin show moderate distribution. Hydrologic systems are occasionally impacted by extreme events such as severe storms, floods, and droughts. The magnitude of an extreme event occurs less frequently than events that are more moderate. The objective of frequency analysis of hydrologic data is to relate the magnitude of extreme events to their frequency of occurrence using probability distributions. The main application of frequency analysis of rainfall for flood predicting at Gibe III dam site catchment may give different outcomes based on the return period of future precipitation of RCP climate scenario comparing base time precipitation in different sub-catchments of Omo-Gibe catchment (Upper Gibe, Lower Gibe, Upper Wabe, Lower Wabe, Great Gibe, and Gojeb). Figures are plotted with different time based on the different year's return period. The annual precipitation change in percentage of rainfall magnitude shows increasing trends in both midterm and long-term scenario with increasing return period like (5, 10, 15, 20, 25, 50, 100, 150, 200, 500, and 1000) years for RCP2.6, RCP4.5, and RCP8.5 as compared to the base time scenario. The RCP8.5 high scenario shows slight increase in the 2080s than in 2050s scenario in Wabe and Gojeb catchments (Figure 7.15). Upper Gibe and Lower Gibe have somewhat decreasing trends in 2080s for RCP2.6 scenario in the 2050s (midterm) and the 2080s (long-term). Besides, the analysis indicates that overall there is increasing trend in both midterm and long-term in predicting rainfall magnitudes in all RCP2.4, RCP4.5, and RCP8.5. In (Figure 7.17) the magnitude of rainfall frequency curve with for upper Omo Gibe catchment for different return period (mid-term and long –term) is compared to base time RCP2.6 scenarios.

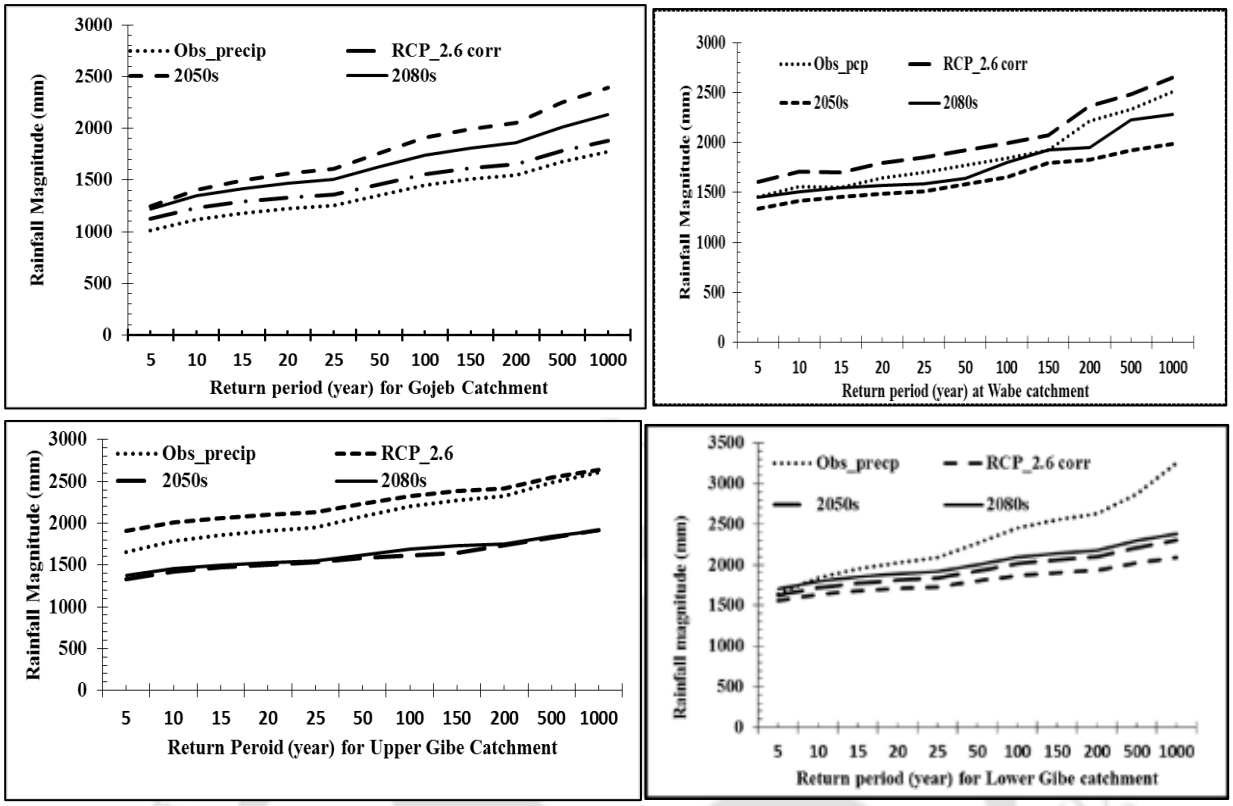

Figure 7. 16 Rainfall frequency curve for Upper Gibe catchment 2050s and 2080s

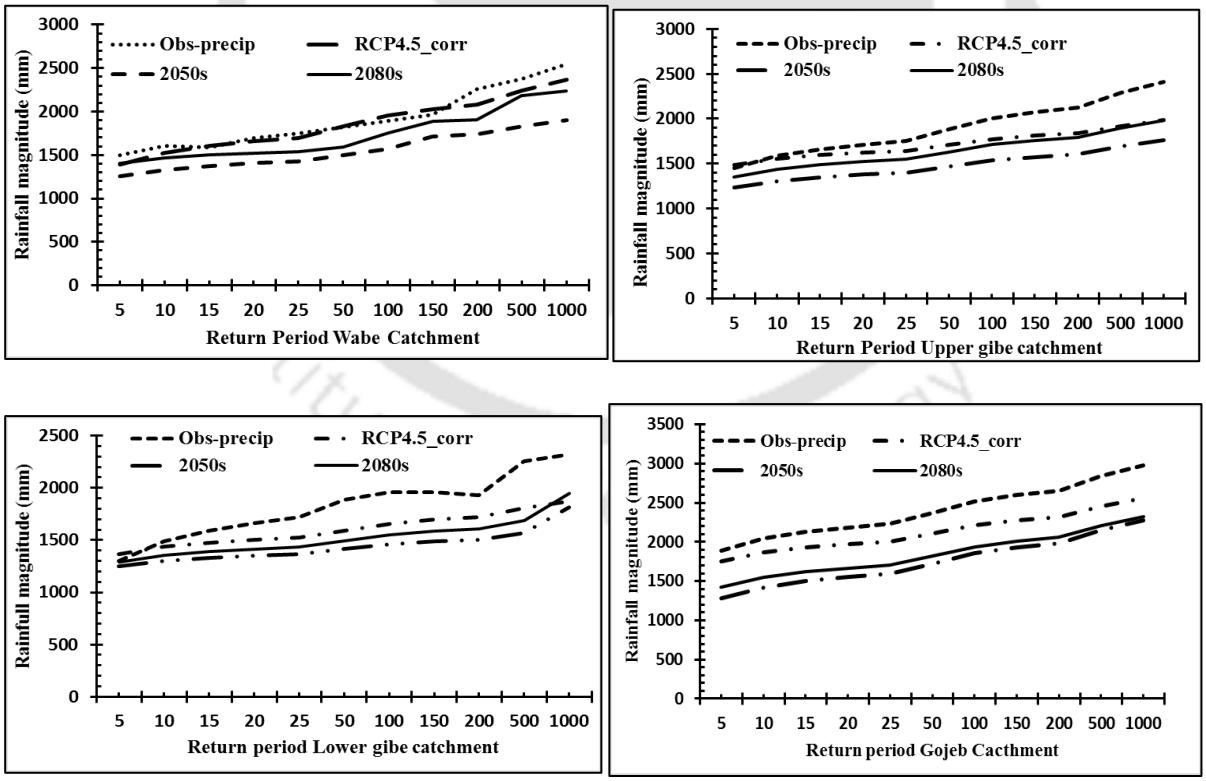

Figure 7.17 Rainfall frequency curve with for Upper Omo Gibe 2050s and 2080s

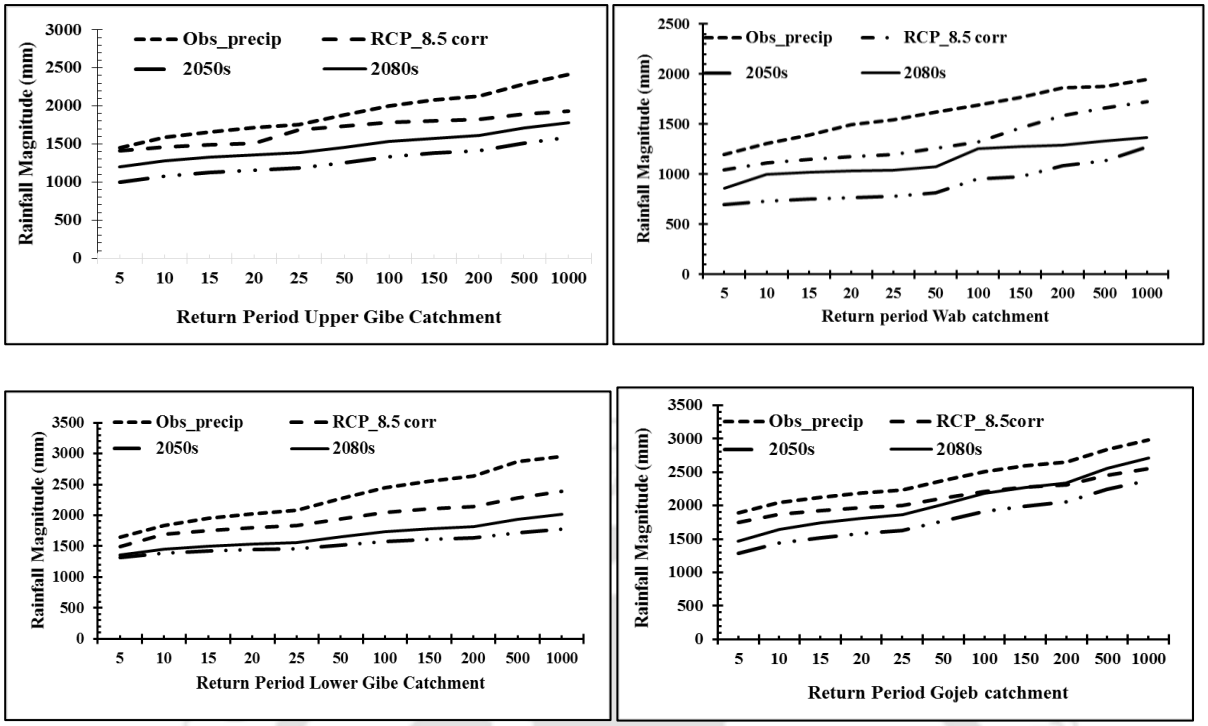

Figure 7.18 Rainfall frequency curve for Upper Gibe catchment using RCP8.5

7.4.7 Flood frequency analysis in Gibe III dam site Catchment considering climate scenario

Using midterm (2050s) and long-term (2080s) scenarios, increasing trends in the magnitude of flood frequency under RCP2.6, RCP4.5, and RCP8.5 scenarios. The flood frequency curve with a return period shows a rising trend, as seen in Figures 6.18 and 6.19. The magnitude of the 1000-year return period flood appears to be increasing in future forecasts using the RCPs emission scenario.

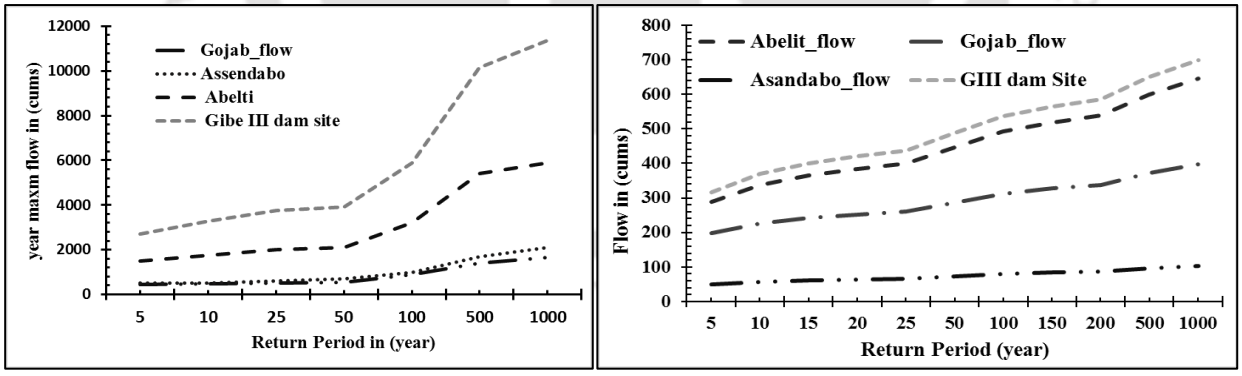

Figure 7.19 year and daily maximum flood frequency curve

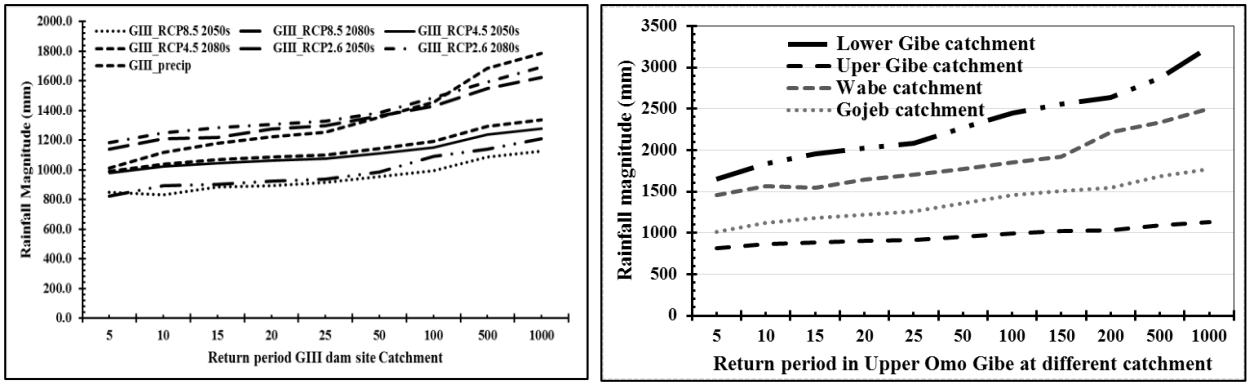

Figure 7.20 Upper Omo Gibe and GIII- dam site catchment rainfall frequency analysis

Therefore, Upper Omo Gibe III dam site catchment for both long-term and midterm scenario shows increasing trends as compared to base line scenario by using RCP2.6, RCP4.5, and RCP8.5 scenario. In (Figure 7.20) flood frequency curve for Abelti, Gojeb, Assandabo and Gibe III dam site catchment the maximum daily discharges and year average river flow with different time of return period is shown. Figure 7.19 and Figure 7.20 shows the Upper Omo Gibe and Gibe III dam site catchment rainfall indicates that with different return period and in both long-term and midterm scenario shows increasing trends. The figure reveals that catchment flow is increasing in Gibe III dam site cathment because of increasing trend of rainfall in both midterm and longterm scenarion.

7.4.8 Impact of hydrological event on Gibe-III dam site catchment.

The discharge from Upper Omo Gibe Basin is the main inflow or contributor for GIII reservoir, which has an area of approximately 34000 sq. km. The regional regression analysis has been applied to analyse the runoff probability curves obtained for the Asandabo, Abelti and Gojeb stations. The impact of climate change on hydropower systems and dam safety assessment is integrated in this study to find the changes in design floods due to climate change. The result of the study shows that the daily maximum flood and year average flood increasing with increasing return period for both rainfall magnitude and runoff in the basin, and this trend indicates that it will affect the safety of the dams in the future as compared to the proposed flood of GIII dam. Therefore, the impact of climate change is to create high or low unusual precipitation patterns. If precipitation is increased, surface water and soil moisture will increase that can positively or negatively affect the reservoir safety. Upper Omo Gibe basin have complex natural resource and rugged topography. The uneven use of natural resource has lead to erosion and sedimentation in reservoir. Safe natural resource management in Upper Omo Gibe basin is very important to keep up Gibe III dam from unexpected high flood and sediment deposition.

7.4.9 Impact of precipitation and evaporation on stream flow.

Climate change will affect the hydrology of the basin and mostly through changes in precipitation and temperature regimes. Temperature is an important factor monitoring many environmental and physical processes of the catchment. Temperature affects the rate of evapotranspiration and surface water moisture that has an impact on the water system. Because of increasing temperatures and increasing surface soil dryness, the catchment hydrological processes are affected. Therefore, integrated land and water management practices through considering climate change impact is crucial to develop different water management scenario and for sustaining the water resources in the area. Changes in temperature, precipitation, and local extreme climatic events have the response changes in water flow and level leading to loss of aquatic habitats, waterfowl, and recreational opportunities. Increasing precipitation lead to increased surface water potential and soil moisture, but decrease in precipitation lead to decreasing surface water and increase in drying of soil moisture. Therefore, precipitation directly relates with surface water and inversely relates with evapotranspiration.

7.4.10 Using Regional Climate Model (RCM) model

Climate change is having an irregular impact on all the weather parameters either in positive or negative perspective. RegCM3 forced by ECHAM5 model provide weather outputs for future scenarios. The baseline period is considered from 1991 to 2000. The future scenarios will be developed by dividing the future time series into two periods of 10 years: 2031-2040 and 2091-2100. Varying precipitation patterns such as extreme events, and shorter but more intense rainfall, can have negative straight and unintended influences on surface stream flow, impact on healthiness and contribute to desertification and inundating, food insecurity, migration and increased water resource conflict on upstream and downstream development basin water potential. Precipitation and temperature produced by RCM for existing and future scenario climates (Figure 7.22) and based on RCM bias corrections for precipitation and temperature. Bias correction is important for coupling of high resolution driving data produced by regional climate models (RCM) and hydrological catchment models.

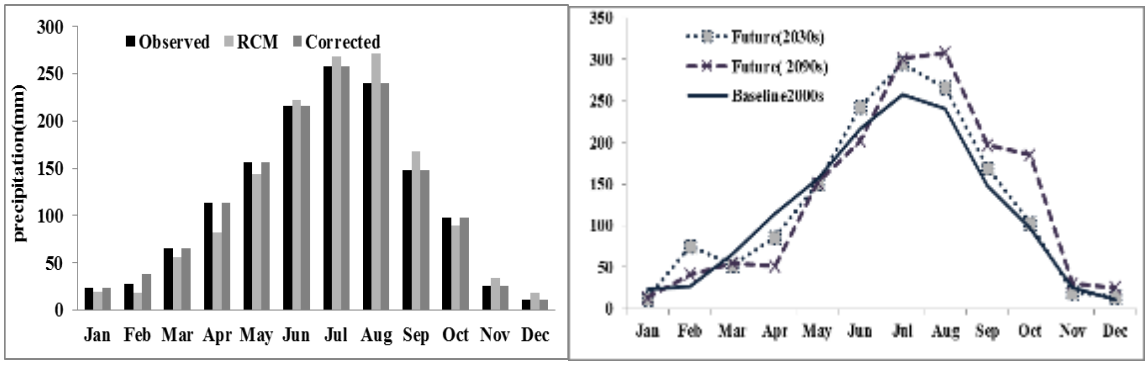

Figure 7.21 Bias-corrected precipitation, at Upper Gibe catchment

The importance of the bias correction depends mostly on the values of the observation. In Figure 7.22, bias-corrected average maximum and minimum future temperature at Upper Gibe is compared with baseline period for the future 2030s and 2090s and it shows increasing trends. However, in Figure 7.24, the bias corrected precipitation at great Gibe is compared with baseline period for the future midterm and long-term scenarios and it shows rising trends.

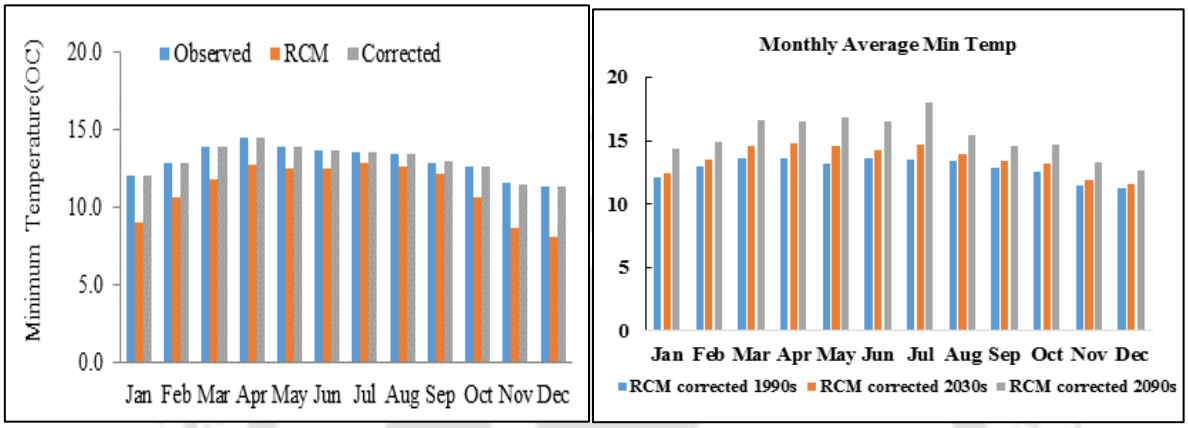

Figure 7.22 Max and min temperature in Upper Gibe for period 2030s and 2090s.

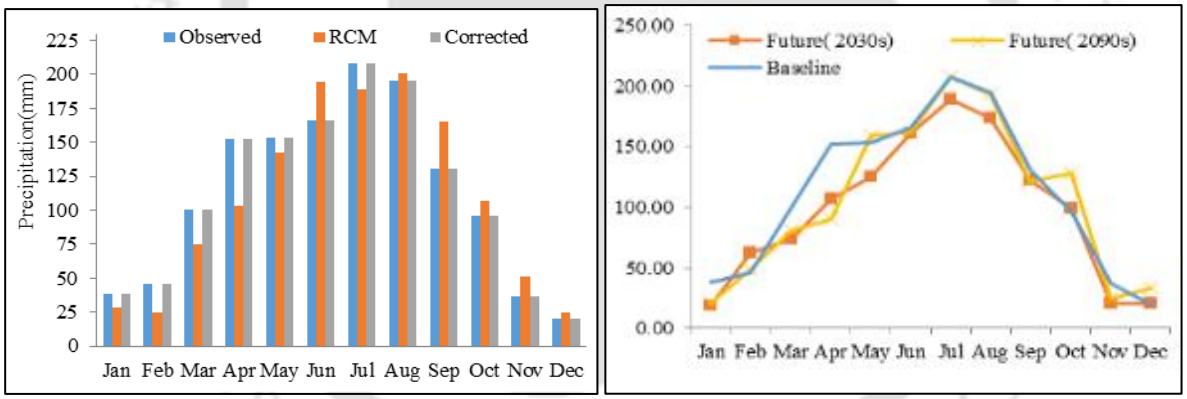

Figure 7. 23 Great Gibe catchment precipitation for midterm and long term scenarios

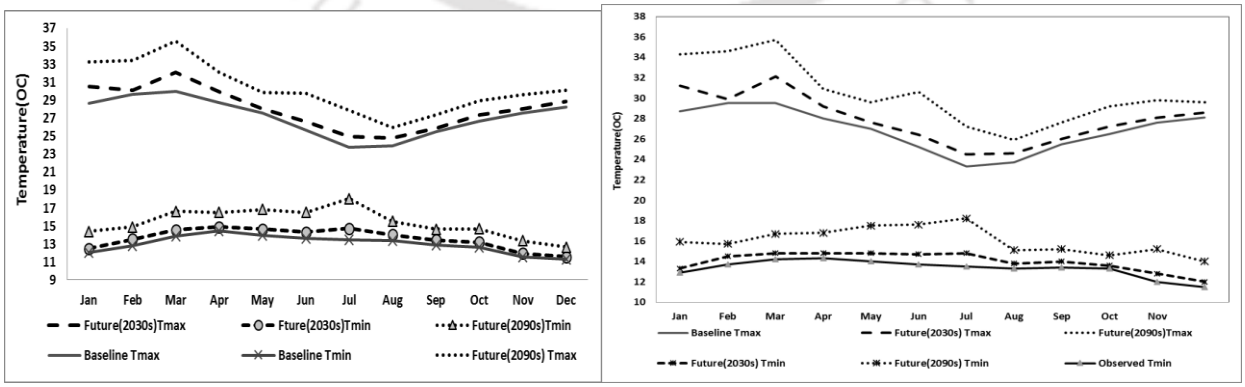

Figure 7.24 Average max and min future temperature at Upper and Lower Gibe

7.4.11 Trends and Scenarios of Climate Change in Gibe-III dam catchment

The Omo River Basin is drained by two major rivers from the highlands, the Gibe River flowing southwards and eastwards and Omo flowing south westwards. Downstream of their confluence only minor tributaries join, as the river continues southwards and enters the deep gorge where the Gibe III dam site has been identified. One of the immediate benefits of impact assessment of the Omo Gibe basin will be the ability to avoid severe drought periods and to control the large flooding downstream, which causes loss of lives, both human and animal, as well as damage to property and infrastructure. Its function will also allow controlling the downstream peak floods, occurring in summer seasons. Therefore, in order to analyse the effects in Lower Gibe due to projects in Upper Gibe basin near to the reservoir it is necessary to discuss here the basic operational output simulated in GCM output and SWAT simulated water balance for the project scenarios. The exercise will examine the hydrological change in upper basin station, change in inflow to lower Gibe in Upper Gibe basin near to reservoir, and change in water level. While comparing the historical climatic variables on observed and generated future climate trends, it is generally observed that the future trends on average basis of maximum and minimum temperature for most of the sub-basins show increasing trend (Figure 7.24). However, in the case of the precipitation, the future condition exhibits a fluctuating trend (i.e. in some of the sub-basin it is increasing and in others, it is decreasing). This fluctuation is due to complicated nature of precipitation processes and its distribution in space and time.

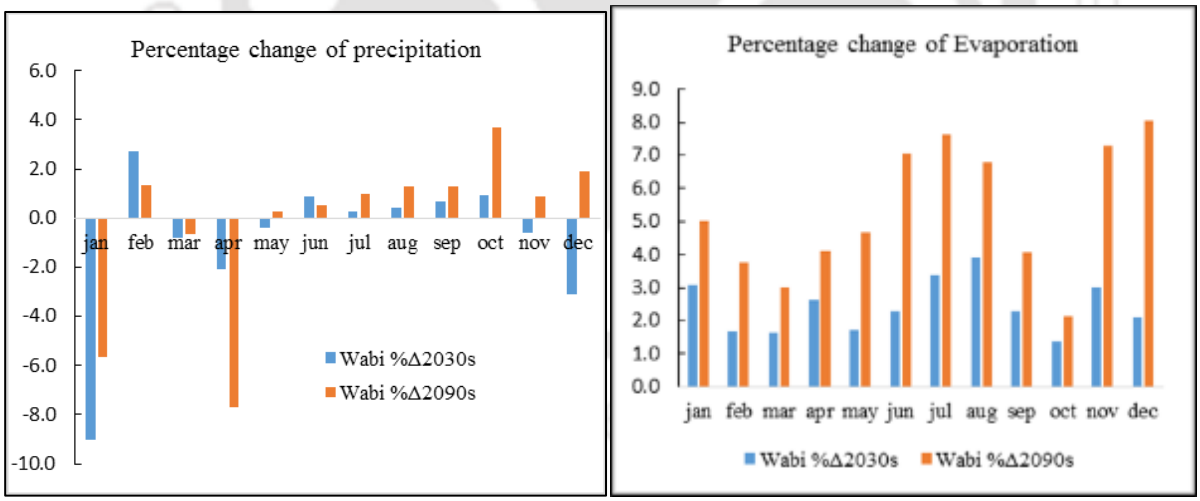

Figure 7.25 Percentage change of precipitation and evaporation Wabe catchment.

The precipitation shows an increasing trend in Upper Gibe sub-basin. Figure 7.26 shows the trend change of precipitation in the 2030s with 2090s for the Wabe sub-basin. It is having decreasing trend in Belg and Bega seasons and increasing trend for Kiremt season. Comparison to the base period and the future period average annual evaporation for Gibe III shows an increasing trend from short-term the (2030s) to long-term (2090s) in A1B scenario. The results of the analysis of the mean

seasonal temperature record clearly showed that all the stations had positive trends in summer seasons. The temperature and evaporation shows an increasing trend in Great Gibe in Upper Gibe basin (Figure 7.29). The percentage change of precipitation is increasing in winter and decreasing in summer season, but evaporation is increasing at Great Gibe site. In the (Figure 7.26) indicate that percentage change of precipitation has increasing trend in summer in both midterm and long-term scenarios and decreasing trends in winter seasons, whereas evaporation has increasing trends in Upper Gibe sub-basin catchment.

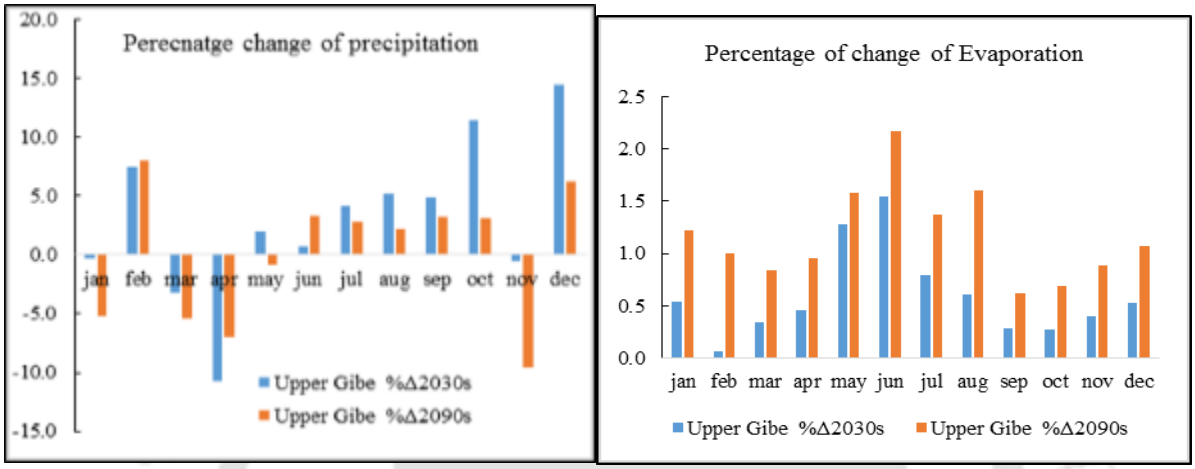

Figure 7.26 Percentage change of precipitation and evaporation Upper Gibe catchment

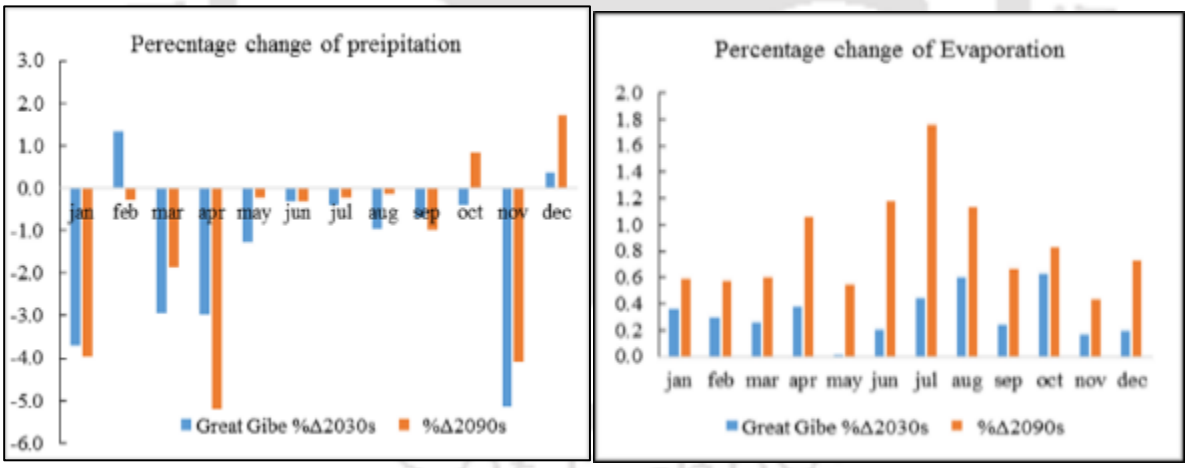

Figure 7.27 Percentage change of precipitation and evaporation Great Gibe catchment.

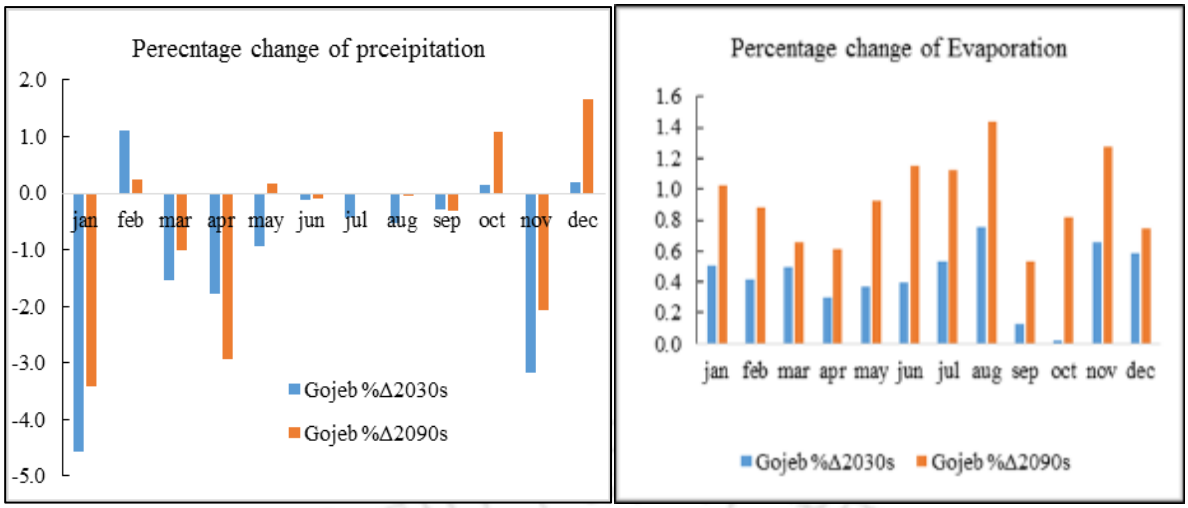

Figure 7.28 Percentage change of precipitation and Evaporation in Gojeb catchment.

7.4.12 Impact of precipitation and evaporation on stream flow using RCM A1B and B2 scenario

Climate change scenarios with expected changes in maximum and minimum temperature and rainfall in the years 2030s and 2090s are applied for generating surface runoff and streamflows in Upper Omo Gibe basin. The assessment for future climate change projections B2 scenario (low emission) and A1B scenario (high emission) was used for the midterm and long-term projection of precipitation and temperature. This analysis (table 7.2) was carried out for a time series of 10 years extending from 1990–2000 as base period and the future midterm 2030s and long-term 2090s. The mean monthly maximum and minimum air temperature and mean annual rainfall were compared with the base period. The analysis shows increase in Gibe III dam site from -32.1 % midterm to 11.58% long-term comparing with base time for mean annual rainfall. The maximum temperature increased by 1.29 ^{o}C and the minimum temperature increased by 1.55 ^{o}C in the 2030s from the base period. Similarly, the maximum temperature increased by 0.65 ^{o}C and the minimum temperature increased by 2.84 ^{o}C in the 2090s scenario. The amounts of rainfall in this catchment was high compared to other basins, where rainfall was increasing and the air temperature was decreasing.

Table 7. 2 the impact of change in precipitation and temperature in A2B scenario.

Sub Basin Name	Catchment area		Scenario	Temperature change (°C)				(%) of change Precipitation	
	Area km^2	% Area	SRES	2030s		2090s		2030s	2090s
				Max	Min	Max	Min		
U-Gibe	11492.7	34.22	A1B	0.32	0.22	1.08	0.82	-0.6	21.0

L-Gibe	9655.28	28.74	A1B	0.31	0.19	1.02	0.78	1.4	14.4
Wabe	4825.52	14.26	A1B	0.13	0.16	0.45	0.61	-13.9	-1.8
Gojeb	3348.44	9.96	A1B	0.11	0.07	0.35	0.27	-11.9	-6.7
G-Gibe	4269.84	12.71	A1B	0.43	0.01	0.66	0.35	-17.1	-14.7
G-III	33591.8	100	A1B	1.29	1.55	0.65	2.84	-32.1	11.85

7.4.13 Impact of precipitation using RCP 2.6, RCP4.5, and RCP8.5 scenarios.

The assessment for future climate change projections assessed by RCPs was used for the midterm and long-term projection of precipitation and temperature. Seasonal Variation of Precipitation in GIII dam site catchment are compared using RCP scenario (Figure 7.29) and SRES A1B scenario (Figure 7.30). The analysis shows that Kiremt precipitation has increasing trend from 12.63% (midterm) to 13.95% long-term while using RCP2.6. It has the same trend on using RCP8.5, but a decreasing trend on using RCP4.5 (from 3.61% midterm to 3.11% long-term) in the dam site catchment. This variation has shown the future pattern of precipitation shift from kiremt to bega and from bega to belg seasons.

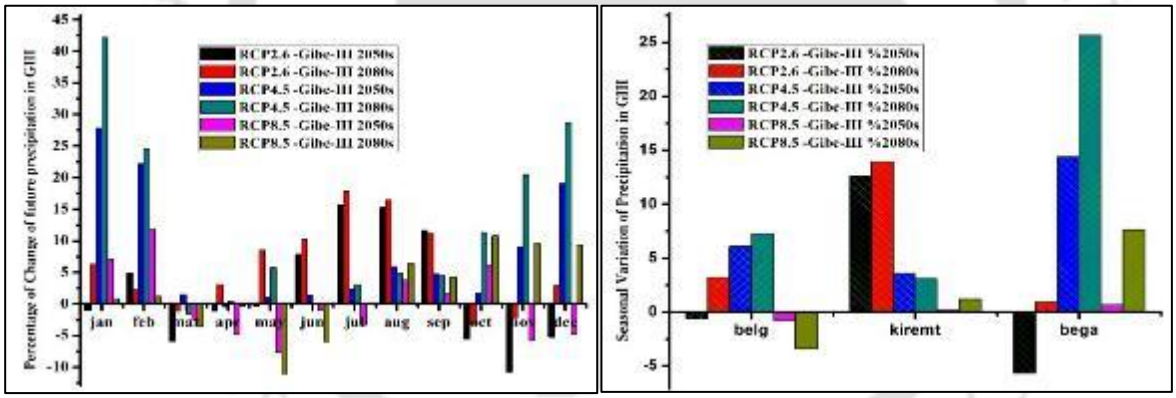

Figure7.29 Percentage of Change of future precipitation and Seasonal Variation in GIII catchment using RCP2.6, RCP4.5, and RCP8.5 scenario

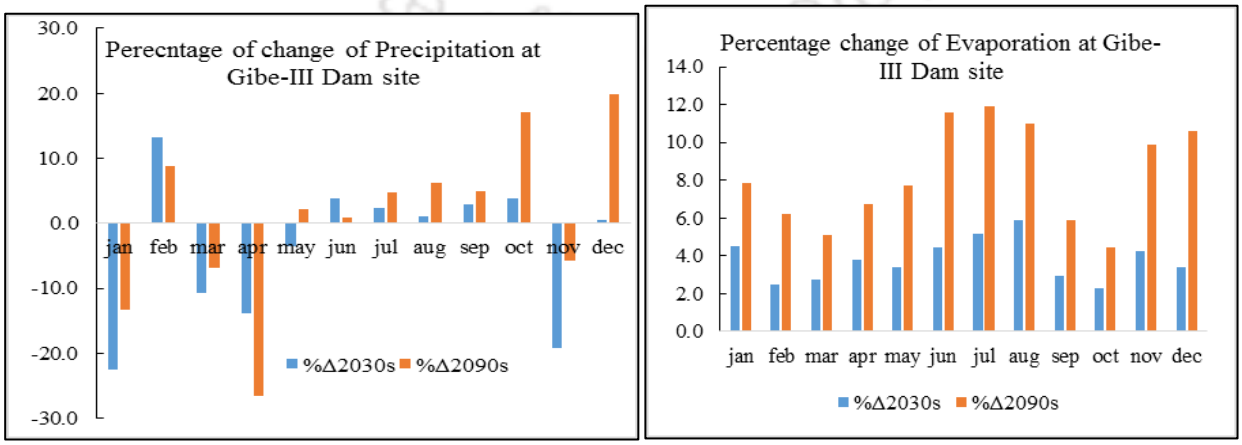

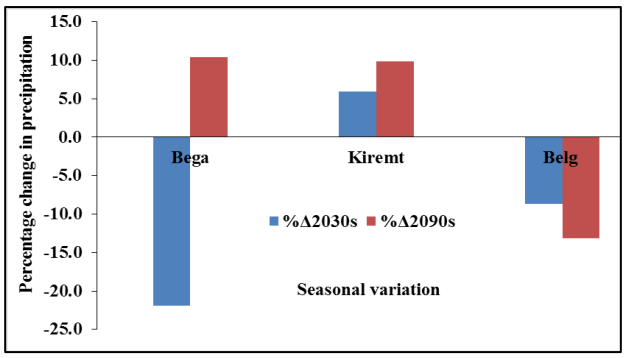

Figure 7.30 Percentage change of future precipitation and Evaporation in Gibe-III catchment

From the Table 6.4 on maximum and minimum temperature and from Ttable 7.5 on percentage of change of Seasonal Precipitation in G-III dam catchment, the G-III long-term percentage change in precipitation and evaporation indicates increasing trend from 6.41% to 18.13% for RCP2.6 (2050s to 2080s), from 24.14% to 36.06% for RCP4.5(2050s to 2080s), and from 0.21% to 5.46% for RCP8.5(2050s to 2080s). Therefore, on comparing both the Climate change assessments, the RCP Scenario was a good representative scenario than RCM A1B Scenario.

Table 7. 3 Percentage of change of Temperature in G-III dam catchment

Mean Annual	2050s			2080s		
	RCP2.6	RCP4.5	RCP8.5	RCP2.6	RCP4.5	RCP8.5
Max Temp	0.75	0.75	0.51	0.79	0.78	0.95
Min Temp	0.92	0.90	1.03	0.92	0.928	0.97

Table 7. 4 Percentage of change of Seasonal Precipitation in G-III dam catchment

Season / RCP	RCP2.6 2050s	RCP2.6 2080s	RCP4.5 2050s	RCP4.5 2080s	RCP8.5 2050s	RCP8.5 2080s
Belg	-0.58	3.23	6.11	7.29	-0.74	-3.37
Kiremt	12.63	13.95	3.61	3.11	0.27	1.19
Bega	-5.64	0.94	14.41	25.68	0.69	7.64
Annual	**6.41**	**18.13**	**24.13**	**36.07**	**0.21**	**5.46**

7.4.14 SWAT Model Sensitivity parameter analysis

The model considered 27 parameters associated with stream flows that were analyzed with a 10 interval of Latin Hypercube and the sensitivity analysis required 270 iterations. The ten parameters were selected for calibration, seven of these mainly affect the surface runoff (CN2, CH_K2, SOL_Z,

REVAPMIN, GW_REVAP, ESCO, and CANMAX), and the remaining three affect base flow generation (SOL_AWC, ALPHA_BF, and GWQMN). Among the sensitivity analysis that ten flow parameters are the most sensitive parameters in Great Gibe catchment as shown in table 7.6, and the remaining seventeen parameters were not considered sensitive to in the Great Gibe catchment.

Table 7.5 the most sensitive parameters in Great Gibe catchment.

Rank	Flow Parameters	Upper/ Lower Bond	Sensitive Value	Class	Description
1	ALPHA_BF	0-1	1.34	V/ High	base flow alpha factor (days)
2	CN2	±25	1.01	High	SCS runoff curve number (%)
3	GWQMN	0-5000	0.456	High	Shallow aquifer required for return flow to occur (H2Omm)
4	GW_REVAP	0-500	0.19	High	Threshold depth of water in the shallow aquifer required for return flow (mm)
5	ESCO	0-1	0.0956	High	Soil Evaporation Compensation factor
6	SOL_Z	0-3000	0.0786	Medium	Total soil depth (mm)
7	CH_K2	0-150	0.0727	Medium	Effective hydraulic conductivity of the main channel (mm/hr.)
8	GW_DELAY	0-0.2	0.0683	Medium	Ground water delay (days)
9	SOL_AWC	0-1	0.0646	Medium	Soil available water capacity (water/mm soil)
10	SURLAG	0-12	0.0939	Medium	Surface lag

7.4.15 Model Calibration and Validation of Great Gibe Sub catchment

Calibration result aimed at overall shape agreement of the observed and simulated discharge using model performance; Nash and Sutcliffe model efficiency (NSE), (Nash, 1970), Pearson's coefficient of determination (R^2) and PBIAS for monthly flow calibration and simulation. As discussed in data analysis section, the flow was calibrated automatically by the model using the observed areal precipitation, areal evapotranspiration, and observed flow at Great Gibe gauging station. The results show that there exists good correlation in monthly flow data (Figure 7.33) and daily flow data (Figure 7.35). The table 7.9 illustrates that the values of these statistical parameters for both simulated and measured flow between monthly observed and simulated stream flows substantiates the use of SWAT for future scenarios in this catchment.

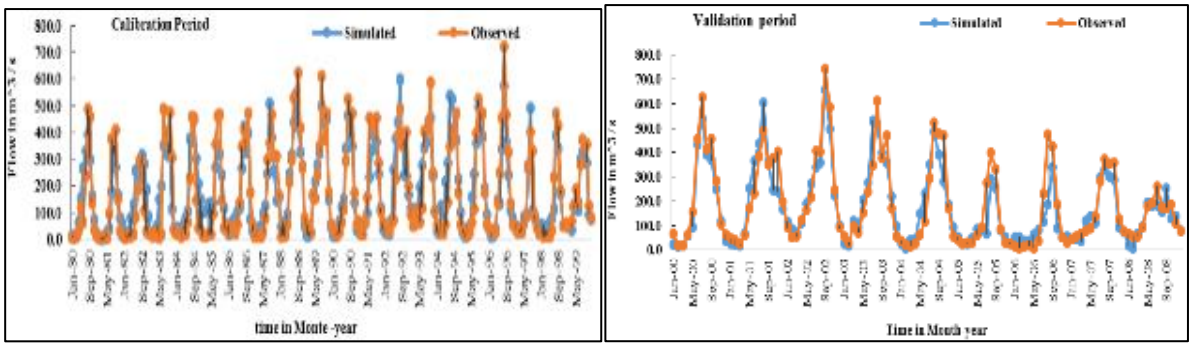

Figure 7.31 Calibration and Validation period at Gojeb gauge station.

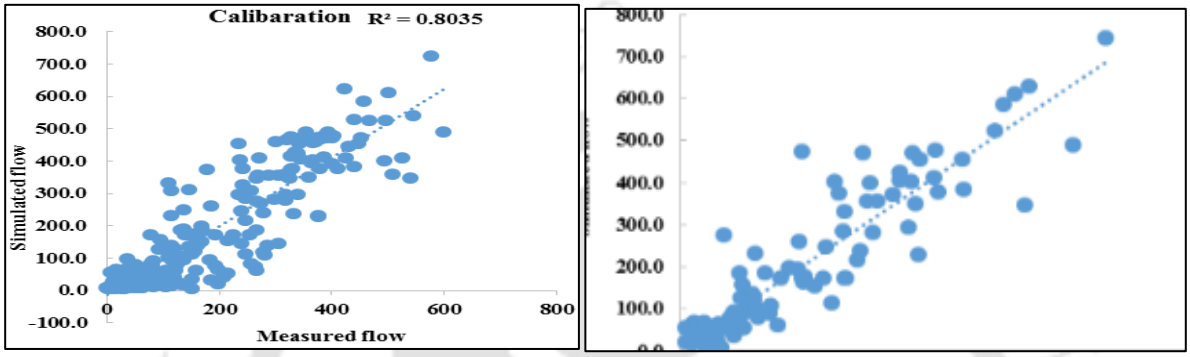

Figure 7.32 Simulation and measured flow during Calibration and Validation period

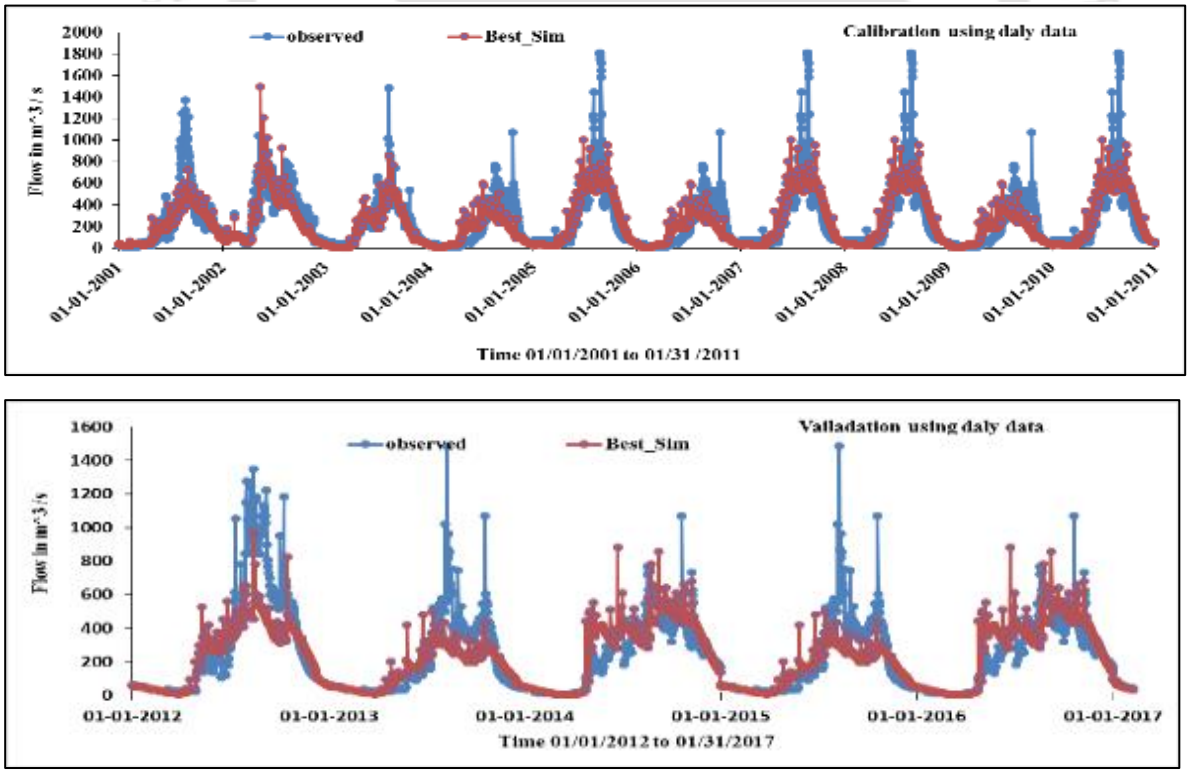

Figure 7.33 Daily data based Calibration and Validation at Gojeb gauge station.

Table 7.8 Calibration and Validation using monthly data model performance

Monthly time step simulation	Mean Stream flow(m3/s)		Model Performance		
	Observed	Simulated	R^2	NSE	PBIAS

Calibration (1980-1999)	170.2322	173.3074	0.893	0.78	-2.39
Validation (2000 to 2008)	184.4572	171.7673	0.835	0.795	-6.22

Table 7. 9 Calibration and Validation using daily data model Performance

Daly time step simulation	Model Performance				
	P-factor	d-factor	R^2	NSE	PBIAS
Calibration (2001- 2011)	0.76	0.71	0.68	0.79	-12.39
Validation (2012 to 2017)	0.72	0.68	0.78	0.76	-4.22

The calibration was performed for twenty years' period from January 1st, 1981 to December 31st, 1999. The R^2 was found to be 0.893, NS=0.78, and PBIAS = -2.39, which shows the simulations' very good correlation with the gauged flow as seen in (Figure 7.33). The validation was performed based on 25 % of the original data years in the period from January 1st, 2000 to December 31st, 2008. The R^2 was found to be 0.835, NS=0.795, and PBIAS = -6.22. Therefore, DEM resolution affects the delineation of the watershed and stream network. A decrease in spatial resolution results in a decrease in the volume of simulated streamflow 90 m by 90 m required to achieve less than -2.39 % error at calibration and -6.22 % in validation error of flow simulation in this basin. Hence, PBIAS value close to 0% is the best estimate, a negative value indicates model overestimation, and a positive value indicates model underestimation. In this study, the value is negative, which indicate overestimation.

7.4.16 Impact of Climate Change scenario on Future Stream flow using SWAT model

The annual streamflow percentage change as a function of annual percentage change of precipitation and evaporation is shown in (Figure 7.33) and the table 7.7. The results indicate that the streamflow is positively correlated with precipitation, but negatively correlated with evaporation. The changes in streamflow ranged from 7.3% to 25.56 % in 2030s and 2090s, respectively, with respect to the changes in precipitation and evaporation as shown in (table 7.7). As expected, the streamflow–precipitation relationship was much stronger than the streamflow– evaporation relationship. As a result, the impact of precipitation on streamflow is treated higher for the catchment and streamflow-precipitation relationship has increasing trends that is reflected in SWAT simulations, also.

Table 7.6 percentage of change of precipitation, evaporation, and stream flow

Hydrological	Midterm and Long-term A1B Scenario using SWAT model

parameter	RCM A1B Scenario			Percentage of Change	
	2000	2030s	2090s	2030s	2090s
Precipitation	1339.2	1407.5	1485.9	5.1	11.4
Evaporation	604.85	659.9	719.9	9.1	16.8
Stream flow	62.31	66.86	71.72	7.3	25.56

The future projected precipitation and temperatures were downscaled using Climate change scenarios (A1B) for the two future periods of (2030s, 2090s). The mean monthly SWAT models were used to derive relationships between precipitation, evaporation, and stream flow. The projections presented in Figure 7.31 indicates increasing trends from base line, medium, and long term scenarios. Changes in stream flow volume and timing with the changes in climatic parameters like precipitation, temperature, evaporation are the main drivers of the future basin stream flow changes. Figure 7.31 shows the SWAT model results for average monthly of mid-term and long term scenario for precipitation. In Figure 7.31, stream flow is increasing in summer and decreasing in winter because of change in precipitation in Upper Omo Gibe basin during summer / Kiremt high rainy season.

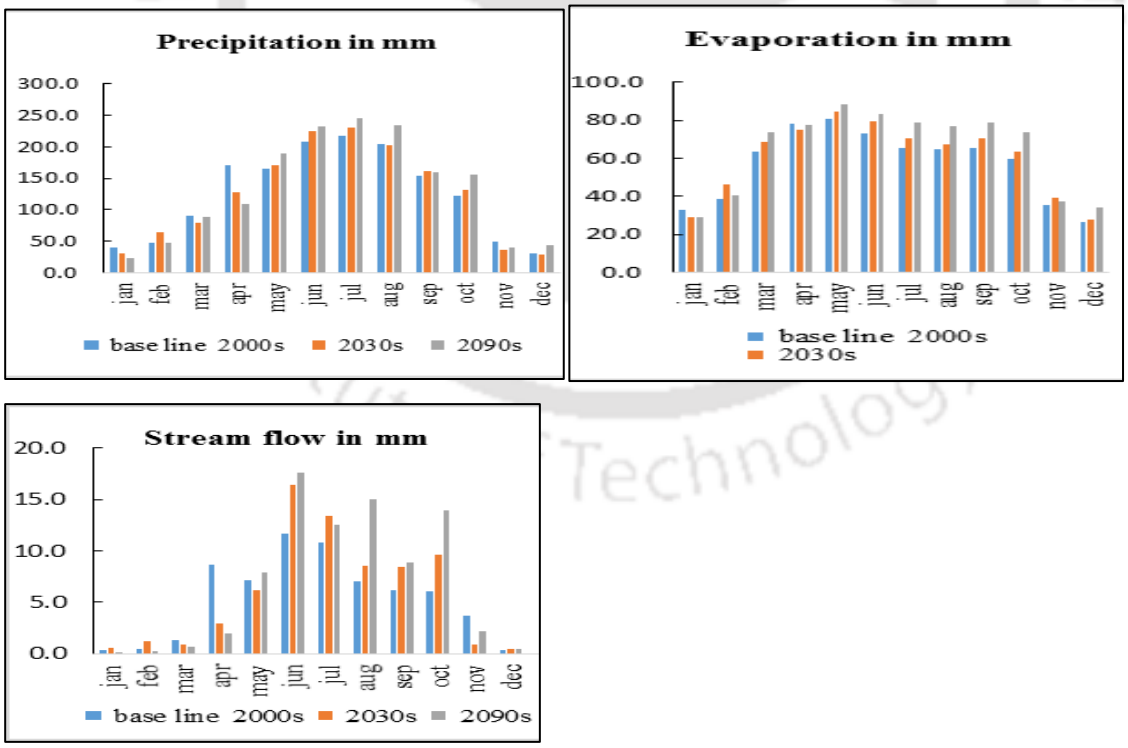

Figure 7. 34 SWAT model results on precipitation, evaporation, and surface runoff.

7.4.17 Effects of Climate Change on stream flow

Watershed management involves developing water resources, finding mechanisms to alert, and provide long-term solutions to water related problems and provide sustainable access to resources. Understanding the regime and the distinctiveness of future high and low stream flows is of vital importance in effective planning, designing, and monitoring the basin resource and assessing direct or indirect factor that affect basin future stream flow. Furthermore, the analyses involve plans to adapt to future water scarcity at the watershed level. This river basin adaptive strategy helps for improving water structures like dam, reservoir, and lakes in a changing climate condition. Increase in temperature results in a rise in evaporation, which could consequence in water scarcities. Climate change raises more alarms with respect to its impact on water resources. This rising temperature form unusual heavy precipitation events, which results in increased runoffs. This also means that there will be reduced groundwater recharges and decreased levels of soil moisture, which can affect in reduced agricultural productivity and thereby affect the socioeconomic activity of the basin.

7.5 Conclusion

Considering the impact of climate change in a water resource management sector is the need of the society to evaluate the vulnerability of infrastructure systems and the effectiveness of different adaptation strategies in managing climate-related stresses. The study addresses the effect of climate change on water resources in the basin and the need for transforming the existing water-infrastructure in the basin to sustain the water resources systems compared to future climate change projection. Seasonal variation of precipitation in Upper Gibe and Gojeb catchment shows increasing trends in all both low and medium emission scenarios. It shows decreasing trends in summer for high emission scenario. The percentage of change of seasonal precipitation in Gibe-III dam catchment shows that Kiremt precipitation is having increasing trends from 2.4% during mid-term to 16.95% in long-term, while using RCP2.6; and 16.34% midterm to 20.6% long-term while using RCP8.5. However, there is a decreasing trend in RCP4.5 from 24.7% midterm to 10.71% long-term. The future projection of maximum temperature under RCP 8.5 indicates an increasing trend for all months and the average annual maximum temperature has been increased with the rate of 0.51°C to 0.95°C for RCP 8.5, 0.75°C to 0.78°C for RCP 4.5, and 0.75°C to 0.79°C for RCP 2.6 from 2050s to 2080s, respectively. The future projection of minimum temperature shows increasing trends for all months in these three RCP scenarios. The average annual minimum temperature shows decreasing trends from 1.03 °C to 0.97 °C for RCP 8.5 from 2050s to 2080s. It shows increasing trends of 0.90 °C to 0.91 °C in RCP 4.5 and 0.92 °C to 0.94 °C for RCP2.6 and from the 2050s to 2080s. Using the SWAT tools the statistical parameters for both simulated and measured streamflow for R^2, NSE and PBIAS was estimated during calibration 0.893, 0.78, and -2.39 and validation

0.835, 0.795, and -6.22, respectively. These statistical parameter values shows the simulation's very good correlation with the gauged flow. The relationship was done between monthly observed and simulated stream flows in great gibe gauging station. The negative value of PBIAS suggested that it was overestimated. Therefore, considering different catchment with a different return period annual precipitation change shows increasing trends in both midterm and long-term scenario with increasing return period. Besides, the analysis indicates that overall increasing trend in both midterm and long-term.

Chapter 8 Climate change impact assessment in South Omo Gibe

8.1 Introduction / Background

The effects of climate change on the water resources system as well as on the water infrastructures have to be assessed through hydrological impact studies to devise suitable management practices (*Tatsumi et al., 2011)*. As precipitation increases, more water is available in the basin and vice versa. Similarly, the change in rates of evapotranspiration also causes variability in available water (*McCain, 2007*). . Water managers face difficult challenges as available land and water resource in the basin are not utilized effectively to improve the livelihood and socio-economic conditions of the inhabitants (*Chaemiso et al. 2016*).

As the climate change impact on water-availability cause demographic and economic deviations, climate change modelling is essential with related to water resouces in a region. The anthropogenic interferences can cause land degradation and increased runoffs (*van Roosmalen et al., 2009; Gumindoga et al., 2014*).Hydrologic modelling along with climate change parameters are essential for estimating water availability as well as assist the water resources management of a basin (*Dwarakish and Ganasri 2015*). The spatio-temporal hydrological modelling aids in visualizing and strategizing different environmentally sustainable management scenarios in a river basin.

Since the maximum and minimum temperatures in Ethiopia have increased at about 0.37 °C and 0.28 °C per decades (NMA, 2007*; Mc Sweeney et al., 2008; Chaemiso et al., 2016*), the presence of climate change phenomenon in Ethiopia is obvious. The vulnerability of the region to climate change are different across the region (*Temesgen et al., 2006*). increasing occurrence of late rains and droughts is consistent with scientific assessments on the impacts of climate change in the basin. Predictions of future temperatures rise and ever-increasing rainfall variability indicated that both droughts and late rains will probably become more pronounced in the coming decades (*Marius, 2009*). The ecosystems and biodiversity are affected as a result of climate change. The master plan of the cascade hydropower project in Omo-Gibe has schemes for irrigation in the downstream.The natural flow of the river is obstructed due to the project. The change in hydrological processes in the basin due to climate change may affect the performances of the water resources project planned at the site. Climate change assessment on the basin hydrology in the present and future scenarios is a vital step for optimal water allocation in the basin.

8.1.1 Objectives

Therefore, the main aim of this study is to evaluate the impact of precipitation and evaporation on streamflow under climate change scenarios using SWAT and geostatistical approaches in the semi-arid sub-basin of South Omo in the Omo-Gibe River Basin.

8.1.2 Specific Objective

Assess the spatial and temporal impact of precipitation and evaporation on streamflow.

Develop SWAT Model Calibration and Validation in South Omo basin.

8.2 Study area

The South Omo river basin has an area of 23,438 Km^2 and it lies between 4° 30' to 6° 00' North Latitude and 36° 00' to 37° East longitude (Figure 8.1). The average annual stream flow from the river basin into Lake Turkana in Kenya was estimated to be 16.6 BCM. The Gilgel Gibe and Gojeb Rivers are major tributaries to the main Omo-Gibe River and it drains the western high lands into the Omo-Gibe river basin. In this basin, a small rainy season occurs from March to May, dry season from December to February, and spring season cover from September to November. Hence, the region is classified as semi-arid by National Meteorology Agency, Ethiopia. The southern parts of Omo were affected by many floods in recent years; however, this is expected to be regulated from the large hydropower dam of the upstream part of the basin (EEPCO, 2008).

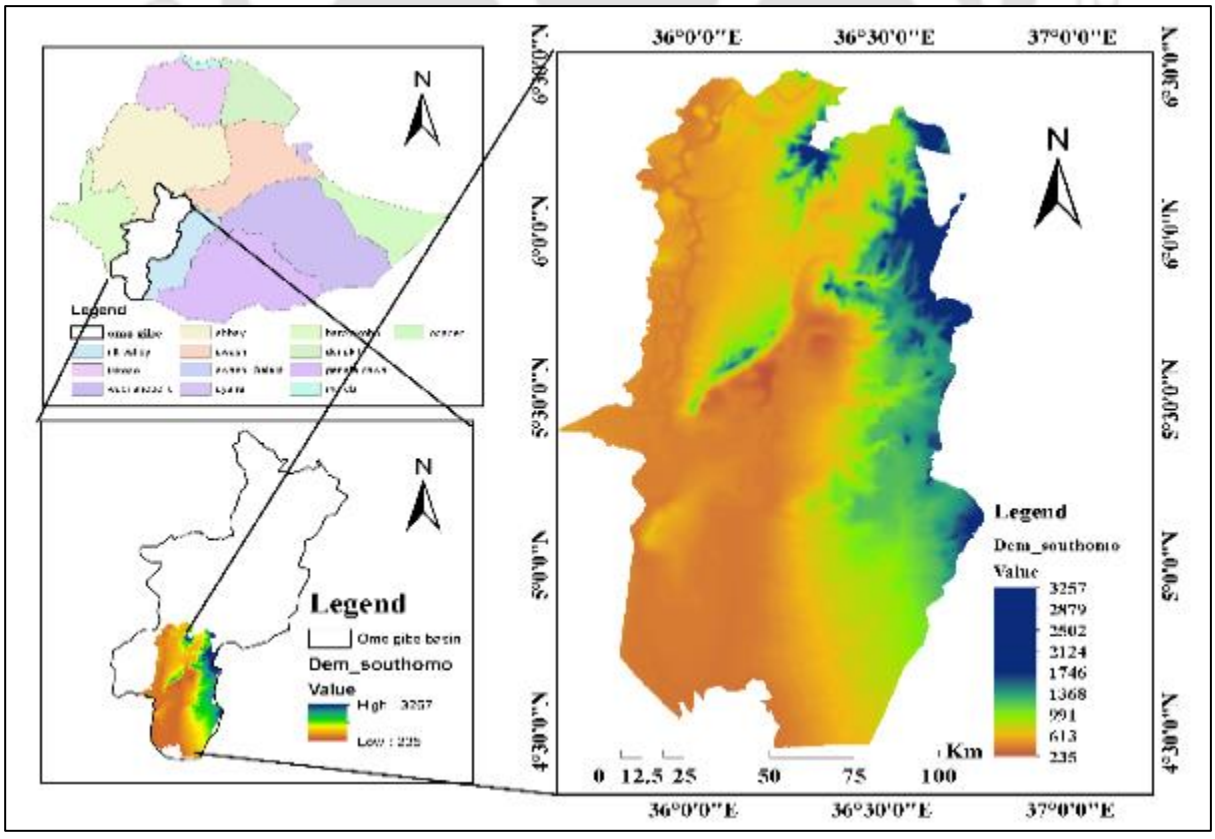

Figure 8. 1 Location map of the study area South Omo in Omo Gibe basin.

The topography of the study area is characterized by a long valley, formed by the erosive action of the Upper Omo-Gibe River and its numerous tributaries, which often separate the plains. The surrounding highland plateau elevations vary from 2000 m above mean sea level (AMSL) or more while the valley elevations range from 342 to 1400 m AMSL. The precipitation decrease with increasing elevation throughout the Omo-Gibe catchments (EEPCO, 2008). The average annual temperature of the basin varies from 16 ^{o}C to 29 ^{o}C. The monthly average temperature rises slightly from January to May and then declines afterward in the months from June to August. This is attributed to the wet season from June to August, in which the region experiences maximum rainfall (EEPCO, 2008). The main land use/land cover and soil type in the basin are shown (Figure 8.2).

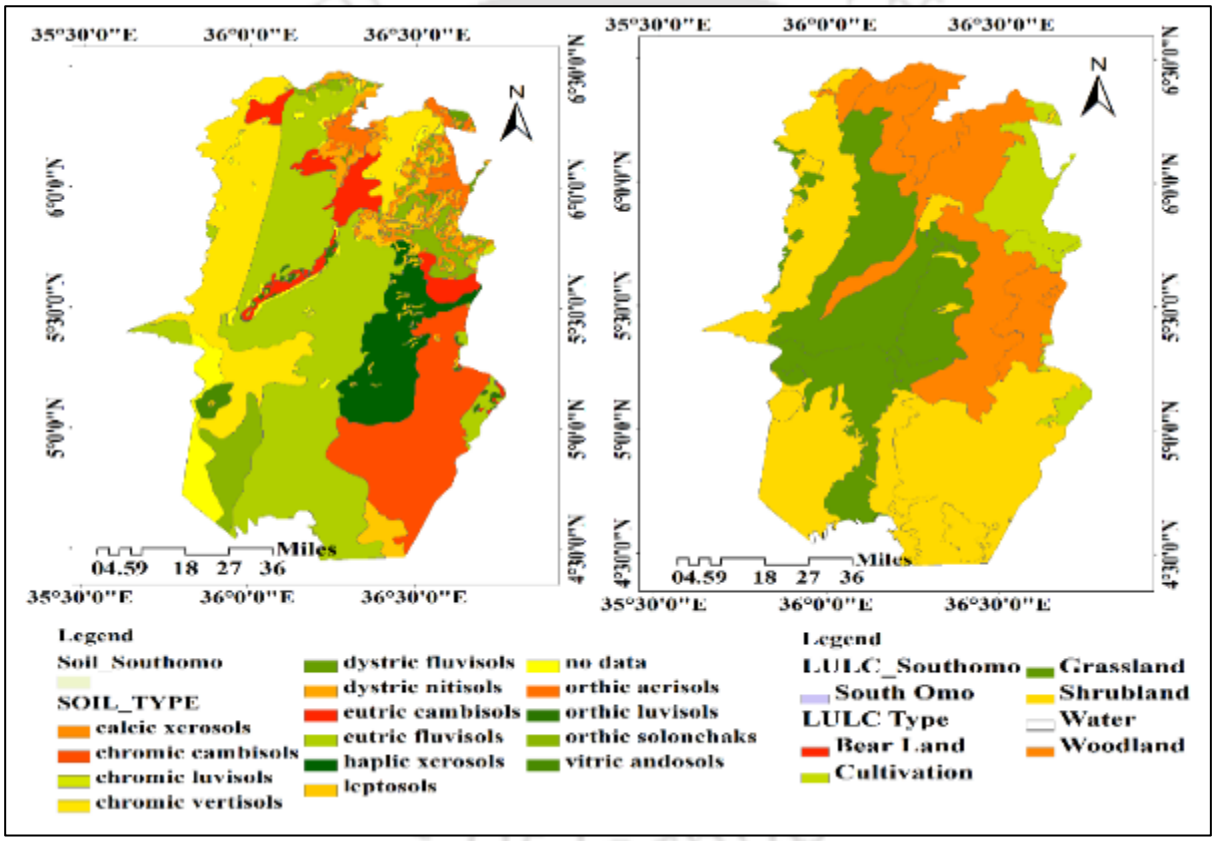

Figure 8.2 Land use/land cover and soil types in the South Omo in Omo-Gibe basin

8.3 Materials and methods

8.3.1 Data used

DEM can be used to analyze the drainage pattern of the watershed, slopes, stream lengths, and widths of the channel within a watershed. The DEM used for this study is 30 m by 30 m spatial resolution from SRTM process and project using ArcGIS v10.2.1. The basin has a varied land use/land cover including agricultural land woodland, natural forest, shrubs land, afro-alpine

grassland plantation, etc. The soil map of Ethiopia was obtained from the Ministry of Water, Irrigation and Energy (MoWIE). The major soil types in the basin are:- Eutriccambisols, Chromic luvisols, Eutricnitisols, Chromic vertisols, Chromic cambisols, Calcic xerosols, Calcic aerosols, and Vitric andosols. The streamflow data of the South Omo Gibe basin were collected from the MoWIE hydrology department for the period from 1995 to 2015. In the present study, the precipitation and temperature data sets for RCP4.5 and RCP8.5 emission scenarios were downloaded from the CORDEX Africa database and subjected to bias corrections (Kiesel 2019). The high grids resolution based on the time sequence from each CORDEX scenario were extracted from the grid cells according to the location of measured climate station.

8.4 Methodology

The general methodology of this study is given in (Figure 8.1)

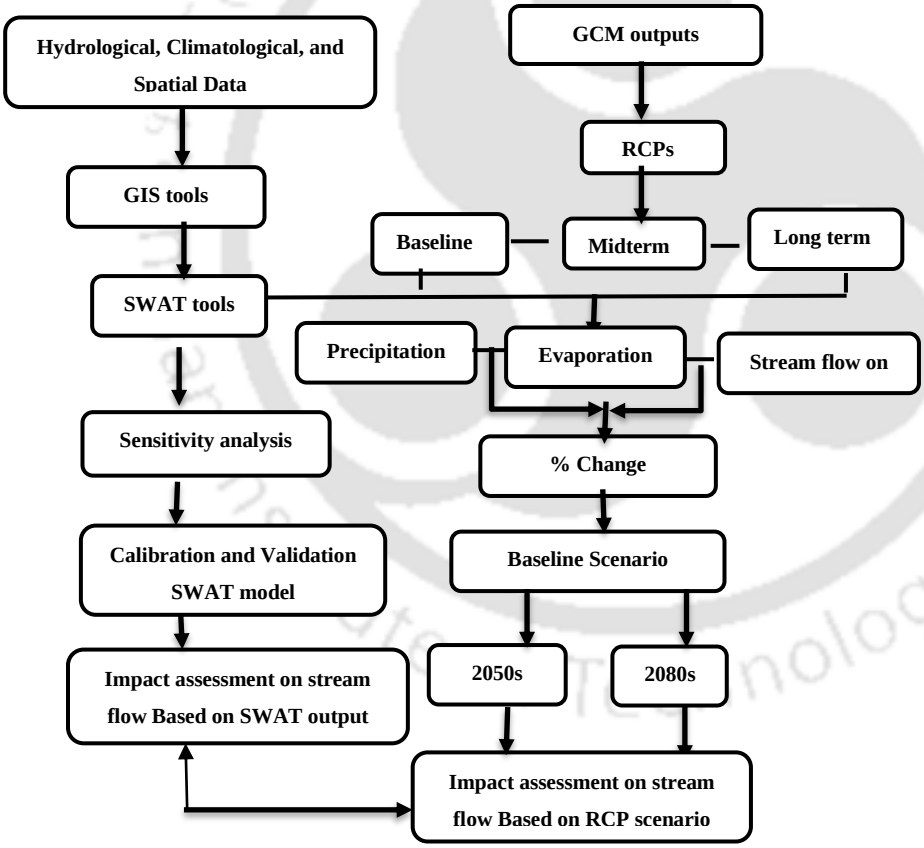

Figure 8.3 The flowchart adopted in the present study

8.5 Hydro-meteorological data analysis, checking homogeneity, and consistency

By checking the consistency and homogeneity of individual stations, the data qualities are investigated and processed. Rainfall of stations within each sub-basin was non-dimensionalized and

plotted to compare the homogeneous stations within the watershed. This helps in filling missed values in the stations. The results of the homogeneity and consistency analysis are shown in (Appendix 5). The homogeneity of dimensionalized monthly precipitation value was calculated as (*Jemberie et al., 2016; Asitatikie 2019*).

There are different methods to estimate potential evapotranspiration (ET_O) using observed and predicted climatological data. For this specific study, the Penman-Monteith method, Hargreaves, and Priestley-Taylor methods were adopted to calculate the daily potential evaporation. Monthly average values were used as estimates of potential evapotranspiration at a certain time of the year. The Penman-Monteith method for estimating potential evapotranspiration using data from different stations depending on the sub-basin locations was (in chapter 2 equation 2.2). The Hargreaves method for estimating the potential evapotranspiration is an empirical radiation-based method, which is extensively used in the conditions of limited weather data (*Hargreaves and Samani, 1985; Neitsch et al., 2005*).

8.6 GIS-based Spatial Rainfall Interpolation techniques

The study adopts ArcGIS's Geo-Statistical Analyst to incorporate IDW and Kriging interpolations (Chapter-4) to the geospatial data (*Yang et al, 2015*). In IDW, the interpolated surface is most influenced by the nearby data that is a locational dependent variable (*Yang et al, 2015*). IDW forecasts the rainfall value at any unmeasured location using the measured values from the nearby location. Presuming the observed values adjoining to the prediction location have more impact on the forecast value than those far apart, more weights are assigned to the nearby observed values. The IDW method of prediction of rainfall is (equation 8.4).

$$z(x) = \frac{\sum_i w_i z_i}{\sum_i w_i} \qquad (8.4)$$

$$w_i = \frac{1}{d_i^2}$$

where z(x) is the unknown precipitation data (mm), z_i is the known or observed precipitation data (mm), i is the number of precipitation stations, w_i is the weighting of each observed precipitation stations, and d_i is the distance from each precipitation stations to the unknown location.

Kriging is a complex and well known geo-statistical process that assesses and generates a surface from a distributed set of points using Ordinary Kriging and Universal Kriging (Equations 4.40 and 4.41, Chapter-4). The prediction errors evaluated in the research are Mean Error; Root Mean Square Error; Average Standard Error; Mean Standardised Error; and Root Mean Square

Standardised Error. These error evaluation techniques are available in the Geostatistical Analyst extension tool in ArcGIS10.2.1.

8.7 SWAT Model

The SWAT Version 2012 was used in this study to model the streamflow in the South Omo-Gibe River Basin. In this study, South Omo basin was divided into 10 sub-basins. The model was calibrated (1995-2007) and validated (2008-2015) including 3 years' warm-up period to initialize the model parameters.

The present study compared the simulated and measured discharges from several gauging stations. The Nash and Sutcliffe efficiency criteria (NSE), the coefficient of determination (R^2), and Percent difference between the simulated and observed streamflow were evaluated to assess the performance of the model (*Rodda & Little 2015*).

8.8 Bias correction method of downscaled climate data

The downscaled RCPs data can be rarely used in direct form for any impact assessment (*Laflamme 2016*), as the computed variables may differ numerically from the observed ones. Bias corrections are applied to compensate the tendencies of overestimating or underestimating the average downscaled variables. In the study, here, the bias corrections are applied for futuristic precipitations and temperatures. The nonlinear bias correction method proposed by (*Mengistu 2009*) and "delta method" were used to calculate the correction factors for each month. The non-linear bias correction for daily rainfall values (P) are obtained using a power transformation equation (Equation 7.13) and temperature bias correction is done using Equation 7.14 (Ashley et al., 2005). As the correction of rainfall and temperature leads to more reasonable results in hydrological impact assessments (*Chen, 2015*), the bias corrections for maximum and minimum temperature and precipitations were applied at each selected station in the study. (CMHyd software is used in this research to correct the biases of RCM of the South Omo portion of Omo-Gibe River Basin.

8.9 Changes in monthly and seasonal climate variable outputs

Precipitation and temperature were generated by RCPs for contemporary and future scenarios and based on RCP bias-corrected precipitation and temperature for the South Omo-Gibe River Basin. The annual rainfall shows diminishing pattern as the river drains from the highlands in the north to Lake Turkana in the south. The bi-modal mean monthly rainfall pattern was found in the lower part of Omo-Gibe basin (Figure 8.4).

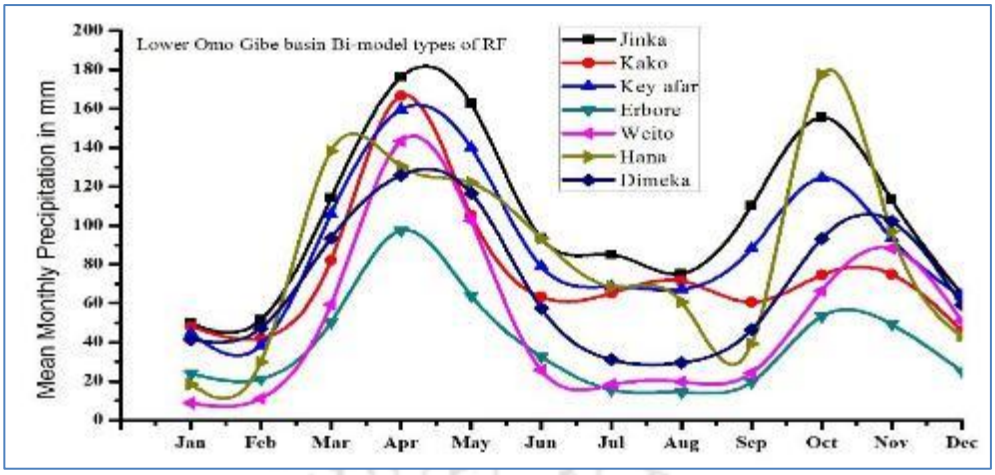

Figure 8. 4 Observed rainfall pattern in the South Omo, Omo-Gibe basin

The variations observed in percentage change in precipitations between the monthly mean of observed measurements and the futuristic RCP scenarios (Figure 8.5, Figure 8.6, and Figure 8.7) reveal the future projections having fluctuating trends in lower Omo-Gibe. Though the analyses were performed for all the sub-basins of Lower Omo-Gibe, however, for brevity, the results of South Omo Jinka site and South Omo Omoratte site are portrayed in this chapter (Figure 8.5, Figure 8.6, and Figure 8.7). Because of the effects of inter tropical convergence zone in Ethiopia the (Figure 8.4) indicates that the two spikes in April and October shows the catchment get annual two times precipitation. These spikes indicate bimodal types of rainfall in south omo gibe catchments (Figure 8. 5). Comparison of a) average monthly precipitation and b) percentage change in mid-term and long-term futuristic precipitation scenarios of Jinka site are shown.

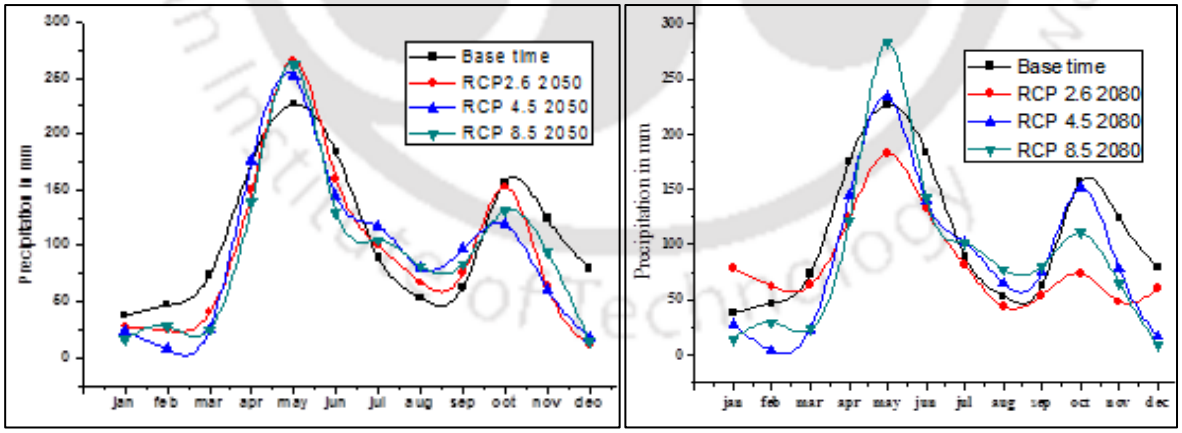

(a)

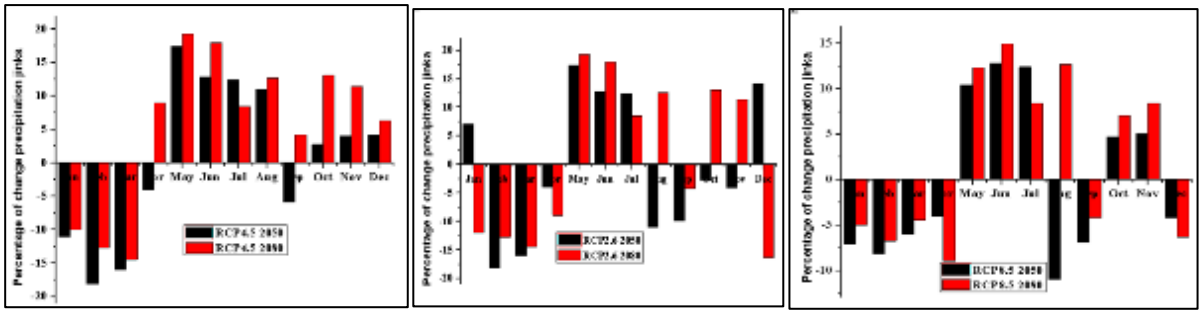

(b)

Figure 8. 6 Comparison of a) average monthly precipitation and b) percentage change in mid-term and long term futuristic precipitation Jinka site

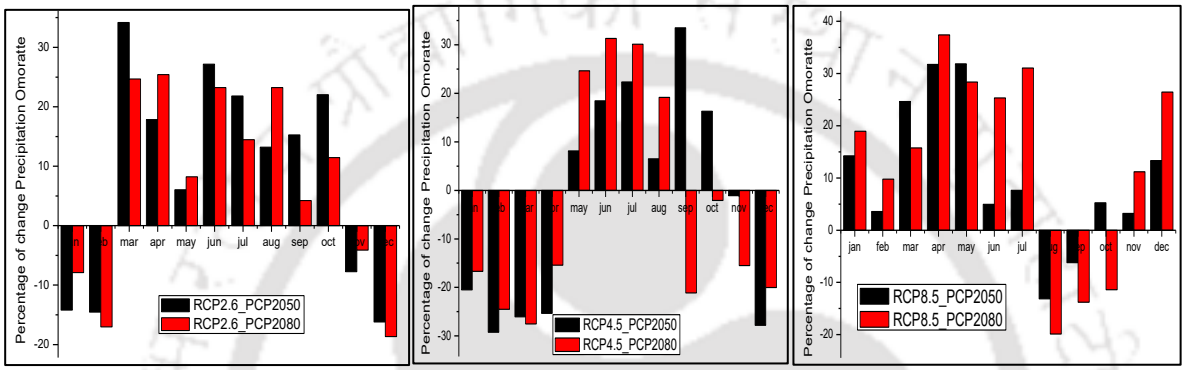

Figure 8. 7 Percentage change in 2050s and 2080s futuristic precipitations Omoratte site

The sub-catchment shows increasing and decreasing trends in seasonal rainfall due to the complicated nature of rainfall processes and its circulation in space and time. (Figure 8.6) compares the percentage change in precipitation in mid-term (the 2050s) and long-term (the 2080s) scenario for the Jinka site sub-basin. The decrease in rainfall is noticed during the Belg season (i.e. less rainy season from February to May) in both the mid-term and long-term predictions for all the RCP scenarios (i.e., 2.6, 4.5, and 8.5). Positive percentage change or increase in rainfall is observed during the Kiremt season (i.e., rainy season from June to September) in both the 2050s and 2080s predictions for all RCPs. However, the predictions of Bega season (i.e., dry season from October to January) shows fluctuating changes in rainfalls for the above classes. Figure (8.6 a, b) summarise the projected mean seasonal rainfall in the mid-term and long-term for the South Omo Jinka site using the RCP2.5, RCP4.5 and RCP8.5 scenarios. Here again, the decreasing trend is observed for Belg season, both in the mid-term and long-term predictions.

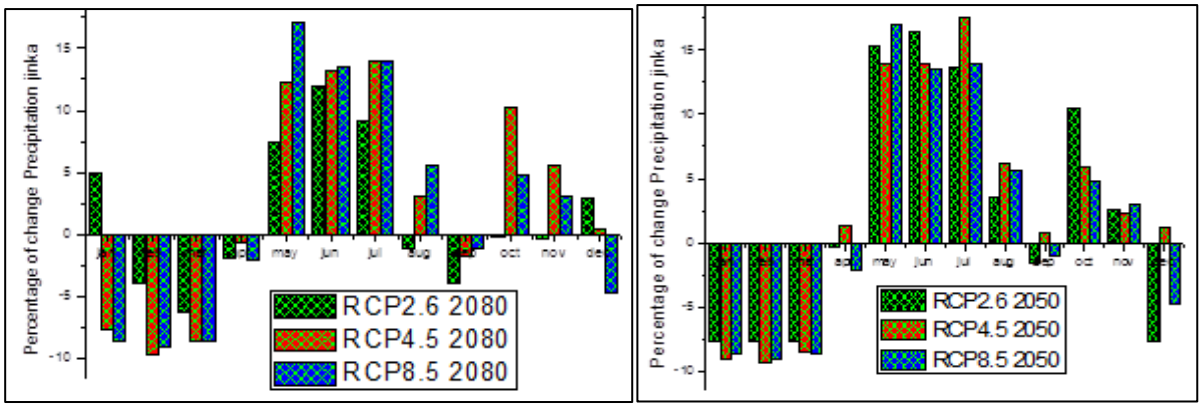

a) b)

Figure 8.8 Percentage change in a) midterm and b) long-term futuristic precipitations Jinka site.

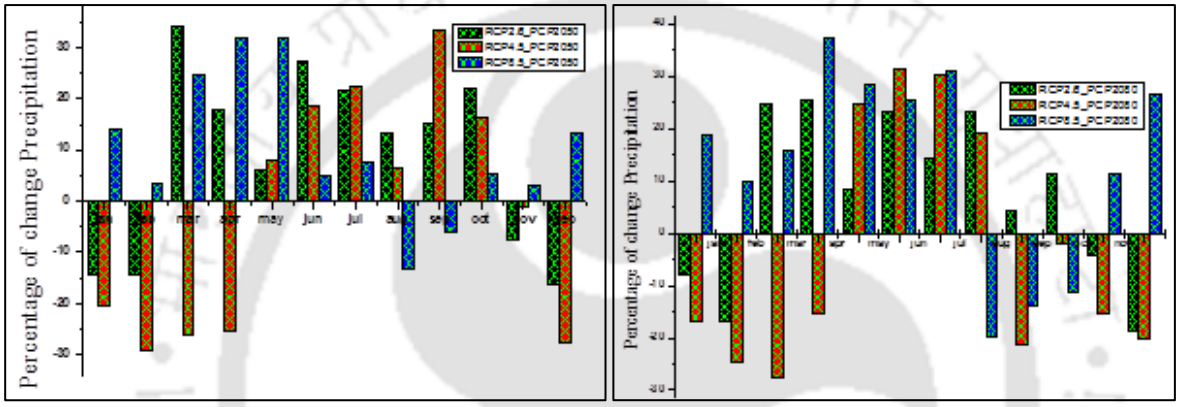

a) b)

Figure 8. 9 Percentage change a) midterm and b) long-term futuristic precipitations Omoratte site.

On the contrary, the Kiremt season showed positive changes for the above and Bega season exhibited fluctuating trends. In a similar tone, the analyses of rainfall predictions in the South Omo Omoratte site are described. The Omoratte site analyses revealed more fluctuating changes in rainfall while considering different RCP scenarios. For Belg season, all the scenarios for the mid-term and long-term predicted a decrease in rainfall for the Omoratte site. The Bega season showed a decrease in mean seasonal rainfall while using RCP2.6 and RCP8.5 during the mid-term predictions. However, in the long-term predictions, the same Bega season revealed a decrease in rainfall only while using the RCP8.5 scenario for the Omoratte site (Figure 8.10).

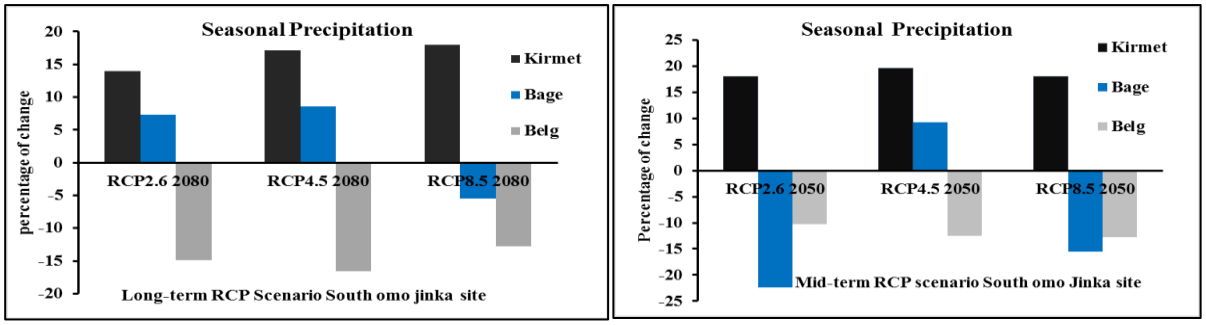

Figure 8. 10 Percentage of changes seasonally precipitation in South Omo Jinka site.

where: Bega (dry season = October–January), Belg (less rainy season = February–May) and Kiremt (rainy season = June –September)

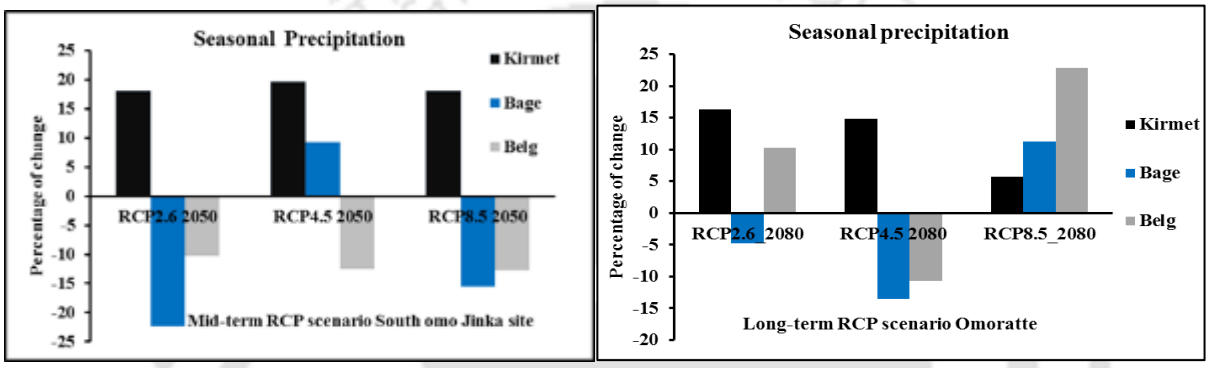

Figure 8.11 Percentage of changes of seasonally precipitation in South Omo Omoratte site.

where: Bega (dry season = October–January), Belg (less rainy season = February–May) and Kiremt (rainy season = June –September)

The monthly average maximum temperatures showed an increasing trend from the baseline temperature for all the emission scenarios, both in the mid-term and long-term temperature predictions (Figure 8.12 A, B). The monthly mean minimum temperatures indicated a significant rise in the temperature for the RCP 8.5 emission scenario in most of the months (Figure 8.12 C, D). In addition, the mean seasonal temperature changes for summer, winter, and spring seasons are compared (Figure 8.13). Except for the mid-term prediction for temperature using the RCP2.6 scenarios, in all other situations, the RCP4.5 emissions is giving larger seasonal temperature change in the mid-term and long-term. On an annual scale, the mean temperatures are expected to increase by 1.34°C, 1.58°C, and 1.47°C, in mid-term 2050s scenario for the RCP2.6, RCP4.5, and RCP8.5, respectively. Similarly, the annual mean temperatures are expected to increase by 0.98°C, 1.03°C and 1.35°C, in the long-term 2080s.

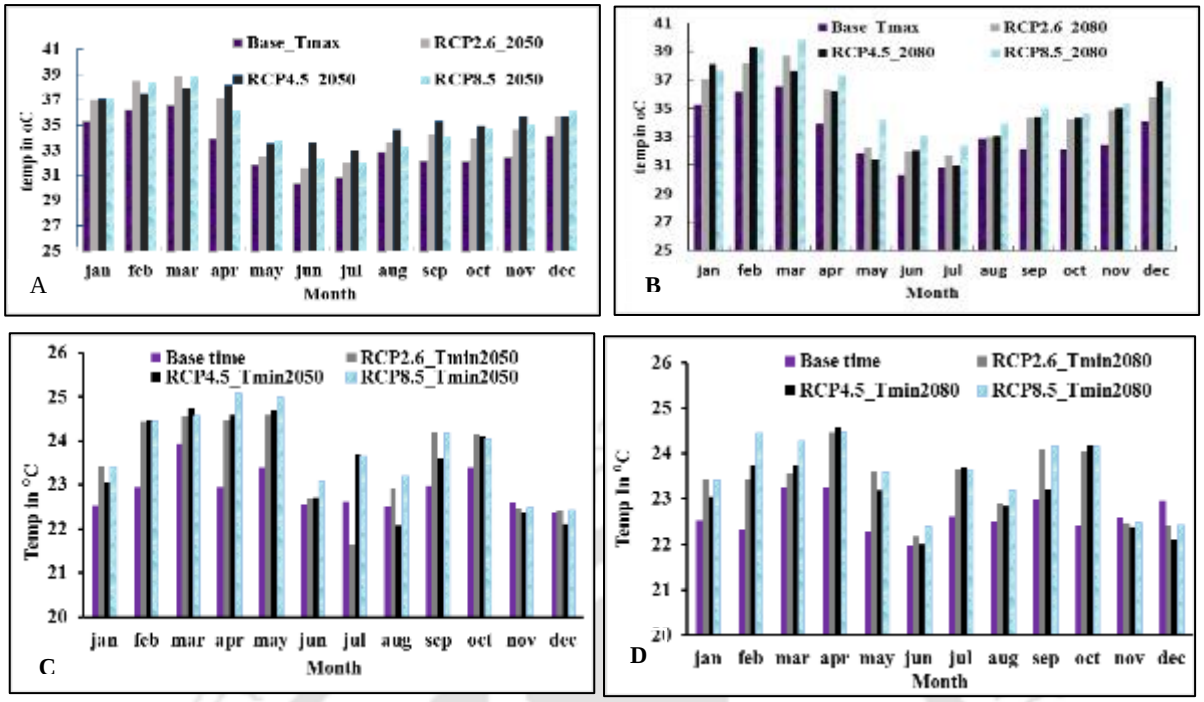

Figure 8.12 Midterm and long-term temperatures (°c): (A and C), maximum and minimum mid-term predicted temperatures; (B and D) maximum and minimum long-term temperature

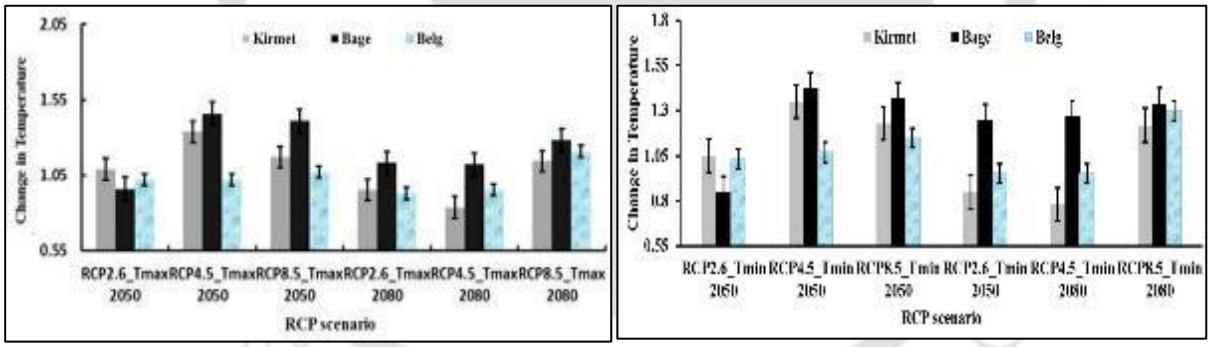

Figure 8.13 Change in mean seasonal maximum temperatures (°C) for long-term and midterm

8.9.1 Spatial Distribution of Rainfall

The spatial distribution of rainfall from the available stations are interpolated using IDW and Kriging to develop the baseline scenario. The mean seasonal, monthly, and annual spatial rainfall interpolations were also performed using the above interpolation techniques. The interpolations again indicate higher values of annual rainfall in the upstream part and lower values in the downstream part of the Lower Omo-Gibe sub-basin. The seasonal data confirms the pattern of a strong wet season and a dry season across the study area (Figure 8.13). The monthly precipitation can also be interpolated by IDW and Kriging approaches in a similar way in (Figure 8.14), however, for the compactness of the script not represented here. Table8.1 shows the min and max, mean and

standard deviation of monthly values of spatially distributed interpolated rainfall values of South Omo sub basin.

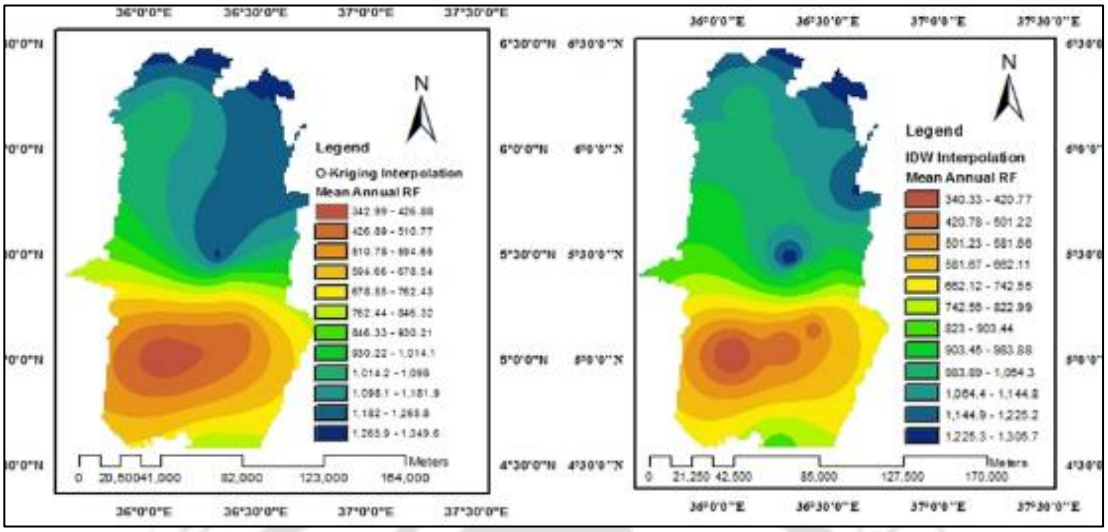

Figure 8. 14Mean annual rainfall interpolation by kriging and IDW for South Omo

The monthly and seasonal rainfall patterns using Ordinary Kriging and IDW were similar for most of the points. The Geostatistical Analyst tool of ArcGIS performs better for normally distributed data. Henceforth, the skewed distributed rainfall data through interpolations are log-transformed to utilize in the software (Yang et al. 2015). Table 8.3 indicates that the values of median and mean are very close, and Table 8.4 Log-transformed data of precipitation (in mm) from interpolations for South Omo shows hence the data distribution is close to normal. Table 8.5 shows the comparison of prediction error statistics for ordinary kriging and IDW interpolation methods. The RMSE and ASE for both kriging and IDW are similar that indicate the predictions are able to incorporate sufficient variability. In this case study, the RMSSE values are close to one for both ordinary Kriging and IDW interpolation. This closeness indicates that both the interpolation techniques are able to incorporate variability and uncertainty effectively.

Table 8.1 Normal data of precipitation (in mm) from interpolations before transforming into log form for South Omo-Gibe

	IDW				Kriging			
	Belg	Bega	Kiremt	Annual	Belg	Bega	Kiremt	Annual
Min	34.03	71.12	22.58	340.15	34.03	71.12	5.98	340.15
Max	582.95	383.2	1085.5	2129.7	956.85	383.2	1085.5	2129.7
Mean	261.95	210.83	420.45	1292.8	295.68	210.83	409.45	1236.6
Std. Dev	191.78	96.47	322.71	387.74	214.98	96.47	312.86	471.01
Skewness	0.353	0.223	0.438	-0.338	0.713	0.22	0.473	-0.30

Kurtosis	1.495	1.622	1.753	3.392	3.29	1.62	1.897	2.92
Median	178.97	213.68	2.68.77	1314.3	290.94	213.68	292.31	1301.5
1st Quartile	79.5	123.75	175.16	1072.6	89.47	123.75	175.16	1031.6
3rd Quartile	447.45	311.4	700.65	1504.3	459.54	331.4	685.72	1501.2

Table 8. 2 Prediction error statistics

	Kriging				IDW			
	Kiremt	Bega	Belg	Annual	Kiremt	Bega	Belg	Annual
ME	-2.24	-2.69	-6.17	-5.806	-2.24	-2.69	-6.17	-5.806
RMSE	228.89	58.78	126.23	271.99	228.89	58.78	126.23	271.99
MSE	0.0025	-0.018	-0.028	-0.034	0.0025	-0.018	-0.028	-0.034
RMSSE	0.965	0.96	0.98	0.975	0.965	0.96	0.98	0.985
ASE	241.38	61.17	125.41	268.366	241.38	61.17	125.41	268.366

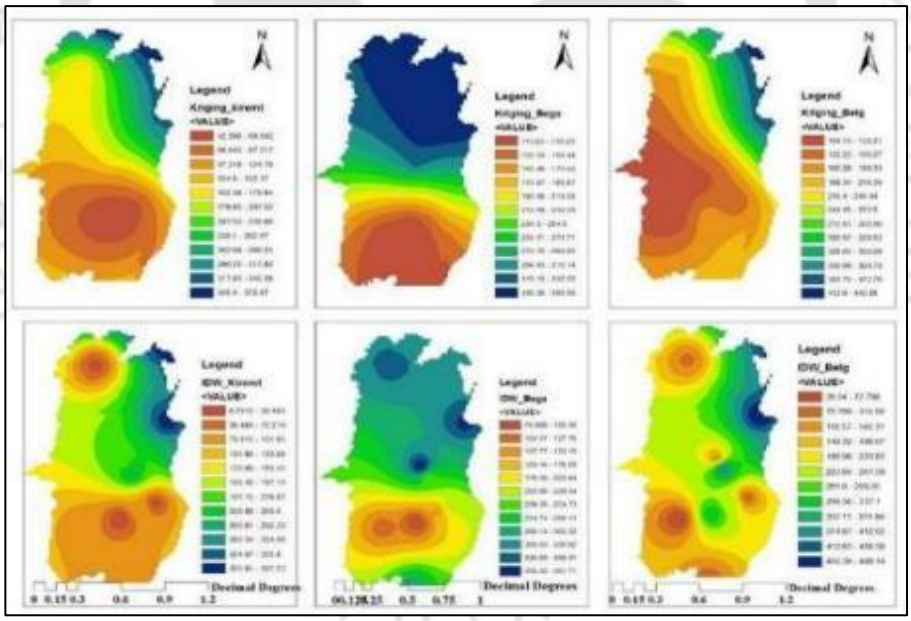

Figure 8.15 Using IDW and Kriging mean rainfall interpolation for South Omo-Gibe

8.9.2 Impact of evapotranspiration on surface water availability

Since the South Omo sub-basin of Omo-Gibe have less meteorological stations, the spatial distribution of data may not be adequate for interpolations. Therefore, the stations located on highland and lowland part of the Omo Gibe basin are also appropriate for interpolating the evapotranspiration. Hence, by making judicious combinations of various neighbouring stations from highland and lowland stations like Jinka, Omoratte, Turmi, Weito, Konso the evapotranspiration in

South Omo is calculated. The meteorological factors determining potential evapotranspiration (ET_o) are hydro-climatological parameters that provide energy for evaporation and eliminate water vapour from the surface. Based on the climatic data, ET_o is calculated using stations Omoratte, Jinka, and Key-Afar. Both the Hargreaves method and Priestley-Taylor method suggested the maximum potential evapotranspiration is during the month of January, whereas the Penman-Montieth method indicated the maximum ET_0 is in the month of March.

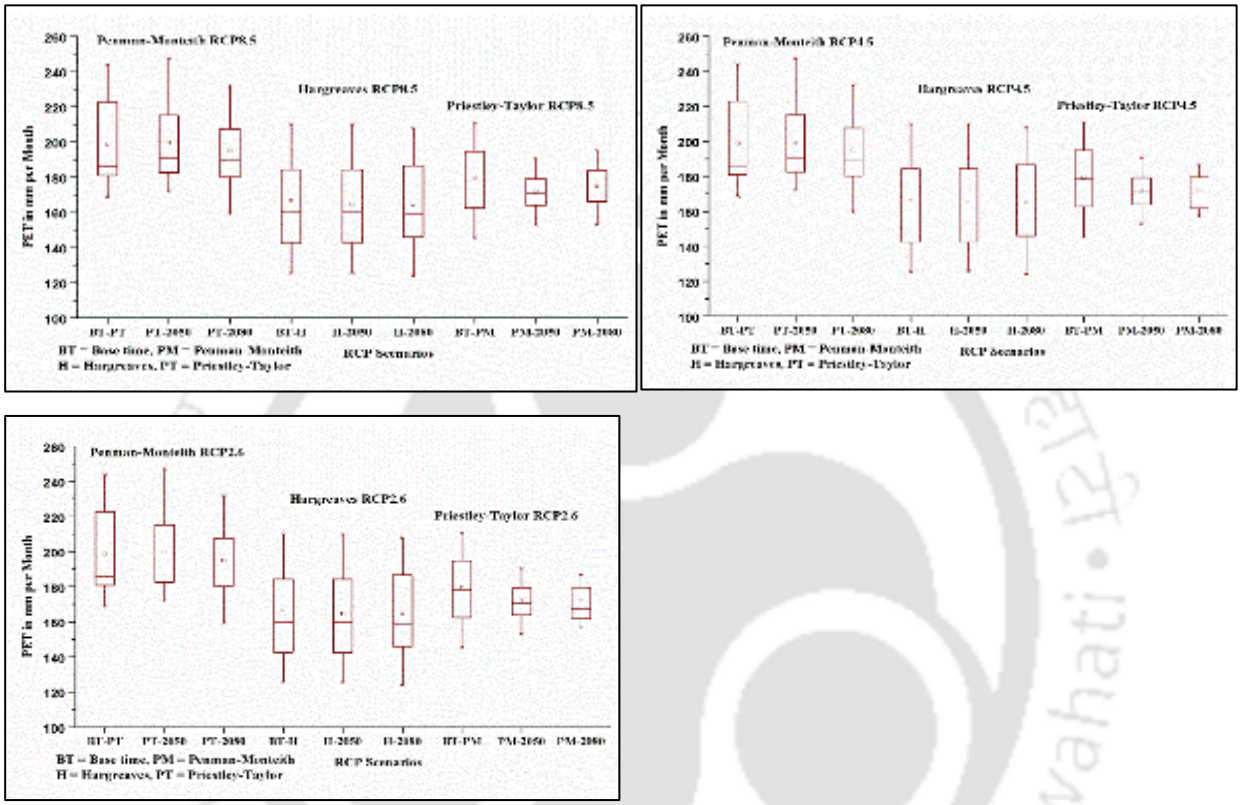

Figure 8.16 Monthly evapotranspiration at South Omo in Omo Gibe basin

As obvious from the fact that evapotranspiration is directly proportional to the temperature, the seasonal variations in potential and actual evapotranspiration show similar trends to that of temperature in the South Omo (Figure 8.16). Seasonal and monthly evapotranspiration using the three different evapotranspiration models show increasing rates during the winter-spring season while using the Penman-Monteith model and decreasing rates from winter to summer and increasing rates from summer to bage season with both Hargreaves and Priestly-Taylor method (Figure 8. 17).

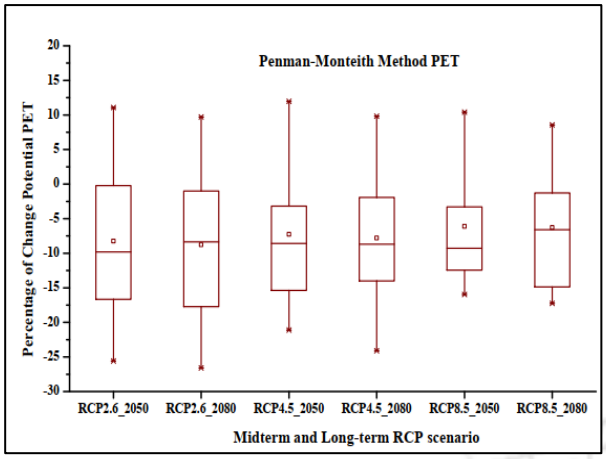

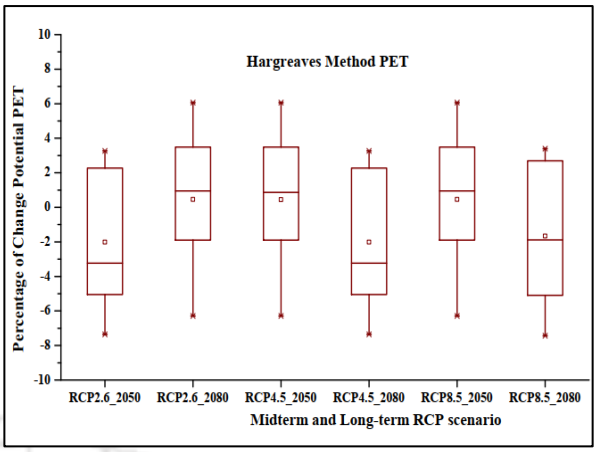

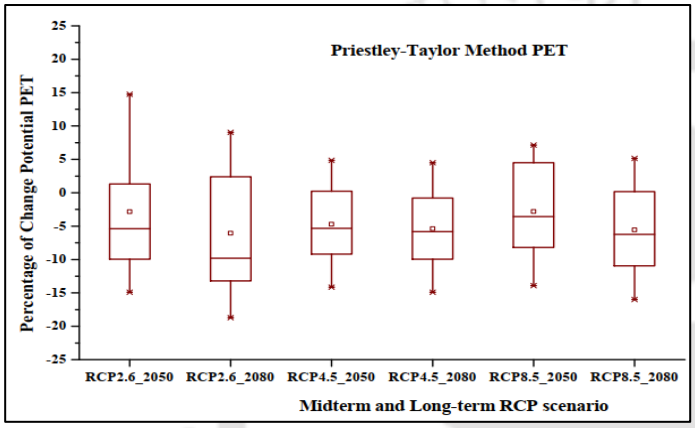

Figure 8.17 Monthly Midterm and Long term RCP evapotranspiration scenario using Penman-Monteith, Hargreves, and Priestley-Taylor methods.

Priestley-Taylor Potential Evaporation suggests a decline in all seasons while using mid-term RCP2.6, long-term RCP4.5, and long-term RCP8.5. However, there is rise in potential evaporation for all other types of scenarios in (Fig 8.17 and 8.16). Hargreaves Mathematical Model shows decreasing trends in all scenarios except for long-term RCP4.5 and mid-term RCP8.5. Penman-Monteith's midterm and long-term RCP scenario for both the Bage and Belg seasons shows declining patterns and rising trends in South Omo during the summer seasons.

Percentage of change of monthly midterm and long-term evapotranspiration scenario at South Omo considering seventy-five and twenty-five percentile is shown in Figure 8.17. In Penman-Monteith analysis, the percentage of change in seasonal PET shows a long-term decrease in kiremt and an increase in long-term and mid-term scenarios in both Baga and Belg. Hargreaves method shows a decrease in PET during Bega and Belg seasons in the mid-term and long-term scenario and an increase during Kiremt season. Priestley-Taylor shows decreasing patterns except for mid-term evapotranspiration in April and May

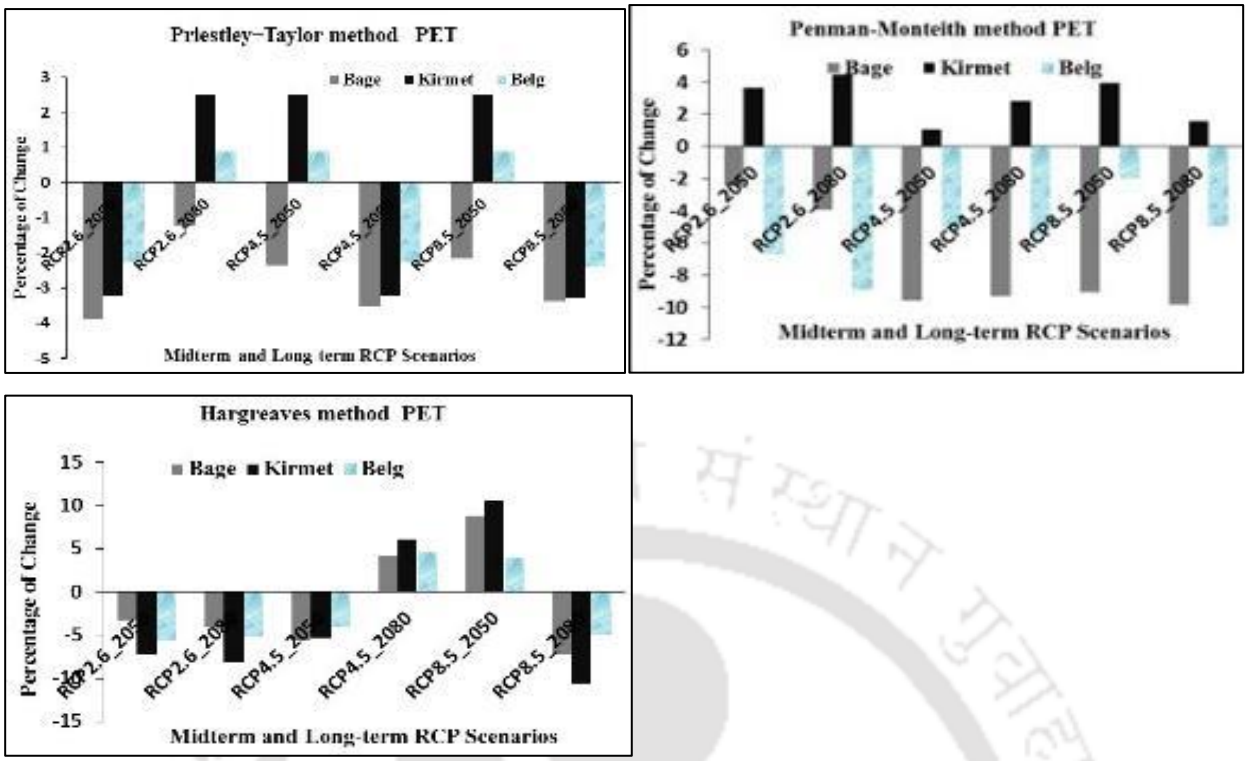

Figure 8.18 Seasonal Midterm and Long term RCP evapotranspiration Scenario

8.10 Hydrological models

8.10.1 SWAT Model Sensitivity parameter analysis

The SWAT model considered 27 parameters associated with stream flows that were analyzed with an interval of Latin Hypercube for the South Omo. Among the ten parameters selected for calibration, seven of them affect the surface runoff (CN2, CH_K2, SOL_Z, REVAPMIN, GW_REVAP, ESCO, and CANMAX), and the remaining three affect base flow generation (SOL_AWC, ALPHA_BF, and GWQMN). The sensitivity analysis indicated that 12 flow parameters are more sensitive to the SWAT model in the 21 sub-basins formed in the study area in South Omo.

8.10.2 Model Calibration and Validation of streamflow of South Omo

The calibration of the SWAT model for South Omo was done for a 12 years' period from January 1st, 1995 to December 31st, 2007. The statistical parameters obtained were - R^2=0.83, NSE=0.76, and PBIAS = -3.37. These statistical parameters' values show a good correlation between the computational model simulation's and observed values. The validation was performed for the period from January 1st, 2008 to December 31st, 2015. The R^2 was found to be 0.856, NSE = 0.825 and PBIAS = -11.42. These values again show the simulation's very good correlation with the measured

flow in table 8.4. The spatial resolution of the digital elevation model data affects the delineation of the catchment, sub-catchment, and stream network of the study area. A change in the value of spatial resolution results in a considerable change in the volume of simulated streamflow. In this study, 30 m by 30 m resolution of the spatial data was used that yielded -3.37% error at calibration and -11.42% in validation for flow simulations. Since the PBIAS was having some negative values, the simulations were overestimating the surface runoff marginally.

Table 8.2 Calibration result of statistic for monthly measured and simulated Stream flow

	Mean Stream flow(m^3/s)		Model Performance		
	Observed	Simulated	R^2	NSE	PBIAS
Calibration (1995-2007)	280.2322	193.374	0.83	0.76	-3.37
Validation (2008 to 2015)	154.4572	181.773	0.856	0.825	-11.42

8.10.3 Impacts of Climate Change on future streamflow and effect of evapotranspiration and precipitation on streamflow

Climatic circumstances affect evapotranspiration and precipitation, thereby, impacting the surface runoff, soil moisture storage, and other sub-components of the hydrological cycle. An increase in precipitation due to climatic conditions causes an increase in streamflow and vice-versa. To compare the futuristic impacts, analyses were done in SWAT to simulate for 10 continuous years for the baseline period (1995-2005), mid-term period (2045-2055), and long-term period (2075-2085). The mean monthly precipitations, evapotranspiration, and streamflow for the above reference periods are compared (Figure 8.20). The plots indicate an increasing trend in the long-term for evapotranspiration and a decreasing trend for streamflow. This assessment is very important to sustain the water balance for future management. The futuristic precipitations showed increased magnitudes for all types of emission scenarios. The evapotranspiration values also rose for all the reference periods and all emission scenarios.

The modelling studies performed in this research aid in identifying future high and low stream flows that are essential for effective planning, designing, and monitoring basin resources. Therefore, assessing the influence of precipitation and evaporations on streamflow is important to know the water balance in the basin in future scenarios. The temperature increase results in a rise of evaporation, which may lead to water scarcities in the region. As the forecast from the research indicated rising minimum and maximum temperatures, they may also lead to unusual heavy

precipitation events during summers, thereby, resulting in the increased runoff. The temperature increase can also cause more evapotranspiration that may lead to a reduction in soil moisture storage.

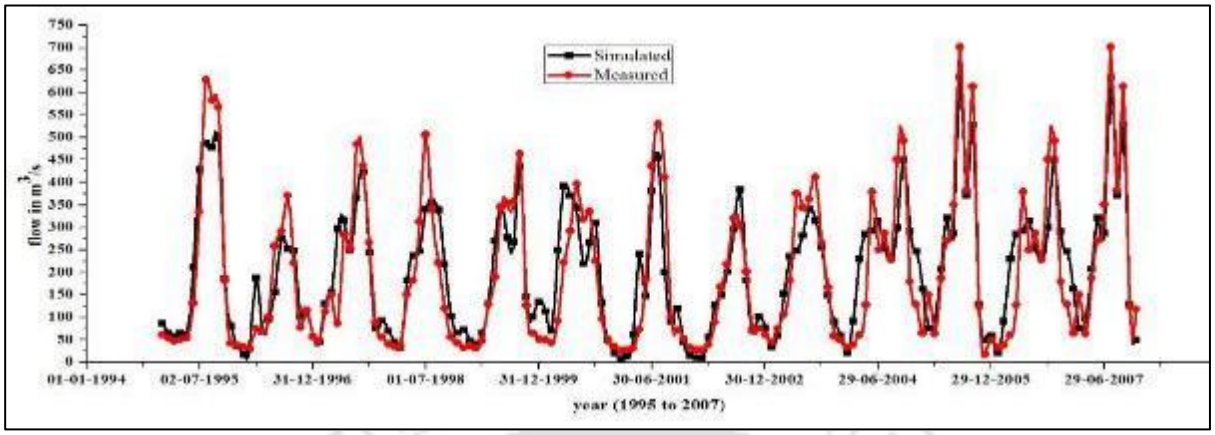

Figure 8.19 Comparison of observed and SWAT simulated surface runoff during calibration outlet of the sub-basin Nerie station: Nr Jinka.

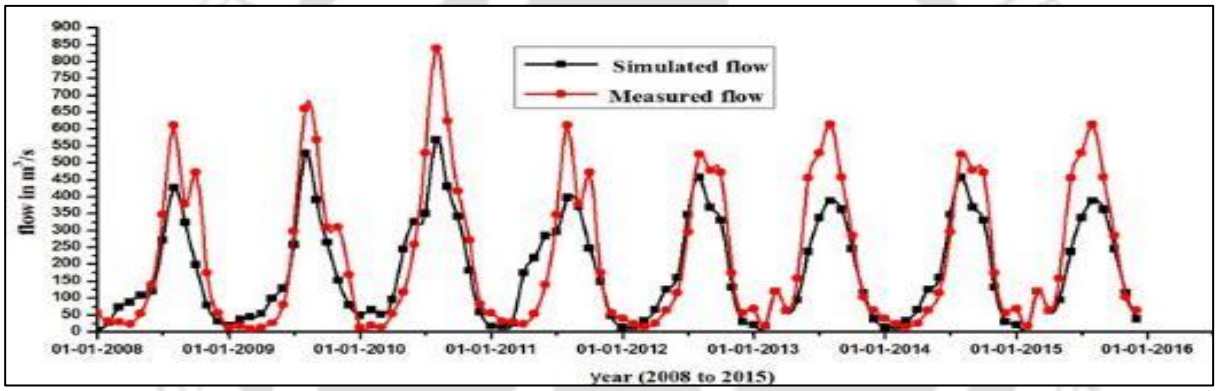

Figure 8.20 Relation between simulation and measured flow during the validation period outlet of the sub-basin Nerie station: Nr Jinka

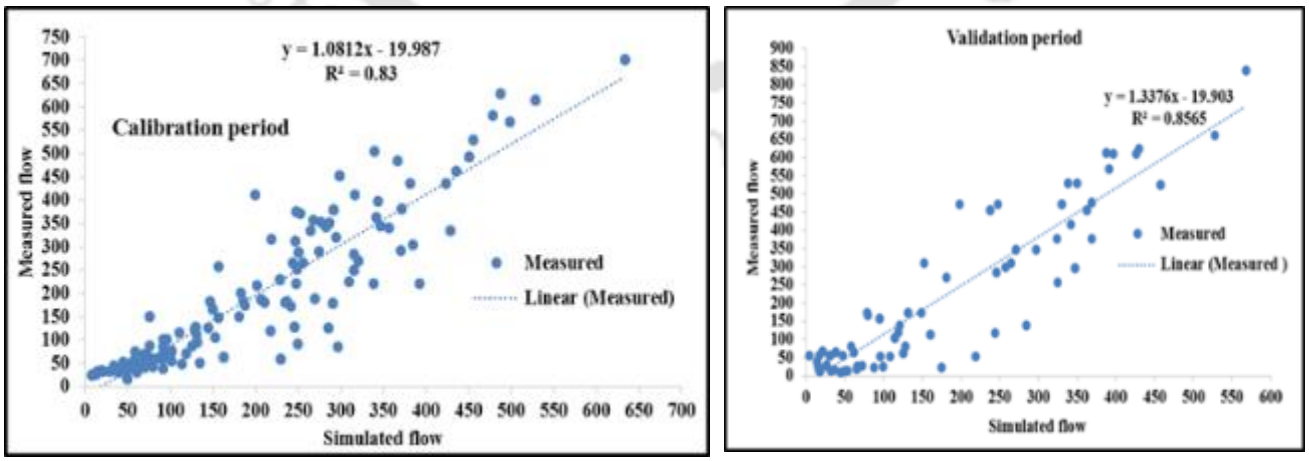

Figure 8.21 Relation between Simulation and measured flow during Validation period

8.10.4 Effect of evapotranspiration and precipitation on streamflow

Climatic circumstances that affect evapotranspiration, such as temperature, wind, relative humidity, seasons, and precipitation directly affect surface runoff and soil moisture. Higher amount of precipitation increases streamflow, but decreasing precipitation reduces surface water potential. Annual precipitation, Evapotranspiration, and streamflow for the reference base period, mid-term, and long-term are compared compared with past time periods Precipitation increased in all cases, and the change was distributed evenly between times. Evapotranspiration also increased, with the greatest change occurring between the reference periods. In most cases, the total increase in ET nearly offset the increase in precipitation, resulting in comparatively small changes in streamflow. Climate change leads to amplified climatic changeability, which would lead to increased frequency and magnitude of weather-related extreme events (*Becker and Bugmann, 1997*). An extreme climatic event will result in higher losses of life in a developing country than in a developed country because of different adaptive capacity (*IPCC, 2001b*). Silting of the river bed and landslides are another cause that changes the river courses, poor natural drainage and so on. Understanding the regime and the distinctiveness of future high and low stream flows is of the vital importance of ineffective planning, designing, and monitoring basin resource.

8.10.5 Impacts of Climate Change on future stream flow based on SWAT tools

Change in magnitude and frequencies of weather related events affect basin water resources. Developing countries are more vulnerable to losses accrued due to climate changes. As Ethiopia is a developing country, its vulnerability to climate change is also huge. Major causes of floods in Ethiopia, as well as lower Omo- Gibe River Basin, include intense precipitation, inadequate river banks to contain high runoff due to this high intense precipitation, deforestation and human interference in nature and landscape. Apart from above, the river bed siltation and landslides can affect drainage as well as changes in river courses. The Figure 8.22 indicate that the relation between precipitation, evaporation, and total water yield in midterm and long-term. It shows an increasing trend in total water yields. Therefore, assessing the influence of precipitation and evaporations on streamflow is important to know that catchment water balance.

The temperature increase results in a rise of evaporation, which may lead to water scarcities in the region. As the forecast from the research indicated rising minimum and maximum temperatures, they may also lead to unusual heavy precipitation events during summers, thereby, resulting in the increased runoff. The temperature increase can also cause more evapotranspiration that may lead to a reduction in soil moisture storage.

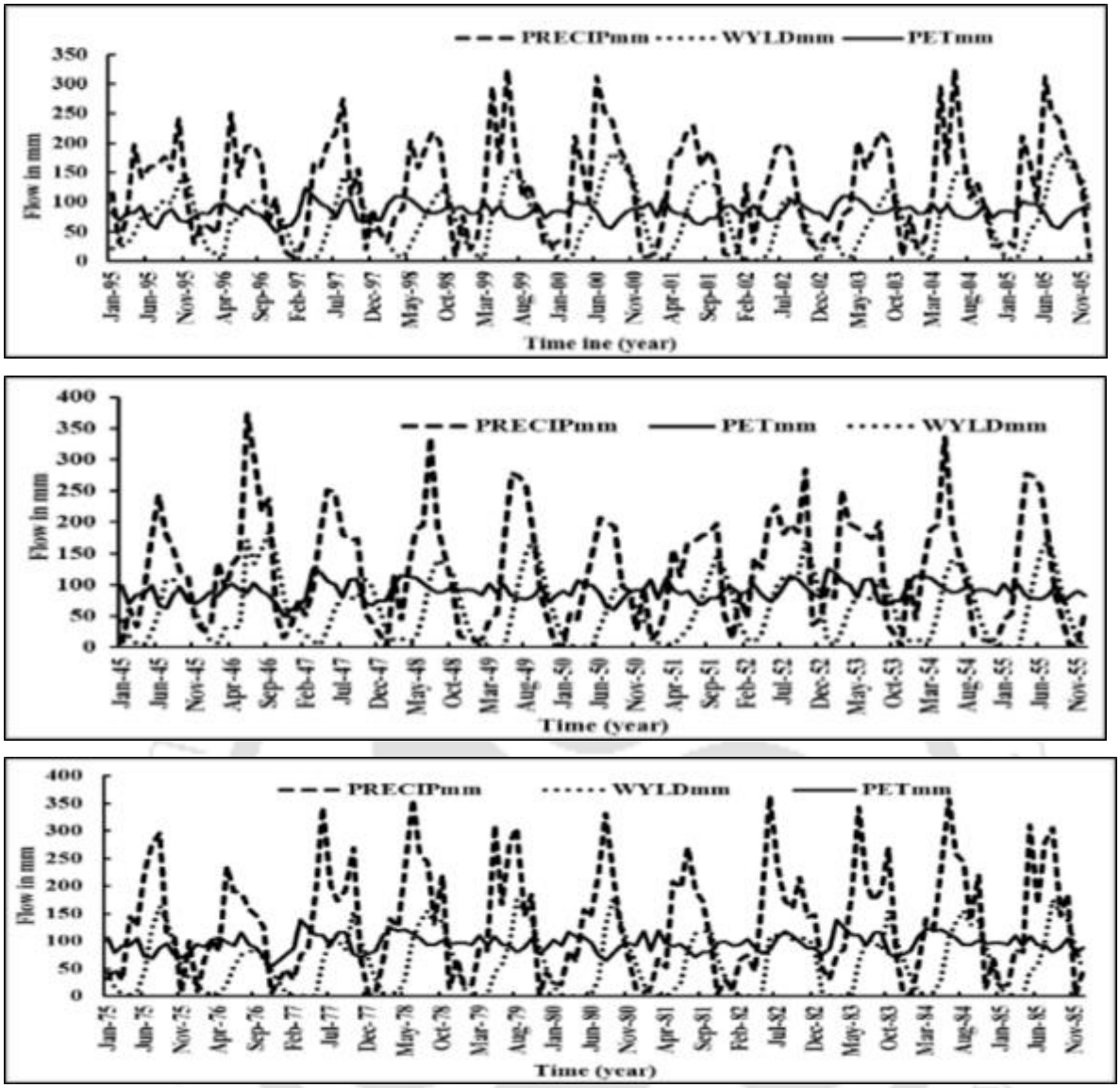

Figure 8.22 Using high emission scenario, precipitation, evapotranspiration, and total water yield

8.11 Conclusion

The chapter analysed the possible climate change effects on water resources systems in South Omo. The validity of the application of SWAT model for streamflow estimation is substantiated by the acceptable values of statistical performance (R^2, NSE, and PBIAS). The SWAT model simulated for the future basin characteristics and estimated streamflows for different emission scenarios (RCP2.6, RCP4.5, and RCP8.5) for short-term, mid-term, and long-term predictions.

Chapter 9 Conclusion and Recommendation

9.1 Conclusions

Analysis on the impact of climate change on water resources sectors are needed to evaluate the vulnerability of infrastructure systems and the effectiveness of different adaptation strategies in managing climate-related stresses. Assessing the effect of climatic variations on hydrological processes and water resources, based on spatial and temporal change are important for measuring water-sensitive parameters in the area and forecasting future water potentials. The research addressed how climate change will affect water resources at the basin level, as well as highlight the need to transform existing water infrastructure in the basin to sustain water resources systems for various climate change forecasts. The study used remote sensing images, GIS analyses, and hydrological SWAT model with additional climate change inputs based on the SRES and RCP Scenario.

The analysis shows that seasonal variation of precipitation in Upper Gibe and Gojeb catchment shows increasing trends in all low (RCP2.6) and medium (RCP4.5) emission scenario and decreasing in summer for high (RCP8.5) emission scenario. In Wabe and Gojeb catchments, the precipitation trends shows increasing, and in Upper Gibe and Lower Gibe catchments, the trends are somewhat decreasing in the 2080s. For RCP2.6 low scenario in the 2050s and the 2080s, the trends are alomost same in Upper Gibe and Lower Gibe but slightly increasing in Gojeb and Wabe as compare to base time scenario. For RCP4.5, the rainfall magnitudes increased with return period for the 2080s in the Wabe catchment. Percentage of change of seasonal precipitation in Gibe-III dam catchment shows that Kiremt precipitation has an increasing trend from 2.4% mid-term to 16.95% long-term in RCP2.6, 16.34% midterm to 20.6% long-term in RCP8.5 but a decreasing trend in RCP4.5 from 24.7% midterm to 10.71% long-term. The average annual maximum temperature in the Upper Omo Gibe basin has been projected from the 2050s to the 2080s and it shows increasing trends when compared to both climate change scenarios (RCP and SRES A1B). The RCP Scenario was a better representative scenario than the SRES (A1B) Scenario.

The statistical performance on the suitability of SWAT hydrological model for streamflow estimation for the study region was satisfactory with permissible values of R^2, NSE, and PBIAS. These testings were done for SWAT simulations of the whole Omo-Gibe basin, and the individual sub-basins like Great Gibe and South Omo.

The mean maximum annual temperatures are estimated to increase by 1.34°C, 1.58°C to 1.47°C, in mid-term 2050s scenario for the RCP2.6, RCP4.5, and RCP8.5, respectively. Similarly, the mean annual minimum temperatures increased by 0.98°C, 1.03°C, and 1.35°C in future long-term 2080s scenario for the above RCPs. The geo-statistical analysis shows that RMSSE is close to 0.98 for both ordinary kriging and IDW interpolations that signify the interpolation method's validity in applying for the requisite hydrological variable.

The ten-year simulations for the baseline period, mid-term future, and long-term future for the South Omo using the high emission scenario disclosed the facts that mid-term period yielded more surface runoff as well as peaks in runoff as compared to the baseline and long-term periods. However, the long-term future precipitations suggested more intensities in storms as the magnitudes of peaks are more for the long term.

GIS tools and remote sensing techniques are important tools for basin planning and management. When understanding a wide range of transition phenomena, the distribution of spatial and temporal LULC is very important. LULC data from remote sensing helps to track changes in land-use trends and use them to predict possible changes in the environment. As such, reliable information on LULC and an understanding of the changes occurring within them is important. The purpose of this study was to determine the hydrological effect of LULC changes in the catchment using the hydrological model over the past years of 1987, 2002, and 2017. The LULC change observed in this catchment was established from collected satellite and ground truth data that provided useful information about land-use changes and allowed us to better understand the causes and effects of land-use change over time.

In the past three 15-years interval data, the Omo Gibe basin had experienced a significant change over land use. It presumed that the rapid increase of the human population has created deforestation and the increase of farmland, and its annual crop production is not proportional in particular to this altered the catchment area. Between 1987 and 2002, land-use changes were rare. However, they changed significantly in the 2017 picture year. It applies to the reduction in forest land and grassland followed by the rise in agricultural and built-up areas, suggesting that the watershed region is under high population pressure. Forest and grasslands have been converted into farmland, and grasslands have been transformed into bare land, woodlands, and bush land.

Reforestation was found to be the Best management scenario and were more effective in reducing sediment than other scenarios in all land use forms. The introduction of BMPs reforestation scenario decreases the sediment output by 49.25%, 34.55%, and 40.84%, respectively for LULC

1987, 2002, and 2017 compared to the second and third scenarios. The reforestation scenario was also more effective than the other scenarios in reducing sediment yields. As a result, land use and climate change could be combined with hydrological models to predict the potential impacts of land-use change on surface and subsurface water. It helps stakeholders and decision-makers make better adoptions for land use and climate change, and consider the planning, control, and management of water resources.

- Climate data was projected from three GCMs output under RCP scenarios.
- Modeling variations in precipitation and evaporation has a significant impact on streamflow in arid and semi-arid areas downstream of the basin, and future climate change for South Omo Gibe anticipates rain and evaporation shifts in season.
- The effects of land use land cover dynamics on stream flow and sediment Yield is detected for most part of the basin.
- The Soil and Water Assessment Tool (SWAT) and SWAT Calibration and Uncertainty program is used to future streamflow modeled through the calibrated and validation SWAT models.
- Most upstream parts of the forest land are converted into cultivated land and human settlement.
- The model results have shown a good agreement with the observed and simulated values.
- Implementing scenario 4 (reforestation) is the best management strategy. Reforestation is potentially found to be the BMP to reduce the sediment yield and safeguard the various hydro-projects in the basin.

9.2 Recommendations

- Based on the statistical principle analysis used to fix optimum number of station for the basin, the assumption helps to obtain number of gauges for a given basin optimally based on an assigned percentage of error estimating for mean aerial rainfall of the area. Because of the limitation in hydrological data, this research strongly recommend to increase the station distribution for hydrological and climatological data.
- The study used the spatial data like DEM and LULC resolution of 30 m by 30 m. The research did not account for the predictive higher classification accuracy for high-resolution. High-resolution satellite images with more detail Land Use Land Cover data will be useful in accurately classifying LULC. The incorporation of better resolution data along with climate projections enhancethe assessment of the impact of climate and LULC dynamics for midterm and long-term projection.

- This study used the Thiessen polygon method to estimate areal rainfall. In additional studies, radar rainfall data should be used in addition to point observations on the ground to reduce model uncertainty caused by poor quality.
- Regionalization of the basin and water resource allocation under climate change using better optimisation tools and new computational algorithms.
- Impact of Dam regulation on streamflow, downstream ecology and Turkana Lake.

References

Abbasi, N. A., Xu, X., Lucas-Borja, M. E., Dang, W., & Liu, B. (2019). The use of check dams in watershed management projects: Examples from around the world. Science of the total environment, 676, 683-691.

Abbate, E., Bruni, P., & Sagri, M. (2015). Geology of Ethiopia: a review and geomorphological perspectives. In Landscapes and landforms of Ethiopia (pp. 33-64). Springer, Dordrecht.

Abdel-Gawad, M., Gass, I. G., Hepworth, J. V., Vail, J. R., Mason, J. F., & Greenwood, J. G. W. (1970). Interpretation of satellite photographs of the Red Sea & Gulf of Aden. Philosophical Transactions for the Royal Society of London., Mathematical and Physical Sciences, 23-40.

Abdo, K. S., Fiseha, B. M., Rientjes, T. H. M., Gieske, A. S. M., & Haile, A. T. (2009). Assessment of climate change impacts on the hydrology of Gilgel Abay catchment in Lake Tana basin, Ethiopia. Hydrological Processes: An International Journal, 23(26), 3661-3669.

Abebe, S. (2005). Land-Use and Land-Cover change in headstream of Abbay watershed, Blue Nile Basin, Ethiopia. Addis Ababa University.

Abeyou, w. (2008). Hydrological balance of Lake Tana, Upper Blue Nile Basin, Ethiopia, International Institute for Geo-information science and Earth observation Netherlands.

Adem, A. A., Tilahun, S. A., Ayana, E. K., Worqlul, A. W., Assefa, T. T., Dessu, S. B., & Melesse, A. M. (2016). Climate change impact on sediment yield in the Upper Gilgel Abay catchment, Blue Nile Basin, Ethiopia. In Landscape dynamics, soils and hydrological processes in varied climates (pp. 615-644). Springer, Cham.

Adeniyi, M. O. (2016). The consequences of the IPCC AR5 RCPs 4.5 and 8.5 climate change scenarios on precipitation in West Africa. Climatic change, 139(2), 245-263.

Agha, O. M. A. M., Bağçacı, S. Ç., & Şarlak, N. (2017). Homogeneity analysis of precipitation series in North Iraq. IOSR Journal of Applied Geology and Geophysics, 5(03), 57-63.

Agrawal, A. (2008). The role of local institutions in adaptation to climate change. World Bank.

Ahmed, K. M., Shamsudduha, M., Chandler, R. E., & Taylor, R. G., (2009). Recent trends in groundwater levels in a highly seasonal hydrological system: the Ganges-Brahmaputra-Meghna Delta. Hydrol Earth Syst Sc, 13(12), 2373-2385.

Alcamo, J., Henrichs, T., & Rösch, T. (2017). World water in 2025: Global modeling and scenario analysis for the world commission on water for the 21st century.

Alemseged, T. H., and Tom, R. (2015). Evaluation of regional climate model simulations of rainfall over the Upper Blue Nile basin. Atmospheric research, 161, 57-64.

Allaby, R. G., Banerjee, M., & Brown, T. A. (1999). Evolution of the high molecular weight

glutenin loci of the A, B, D, and G genomes of wheat. Genome, 42(2), 296-307.

Allen, J. C., & Barnes, D. F. (1985). The causes of deforestation in developing countries. Annals of the association of American Geographers, 75(2), 163-184.

Almeida, A., Loy, A., & Hofmann, H. (2018). ggplot2 Compatible Quantile-Quantile Plots in R. R J., 10(2), 248.

Altobelli, M., Cipolla, S. S., & Maglionico, M. (2020). Combined Application of Real-Time Control and Green Technologies to Urban Drainage Systems. Water, 12(12), 3432.

Amin, A., Iqbal, J., Asghar, A., & Ribbe, L. (2018). Analysis of current and future water demands in the Upper Indus Basin under IPCC climate and socio-economic scenarios using a hydro-economic WEAP model. Water, 10(5), 537.

Andersen, M. S. (2007). An introductory note on the environmental economics of the circular economy. Sustainability science, 2(1), 133-140.

Aneseyee, A.B., Elias, E., Soromessa, T., and Feyisa, G.L., 2020. Land use/land cover change effect on soil erosion and sediment delivery in the Winike watershed, Omo Gibe Basin, Ethiopia. Science of The Total Environment, 728, 138776.

Aneseyee, A.B., Soromessa, T., and Elias, E., 2019. The effect of land use/land cover changes on ecosystem services valuation of Winike watershed, Omo Gibe basin, Ethiopia. Human and Ecological Risk Assessment: An International Journal, 1–20.

Anjomshoaa, A., & Salmanzadeh, M. (2019). Filling missing meteorological data in heating and cooling seasons separately. International Journal of Climatology, 39(2), 701-710.

Araya, A., Keesstra, S. D., & Stroosnijder, L. (2010). A new agro-climatic classification for crop suitability zoning in northern semi-arid Ethiopia. Agricultural and forest meteorology, 150 (7-8), 1057-1064.

Araya, A., Keesstra, S. D., & Stroosnijder, L. (2010). A new agro-climatic classification for crop suitability zoning in northern semi-arid Ethiopia. Agricultural and Forest Meteorology, 150(7-8), 1057-1064.

Arnold, J.G and N. Fohrer, (2005). SWAT-2000 current capabilities and research in applied watershed modeling. Journal of Hydrology (19) pp53-572.

Arnold, J.G., Allen, P.M, and Bernhardt, G., (1993). A comprehensive surface-groundwater flow model, Journal of Hydrology 142: pp47-69.

Arnold, J.G., Kiniry, J.R., Srinivasan, R., Williams, J.R., Haney, E.B., Neitsch, S.L. (2012). Soil and Water Assessment Tool Input/Output Documentation Version 2012

Arnold, J.G., Srinivasan, R., Muttiah, R.S., and Williams, J.R., 1998. Large area hydrologic modeling and assessment Part I: Model development. Journal of the American Water

Resources Association, 34 (1), 73–89.

Arsiso, B. K., Tsidu, G. M., Stoffberg, G. H., & Tadesse, T. (2018). Influence of urbanization-driven land use/cover change on climate: The case of Addis Ababa, Ethiopia. Physics and Chemistry of the Earth, Parts A/B/C, 105, 212-223.

Asefa, D. (2011). Water use and operation analysis of water resource systems in Omo Gibe river basin (Doctoral dissertation, Addis Ababa University).

Ashley, R. M., Balmforth, D. J., Saul, A. J., & Blanskby, J. D. (2005). Flooding in the future–predicting climate change, risks and responses in urban areas. Water Science and Technology, 52(5), 265-273.

Asitatikie, A. N. (2019). Impact of Land Use/Land Cover Change on Hydrology of the Catchment: The Case of Upper Ribb Catchment, Lake Tana Sub Basin, Ethiopia.

Aslami, F., & Ghorbani, A. (2018). Object-based land-use/land-cover change detection using Landsat imagery: a case study of Ardabil, Namin, and Nir counties in northwest Iran. Environmental monitoring and assessment, 190(7), 1-14.

Asl-Rousta, B., Mousavi, S. J., Ehtiat, M., & Ahmadi, M. (2018). SWAT-based hydrological modelling using model selection criteria. Water resources management, 32(6), 2181-2197.

Auffhammer, M., Hsiang, S. M., Schlenker, W., & Sobel, A. (2013). Using weather data and climate model output in economic analyses of climate change. Review of Environmental Economics and Policy, 7(2), 181-198.

Avery, S., & Eng, C. (2012). Lake Turkana & the Lower Omo: hydrological impacts of major dam and irrigation developments. African Studies Centre, the University of Oxford.

Avery, S., & Eng, C. (2012). Lake Turkana and the Lower Omo: hydrological impacts of major dam and irrigation developments. African Studies Centre, the University of Oxford.

Awulachew, S. B., Yilma, A. D., Loulseged, M., Loiskandl, W., Ayana, M., & Alamirew, T. (2007). Water resources and irrigation development in Ethiopia (Vol. 123).

Ayalew, L. (2009). Analyzing the effects of historical and recent floods on channel pattern and the environment in the Lower Omo basin of Ethiopia using satellite images and GIS. Environmental geology, 58(8), 1713-1726.

Ayalew, L. (2009). Analyzing the effects of historical and recent floods on channel pattern and the environment in the Lower Omo basin of Ethiopia using satellite images and GIS. Environmental geology, 58(8), 1713-1726.

Babovic, V., & Keijzer, M. (2002). Rainfall runoff modelling based on genetic programming. Hydrology Research, 33(5), 331-346.

Baede, A. P. M., Ahlonsou, E., Ding, Y., & Schimel, D. E. (2001). Climate change 2001: The

scientific basis. The climate system: An overview.

Bagdonavicius, V., & Nikulin, M. S. (2011). Chi-squared goodness-of-fit test for right censored data. The International Journal of Applied Mathematics and Statistics, 24(1), 1-11.

Baker, C., Lawrence, R., Montagne, C., & Patten, D. (2006). Mapping wetlands and riparian areas using Landsat ETM+ imagery & decision-tree-based models. Wetlands, 26(2), 465.

Bates, B., Kundzewicz, Z., & Wu, S. (2008). Climate change and water. Intergovernmental Panel on Climate Change Secretariat.

Becker, A., & Bugmann, H. (1997). Predicting global change impacts on mountain hydrology and ecology: integrated catchment hydrology/altitudinal gradient studies: workshop report: Kathmandu, Nepal, 30 March 1996. Global Change Report (Sweden).

Behr, A., & Tente, S. (2008). Stochastic frontier analysis by means of maximum likelihood and the method of moments.

Berihun, M.L., Tsunekawa, A., Haregeweyn, N., Meshesha, D.T., Adgo, E., Tsubo, M., Masunaga, T., Fenta, A.A., Sultan, D., Yibeltal, M., Ebabu, K. (2019). Hydrological responses to land use/land cover change and climate variability in contrasting agro-ecological environments of the Upper Blue Nile basin, Ethiopia. Science of the Total Environment 689, pp 347-365

Betrie, G. D., Mohamed, Y. A., van Griensven, A., and Srinivasan, R. (2011). Sediment management modelling in the Blue Nile Basin using SWAT model.

Betrie, G.D., Mohamed, Y.A., van Griensven, A., and Srinivasan, R., 2011. Sediment management modelling in the Blue Nile Basin using SWAT model. Hydrology and Earth System Sciences, 15 (3), 807–818.

Beyer, R., Krapp, M., & Manica, A. (2019). A systematic comparison of bias correction methods for paleoclimate simulations. Clim. Past Discuss, 11, 1-23.

Bhunia, G. S., Shit, P. K., & Maiti, R. (2018). Comparison of GIS-based interpolation methods for spatial distribution of soil organic carbon (SOC). Journal of the Saudi Society of Agricultural Sciences, 114-126.

Biniyam, Y., & Kemal, A. (2017). The impacts of climate change on rainfall and flood frequency: the case of Hare Watershed, Southern Rift Valley of Ethiopia. J. Earth Sci. cc, 8, 383.

Boivin, N. L., Zeder, M. A., Fuller, D. Q., Crowther, A., Larson, G., Erlandson, J. M., and Petraglia, M. D. (2016). Ecological consequences of human niche construction: Examining long-term anthropogenic shaping of global species distributions. Proceedings of the National Academy of Sciences, 113(23), 6388-6396.

Borrelli, P., Alewell, C., Alvarez, P., Anache, J. A. A., Baartman, J., Ballabio, C., ... & Panagos, P. (2021). Soil erosion modelling: A global review and statistical analysis. Science of the total

environment, 146494.

Bosworth, W., Huchon, P., & McClay, K. (2005). The red sea and Gulf of Aden basins. Journal of African Earth Sciences, 43(1-3), 334-378.

Bouwer, L. M. (2011). Have disaster losses increased due to anthropogenic climate change?. Bulletin of the American Meteorological Society, 92(1), 39-46.

Bracmort, K.S., Arabi, M., Frankenberger, J.R., Engel, B.A., and Arnold, J.G., 2006. Modeling long-term water quality impact of structural BMPs. Transactions of the ASABE, 49 (2), 367–374.

Bronstert, A., Niehoff, D. and Burger, G. (2002). Effects of Climate and Land-Use Change on Storm Runoff Generation: Present Knowledge and Modelling Capabilities. Hydrol. Process, 16, 509–529.

Busuioc, A., & Dumitrescu, A. (2018). Empirical-Statistical Downscaling: Nonlinear Statistical Downscaling. In Oxford Research Encyclopedia of Climate Science.

Butt, A., Shabbir, R., Ahmad, S. S., and Aziz, N. (2015). Land use change mapping and analysis using Remote Sensing and GIS: A case study of Simly watershed, Islamabad, Pakistan. The Egyptian Journal of Remote Sensing and Space Science, 18(2), 251-259.

Calder, I.R. (1998). Water Resource and Land-Use Issues, SWIM Paper 3, International Water.

Campozana, F. P., & Lake, L. W. (2008). A Novel Kriging Approach for Incorporating Nonlinear Constraints. In ECMOR XI-11th European Conference on the Mathematics of Oil Recovery.

Carmona, G., Varela-Ortega, C., & Bromley, J. (2013). Supporting decision making under uncertainty: development of a participatory integrated model for water management in the middle Guadiana river basin. Environmental modelling & software, 50, 144-157.

Carter, T. R., La Rovere, E. L., Jones, R. N., Leemans, R., Mearns, L. O., Nakicenovic, N., ... & Skea, J. (2001). Developing and applying scenarios. Climate change, 200, 145-190.

Castillo, E., Hadi, A. S., Balakrishnan, N., & Sarabia, J. M. (2005). Extreme value and related models with applications in engineering and science.

Catholic Relief Services (CRS) , (2009). Adapting to Climate Change a case Study: Ethiopia change, risks, and responses in urban areas. Water Sci Technol 52: 265-273.1-30

Catholic Relief Services, (2009). Adapting to Climate Change a case Study: Ethiopia 1-30.

Cavallaro, G., Riedel, M., Richerzhagen, M., Benediktsson, J. A., & Plaza, A. (2015). On understanding big data impacts in remotely sensed image classification using support vector machine methods. IEEE journal of selected topics in applied earth observations and remote sensing, 8(10), 4634-4646.

Chaemiso, S.E., Abebe, A., & Pingale, S.M. (2016). Assessment of the impact of climate change on

surface hydrological processes using SWAT: a case study of Omo-Gibe river basin, Ethiopia. Modeling Earth Systems and Environment 2, pp 205

Chandra, P., Patel, P. L., Porey, P. D., & Gupta, I. D. (2014). Estimation of sediment yield using SWAT model for Upper Tapi basin. ISH Journal of Hydraulic Engineering, 20(3), 291-300.

Chandramohan, T., Jose, M. K., Purandara, B. K., & Venkatesh, B. (2018). Revision of Empirical Coefficients of Commonly Used Flood Formulae Using Flow Data from Karnataka Rivers. In Hydrologic Modeling (pp. 555-563). Springer, Singapore.

Chang, H., & Franczyk, J. (2008). Climate change, land-use change, and floods: Toward an integrated assessment. Geography Compass, 2(5), 1549-1579.

Chang, J., Wang, Y., Istanbulluoglu, E., Bai, T., Huang, Q., Yang, D., & Huang, S. (2015). Impact of climate change and human activities on runoff in the Weihe River Basin, China. Quaternary International, 380, 169-179.

Change, I. P. O. C. (2001). Climate change 2007: Impacts, adaptation and vulnerability. Genebra, Suíça.

Change, N. G. C. (2020). The Causes of Climate Change. nd https://climate. nasa. gov/causes.

Chekol, D. A. (2006). Modeling of hydrology and soil erosion of Upper Awash River Basin (p. 235). Cuvillier.

Chekol, D.A., 2006. Modeling of Hydrology and Soil Erosion of Upper Awash River Basin. Cuvillier Verlag.

Chen, J., Brissette, F. P., & Lucas-Picher, P. (2015). Assessing the limits of bias-correcting climate model outputs for climate change impact studies. Journal of Geophysical Research 120(3), 1123-1136.

Chen, Y. C., Wei, C., & Yeh, H. C. (2008). Rainfall network design using kriging and entropy. Hydrological Processes: An International Journal, 22(3), 340-346.

Chepkochei, L. C. (2011,). Object-oriented image classification of individual trees using Erdas Imagine objective: case study of Wanjohi area, Lake Naivasha Basin, Kenya. In Proceedings of the Kenya Geothermal Conference, Nairobi, Kenya (Vol. 2123).

Cheung, W. H., Senay, G. B., & Singh, A. (2008). Trends and spatial distribution of annual and seasonal rainfall in Ethiopia. International Journal of Climatology: A Journal of the Royal Meteorological Society, 28(13), 1723-1734.

Chok, N. S. (2010). Pearson's versus Spearman's and Kendall's correlation coefficients for continuous data (Doctoral dissertation, University of Pittsburgh).

Choto, M. and Fetene, A., 2019. Impacts of land use/land cover change on stream flow and sediment yield of Gojeb watershed, Omo-Gibe basin, Ethiopia. Remote Sensing Applications: Society

and Environment, 14 (January), 84–99.

Choto, M., & Fetene, A. (2019). Impacts of land use/land cover change on stream flow and sediment yield of Gojeb watershed, Omo-Gibe basin, Ethiopia. Remote Sensing Applications: Society and Environment, 14, 84-99.

Chow, V.T., Maidment, D.R., & Mays, L.W. (1988) Applied Hydrology. McGraw-Hill International Editions, Singapore

Chow, V.T., Maidment, D.R., and Mays, L.W., 2010. Applied Hydrology. Tata McGraw-Hill Education.

Cirrone, G. A. P., Donadio, S., Guatelli, S., Mantero, A., Mascialino, B., Parlati, S., & Viarengo, P. (2004). A goodness-of-fit statistical toolkit. IEEE Transactions on Nuclear Science, 51(5), 2056-2063.

Congalton, R.G., 1991. A review of assessing the accuracy of classifications of remotely sensed data. Remote Sensing of Environment, 37 (1), 35-46.

Conway, G. (2009). The science of climate change in Africa: impacts and adaptation. Grantham Institute for Climate Change Discussion Paper, 1, 24.

Cosgrove, W. J., & Loucks, D. P. (2015). Water management: Current and future challenges and research directions. Water Resources Research, 51(6), 4823-4839.

Cressie, N. (1990). The origins of kriging. Mathematical Geology, 22(3), 239-252.

Cunderlik, J. (2003). Hydrologic model selection for the CFCAS project: assessment of water resources risk and vulnerability to changing climatic conditions. Department of Civil and Environmental Engineering, The University of Western Ontario

Cunderlik, J. M., & Burn, D. H. (2003). Non-stationary pooled flood frequency analysis. Journal of Hydrology, 276(1-4), 210-223.

Cunnane, C. (1989). Statistical distributions for flood frequency analysis. Operational hydrology report (WMO).

Daba, M. H., & You, S. (2020). Assessment of climate change impacts on river flow regimes in the upstream of Awash Basin, Ethiopia: based on IPCC fifth assessment report (AR5) climate change scenarios. Hydrology, 7(4), 98.

Dagnachew, M., Kebede, A., Moges, A., & Abebe, A. (2020). Effects of Climate Variability on Normalized Difference Vegetation Index (NDVI) in the Gojeb River Catchment, Omo-Gibe Basin, Ethiopia. Advances in Meteorology, 2020.

Dahamsheh, A., & Aksoy, H. (2007). Structural characteristics of annual precipitation data in Jordan. Theoretical and Applied Climatology, 88(3-4), 201-212.

Dale, V. H., Efroymson, R. A., & Kline, K. L. (2011). The land use–climate change–energy nexus.

Landscape ecology, 26(6), 755-773.

De Sherbinin, A. (2002). Land-Use and Land-Cover Change, A CIESIN Thematic Guide. Center For International Earth Science Information Network (CIESIN) of Columbia University, Palisades, NY, USA. Discharge in Denmark. Ph.D. diss. Dep. of Geography and Geology, Univ. of Copenhagen.

de Sherbinin, A., 2002. A CIESIN thematic guide to land-use and land-cover change (LUCC). Center for International Earth Science Information Network, Columbia University, (September), 67.

De Sherbinin, A., VanWey, L. K., McSweeney, K., Aggarwal, R., Barbieri, A., Henry, S., & Walker, R. (2008). Rural household demographics, livelihoods and the environment. Global environmental change, 18(1), 38-53.

De Vente, J., Reed, M., Stringer, L., Valente, S., & Newig, J. (2016). How does the context and design of participatory decision making processes affect their outcomes? Evidence from sustainable land management in global drylands. Ecology and Society, 21(2).

Deb, P., Babel, M. S., & Denis, A. F. (2018). Multi-GCMs approach for assessing climate change impact on water resources in Thailand. Modeling Earth Systems and Environment, 4(2), 825-839.

Den Elzen, M., & Schaeffer, M. (2002). Responsibility for past and future global warming: uncertainties in attributing anthropogenic climate change. Climatic change, 54(1), 29-73.

Deng, J. S., Wang, K., Deng, Y. H., & Qi, G. J. (2008). PCA-based land-use change detection and analysis using multitemporal and multisensor satellite data. InternationalJournal of Remote Sensing, 29(16), 4823-4838.

Deng, J.S., Wang, K., Deng, Y.H., and Qi, G.J., 2008. PCA-based land-use change detection and analysis using multitemporal and multisensor satellite data. International Journal of Remote Sensing, 29 (16), 4823–4838.

Dennison, P. E., Roberts, D. A., Peterson, S. H., & Rechel, J. (2005). Use of normalized difference water index for monitoring live fuel moisture. International journal of remote sensing, 26(5), 1035-1042.

Deribew, K., Jaleta, E., Mandefro, B., Mekonnen, Z., Yewhalaw, D., Abdie, Y., & Mereta, S. T. (2020). Effects of land use on intermediate snail host fauna, abundance, distribution and cercariae infection rate in Omo-Gibe river basin, Ethiopia.

Deshmukh, D. S., Chaube, U. C., Hailu, A. E., Gudeta, D. A., & Kassa, M. T. (2013). Estimation and comparision of curve numbers based on dynamic land use land cover change, observed rainfall-runoff data and land slope. Journal of Hydrology, 492, 89-101.

Deshmukh, D.S., Chaube, U.C., Hailu, A.E., Gudeta, D.A., and Kassa, M.T., 2013. Estimation and comparision of curve numbers based on dynamic land use land cover change, observed rainfall-runoff data and land slope. Journal of Hydrology, 492, 89–101.

Diggle, P. J., & Ribeiro Jr, P. J. (2002). Bayesian inference in Gaussian model-based geostatistics. Geographical and environmental modelling, 6(2), 129-146. Gunarathna, M. H. J. P., Kumari, M. K. N., & Nirmanee, K. G. S. (2016). Evaluation of interpolation methods for mapping pH of groundwater. International journal of latest technology in engineering, management & applied science, 3, 1-5.

Dosdogru, F., Kalin, L., Wang, R., and Yen, H., 2020. Potential impacts of land use/cover and climate changes on ecologically relevant flows. Journal of Hydrology, 584 (March 2019), 124654.

Duhachek, A., Coughlan, A. T., & Iacobucci, D. (2005). Results on the standard error of the coefficient alpha index of reliability. Marketing Science, 24(2), 294-301.

Duinker, P. N., & Greig, L. A. (2007). Scenario analysis in environmental impact assessment: Improving explorations of the future. Environmental impact assessment review, 27(3), 206-219.

Dwarakish, G. S., & Ganasri, B. P. (2015). Impact of land use change on hydrological systems: A review of current modeling approaches. Cogent Geoscience, 1(1), 1115691.

Easterling, D. R., Evans, J. L., Groisman, P. Y., Karl, T. R., Kunkel, K. E., & Ambenje, P. (2000). Observed variability and trends in extreme climate events: a brief review. Bulletin of the American Meteorological Society.

Easton, G. S., & McCulloch, R. E. (1990). A multivariate generalization of quantile-quantile plots. Journal of the American Statistical Association, 85(410), 376-386.

EEPCo. (2004) Gilgel Gibe II hydroelectric project design (General report) Prepared by Salini contractor, submitted to Ethiopian power and electric corporation Addis Ababa Ethiopia 42p

EEPCO. (2009) Environmental and social management plan for Gibe III hydroelectric project: prepared by Salini contractor and MDI international consulting engineers 238p

Egeru, A., Barasa, B., Nampijja, J., Siya, A., Makooma, M. T., & Majaliwa, M. G. J. (2019). Past, present and future climate trends under varied representative concentration pathways for a sub-humid region in Uganda. Climate, 7(3), 35.

Ehsani, A. H., & Quiel, F. (2010). Efficiency of Landsat ETM+ Thermal Band for Land Cover Classification of the Biosphere Reserve (Central Europe) Using SMAP and MLAlgorithms. International Journal of Environmental Research, 4(4), 741-750.

Ekström, M., Grose, M. R., & Whetton, P. H. (2015). An appraisal of downscaling methods used in

climate change research. Wiley Interdisciplinary Reviews: Climate Change, 6(3), 301-319.

Elliott, J., Deryng, D., Müller, C., Frieler, K., Konzmann, M., Gerten, D., and Eisner, S. (2014). Constraints and potentials of future irrigation water availability on agricultural production under climate change. Proceedings of the National Academy of Sciences, 111(9), 3239-3244.

Ellis, E. C., Kaplan, J. O., Fuller, D. Q., Vavrus, S., Goldewijk, K. K., and Verburg, P. H. (2013). Used planet: A global history. Proceedings of the National Academy of Sciences, 110(20), 7978-7985.

Engmann, S., & Cousineau, D. (2011). Comparing distributions: the two-sample Anderson-Darling test as an alternative to the Kolmogorov-Smirnoff test. Journal of applied quantitative methods, 6(3), 1-17.

Estifanos, T. H. (2014). Modeling-Impact of Land Use/Cover Change on Reservoir Sedimentation.

Evaluation and comparison different methods of preparation of sediment rating curve in Telezang station of the Dez River. Austr. J. Basic Appl. Sci, 4(5), 717-723.

Evangelista, P., Young, N., & Burnett, J. (2013). How will climate change spatially affect agriculture production in Ethiopia? Case studies of important cereal crops. Climatic change, 119(3), 855-873.

Ewemoje, T. A., and Ewemooje, O. S. (2011). Best distribution and plotting positions of daily maximum flood estimation at Ona River in Ogun-Oshun river basin, Nigeria.

Ewemoje, T. A., and Ewemooje, O. S. (2017). Estimating Annual Maximum and Minimum Flows at Ona River Gauging Station in Ibadan, Nigeria Using a Modified Mixed Gamma Distribution. In 2017 ASABE Annual International Meeting (p. 1). American Society of Agricultural and Biological Engineers.

Fang, G. H., Yang, J., Chen, Y. N. and Zammit, C. (2015). Comparing bias correction methods in downscaling meteorological variables for a hydrologic impact study in an arid area in China. Hydrology and Earth System Sciences, 19, 2547-2559.

FAO, 1995. Digital Soil Map of the World and Derived Soil Properties (CDROM) Food and Agriculture Organization of the United Nations.

FAO, 1998. The Soil and Terrain Database for north eastern Africa (CDROM) FAO, Rome,

FAO, 2002. Major Soils of the World. Land and Water Digital Media Series Food and Agricultural Organization of the United Nations, Rome. CD-ROM,

Favre, A. C., El Adlouni, S., Perreault, L., Thiémonge, N., & Bobée, B. (2004). Multivariate hydrological frequency analysis using copulas. Water resources research, 40(1).

Fazeli Sangani, M., Owens, G., & Fotovat, A. (2018). Transport of engineered nanoparticles in soils and aquifers. Environmental Reviews, 27(1), 43-70.

Federal Democratic Republic of Ethiopia Population Census Commission. (2008). Summary & Statistical Report of the 2007 Population and Housing Census Results. Addis Ababa.

Feng, S., Hu, Q., & Qian, W. (2004). Quality control of daily meteorological data in China, 1951–2000: a new dataset. International Journal of Climatology: A Journal of the Royal Meteorological Society, 24(7), 853-870.

Field, C. B. (Ed.). (2014). Climate change 2014–Impacts, adaptation and vulnerability: Regional aspects. Cambridge University Press.

Field, C. B., Barros, V., Stocker, T. F., & Dahe, Q. (Eds.). (2012). managing the risks of extreme events and disasters to advance climate change adaptation: special report of the intergovernmental panel on climate change. Cambridge University Press.

Flato, G.M., G.J. Boer, W.G. Lee, N.A. McFarlane, D. Ramsden, M.C. Reader and A.J. Weaver, 2000: The Canadian Centre for Climate Modelling and Analysis global coupled model and its climate. Clim. Dyn., 16, 451-467.

Foerster, V., Junginger, A., Langkamp, O., Gebru, T., Asrat, A., Umer, M.,& Trauth, M. H. (2012). Climatic change recorded in the sediments of the Chew Bahir basin, southern Ethiopia, during the last 45,000 years. Quaternary International, 274, 25-37.

Foley, J.A., DeFries, R., Asner, G.P., Harford, C., Bonan, G., Carpenter, S.R., Chapin, F.S.,Coe, M.T., Daily, G.C., Gibbs, H.K., Helkowski, J.H., Holloway, T., Howard, E.A., Kucharik, C.J., Monfreda, C., Patz, J.A., Hamed, K., & Rao, A. R. (1999). Flood frequency analysis. CRC press.

Ford, B., Val Martin, M., Zelasky, S. E., Fischer, E. V., Anenberg, S. C., Heald, C. L., & Pierce, J. R. (2018). Future fire impacts on smoke concentrations, visibility, and health in the contiguous United States. GeoHealth, 2(8), 229-247.

Francesconi, W., Srinivasan, R., Pérez-Miñana, E., Willcock, S. P., & Quintero, M. (2016). Using the Soil and Water Assessment Tool (SWAT) to model ecosystem services: A systematic review. Journal of Hydrology, 535, 625-636.

Friedrich, T., Timmermann, A., Tigchelaar, M., Timm, O. E., & Ganopolski, A. (2016). Nonlinear climate sensitivity and its implications for future greenhouse warming. Science Advances, 2(11), e1501923.

Furevik, T., Bentsen, M., Drange, H., Kindem, I. K. T., Kvamstø, N. G., & Sorteberg, A. (2003). Description and evaluation of the Bergen climate model: ARPEGE coupled with MICOM. Climate Dynamics, 21(1), 27-51.

Gao, B. C. (1996). NDWI—A normalized difference water index for remote sensing of vegetation liquid water from space. Remote sensing of environment, 58(3), 257-266.

Gawatre, D. W., Kandgule, M. H., & Kharat, S. D. (2016). Comparative Study of Population Forecasting Methods. Population, 40(3), 13-5133.

Gebremicael, T. G., Mohamed, Y. A., & Van der Zaag, P. (2019). Attributing the hydrological impact of different land use types and their long-term dynamics through combining parsimonious hydrological modelling, alteration analysis and PLSR analysis. Science of the Total Environment, 660, 1155-1167.

George, J., Baby, L., Arickal, A. P., Vattoly, J. D., & Use, L. (2016). Land use/land cover mapping with change detection analysis of Aluva Taluk using remote sensing and GIS. International Journal of Science, Engineering and Technology, 4(2), 383-389.

Ginos, B. F. (2009). Parameter estimation for the lognormal distribution.

Giorgi, F., M.R. Marinucci and G. T. Bates, 1993: Development of a second generation regional climate model (RegCM2). Part I Boundary layer and radiative transfer processes. Mon. Weather Rev., 121, 2794-2813.

Giorgi, F., M.R. Marinucci, G. T. Bates and G. DeCanio, 1993: Development of a second generation regional climate model (RegCM2). Part II Convective processes and assimilation of lateral boundary conditions. Mon. Weather Rev., 121, 2814-2832.

Gleeson, T., Wada, Y., Bierkens, M. F., & van Beek, L. P. (2012). Water balance of global aquifers revealed by groundwater footprint. Nature, 488(7410), 197.

Global Runoff Data Sets and Grid Estimation, 10-15 Nov. 1988, Koblenz. World Climate

Gordon, C., C. Cooper, C.A. Senior, H.T. Banks, J.M. Gregory, T.C. Johns, J.F.B. Mitchell and R.A. Wood, 2000: The simulation of SST, sea ice extents and ocean heat transports in a version of the Hadley Centre coupled model without flux adjustments. Clim. Dyn., 16, 147-168.

Gornall, J., Betts, R., Burke, E., Clark, R., Camp, J., Willett, K., & Wiltshire, A. (2010). Implications of climate change for agricultural productivity in the early twenty-first century. Philosophical Transactions of the Royal Society B: Biological Sciences, 365(1554), 2973-2989.

Goswami, B. N. (2005). South Asian monsoon. In Intra seasonal variability in the atmosphere-ocean climate system (pp. 19-61). Springer, Berlin, Heidelberg.

Gotway, C. A., Ferguson, R. B., Hergert, G. W., & Peterson, T. A. (1996). Comparison of kriging and IDW for mapping soil parameters. Soil Science Society of America Journal, 60(4), 1237-1247

Goual, H., & Seddik-Ameur, N. (2014). Chi-squared type test for the AFT-generalized inverse Weibull distribution. Communications in statistics-Theory and Methods, 43(13), 2605-2617.

Greenwood, P. J., Harvey, P. H., & Perrins, C. M. (1979). Kin selection and territoriality in birds?

A test. Animal Behaviour, 27, 645-651.

Gumbel, E. J. (1954). The maxima of the mean largest value and of the range. The Annals of Mathematical Statistics, 76-84.

Gumindoga, W., Rientjes, T. H. M., Haile, A. T., & Dube, T. (2014). Predicting streamflow for land cover changes in the Upper Gilgel Abay River Basin, Ethiopia: A TOPMODEL based approach. Physics and Chemistry of the Earth, Parts A/B/C, 76, 3-15.

Haan, C. T. (1989). Parametric uncertainty in hydrologic modeling. Transactions of the ASAE, 32(1), 137-0146.

Haile, A. T., Habib, E., & Rientjes, T. (2013). Evaluation of the climate prediction center (CPC) morphing technique (CMORPH) rainfall product on hourly time scales over the source of the Blue Nile River. Hydrological processes, 27(12), 1829-1839.

Hansen, M. C., & Loveland, T. R. (2012). A review of large area monitoring of land cover change using Landsat data. Remote sensing of Environment, 122, 66-74.

Hanssen-Bauer, I., Achberger, C., Benestad, R. E., Chen, D., & Førland, E. J. (2005). Statistical downscaling of climate scenarios over Scandinavia. Climate Research, 29(3), 255-268.

Hargreaves, G. H., & Samani, Z. A. (1985). Reference crop evapotranspiration from temperature. Applied engineering in agriculture, 1(2), 96-99.

Harms, A. A., & Campbell, T. H. (1967). An extension to the Thomas-Fiering Model for the sequential generation of streamflow. Water Resources Research, 3(3), 653-661.

Hassan, Z., Shamsudin, S., & Harun, S. (2014). Application of SDSM and LARS-WG for simulating and downscaling of rainfall and temperature. Theoretical and applied climatology, 116(1-2), 243-257.

Herweg, K. and Ludi, E., 1999. The performance of selected soil and water conservation measures—case studies from Ethiopia and Eritrea. Catena, 36 (1–2), 99–114.

Hewitson, B. C., & Crane, R. G. (1996). Climate downscaling: techniques and application. Climate Research, 7(2), 85-95.

Higaki, D., Karki, K. K., & Gautam, C. S. (2005). Soil erosion control measures on degraded sloping lands: A case study in Midlands of Nepal. Aquatic Ecosystem Health & Management, 8(3), 243-249.

Hooke, J. M. (2006). Human impacts on fluvial systems in the Mediterranean region. Geomorphology, 79(3-4), 311-335.

Hosking, J. R. (1986). The theory of probability weighted moments (pp. 3-16). IBM Research Division, TJ Watson Research Center.

Houghton, J. (2009). Global warming: the complete briefing. Cambridge university press.

Houghton, J. (2009). Global warming: the complete briefing. Cambridge university press.

Hougton, J. T. (1995). Climate Change 1995. The Science of Climate Change. WG1, to the Second Assessment Report of the IPCC.

Huang, J., Zhang, J., Zhang, Z., Xu, C., Wang, B., & Yao, J. (2011). Estimation of future precipitation change in the Yangtze River basin by using statistical downscaling method. Stochastic Environmental Research and Risk Assessment, 25(6), 781-792.

Hughes, T. P., Baird, A. H., Bellwood, D. R., Card, M., Connolly, S. R., Folke, C., & Lough, J. M. (2003). Climate change, human impacts, and the resilience of coral reefs. Science, 301(5635), 929-933.

Hurni, H. (1985). Erosion-productivity-conservation systems in Ethiopia.

Hussen, B., Mekonnen, A., & Pingale, S. M. (2018). Integrated water resources management under climate change scenarios in the sub-basin of Abaya-Chamo, Ethiopia. Modeling Earth Systems and Environment, 4(1), 221-240.

Ibbitt, R. P., & Henderson, R. D. (1998, November). Filling in missing data in flow records. In INTERNATIONAL SYMPOSIUM ON HYDROLOGY WATER RESOURCES AND ENVlRONMENT DR (ELOPMENT AND MANAGEMENT IN SOUTHEAST ASIA AND THE PACIFIC (p. 16).

Ibbitt, R. P., & Henderson, R. D. (1998, November). Filling in missing data in flow records. In international symposium on hydrology water resources and envlronment dr (elopment and management in southeast asia and the pacific (p. 16).

IKHSAN, J. (2010). Study on Integrated Sediment Management in an Active Volcanic Basin.

Im, E. S., Ahn, J. B., & Kim, D. W. (2012). An assessment of future dryness over Korea based on the ECHAM5-RegCM3 model chain under A1B emission scenario. Asia-Pacific Journal of Atmospheric Sciences, 48(4), 325-337.

Ines, A. V. M. & Hansen, J. W. (2006). Bias correction of daily GCM rainfall for crop simulation studies. Agricultural and Forest Meteorology, 138, 44-53.

IPCC, (1996a). Climate change 1995: economic and social dimensions of climate change. Contribution of working group III of the Second Assessment Report of the Intergovernmental Panel on Climate Change [Bruce, J.P., H. Lee and E.F. Haites (eds.)]. Cambridge University Press, Cambridge

IPCC, (2001b). Climate Change 2001): Impacts, Adaptation, and Vulnerability. Contribution of WG II to TAR of the Intergovernmental Panel on Climate Change [McCarthy, M.C.O.F. Canziani, N.A. Leary, D.J.Dokken and K.S. White (eds.)] Cambridge, pp1031.

IPCC, (2001c): Climate Change 2001: The scientific basis. Contribution of Working Group I to the

Third Assessment report of the Intergovernmental Panel on Climate Change [Houghton, J.T., Y. Ding, D.J. Griggs, M. Noguer, P.J. van der Linden, X. Dai, K. Maskell and C.A. Johnson (eds.)]. Cambridge University Press, Cambridge, pp881.

IPCC, S.R.E.S., (2007). Climate Change 2007: The physical Science Basis, Contribution of Working Group I to the Fourth Assesment Report of the IPCC, 2007.

IPCC. (2001). Climate Change 2001: The Scientific Basis. Technical Summary of the Working Group I Report. [Houghton, J.T., Y. Ding, D.J. Griggs, M. Noguer, P.J. van der Linden, X. Dai, K. Maskell, and C.A. Johnson (eds.)] . Cambridge University Press, Cambridge, United Kingdom and New York, NY, USA, 94pp.

IPCC: Climate Change. (2013) Synthesis Report, Cambridge Press, Cambridge

Isard, W. (1966). Methods of regional analysis. Рипол Классик.

Islam, S., Chu, C., & Smart, J. C. (2020). Challenges in integrating disaster risk reduction and climate change adaptation: Exploring the Bangladesh case. International journal of disaster risk reduction, 47, 101540.

Izinyon, O. C., & Ehiorobo, J. O. (2014). L-moments approach for flood frequency analysis of river Okhuwan in Benin-Owena River basin in Nigeria. Nigerian Journal of Technology, 33(1), 10-18.

Jain, A. O., Thaker, T. P., Misra, A. K., Singh, A. K., & Kumari, P. (2021). Determination of sensitivity of drainage morphometry towards hydrological response interactions for various datasets. Environment, Development and Sustainability, 23(2), 1799-1822.

Janssen, P.H.M. and Heuberger, P.S.C., 1995. Calibration of process-oriented models. Ecological Modelling, 83 (1–2), 55–66.

Jemberie, M., Gebrie, T., & Gebremariam, B. (2016). Evaluation of Land Use Land Cover Change on Stream Flow: A Case Study of dedissa Sub Basin, Abay Basin, South Western Ethiopia. Evaluation, 3(8).

Jena, J., & Nath, S. (2020). An empirical formula for design flood estimation of un-gauged catchments in Brahmani Basin, Odisha. Journal of The Institution of Engineers (India): Series A, 101(1), 1-6.

Jiang, D., Sui, Y., & Lang, X. (2016). Timing and associated climate change of a 2 C global warming. International Journal of Climatology, 36(14), 4512-4522.

Jiang, Z., Huete, A.R., Chen, J., Chen, Y., Li, J., Yan, G., and Zhang, X., 2006. Analysis of NDVI and scaled difference vegetation index retrievals of vegetation fraction. Remote Sensing of Environment.

Joel, C. E. (2010). Population and climate change. Proceedings of the American Philosophical

Society, 154(2), 158-182.

Johns, T. C., Gregory, J. M., Ingram, W. J., Johnson, C. E., Jones, A., Lowe, J. A., ... & Woodage, M. J. (2003). Anthropogenic climate change for 1860 to 2100 simulated with the HadCM3 model under updated emissions scenarios. Climate dynamics, 20(6), 583-612.

Johns, T.C., R.E. Carnell, J.F. Crossley, J.M. Gregory, J.F.B. Mitchell, C.A. Senior, S.F.B. Tett and R.A. Wood, 1997: The second Hadley Centre coupled ocean-atmosphere GCM: model description, spinup and validation. Clim. Dyn., 13, 103-134.

Johnston, K., Ver Hoef, J. M., Krivoruchko, K., & Lucas, N. (2001). Using ArcGIS geostatistical analyst (Vol. 380). Redlands: Esri.

Kahya, E., & Kalaycı, S. (2004). Trend analysis of streamflow in Turkey. Journal of Hydrology, 289(1-4), 128-144.

Kang, D. B., & Ko, K. N. (2018). An Application of the Probability Plotting Positions for the Lnleast Method for Estimating the Parameters of Weibull Wind Speed Distribution. Journal of the Korean Solar Energy Society, 38(5), 11-25.

Karl, T. R., Melillo, J. M., Peterson, T. C., & Hassol, S. J. (Eds.). (2009). Global climate change impacts in the United States. Cambridge University Press.

Kiesel, J., Gericke, A., Rathjens, H., Wetzig, A., Kakouei, K., Jähnig, S. C., & Fohrer, N. (2019). Climate change impacts on ecologically relevant hydrological indicators in three catchments in three European ecoregions. Ecological engineering, 127, 404-416.

Kim, S., Shin, H., Ahn, H., & Heo, J. H. (2015). Development of an unbiased plotting position formula considering the coefficient of skewness for the generalized logistic distribution. Journal of Hydrology, 527, 471-481.

Kinthada N R., Gurram M K., Eadara A., & Velagala V R.(2014). Land Use/Land Cover and NDVI Analysis for Monitoring the Health of Micro-watersheds of Sarada River Basin, Visakhapatnam District, India." J Geo. Geosci.3 (2).

Kite, G.W., Dalton, A. and Dion, K. (1994). Simulation of stream flow in a macro-scale watershed using GCM data. Water Research Paper 30 (5): pp1547-1559.

Korkmaz, S., Göksülük, D., & Zararsiz, G. Ö. K. M. E. N. (2014). MVN: An R package for assessing multivariate normality. R JOURNAL, 6(2).

Kotsiantis, S., Kostoulas, A., Lykoudis, S., Argiriou, A., & Menagias, K. (2006, July). Filling missing temperature values in weather data banks. In 2006 2nd IET International Conference on Intelligent Environments-IE 06 (Vol. 1, pp. 327-334). IET.

Kotz, S., & Nadarajah, S. (2000). Extreme value distributions: theory and applications. World Scientific.

Krivoruchko, K., & Gotay, C. A. (2003, July). Using spatial statistics in GIS. In International congress on modelling and simulation (pp. 713-736).

Kumar, S., Radhakrishnan, N., & Mathew, S. (2014). Land use change modelling using a Markov model and remote sensing. Geomatics, Natural Hazards and Risk, 5(2), 145-156.

Kundzewicz, Z. W. (2008). Climate change impacts on the hydrological cycle. Ecohydrology & Hydrobiology, 8(2-4), 195-203.

Kundzewicz, Z. W., Kanae, S., Seneviratne, S. I., Handmer, J., Nicholls, N., Peduzzi, P., & Muir-Wood, R. (2014). Flood risk and climate change: global and regional perspectives.

Lacombe, G., Ribolzi, O., Rouw, A. D., Pierret, A., Latsachak, K., Silvera, N& Robain, H. (2016). Contradictory hydrological impacts of afforestation in the humid tropics evidenced by long-term field monitoring and simulation modelling. Hydrology and Earth System Sciences, 20(7), 2691-2704.

Laflamme, E. M., Linder, E., & Pan, Y. (2016). Statistical downscaling of regional climate model output to achieve projections of precipitation extremes. Weather and Climate Extremes, 12,15-23.

Lake, P. S., Bond, N. R., & Arthington, A. H. (2008). The impacts of drought on freshwater ecosystems: an Australian perspective. Hydrobiologia, 600(1), 3-16.

Lambin, E. F.,Samuel, B. and Geist, H. J. (2003). Global Land-Use and Land-Cover Change: What Have We Learned So Far? Global Change Newsletter, Land-Use/Cover Change.

Lambin, E.F., Geist, H.J., and Lepers, E., 2003. Dynamics of landuse and landcover change in tropical regions. Annual Review of Environment and Resources, 28 (1), 205–241.

Leander, R., & Buishand, T. A. (2007). Resampling of regional climate model output for the simulation of extreme river flows. Journal of Hydrology, 332(3-4), 487-496.

Lee, D. R. (2005). Agricultural sustainability and technology adoption: Issues and policies for developing countries. American journal of agricultural economics, 87(5), 1325-1334.

Legesse, D., C. Vallet-Coulomb, and F. Gasse. (2003). Hydrological response of a catchment to climate and land use change in tropical Africa: Case study south central Ethiopia. J. Hydrol. 275(1-2): 67-85.

Levermann, A., Clark, P. U., Marzeion, B., Milne, G. A., Pollard, D., Radic, V., & Robinson, A. (2013). The multimillennial sea-level commitment of global warming. Proceedings of the National Academy of Sciences, 110(34), 13745-13750.

Li, M., Zang, S., Zhang, B., Li, S., & Wu, C. (2014). A review of remote sensing image classification techniques: The role of spatio-contextual information. European Journal of Remote Sensing, 47(1), 389-411.

Li, W., Du, Z., Ling, F., Zhou, D., Wang, H., Gui, Y., & Zhang, X. (2013). A comparison of land surface water mapping using the normalized difference water index from TM, ETM+ and ALI. Remote Sensing, 5(11), 5530-5549.

Liang, X. Z., Kunkel, K. E., Meehl, G. A., Jones, R. G., & Wang, J. X. (2008). Regional climate models downscaling analysis of general circulation models present climate biases propagation into future change projections. Geophysical research letters, 35(8).

Liu, W., Zhang, Z. H. E., & Wan, S. (2009). Predominant role of water in regulating soil and microbial respiration and their responses to climate change in a semiarid grassland. Global Change Biology, 184-195.

López-Ballesteros, A., Senent-Aparicio, J., Srinivasan, R., & Pérez-Sánchez, J. (2019). Assessing the impact of best management practices in a highly anthropogenic and ungauged watershed using the SWAT model: A case study in the El Beal Watershed (Southeast Spain). Agronomy, 9(10), 576.

Lutz, W. (2017). How population growth relates to climate change. Proceedings of the National Academy of Sciences, 114(46), 12103-12105.enty-first century. OUP Oxford.

Machiwal, D., & Jha, M. K. (2012). Methods for time series analysis. In Hydrologic Time Series Analysis: Theory and Practice (pp. 51-84). Springer, Dordrecht.1), 41.Management Institute, Colombo, Sri Lanka.

Mahmood, R., & Babel, M. S. (2013). Evaluation of SDSM developed by annual and monthly sub-models for downscaling temperature and precipitation in the Jhelum basin, Pakistan and India. Theoretical and applied climatology, 113(1-2), 27-44.

Maity, R. (2018). Statistical Methods in Hydrology and Hydroclimatology. Springer Transactions in Civil and Environmental Engineering.

Mango, L. M., Melesse, A. M., McClain, M. E., Gann, D., & Setegn, S. G. (2011). Land use and climate change impacts on the hydrology of the upper Mara River Basin, Kenya: results of a modeling study to support better resource management. Hydrology and Earth System Sciences, 15(7), 2245-2258.

Maraun, D., & Widmann, M. (2018). Cross-validation of bias-corrected climate simulations is misleading. Hydrology and Earth System Sciences, 22(9), 4867-4873.

Maraun, D., Wetterhall, F., Ireson, A. M., Chandler, R. E., Kendon, E. J., Widmann, M., ... & Venema, V. K. C. (2010). Precipitation downscaling under climate change: Recent developments to bridge the gap between dynamical models and the end user. Reviews of Geophysics, 48(3).

Maraun, D., Widmann, M., & Gutiérrez, J. M. (2019). Statistical downscaling skill under present

climate conditions: A synthesis of the VALUE perfect predictor experiment. International Journal of Climatology, 39(9), 3692-3703.

Marengo, J. A., & Espinoza, J. C. (2016). Extreme seasonal droughts and floods in Amazonia: causes, trends and impacts. International Journal of Climatology, 36(3), 1033-1050.

Marius K., (2009). Climate Risks and Development Projects Assessment Report for community Level Project in Guduru, Oromiya, Ethiopia, pp1-13.

Matewos, T. (2020). The state of local adaptive capacity to climate change in drought-prone districts of rural Sidama, southern Ethiopia. Climate Risk Management, 27, 100209.

Mather, A. S., & Needle, C. L. (2000). The relationships of population and forest trends. Geographical Journal, 166(1), 2-13.

Mc Sweeney, C., New, M., and Lizcano, G., (2008). UNDP Climate Change Country Profiles Ethiopia. Available at: http://country-profiles.geog.ox.ac.uk.

McCain, C. M. (2007). Could temperature and water availability drive elevational species richness patterns? A global case study for bats. Global Ecology and biogeography, 16(1), 1-13.

McCarthy, J. J., Canziani, O. F., Leary, N. A., Dokken, D. J., & White, K. S. (Eds.). (2001). Climate change 2001: impacts, adaptation, and vulnerability: contribution of Working Group II to the third assessment report of the IPCC (Vol. 2). Cambridge University Press.

McDowell, G., Ford, J. D., Lehner, B., Berrang-Ford, L., & Sherpa, A. (2013). Climate-related hydrological change and human vulnerability in remote mountain regions: a case study from Khumbu, Nepal. Regional Environmental Change, 13(2), 299-310.

Meng, F., Liu, T., Wang, H., Luo, M., Duan, Y., & Bao, A. (2018). An alternative approach to overcome the limitation of HRUs in analyzing hydrological processes based on land use/cover change. Water, 10(4), 434.

Mengistu, K. T. (2009). Watershed hydrological responses to changes in land use and land cover, and management practices at Hare Watershed, Ethiopia.

Mereta, S. T., Bedewi, J., Yewhalaw, D., Mandefro, B., Abdie, Y., Tegegne, D., ... & Kloos, H. (2019). Environmental determinants of distribution of freshwater snails and trematode infection in the Omo Gibe River Basin, southwest Ethiopia. Infectious diseases of poverty, 8(1), 1-10.

Merrick, B. (2018). The power of hydrology in the Omo-Gibe River Basin: Gibe III and flood retreat agriculture on the river omo. Masters Thesis Series in Environmental Studies and Sustainability Science.

Mesa-Mingorance, J. L., & Ariza-López, F. J. (2020). Accuracy Assessment of Digital Elevation Models (DEMs): A Critical Review of Practices of the Past Three Decades. Remote Sensing,

12(16), 2630.

Midhuna, T. M., & Dimri, A. P. (2019). Future projection of winter precipitation over northwest India and associated regions using CORDEX-SA experiments. Theoretical and Applied Climatology, 1-15.

Miller, C. R. (1951). Analysis of flow-duration: Sediment-rating curve method of computing sediment yield. United States Department of Interior, Bureau of Reclamation.

Miller, J. D., Stewart, E., Hess, T., & Brewer, T. (2020). Evaluating landscape metrics for characterising hydrological response to storm events in urbanised catchments. Urban Water Journal, 17(3), 247-258.

Mohammed, A. K. (2013). The Effect of Climate Change on Water Resources Potential of Omo Gibe Basin, Ethiopia (Doctoral dissertation, Universitätsbibliothek der Universität der Bundeswehr München)

Moog, D. B., Whiting, P. J., & Thomas, R. B. (1999). Streamflow record extension using power transformations and application to sediment transport. Water Resources Research, 35(1), 243-254.

Moore, I. D., Grayson, R. B., & Ladson, A. R. (1991). Digital terrain modelling: a review of hydrological, geomorphological, and biological applications. Hydrological processes, 5(1), 3-30.

Moore, T. J., Sadler, B. M., & Kozick, R. J. (2008). Maximum-likelihood estimation, the Cramér–Rao bound, and the method of scoring with parameter constraints. IEEE Transactions on Signal Processing, 56(3), 895-908.

Moriasi, D. N., Arnold, J. G., Van Liew, M. W., Bingner, R. L., Harmel, R. D., & Veith, T. L. (2007). Model evaluation guidelines for systematic quantification of accuracy in watershed simulations. Transactions of the ASABE, 50(3), 885-900.

MoWR (Ministry of Water Resources), (1996). Integrated Development of Omo-Gibe River Basin Master Plan Study, Vol. XI F1, F2, F3, and Addis Ababa: Ethiopia.

Mueller, T. G., Pusuluri, N. B., Mathias, K. K., Cornelius, P. L., Barnhisel, R. I., & Shearer, S. A. (2004). Map quality for ordinary kriging and inverse distance weighted interpolation. Soil Science Society of America Journal, 68(6), 2042-2047.

Musy, A., Meylan, P., & Favre, A. C. (2012). Predictive hydrology: A frequency analysis approach. CRC Press.

Myles R. Allen, (2011). IPCC WGI Fifth Assessment Report. Long-term Climate Change: Projections, Commitments and Irreversibility.

Nakicenovic, N., Alcamo, J., Davis, G., Vries, B. D., Fenhann, J., Gaffin, S., ... & Zhou, D. (2000).

Special report on emissions scenarios.

Namrata P, N., & Heijnen, H. (2004). Rainwater Harvesting and Health Aspects-Working on WHO Guidance. University of Hawaii: Honolulu, HI, USA.

Narsimlu, B., Gosain, A. K., Chahar, B. R., Singh, S. K., & Srivastava, P. K. (2015). SWAT model calibration and uncertainty analysis for streamflow prediction in the Kunwari River Basin, India, using sequential uncertainty fitting. Environmental Processes, 2(1), 79-95.

Nash, J.E. and J.E. Sutcliffe, (1970). River Flow Forecasting Through Conceptual Models -Part 1-A: Discussion of Principles. Journal of Hydrology 10(82): pp282-290.

Nathan, R. J., McMahon, T. A., Peel, M. C., & Horne, A. (2019). Assessing the degree of hydrologic stress due to climate change. Climatic Change, 156(1), 87-104.

National Meteorology Agency, (2007). National Adaptation Programme of Action of Ethiopia (NAPA). National Meteorological Agency, Addis Ababa

Nearing, M. A., Foster, G. R., Lane, L. J., & Finkner, S. C. (1989). A process-based soil erosion model for USDA-Water Erosion Prediction Project technology. Transactions of the ASAE, 32(5), 1587-1593.

Neitsch, S. L., Arnold, J. G., Kiniry, J. R., & Williams, J. R. (2011). Soil and water assessment tool theoretical documentation version 2009. Texas Water Resources Institute.

Neitsch, S.L., Arnold, J.G., Kiniry, J.R., Williams, J.R. (2005). Soil and Water Assessment Tool Theoretical Documentation Version 2005

Ngana, J. O. (2002). Integrated Water Resources Management: The Case of the Pangani River Basin.

Nie, W., Yuan, Y., Kepner, W., Nash, M. S., Jackson, M., & Erickson, C. (2011). Assessing impacts of Land use and Land cover changes on hydrology for the upper San Pedro watershed. Journal of Hydrology, 407(1-4), 105-114

Nigussie, A., 2007. Impact of Land use Land cover change on Stream flow (CASE STUDY GILGEL GIBE III), PhD Thesis.

Niraula, R., Meixner, T., and Norman, L.M., 2015. Determining the importance of model calibration for forecasting absolute/relative changes in streamflow from LULC and climate changes. Journal of Hydrology, 522, 439–451.

Noe, R. A., Hollenbeck, J. R., Gerhart, B., & Wright, P. M. (2017). Human resource management: Gaining a competitive advantage. New York, NY: McGraw-Hill.

Nordbo, A., Launiainen, S., Mammarella, I., Leppäranta, M., Huotari, J., Ojala, A., & Vesala, T. (2011). Long-term energy flux measurements and energy balance over a small boreal lake using eddy covariance technique. Journal of Geophysical Research: Atmospheres, 116(D2).

Nordhaus, W. (2019). Climate change: The ultimate challenge for economics. American Economic Review, 109(6), 1991-2014.

O'Neill, B. C., Carter, T. R., Ebi, K., Harrison, P. A., Kemp-Benedict, E., Kok, K., ... & Pichs-Madruga, R. (2020). Achievements and needs for the climate change scenario framework. Nature climate change, 10(12), 1074-1084.

Ojeda Olivares, E. A., Sandoval Torres, S., Belmonte Jiménez, S. I., Campos Enríquez, J. O., Zignol, F., Reygadas, Y., & Tiefenbacher, J. P. (2019). Climate Change, Land Use/ Land Cover Change, and Population Growth as Drivers of Groundwater Depletion in the Central Valleys, Oaxaca, Mexico. Remote Sensing, 11(11), 1290.

Owens, P. N. (2008). Sediment behaviour, functions and management in river basins. In Sustainable management of sediment resources (Vol. 4, pp. 1-29). Elsevier.

Pachauri, R. K., Allen, M. R., Barros, V. R., Broome, J., Cramer, W., Christ, R., ... & Dubash, N. K. (2014). Climate change 2014: synthesis report. Contribution of Working Groups I, II and III to the fifth assessment report of the Intergovernmental Panel on Climate Change (p. 151). Ipcc.

Pachauri, R. K., Allen, M. R., Barros, V. R., Broome, J., Cramer, W., Christ, R., & Dubash, N. K. (2014). Climate change 2014: synthesis report. Contribution of Working Groups I, II and III to the fifth assessment report of the Intergovernmental Panel on Climate Change (p. 151). IPCC.

Palm, R., Lewis, G. B., & Feng, B. (2017). What causes people to change their opinion about climate change?. Annals of the American Association of Geographers, 107(4), 883-896.

Pandey, A., Bishal, K. C., Kalura, P., Chowdary, V. M., Jha, C. S., & Cerdà, A. (2021). A soil water assessment tool (SWAT) modeling approach to prioritize soil conservation management in river basin critical areas coupled with future climate scenario analysis. Air, Soil and Water Research, 14, 11786221211021395.

Papritz, A., & Stein, A. (1999). Spatial prediction by linear kriging. In Spatial statistics for remote sensing (pp. 83-113). Springer, Dordrecht.

Partal, T., & Kahya, E. (2006). Trend analysis in Turkish precipitation data. Hydrological processes, 20(9),

Patel, A. D., Dholakia, M. B., Patel, D. P., Prakash, I., & Mahmood, K. (2016). Analysis of optimum number of rain gauge in Shetrunji River Basin, Gujarat-India. International Journal of Science Technology & Engineering, 2(11), 380-384.

Pechlivanidis, I. G., Jackson, B. M., McIntyre, N. R., & Wheater, H. S. (2011). Catchment scale hydrological modelling: a review of model types, calibration approaches and uncertainty analysis methods in the context of recent developments in technology and applications. Global

NEST journal, 13(3), 193-214.

Peng, T., & Wang, S. J. (2012). Effects of land use, land cover and rainfall regimes on the surface runoff and soil loss on karst slopes in southwest China. Catena, 90, 53-62.

Pereira, H. C. (1989). Policy and Practice of Water Management in Tropical Areas. Boulder, Co: Westview Press.

Peter W. G., David L. Smith, Anand P. Patil, Andrew J. Tatem, Robert W. Snow, and Simon I. Hay. "Climate change and the global malaria recession." Nature 465, no. 7296 (2010): 342-345.

Peterson, T. C., Heim Jr, R. R., Hirsch, R., Kaiser, D. P., Brooks, H., Diffenbaugh, N. S., ... & Katz, R. W. (2013). Monitoring and understanding changes in heat waves, cold waves, floods, and droughts in the United States: state of knowledge. Bulletin of the American Meteorological Society, 94(6), 821-834.

Piao, S., Ciais, P., Huang, Y., Shen, Z., Peng, S., Li, J., & Friedlingstein, P. (2010). The impacts of climate change on water resources and agriculture in China. Nature, 467(7311).

Pierce, D. W., Cayan, D. R., & Dehann, L. (2016). Creating Climate Projections to Support the 4th California Climate Assessment. University of California at San Diego, Scripps Institution of Oceanography: La Jolla, CA, USA.

Pinakkattu, J. S., Gurugnanam, B., & Bairavi, S. (2018). Analysis of Land Use/Land Cover Changes Using Remote Sensing Data in Dindigul District, Tamil Nadu, India.

Pohlert, T. (2016). Non-parametric trend tests and change-point detection. CC BY-ND, 4.

Popova, E. E., Yool, A., Coward, A. C., Dupont, F., Deal, C., Elliott, S., ... & Zhang, J. (2012). What controls primary production in the Arctic Ocean? Results from an intercomparison of five general circulation models with biogeochemistry. Journal of Geophysical Research: Oceans, 117(C8).

Pour, S. H., Harun, S. B., & Shahid, S. (2014). Genetic programming for the downscaling of extreme rainfall events on the East Coast of Peninsular Malaysia. Atmosphere, 5(4), 914-936.

Prein, A. F., Langhans, W., Fosser, G., Ferrone, A., Ban, N., Goergen, K., & Brisson, E. (2015). A review on regional convection-permitting climate modeling: Demonstrations, prospects, and challenges. Reviews of geophysics, 53(2), 323-361.

Priestley, C. H. B., and R. J. Taylor (1972), on the assessment of surface heat flux and evaporation using large-scale parameters, Mon. Weather Rev., 100, 81–92.

Rahman, K., Maringanti, C., Beniston, M., Widmer, F., Abbaspour, K., & Lehmann, A. (2013). Streamflow modeling in a highly managed mountainous glacier watershed using SWAT: the Upper Rhone River watershed case in Switzerland. WRM, 27(2), 323-339.

Rajan, K. S., & Shibasaki, R. (2001, November). A GIS based integrated land use/cover change

model to study agricultural and urban land use changes. In 22nd Asian Conference on Remote Sensing (Vol. 9).

Ramírez Villegas, J., & Jarvis, A. (2010). Downscaling global circulation model outputs: the delta method decision and policy analysis Working Paper No. 1.

Ran, L., Lu, X. X., Xin, Z., & Yang, X. (2013). Cumulative sediment trapping by reservoirs in large river basins: A case study of the Yellow River basin. Global and Planetary Change, 100, 308-319.

Ranzi, R., Le, T. H., & Rulli, M. C. (2012). A RUSLE approach to model suspended sediment load in the Lo river (Vietnam): Effects of reservoirs and land use changes. Journal of Hydrology, 422, 17-29.

Rasul, G., Pasakhala, B., Mishra, A., & Pant, S. (2020). Adaptation to mountain cryosphere change: issues and challenges. Climate and Development, 12(4), 297-309.

Rathjens, H., Bieger, K., Srinivasan, R., Chaubey, I., & Arnold, J. G. (2016). CMhyd User Manual.

Refsgaard, J. C., & Knudsen, J. (1996). Operational validation and intercomparison of different types of hydrological models. Water Resources Research, 32(7), 2189-2202.

Reid, R.S., Kruska, R.L., Muthui, N., Taye, A., Wotton, S., Wilson, C.J., and Mulatu, W., 2000. Land-use and land-cover dynamics in response to changes in climatic, biological and socio-political forces: The case of southwestern Ethiopia. Landscape Ecology, 15 (4), 339–355.

Riahi, K., Grübler, A., & Nakicenovic, N. (2007). Scenarios of long-term socio-economic and environmental development under climate stabilization. Technological Forecasting and Social Change, 74(7), 887-935.

Riahi, K., Rao, S., Krey, V., Cho, C., Chirkov, V., Fischer, G., and Rafaj, P. (2011). RCP 8.5-A scenario of comparatively high greenhouse gas emissions. Climatic Change, 109(1-2), 33.

Richard Jones, Maria Noguer, David Hassell, Debbie Hudson,Simon Wilson, Geoff Jenkins And John Mitchel, (2004). Generating High Resolution Climate Change Scenario Usin PRECI. Hadley Centre for Climate Prediction and Research, UK. PRECIS Providing Regional Climates for Impacts Studies.

Robert Leander and T. AdriBuishand. (2006). Combining RCM Output and Resampling. Royal Netherlands Meteorological Institute (KNMI), 3730 AE De Bilt, Netherlands.

Rodda, H.J.E., Little, M.A. (2015) Understanding Mathematical and Statistical Techniques in Hydrology. John Wiley & Sons.

Roeckner, E., K. Arpe, L. Bengtsson, M. Christoph, M. Claussen, L. Dümenil, M. Esch, M. Giorgetta, U. Schlese and U. Schulzweida, 1996: The atmospheric general circulation model ECHAM-4: model description and simulation of present-day climate. MaxPlanck Institute for

Meteorology, Report No.218, Hamburg, Germany, 90 pp.

Rowntree, P,(1989). The Needs of Climate Modellers for Water Runoff Data. Workshop on

Roy, K., Ambure, P., & Aher, R. B. (2017). How important is to detect systematic error in predictions and understand statistical applicability domain of QSAR models. Chemometrics and Intelligent Laboratory Systems, 162, 44-54.

Rukhin, A. L., Biggerstaff, B. J., & Vangel, M. G. (2000). Restricted maximum likelihood estimation of a common mean and the Mandel–Paule algorithm. Journal of Statistical Planning and Inference, 83(2), 319-330.

Rukhin, A. L., Biggerstaff, B. J., & Vangel, M. G. (2000). Restricted maximum likelihood estimation of a common mean and the Mandel–Paule algorithm. Journal of Statistical Planning and Inference, 83(2), 319-330.

Rummukainen, M. (2016). Added value in regional climate modeling. Wiley Interdisciplinary Reviews: Climate Change, 7(1), 145-159.

Russo, S., Marchese, A. F., Sillmann, J., & Immé, G. (2016). When will unusual heat waves become normal in a warming Africa?. Environmental Research Letters, 11(5), 054016.

Russo, S., Sillmann, J., & Fischer, E. M. (2015). Top ten European heatwaves since 1950 and their occurrence in the coming decades. Environmental Research Letters, 10(12), 124003.

Rwanga, S. S., & Ndambuki, J. M. (2017). Accuracy assessment of land use/land coverclassification using remote sensing and GIS. Int. J. Geosci, 8(4), 611-622.

Sahebjalal, E. and K. Dashtekian. (2013). Analysis of land use-land covers changes using normalized difference vegetation index (NDVI) differencing and classification methods. African Journal of Agricultural Research,. 8(37): p. 4614-4622.

Sailor, D. J., Hu, T., Li, X., & Rosen, J. N. (2000). A neural network approach to local downscaling of GCM output for assessing wind power implications of climate change. Renewable Energy, 19(3), 359-378.

Samadi, S.Z., Mahdavi, M., Sharifi, F. and Bihamta, M.R. (2009) 'Methodology for selecting the best predictor for climate change impact assessment in Karkheh Basin, Iran', Journal of Environmental Science and Engineering (JESE), Vol. 51, No. 4, pp.249–256.

Santhi, C., Arnold, J. G., Williams, J. R., Dugas, W. A., Srinivasan, R., & Hauck, L. M. (2001). Validation of the swat model on a large rwer basin with point and nonpoint sources 1. JAWRA Journal of the American Water Resources Association, 37(5), 1169-1188.

Sass, L., & Oxman, R. (2006). Materializing design: the implications of rapid prototyping in digital design. Design Studies, 27(3), 325-355.

Schaefer, K., Lantuit, H., Romanovsky, V. E., Schuur, E. A., & Witt, R. (2014). The impact of the

permafrost carbon feedback on global climate. Environmental Research Letters, 9(8), 085003.

Schmidli, J., Frei, C. & Vidale, P. L. (2006). Downscaling from GCM precipitation: a benchmark for dynamical and statistical downscaling methods. International Journal of Climatology, 26, 679-689

Schober, P., Boer, C., & Schwarte, L. A. (2018). Correlation coefficients: appropriate use and interpretation. Anesthesia & Analgesia, 126(5), 1763-1768.

Schroeder, W., Prins, E., Giglio, L., Csiszar, I., Schmidt, C., Morisette, J., & Morton, D. (2008). Validation of GOES and MODIS active fire detection products using ASTER and ETM+ data. Remote Sensing of Environment, 112(5), 2711-2726.

Seddon, N., Chausson, A., Berry, P., Girardin, C. A., Smith, A., & Turner, B. (2020). Understanding the value and limits of nature-based solutions to climate change and other global challenges. Philosophical Transactions of the Royal Society B, 375(1794), 20190120.

Setyorini, A., Khare, D., and Pingale, S.M., 2017. Simulating the impact of land use/land cover change and climate variability on watershed hydrology in the Upper Brantas basin, Indonesia. Applied Geomatics, 9 (3), 191–204.

Seyfried, M. S. (1991). Infiltration patterns from simulated rainfall on a semiarid rangeland soil. Soil Science Society of America Journal, 55(6), 1726-1734.

Shabri, A., & Jemain, A. A. (2013). Regional flood frequency analysis for S outhwest P eninsular M alaysia by LQ-moments. Journal of Flood Risk Management, 6(4), 360-371.

Shahbeik, S., Afzal, P., Moarefvand, P., & Qumarsy, M. (2014). Comparison between ordinary kriging (OK) and inverse distance weighted (IDW) based on estimation error. Case study: Dardevey iron ore deposit, NE Iran. Arabian Journal of Geosciences, 7(9), 3693-3704.

Shahidi, M., & Abedini, M. J. (2018). Optimal selection of number and location of rain gauge stations for areal estimation of annual rainfall using a procedure based on inverse distance weighting estimator. Paddy and Water Environment, 16(3), 617-629.

Shaohong, W., & Zongci, Z. (2009). Updated Understanding of Climate Change and Water [J]. Advances in Climate Change Research, 3.

Sheskin, D. J. (2011). Parametric Versus Nonparametric Tests. International encyclopedia of statistical science, 10, 978-3.

Shiferaw, B., Tesfaye, K., Kassie, M., Abate, T., Prasanna, B. M., & Menkir, A. (2014). Managing vulnerability to drought and enhancing livelihood resilience in sub-Saharan Africa: Technological, institutional and policy options. Weather and Climate Extremes, 3, 67-79.

Shrestha, B., Cochrane, T. A., Caruso, B. S., Arias, M. E., & Piman, T. (2016). Uncertainty in flow and sediment projections due to future climate scenarios for the 3S Rivers in the Mekong Basin.

Journal of Hydrology, 540, 1088-1104.

Siderius, C., Gannon, K. E., Ndiyoi, M., Opere, A., Batisani, N., Olago, D., ... & Conway, D. (2018). Hydrological response and complex impact pathways of the 2015/2016 El Niño in Eastern and Southern Africa. Earth's Future, 6(1), 2-22.

Sinclair, C. D., Spurr, B. D., & Ahmad, M. I. (1990). Modified anderson darling test. Communications in Statistics-Theory and Methods, 19(10), 3677-3686.

Smakhtin, V.U. (2001). Low Flow Hydrology: A Review. J. Hydrol., 240 (3/4), 147–186.

Smith, P., House, J. I., Bustamante, M., Sobocká, J., Harper, R., Pan, G., & Paustian, K. (2016). Global change pressures on soils from land use and management. Global Change Biology, 22(3), 1008-1028.

Smith, P., House, J.I., Bustamante, M., Sobocká, J., Harper, R., Pan, G., West, P.C., Clark, J.M., Adhya, T., Rumpel, C., Paustian, K., Kuikman, P., Cotrufo, M.F., Elliott, J.A., Mcdowell, R., Griffiths, R.I., Asakawa, S., Bondeau, A., Jain, A.K., Meersmans, J., and Pugh, T.A.M., 2016. Global change pressures on soils from land use and management. Global Change Biology, 22 (3), 1008–1028.

Smitha, P. S., Narasimhan, B., Sudheer, K. P. & Annamalai, H. (2018). An improved bias correction method of daily rainfall data using a sliding window technique for climate change impact assessment. Journal of Hydrology, 556, 100-118.

Snedecor, G. W., & Cochran, W. G. (1989). Statistical methods., 8th edn.(Iowa State University Press: Ames, IA).

Spera, S. A., Galford, G. L., Coe, M. T., Macedo, M. N., & Mustard, J. F. (2016). Land-use change affects water recycling in Brazil's last agricultural frontier. Global change biology, 22(10), 3405-3413.

Spinoni, J., Naumann, G., Vogt, J., & Barbosa, P. (2015). European drought climatologies and trends based on a multi-indicator approach. Global and Planetary Change, 127, 50-57.

Spitzer, M., Wildenhain, J., Rappsilber, J., & Tyers, M. (2014). BoxPlotR: a web tool for generation of box plots. Nature methods, 11(2), 121.

Staffordshire Learning Net (2013). River flooding-Flood alert: Geographical web enquiries.

Steffen, W., Sanderson, R. A., Tyson, P. D., Jäger, J., Matson, P. A., Moore III, B & Wasson, R. J. (2006). Global change and the earth system: a planet under pressure. Springer Science & Business Media.

Stevenson, E. G. (2018). Plantation Development in the Turkana Basin: The Making of a New Desert?. Land, 7(1), 16.

Stocker, T. F., Qin, D., Plattner, G. K., Tignor, M., Allen, S. K., Boschung, J & Midgley, B. M.

(2013). IPCC, 2013: climate change 2013: the physical science basis. Contribution of working group I to the fifth assessment report of the intergovernmental panel on climate change. .

Strahler, A. N. (1954). Statistical analysis in geomorphic research. The journal of Geology, 62(1), 1-25.

Subramanya, K., (1998).Engineering Hydrology, Tata McGraw-Hill 2nd Edition.

Sun, G. (2013). Impacts of climate change and variability on water resources in the Southeast USA. In Climate of the Southeast United States (pp. 210-236). Island Press, Washington, DC.

Swart, R., Robinson, J., & Cohen, S. (2003). Climate change and sustainable development: expanding the options. Climate policy, 3(sup1), S19-S40.

Sweeney, V. (2017). Consolidating 20 years of GPA and its activities in improving sustainable use of oceans. In Handbook on the Economics and Management of Sustainable Oceans. Edward Elgar Publishing.

Tabatabaei, M., & Salehpour Jam, A. (2017). Optimization of sediment rating curve coefficients using evolutionary algorithms and unsupervised artificial neural network. Caspian Journal of Environmental Sciences, 15(4), 385-399.

Tan, M. L., Ibrahim, A. L., Yusop, Z., Duan, Z., & Ling, L. (2015). Impacts of land-use and climate variability on hydrological components in the Johor River basin, Malaysia. Hydrological Sciences Journal, 60(5), 873-889.

Tang, Z., B. A. Engel, B. C. Pijanowski, and K. J. Lim. (2005). Forecasting land use change and its environmental impact at a watershed scale. Journal of Environmental Management 76:35-45.

Tatalovich, Z., Wilson, J. P., & Cockburn, M. (2006). A comparison of thiessen polygon, kriging, and spline models of potential UV exposure. Cartography and Geographic Information Science, 33(3), 217-231.

Tatsumi, K., Yamashiki, Y., Valmir da Silva, R., Takara, K., Matsuoka, Y., Takahashi, K., & Kawahara, N. (2011). Estimation of potential changes in cereals production under climate change scenarios. Hydrological Processes, 25(17), 2715-2725.

Taye, M., Simane, B., Zaitchik, B. F., Selassie, Y. G., & Setegn, S. (2019). Rainfall Variability across the Agro-Climatic Zones of a Tropical Highland: The Case of the Jema Watershed, Northwestern Ethiopia. Environments, 6(11), 118.

Taye, W., Adugna, T., & Temam, D. (2018). Evaluation of Groundwater Potential and Sustainable Management in Upper Gilgel Gibe Watershed, Omo Gibe River Basin, Ethiopia (Doctoral dissertation).

Taylor, K. E., Stouffer, R. J., & Meehl, G. A. (2012). An overview of CMIP5 and the experiment design. Bulletin of the American meteorological Society, 93(4), 485-498.

Temesgen T. Deressa, Rashid M. Hassan, and Claudia Ringler, (2006). Measuring Ethiopian Farmers' Vulnerability to Climate Change across Regional States, Washington D.C USA.

Tensay, G. (2011). Sedimentation modeling for Ribb dam (Doctoral dissertation, MSc thesis University of Addis Ababa, Ethiopia).

Teutschbein, C. & Seibert, J. (2012). Bias correction of regional climate mode simulations for hydrological climate-change impact studies: Review and evaluation of different methods. Journal of Hydrology, 456, 12-29.

Teutschbein, C., & Seibert, J. (2012). Bias correction of regional climate model simulations for hydrological climate-change impact studies: Review and evaluation of different methods. Journal of hydrology, 456, 12-29.

Teutschbein, C., & Seibert, J. (2013). Is bias correction of regional climate model (RCM) simulations possible for non-stationary conditions?. Hydrology and Earth System Sciences, 17(12), 5061-5077.

Thenkabail, P. S., & Lyon, J. G. (2016). Hyperspectral remote sensing of vegetation. CRC press.

Thomson, A. M., Calvin, K. V., Smith, S. J., Kyle, G. P., Volke, A., Patel, P., & Edmonds, J. A. (2011). RCP4. 5: a pathway for stabilization of radiative forcing by 2100. CC, 109(1-2),

Tian, D., Dong, W., Zhang, H., Guo, Y., Yang, S., & Dai, T. (2017). Future changes in coverage of 1.5° C and 2° C warming thresholds. Science bulletin, 62(21), 1455-1463.

Tigabu, T. B., Wagner, P. D., Hörmann, G., Kiesel, J., & Fohrer, N. (2021). Climate change impacts on the water and groundwater resources of the Lake Tana Basin, Ethiopia. Journal of Water and Climate Change, 12(5), 1544-1563.

Tilmant, A., Pina, J., Salman, M., Casarotto, C., Ledbi, F., & Pek, E. (2020). Probabilistic trade-off assessment between competing and vulnerable water users–The case of the Senegal River basin. Journal of Hydrology, 587, 124915.

Tirumala, C., Vignesh, M., & Balaji, R. (2017, April). Data analysis using Box and Whisker plot for Lung Cancer. In 2017 Innovations in Power and Advanced Computing Technologies (i-PACT) (pp. 1-6). IEEE.

Trenberth, K. E. (2011). Changes in precipitation with climate change. Climate Research, 47(1-2), 123-138.

Tu_Min. (2006).Assessment of the Effects of Climate Variability and Land-Use Change on the Hydrology of Meuse River Basin. PhD Thesis, Netherland: UNESCO-IHE Institute for Water Education.

USDA, S. (1972). National engineering handbook, section 4: Hydrology. Washington, DC.

Ustin, S. L., Palacios-Orueta, A., Whiting, M. L., Jacquemoud, S., & Li, L. (2009). Remote sensing

based assessment of biophysical indicators for land degradation and desertification. In Recent advances in remote sensing and geoinformation processing for land degradation assessment (pp. 35-64). CRC Press.

van Delden, H., Seppelt, R., White, R., & Jakeman, A. J. (2011). A methodology for the design and development of integrated models for policy support. Environmental Modelling & Software, 26(3), 266-279.

Van Lieshout, M., Kovats, R. S., Livermore, M. T. J., & Martens, P. (2004). Climate change and malaria: analysis of the SRES climate and socio-economic scenarios. Global Environmental Change, 14(1), 87-99.

Van Roosmalen,L., Sonnenborg,T. O., & Jensen,K.H. (2009). Impact of climate and land use change on the hydrology of large-scale agricultural catchment. Water Resources Research,45(7).

Van Vuuren, D. P., Edmonds, J., Kainuma, M., Riahi, K., Thomson, A., Hibbard, K., & Masui, T. (2011). The representative concentration pathways: an overview. Climatic change,109(1-2), 5.

Vieira, D. C. S., Serpa, D., Nunes, J. P. C., Prats, S. A., Neves, R., & Keizer, J. J. (2018). Predicting the effectiveness of different mulching techniques in reducing post-fire runoff and erosion at plot scale with the RUSLE, MMF and PESERA models. Environmental research, 165, 365-378.

Wale, A., Rientjes, T. H. M., Dost, R. J. J., & Gieske, A. (2008). Hydrological balance of Lake Tana Upper Blue Nile basin, Ethiopia. The Netherlands: ITC.

Wang, Q. J. (1997). LH moments for statistical analysis of extreme events. Water Resources Research, 33(12), 2841-2848.

Wang, R., Kalin, L., Kuang, W., & Tian, H. (2014). Individual and combined effects of land use/cover and climate change on Wolf Bay watershed streamflow in southern Alabama. Hydrological Processes, 28(22), 5530-5546.

Wang, W., Shao, Q., Yang, T., Peng, S., Xing, W., Sun, F., & Luo, Y. (2013). Quantitative assessment of the impact of climate variability and human activities on runoff changes: a case study in four catchments of the Haihe River basin, China., 27(8), 1158-1174.

Wang, Y., Leung, L. R., McGREGOR, J. L., Lee, D. K., Wang, W. C., Ding, Y., & Kimura, F. (2004). Regional climate modeling: progress, challenges, and prospects. Journal of the Meteorological Society of Japan. Ser. II, 82(6), 1599-1628.

Watson, R. T., Zinyowera, M. C., Moss, R. H., & Dokken, D. J. (1998). The regional impacts of climate change. An assessment of vulnerability: A Special Report of IPCC WG-II, 517.

Wayne, G. P. (2014). Representative Concentration Pathways. Skeptical science, 24.

West, M., & Harrison, J. (2006). Bayesian forecasting and dynamic models. Springer Science &

Business Media.

White, J. W., Tanner, D. G., & Corbett, J. D. (2001). An agro-climatological characterization of bread wheat production areas in Ethiopia.

Wilby, R. L., Dawson, C. W., & Barrow, E. M. (2002). SDSM—a decision support tool for the assessment of regional climate change impacts. Environmental Modelling & Software, 17(2), 145-157.

Wilby, R. L., Hay, L. E., & Leavesley, G. H. (1999). A comparison of downscaled and raw GCM output: implications for climate change scenarios in the San Juan River basin, Colorado. Journal of Hydrology, 225(1-2), 67-91.

Wolka, K. and Zeleke, G., 2016. Understanding farmers' perception on climate change and adaptation strategies in Karetha watershed, Omo-gibe basin, Ethiopia. Asian Journal of Earth Sciences, 10 (1), 22–32.

Worqlul, A. W., Dile, Y. T., Ayana, E. K., Jeong, J., Adem, A. A., & Gerik, T. (2018). Impact of climate change on streamflow hydrology in headwater catchments of the Upper Blue Nile Basin, Ethiopia. Water, 10(2), 120.

Worqlul, A. W., Tulu, T., Argaw, M., & Gashaw, T., (2018). Modeling the hydrological impacts of land use/land cover changes in the Andassa watershed, Blue Nile Basin, Ethiopia. Science of the Total Environment, 619, 1394-1408.

Wu, C. L., Herrington, S. J., Charry, B., Chu, M. L., & Knouft, J. H. (2021). Assessing the potential of riparian reforestation to facilitate watershed climate adaptation. Journal of Environmental Management, 277, 111431.

Wuebbles, D. J., & Jain, A. K. (2001). Concerns about climate change and the role of fossil fuel use. Fuel processing technology, 71(1-3), 99-119.

Xu, H. (2007). Extraction of urban built-up land features from Landsat imagery using a thematicoriented index combination technique. Photogrammetric Engineering & Remote Sensing, 73(12), 1381-1391.

Xu, Z., Han, Y., & Yang, Z. (2019). Dynamical downscaling of regional climate: A review of methods and limitations. Science China Earth Sciences, 62(2), 365-375.

Yacob, A., Milman, A., &. (2014). Climate adaptation and development: Contradictions for human security in Gambella, Ethiopia. Global environmental change, 29, 349-359.

Yang, X., & Lu, X. X. (2014). Estimate of cumulative sediment trapping by multiple reservoirs in large river basins: An example of the Yangtze River basin. Geomorphology, 227, 49-59.

Yang, X., Xie, X., Liu, D. L., Ji, F., & Wang, L. (2015). Spatial interpolation of daily rainfall data for local climate impact assessment over greater Sydney region. Advances in Meteorology,

Yates, D. N., & Strzepek, K. M. (1998). Modeling the Nile Basin under climatic change. Journal of Hydrologic Engineering, 3(2), 98-108.

Yongqiang, Y., Xuehong, Z., & Yufu, G. (2004). Global coupled ocean-atmosphere general circulation models in LASG/IAP. Advances in Atmospheric sciences, 21(3), 444

You, Q., Min, J., Fraedrich, K., Zhang, W., Kang, S., Zhang, L., & Meng, X. (2014). Projected trends in mean, maximum, and minimum surface temperature in China from simulations. Global and Planetary Change, 112, 53-63.

Yuan, S., Quiring, S. M., Kalcic, M. M., Apostel, A. M., Evenson, G. R., & Kujawa, H. A. (2020). Optimizing climate model selection for hydrological modeling: A case study in the Maumee River basin using the SWAT. Journal of Hydrology, 588, 125064.

Yue N. G., Yang, Z. L., Dickinson, R. E., Gulden, L. E., & Su, H. (2007). Development of a simple groundwater model for use in climate models and evaluation with Gravity Recovery and Climate Experiment data. Journal of Geophysical Research: Atmospheres, 112(D7).

Yue, H., & Jin-yang, Y. (2016). Quantile-Quantile Plot Compared with Stablized Probability Plot in Figure on the Distribution of the Test Research. American Journal of Applied Mathematics, 4(2), 110-113.

Zakaria, N. A., & Noor, N. M. (2018). Imputation methods for filling missing data in urban air pollution data formalaysia. Urbanism. Arhitectura. Constructii, 9(2), 159.

Zeleke, G., & Hurni, H. (2001). Implications of land use and land cover dynamics for mountain resource degradation in the North-western Ethiopian highlands. Mountain research and development, 21(2), 184-192.

Zeng, X., Wang, D., & Wu, J. (2015). Evaluating the three methods of goodness of fit test for frequency analysis. Journal of Risk Analysis and Crisis Response, 5(3), 178-187.

Zhang, L., Nan, Z., Yu, W., & Ge, Y. (2015). Modeling land-use and land-cover change and hydrological responses under consistent climate change scenarios in the Heihe River Basin, China. Water resources management, 29(13), 4701-4717.

Zhang, X., Srinivasan, R., & Bosch, D. (2009). Calibration and uncertainty analysis of the SWAT model using Genetic Algorithms and Bayesian Model Averaging. Journal of Hydrology, 374(3-4), 307-317.

Zhao, H., & Chen, X. (2005,). Use of normalized difference bareness index in quickly mapping bare areas from TM/ETM+. In International geoscience and remote sensing symposium (Vol. 3, p. 1666).

Zhao, Y., Wang, C., Wang, S., & Tibig, L. V. (2005). Impacts of present and future climate variability on agriculture and forestry in the humid and sub-humid tropics. Climatic Change,

70(1-2), 73-116

Zorn, M. and Komac, B., 2013. Erosivity. In: P.T. Bobrowsky, ed. Dordrecht: Springer Netherlands, 289–290.

Appendix 1 Hydrological data Normality test using Chi-squared test and Kolmogorov-Smirnov test[a]

Table A1.1 Chi-squared test

Variable	Abelit_flow	Asandabo_flow	Gojab_NR.Shebe
Sample size	1985-2016	1985-2016	1985-2016
Variance	6102.9628	123.7558	265.7855
Standard deviation	78.1215	11.1246	16.3029
Relativestandard deviation	0.3436 (34.36%)	0.2771 (27.71%)	0.2630 (26.30%)
Standard error of the mean	13.8101	1.9666	2.882
Coefficient of Skewness	0.1055 (P=0.7875)	0.1213 (P=0.7567)	0.2893 (P=0.4639)
Coefficient of Kurtosis	-0.9422 (P=0.1118)	-1.1613 (P=0.0215)	-0.9994 (P=0.0788)
Chi-squared test for Normal Distributiont	AN (P=0.7520) (Chi-squared=1.92 DF = 4	AN (P=0.356) (Chi-squared=4.38 DF=4)	AN (P=0.256) (Chi-squared=6.55 DF=5)

Megecha_flow	Kiulit_flow	Awuti_flow	Ghibe_flow
1985-2016	1985-2016	1985-2016	1985-2016
176.7036	2.1294	2.4099	4.4123
13.293	1.4592	1.5524	2.1006
0.4987	0.3307	0.7567	0.5499
(49.87%)	(33.07%)	(75.67%)	(54.99%)
2.3499	0.258	0.2744	0.3713
0.7292	0.2818	0.9564	0.2327
(P=0.0785)	(P=0.4753)	(P=0.0258)	(P=0.5544)
-0.2323	-0.2011	0.4329	-1.3015
(P=0.9165)	(P=0.9548)	(P=0.4557)	(P=0.0041)
AN (P=0.1952)	AN (P=0.0630)	RN (P=0.0054)	RN (P=0.0029)
(Chi-squared=6.13	(Chi-squared=8.93	(Chi-squared=14.78	(Chi-squared=16.19
DF=4)	DF=4)	DF=4	DF=4)

NB: AN = Accept Normality, RN =Reject Normality

Table A1.2 Kolmogorov-Smirnov test

Variable	Abelit_flow	Asandabo	Gojab__NR.Shebe	Kiulit_flow
Sample size	1985-2016	1985-2016	1985-2016	1985-2016
Mean	372.9563	40.1442	61.9941	2.1294
Meida	223.3245	38.6042	60.6645	1.4592
Variance	6102.9628	123.7558	265.7855	2.1294
Standard deviation	78.1215	11.1246	16.3029	1.4592
Relative standard deviation	0.3436 (34.36%)	0.2771 (27.71%)	0.2656478 (26.30%)	0.3307 (33.07%)
Standard error of the mean	13.8101	1.9666	2.882	0.258
Coefficient of Skewness	0.1055 (P=0.785)	0.1213 (P=0.77)	0.2965454 (P=0.45)	0.2818 (P=0.475)
Coefficient of Kurtosis	-0.9422 (P=0.118)	-1.163 (P=0.025)	-0.94546 (P=0.0788)	-0.2011 (P=0.98)
Kolmogorov-Smirnov test	D=0.1198	D=0.1244	D=0.1211	D=0.148
Normal distribution	AN ((P>0.10)	(P>0.10)	(P>0.10)	(P=0.12))

Megecha_flow	Wabe_flow	Walge_flow	Ghibe_flow
1985-2016	1985-2016	1985-2016	1985-2016
26.6549	18.3083	3.2499	0.9717
23.8333	94.125	26.1521	7.4988
176.7036	435.6165	31.6596	4.4123
13.293	20.8714	5.6267	2.1006
0.4987	0.4088	0.5029	0.5499
(49.87%)	(40.88%)	(50.29%)	(54.99%)
2.3499	3.6896	0.9947	0.3713
0.7292	0.1854	0.6388	0.2327
(P=0.0785)	(P=0.6368)	(P=0.1187)	(P=0.5544)
-0.2323 (P=0.9165)	-0.6897 (P=0.3396)	-0.07711 (P=0.9004)	-1.3015 (P=0.0041)
D=0.1333	D=0.1170	D=0.1516	D=0.1551
Normality (P>0.10)	AN (P>0.10)	AN (P=0.0595)	RN (P=0.0487)

NB: AN = Accept Normality, RN =Reject Normality

Number	Gojbe_ flow Distribution	Kolmogorov Smirnov		Anderson Darling		Chi-Squared	
		Statistic	Rank	Statistic	Rank	Statistic	Rank
1	Gamma	0.09513	7	0.3569	7	0.87345	1
2	Gamma (3P)	0.08799	4	0.24778	4	1.9996	5
3	Gen. Extreme Value	0.07543	2	0.21452	1	1.8666	4
4	Gen. Pareto	0.09666	8	7.6787	9	N/A	0
5	Log-Pearson 3	0.06985	1	0.2202	2	2.5093	8
6	Lognormal	0.1195	9	0.5182	8	1.5042	2
7	Lognormal (3P)	0.08857	5	0.25096	5	2.0079	6
8	Pareto	0.36738	10	7.7335	10	11.723	9
9	Weibull	0.09346	6	0.27914	6	1.6816	3
10	Weibull (3P)	0.08371	3	0.24568	3	2.1585	7

Number	Abelit_flow Distribution	Kolmogorov Smirnov		Anderson Darling		Chi-Squared	
		Statistic	Rank	Statistic	Rank	Statistic	Rank
1	Gamma	0.12339	7	0.48449	6	1.8912	4
2	Gamma (3P)	0.1212	6	0.47362	5	3.2891	9
3	Gen. Extreme Value	0.10843	2	0.38608	2	2.2847	5
4	Gen. Pareto	0.08112	1	0.2319	1	0.27768	1
5	Log-Pearson 3	0.1171	3	0.43393	3	1.7346	3
6	Lognormal	0.12072	4	0.49657	9	3.1478	8
7	Lognormal (3P)	0.12427	8	0.49508	8	2.6471	6
8	Pareto	0.23555	10	6.4885	10	5.1307	10
9	Weibull	0.12807	9	0.49282	7	2.7764	7
10	Weibull (3P)	0.12073	5	0.45967	4	1.6859	2

Number	Megecha_flow Distribution	Kolmogorov Smirnov		Anderson Darling		Chi-Squared	
		Statistic	Rank	Statistic	Rank	Statistic	Rank
1	Gen. Pareto	0.08975	1	4.2648	9	N/A	

2	Gen. Extreme Value	0.10311	2	0.39054	1	1.5964	8
3	Log-Pearson 3	0.10938	3	0.42275	2	0.14279	1
4	Weibull	0.11297	4	0.42558	3	0.18915	2
5	Weibull (3P)	0.11474	5	0.46132	4	0.2168	5
6	Lognormal (3P)	0.11614	6	0.48164	6	0.66627	7
7	Gamma (3P)	0.11819	7	0.47787	5	0.65795	6
8	Lognormal	0.12262	8	0.6031	8	0.20028	4
9	Gamma	0.12508	9	0.55133	7	0.19334	3
10	Pareto	0.3218	10	6.6929	10	7.2908	9

Number	Asandabo_flow Distribution	Kolmogorov Smirnov		Anderson Darling		Chi-Squared	
		Statistic	Rank	Statistic	Rank	Statistic	Rank
1	Gamma	0.12339	7	0.48449	6	1.8912	4
2	Gamma (3P)	0.1212	6	0.47362	5	3.2891	9
3	Gen. Extreme Value	0.10843	2	0.38608	2	2.2847	5
4	Gen. Pareto	0.08112	1	0.2319	1	0.27768	1
5	Log-Pearson 3	0.1171	3	0.43393	3	1.7346	3
6	Lognormal	0.12072	4	0.49657	9	3.1478	8
7	Lognormal (3P)	0.12427	8	0.49508	8	2.6471	6
8	Pareto	0.23555	10	6.4885	10	5.1307	10
9	Weibull	0.12807	9	0.49282	7	2.7764	7
10	Weibull (3P)	0.12073	5	0.45967	4	1.6859	2

Number	Wabe _flow Distribution	Kolmogorov Smirnov		Anderson Darling		Chi-Squared	
		Statistic	Rank	Statistic	Rank	Statistic	Rank
1	Gen. Extreme Value	0.11133	1	0.41649	1	1.253	2
2	Weibull	0.13727	4	0.45064	2	4.598	8
3	Log-Pearson 3	0.14095	5	0.51483	3	3.7492	4
4	Lognormal (3P)	0.13131	3	0.52148	4	3.7948	6
5	Gamma (3P)	0.14365	6	0.56201	5	3.7797	5
6	Weibull (3P)	0.14502	7	0.57666	6	3.9334	7
7	Gamma	0.15449	8	0.69725	7	1.1929	1

8	Lognormal	0.16988	9	0.79346	8	2.2287	3
9	Pareto	0.26956	10	7.2349	9	6.6339	9
10	Gen. Pareto	0.11836	2	7.7265	10	N/A	

Appendix 2: Parameter Estimation Using Method of Momentum (MoM)

Megecha flow: Parameter estimation by using Method of Momentum

Parameter Estimation	μ	α	δ	κ	β	γ
Gamma		4.02			6.63	
Gamma(3p)		2.56			8.60	4.58
GEV	20.30		10.66	0.02		
Log-pearson 3		49.05			-0.07	6.83
Lognormal	3.16		0.52			
Weibull		2.20			29.18	
Gen.Pareto	8.72		24.82	-0.38		

Abelit flow: Parameter estimation by using Method of Momentum

Parameter Estimation	μ	α	δ	κ	β	γ
Gamma		8.47			26.85	
Gamma(3p)		27.83			14.70	-181.9
GEV	197.49		77.96	-0.24		
Log-pearson 3		15.21			-0.09	6.82
Lognormal	5.36	0.37				
Weibull		3.05			249.84	
Gen.Pareto	96.04		249.29	-0.89		

Asendabo flow: Parameter estimation by using Method of Momentum

Parameter Estimation	μ	α	δ	κ	β	γ
Gamma		8.47			2.85	
Gamma(3p)		27.83			14.70	-181.9
GEV	197.49		77.96	-0.27		
Log-pearson 3		15.27			-0.09	6.82
Lognormal	5.36		0.37			
Weibull		3.05			249.84	
Gen.Pareto	96.04		249.29	-0.89		

Wabe: Parameter estimation by using Method of Momentum

Parameter Estimation	μ	α	δ	κ	β	γ
Gamma		5.98			8.53	

Gamma(3p)		9.55			6.83	-14.19
GEV	43.18		20.95	-0.24		
Log-pearson 3		14.22			-0.12	5.56
Lognormal	3.84	0.45				
Weibull		2.49			56.41	
Gen. Pareto	16.01		66.98	-0.91		

Table: Gojeb flow near to Shebe: Parameter estimation by using Method of Momentum

Parameter Estimation	μ	α	δ	κ	β	γ
Gamma		7.12			20.24	
Gamma(3p)		45.71			7.88	-216.4
GEV	122.72		52.67	-0.21		
Log-pearson 3		5.29			-0.19	5.88
Lognormal	4.89		0.43			
Weibull	2.67				159.35	
Gen. Pareto	55.80		161.49	-0.83		

Appendix 3: Selected Omo Gibe river basin streamflow time series

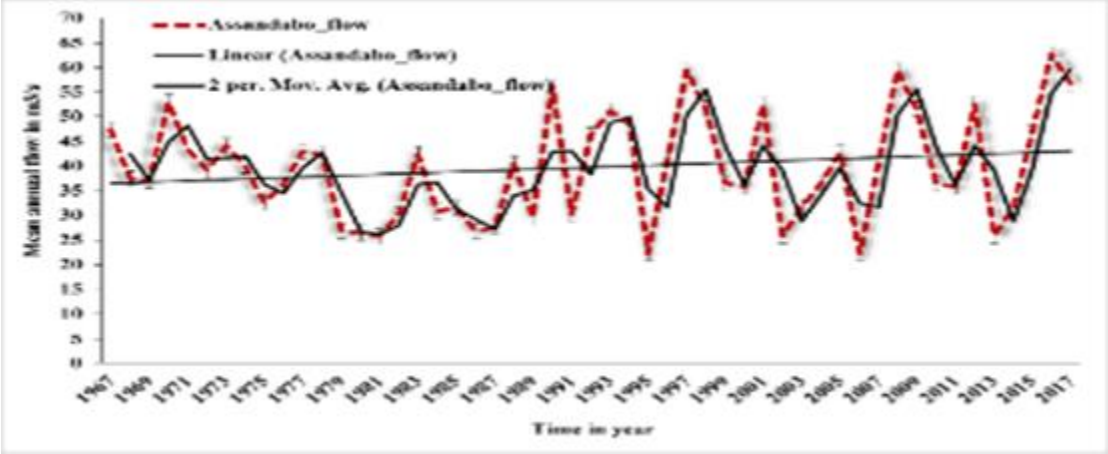

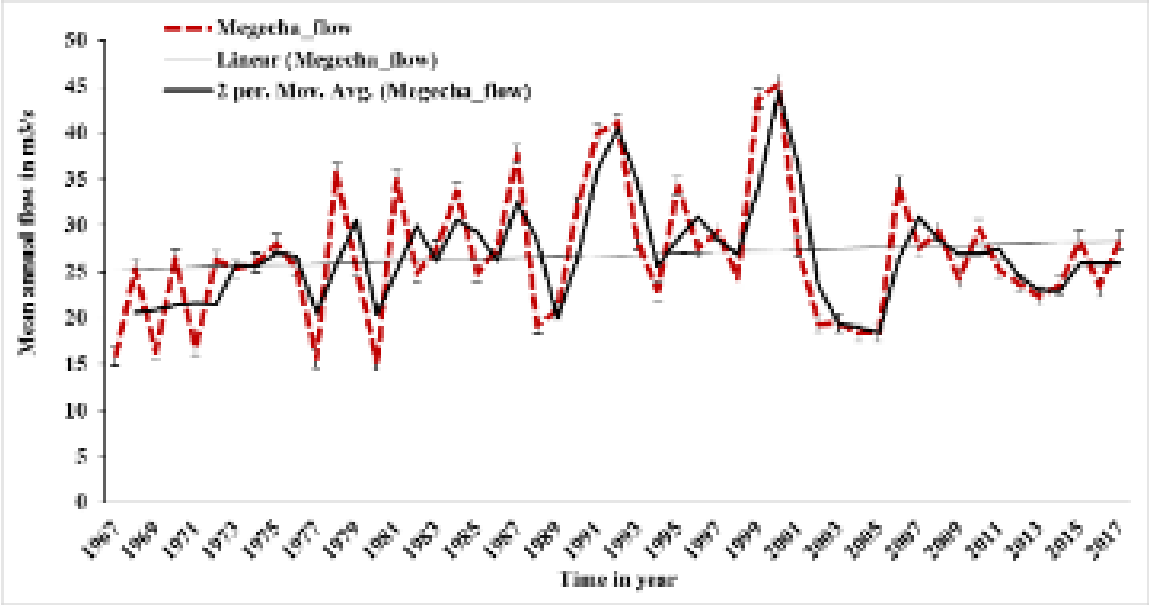

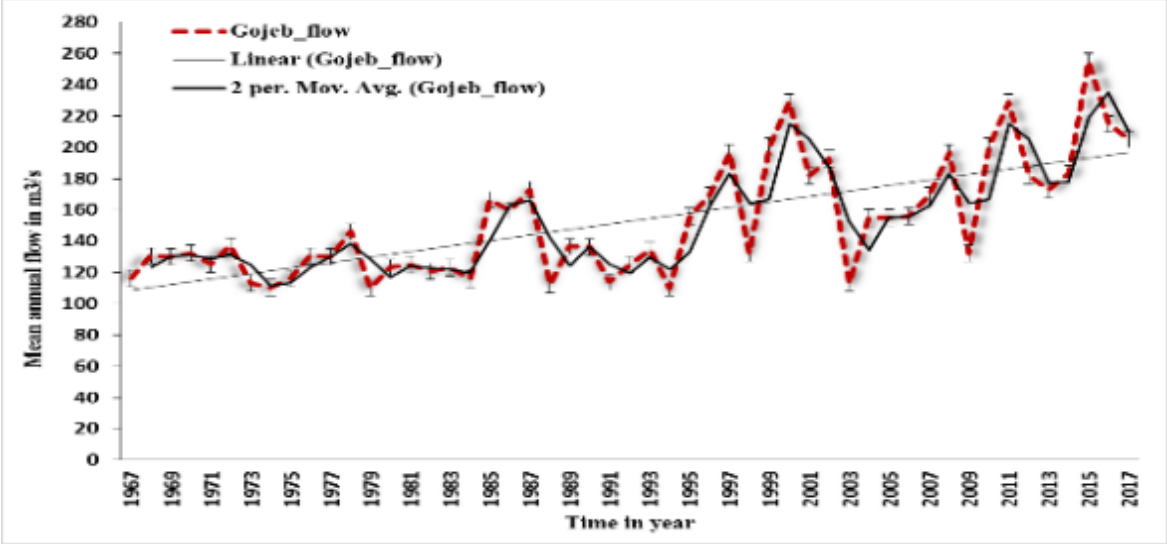

Appendix 4 Spatial Interpolation Minimum and maximum RF using IDW and Ordinary Kriging

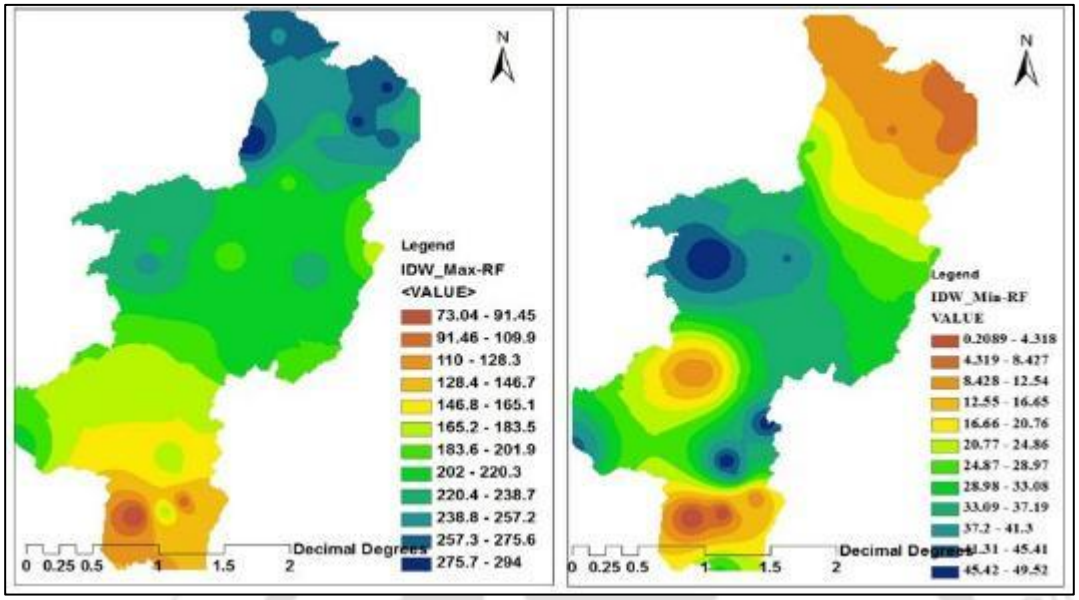

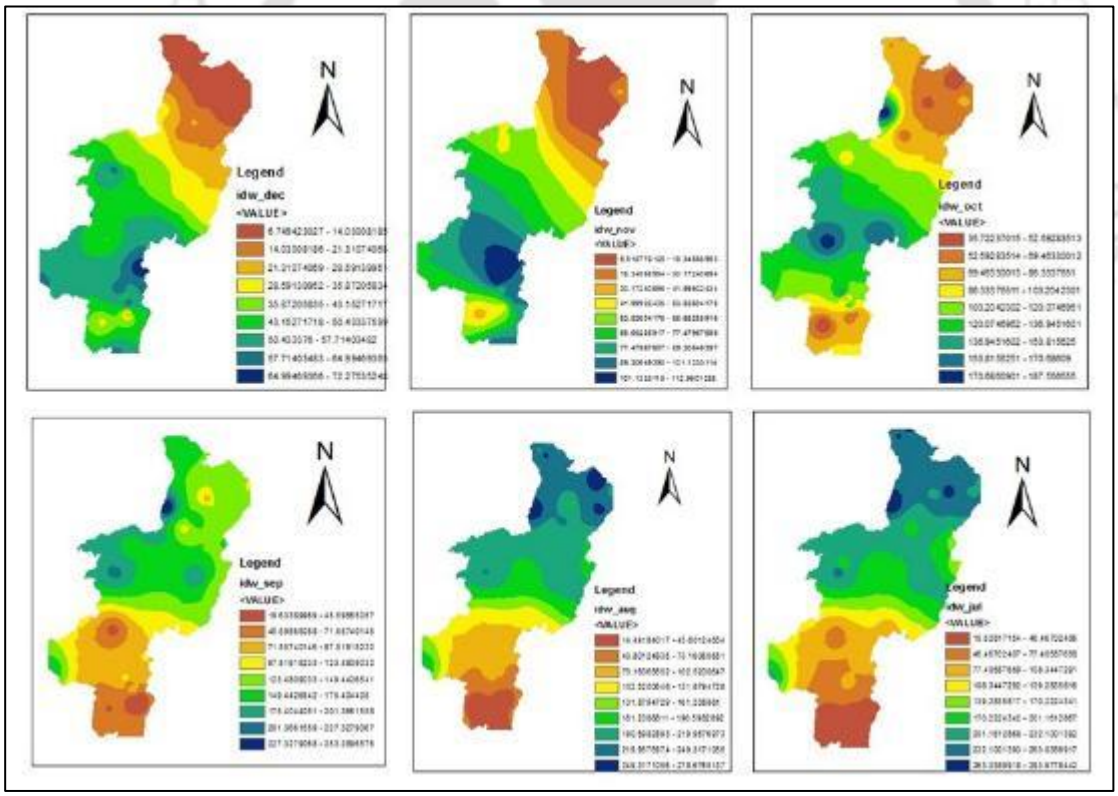

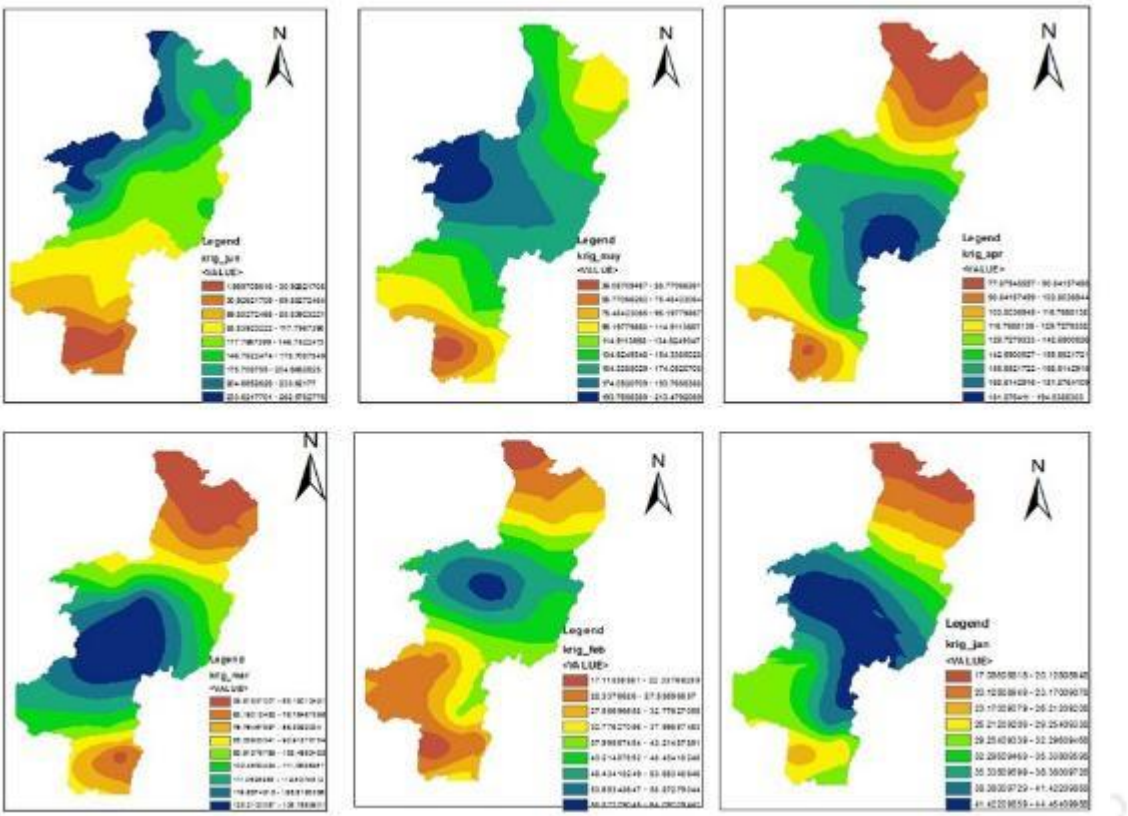

Appendix 5: Checking Homogeneity and Consistency of the Rainfall Stations.

Consistency of the Rainfall Stations

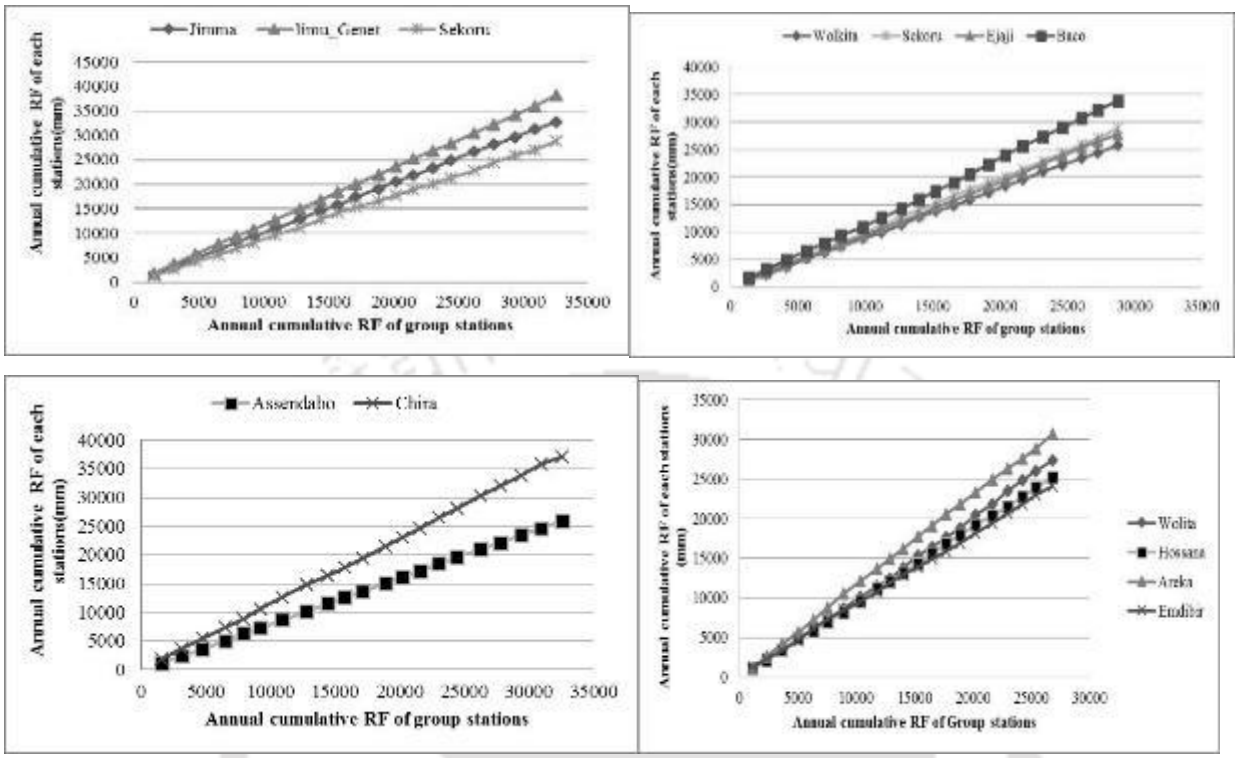

Checking Homogeneity of Rainfall Station

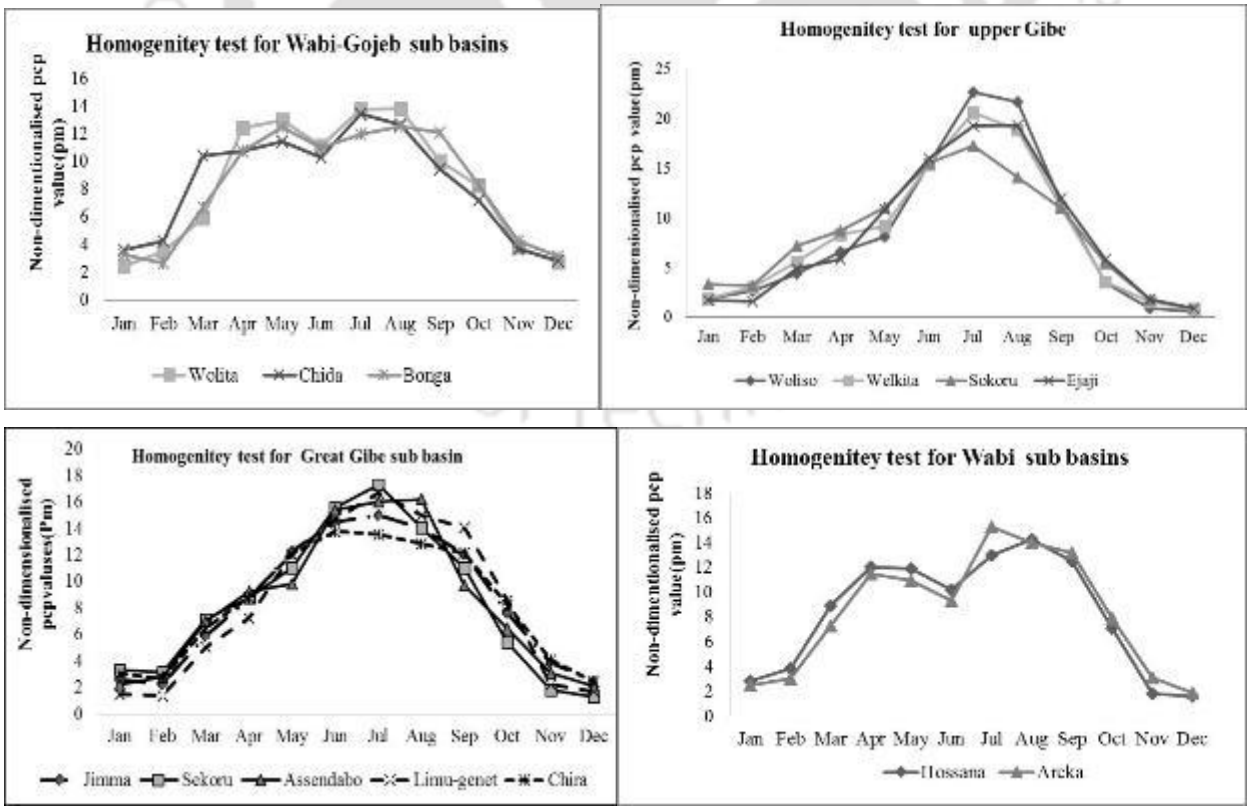

Appendix 6: Hydrological Data

Mean Monthly Magach Station flow In m^3/s															
Y/M	Jan.	Feb.	Mar.	Apr.	May.	Jun.	Jul.	Aug.	Sep.	Oct.	Nov.	Dec.	Mean	Max	Min
1980	8.78	6.80	7.69	17.29	48.86	122.16	118.94	134.90	89.88	50.23	21.05	13.18	53.31	134.90	6.80
1981	10.03	8.09	11.65	6.15	21.80	49.69	68.68	237.63	134.98	79.36	19.23	9.93	54.77	237.63	6.15
1982	11.09	7.93	6.81	9.50	20.48	61.90	90.98	129.47	108.95	112.58	28.26	22.80	50.90	129.47	6.81
1983	9.95	8.55	8.96	10.51	18.16	35.31	54.37	132.67	235.98	73.07	31.31	19.52	53.20	235.98	8.55
1984	12.54	9.19	8.64	14.96	19.95	57.15	104.09	128.71	119.99	29.32	25.79	18.67	45.75	128.71	8.64
1985	10.48	8.26	8.62	14.08	43.13	68.57	103.56	149.59	156.84	54.03	27.54	14.59	54.94	156.84	8.26
1986	9.24	9.91	12.81	16.58	22.37	78.93	78.47	100.25	117.80	41.01	16.81	13.91	43.17	117.80	9.24
1987	8.73	7.80	12.18	14.01	22.37	43.06	83.62	95.35	86.06	58.94	39.33	17.30	40.73	95.35	7.80
1988	35.81	29.18	23.65	17.85	46.38	114.78	205.75	551.02	510.49	498.22	72.07	36.81	178.50	551.02	17.85
1989	31.94	29.65	27.96	65.57	60.21	88.55	226.37	255.44	324.95	193.52	67.20	101.93	122.77	324.95	27.96
1990	48.44	43.50	63.49	60.84	75.35	222.65	221.52	425.46	383.56	233.63	77.07	48.72	158.69	425.46	43.50
1991	35.78	30.19	31.20	44.42	124.48	274.43	443.80	298.79	193.89	104.98	48.40	37.83	139.02	443.80	30.19
1992	27.91	31.47	27.03	42.50	112.33	165.93	302.05	309.57	313.68	406.43	110.86	56.32	158.84	406.43	27.03
1993	44.67	43.59	37.53	81.07	195.02	256.17	348.44	278.56	294.36	198.21	84.11	41.59	158.61	348.44	37.53
1994	30.32	22.52	24.03	27.12	64.29	161.18	383.12	465.12	360.91	89.21	63.00	45.74	144.71	465.12	22.52
1995	28.95	23.90	23.64	33.93	77.22	146.44	191.33	280.69	267.00	176.30	61.04	66.71	114.76	280.69	23.64
1996	53.33	39.01	65.64	92.91	159.17	329.47	301.63	318.59	361.53	233.64	67.09	51.52	172.79	361.53	39.01
1997	43.54	28.88	33.46	52.63	111.45	332.33	218.92	252.23	200.78	396.11	432.13	156.89	188.28	432.13	28.88
1998	112.88	56.29	131.37	55.21	163.37	237.64	307.25	615.17	335.13	538.48	106.96	14.99	222.90	615.17	14.99
1999	2.53	0.78	0.57	7.29	107.30	172.17	379.21	332.27	185.83	364.59	73.01	7.02	136.05	379.21	0.57
2000	3.69	0.47	0.35	59.75	204.85	222.20	395.21	382.95	339.62	403.11	197.55	33.91	186.97	403.11	0.35

2001	7.46	2.69	14.20	36.01	83.35	294.84	457.17	588.15	644.30	355.10	203.63	33.95	226.74	644.30	2.69
2002	44.83	29.84	32.45	41.22	35.95	107.25	180.74	260.78	204.28	125.39	37.67	30.92	94.28	260.78	29.84
2003	12.30	7.44	34.11	54.21	32.63	106.37	260.30	275.38	341.96	107.26	43.80	44.06	109.99	341.96	7.44
2004	35.09	32.79	24.59	25.97	68.06	135.68	230.05	314.92	368.50	272.78	28.92	26.48	130.32	368.50	24.59
2005	27.91	31.47	27.03	42.50	112.33	165.93	302.05	309.57	313.68	406.43	110.86	56.32	158.84	406.43	27.03
2006	44.67	43.59	37.53	81.07	195.02	256.17	348.44	278.56	294.36	198.21	84.11	41.59	158.61	348.44	37.53
2007	30.32	22.52	24.03	27.12	64.29	161.18	383.12	465.12	360.91	89.21	63.00	45.74	144.71	465.12	22.52
2008	28.95	23.90	23.64	33.93	77.22	146.44	191.33	280.69	267.00	176.30	61.04	66.71	114.76	280.69	23.64
2009	53.33	39.01	65.64	92.91	159.17	329.47	301.63	318.59	361.53	233.64	67.09	51.52	172.79	361.53	39.01
2010	43.54	28.88	33.46	52.63	111.45	332.33	218.92	252.23	200.78	396.11	432.13	156.89	188.28	432.13	28.88
2011	112.88	56.29	131.37	55.21	163.37	237.64	307.25	615.17	335.13	538.48	106.96	14.99	222.90	615.17	14.99
2012	2.53	0.78	0.57	7.29	107.30	172.17	379.21	332.27	185.83	364.59	73.01	7.02	136.05	379.21	0.57
2013	3.69	0.47	0.35	59.75	204.85	222.20	395.21	382.95	339.62	403.11	197.55	33.91	186.97	403.11	0.35
2014	7.46	2.69	14.20	36.01	83.35	294.84	457.17	588.15	644.30	355.10	203.63	33.95	226.74	644.30	2.69
2015	112.88	56.29	131.37	55.21	163.37	237.64	307.25	615.17	335.13	538.48	106.96	14.99	222.90	615.17	14.99
2016	2.53	0.78	0.57	7.29	107.30	172.17	379.21	332.27	185.83	364.59	73.01	7.02	136.05	379.21	0.57
2017	3.69	0.47	0.35	59.75	204.85	222.20	395.21	382.95	339.62	403.11	197.55	33.91	186.97	403.11	0.35
2018	7.46	2.69	14.20	36.01	83.35	294.84	457.17	588.15	644.30	355.10	203.63	33.95	226.74	644.30	2.69

Mean Monthly Assandebo Station flow In m^3/s															
Y/M	Jan.	Feb.	Mar.	Apr.	May.	Jun.	Jul.	Aug.	Sep.	Oct.	Nov.	Dec.	mean	Max	Min
1980	3.62	2.31	3.11	6.23	9.51	44.97	63.91	95.18	56.93	20.98	7.61	3.83	26.52	95.18	2.31
1981	2.03	2.39	10.70	6.92	7.75	18.91	70.86	92.86	33.69	45.54	12.61	5.09	25.78	92.86	2.03
1982	4.45	2.29	2.32	2.77	7.76	16.81	32.25	67.83	108.11	54.49	38.41	24.32	30.15	108.11	2.29
1983	9.42	5.80	3.43	7.36	9.65	35.70	36.59	80.08	161.89	142.44	61.48	19.92	47.81	161.89	3.43

1984	9.48	3.80	2.41	3.82	9.45	47.30	87.86	93.37	78.38	19.64	8.89	6.42	30.90	93.37	2.41
1985	2.58	1.87	1.25	5.64	14.90	36.68	74.34	117.94	91.75	36.98	12.79	6.06	33.56	117.94	1.25
1986	2.14	2.60	4.02	3.62	4.41	34.40	74.96	70.72	87.08	33.19	10.34	7.08	27.88	87.08	2.14
1987	3.29	2.20	7.54	5.54	16.05	41.66	57.56	61.43	77.23	35.67	15.35	6.96	27.54	77.23	2.20
1988	3.99	4.18	1.67	1.46	3.48	10.81	56.36	157.91	123.57	95.55	20.66	7.46	40.59	157.91	1.46
1989	4.80	5.04	3.55	21.13	11.51	27.44	52.61	77.31	78.54	41.85	15.05	17.26	29.67	78.54	3.55
1990	8.24	6.51	9.70	8.97	16.43	48.90	92.15	76.78	121.81	181.07	94.00	9.57	56.18	181.07	6.51
1991	6.30	5.30	7.49	4.64	10.61	34.83	67.72	114.16	85.29	20.41	3.10	2.63	30.21	114.16	2.63
1992	0.64	1.42	0.13	1.29	12.00	42.49	86.26	189.58	119.82	75.38	20.04	7.80	46.40	189.58	0.13
1993	7.32	10.67	4.49	20.37	53.71	78.46	129.22	120.22	85.00	60.92	33.42	10.25	51.17	129.22	4.49
1994	5.92	3.21	4.36	5.02	21.57	70.90	131.87	170.04	125.93	27.44	11.37	5.87	48.63	170.04	3.21
1995	3.26	3.07	2.54	8.12	11.86	15.26	45.45	65.42	79.09	18.85	8.01	6.24	22.27	79.09	2.54
1996	3.26	3.07	2.54	8.12	11.86	91.21	85.50	125.14	90.82	46.75	17.35	8.93	41.21	125.14	2.54
1997	6.58	12.62	2.44	17.21	26.34	70.84	70.56	105.85	72.40	134.48	140.04	53.97	59.44	140.04	2.44
1998	27.67	16.25	16.40	11.79	20.91	30.27	85.82	174.10	100.33	85.57	34.34	15.03	51.54	174.10	11.79
1999	10.07	5.87	7.30	6.05	16.58	35.55	79.59	108.69	59.56	72.57	26.01	11.01	36.57	108.69	5.87
2000	6.36	3.70	2.38	7.27	19.90	29.80	62.93	82.78	87.82	75.47	36.51	15.36	35.86	87.82	2.38
2001	22.94	23.58	24.68	23.97	36.55	67.65	117.56	106.54	77.50	49.86	29.78	50.17	52.56	117.56	22.94
2002	9.78	5.88	7.23	9.74	7.13	29.69	57.77	76.41	61.24	21.91	12.23	12.61	25.97	76.41	5.88
2003	10.64	5.28	9.01	10.01	5.74	24.30	80.97	85.15	94.59	30.78	12.74	9.90	31.59	94.59	5.28
2004	6.46	4.77	4.12	6.70	13.44	32.60	65.19	99.09	95.64	77.73	20.45	13.21	36.62	99.09	4.12
2005	9.16	4.84	10.28	8.79	40.68	34.71	67.98	129.46	125.73	51.90	19.70	9.88	42.76	129.46	4.84
2006	7.69	9.23	9.79	12.12	14.40	35.93	121.09	169.05	108.89	52.03	29.52	23.48	49.43	169.05	7.69
2007	15.22	15.33	9.34	15.30	20.91	57.78	98.19	115.38	138.30	65.74	16.82	9.32	48.14	138.30	9.32
2008	3.26	3.07	2.54	8.12	11.86	91.21	85.50	125.14	90.82	46.75	17.35	8.93	41.21	125.14	2.54

2009	6.58	12.62	2.44	17.21	26.34	70.84	70.56	105.85	72.40	134.48	140.04	53.97	59.44	140.04	2.44
2010	27.67	16.25	16.40	11.79	20.91	30.27	85.82	174.10	100.33	85.57	34.34	15.03	51.54	174.10	11.79
2011	9.78	5.88	7.23	9.74	7.13	29.69	57.77	76.41	61.24	21.91	12.23	12.61	25.97	76.41	5.88
2012	10.64	5.28	9.01	10.01	5.74	24.30	80.97	85.15	94.59	30.78	12.74	9.90	31.59	94.59	5.28
2013	6.46	4.77	4.12	6.70	13.44	32.60	65.19	99.09	95.64	77.73	20.45	13.21	36.62	99.09	4.12
2014	9.16	4.84	10.28	8.79	40.68	34.71	67.98	129.46	125.73	51.90	19.70	9.88	42.76	129.46	4.84
2015	7.69	9.23	9.79	12.12	14.40	35.93	121.09	169.05	108.89	52.03	29.52	23.48	49.43	169.05	7.69
2016	6.58	12.62	2.44	17.21	26.34	70.84	70.56	105.85	72.40	134.48	140.04	53.97	59.44	140.04	2.44
2017	3.99	4.18	1.67	1.46	3.48	10.81	56.36	157.91	123.57	95.55	20.66	7.46	40.59	157.91	1.46
2018	4.80	5.04	3.55	21.13	11.51	27.44	52.61	77.31	78.54	41.85	15.05	17.26	29.67	78.54	3.55

Mean Monthly Abeilt Station flow In m^3/s															
	Jan.	Feb.	Mar.	Apr.	May.	Jun.	Jul.	Aug.	Sep.	Oct.	Nov.	Dec.	Mean	Max	Min
1980	243.93	60.38	49.82	33.62	34.14	49.39	295.69	425.67	284.52	122.97	43.06	42.67	140.49	425.67	33.62
1981	27.15	27.71	22.26	19.19	18.98	33.27	197.35	534.17	502.97	230.04	41.02	19.47	139.47	534.17	18.98
1982	16.53	10.63	42.67	38.59	23.60	67.93	180.28	439.58	320.19	286.53	91.75	50.92	130.77	439.58	10.63
1983	19.24	15.00	15.71	17.39	54.58	90.58	202.69	663.82	558.79	454.84	134.49	53.75	190.07	663.82	15.00
1984	25.87	16.66	12.46	10.28	18.68	91.37	313.76	491.82	160.60	66.55	19.59	13.42	103.42	491.82	10.28
1985	7.92	4.86	2.91	4.81	20.51	62.81	238.65	519.84	461.63	139.23	35.70	14.83	126.14	519.84	2.91
1986	8.20	6.79	8.38	8.81	7.49	97.13	375.24	350.23	409.88	151.09	30.02	14.31	122.30	409.88	6.79
1987	7.27	5.81	12.38	11.76	20.18	82.71	186.19	297.85	278.53	111.14	32.73	11.73	88.19	297.85	5.81
1988	6.67	6.29	4.52	2.17	4.62	19.93	589.27	993.06	758.43	675.91	308.05	29.71	283.22	993.06	2.17
1989	24.40	16.77	12.21	36.58	20.47	62.43	227.51	459.83	453.48	145.30	41.84	35.68	128.04	459.83	12.21
1990	12.86	15.48	15.17	16.81	19.94	95.03	355.67	663.91	567.07	145.30	41.84	35.68	165.40	663.91	12.86
1991	54.72	30.81	27.91	22.42	54.27	139.42	346.51	611.44	377.14	471.18	173.36	55.02	197.02	611.44	22.42

1992	12.06	16.14	8.63	8.94	25.87	80.42	298.42	960.99	568.56	309.24	310.68	167.55	230.62	960.99	8.63
1993	12.06	17.76	13.63	54.31	117.20	257.55	530.14	839.57	624.50	417.13	269.97	81.64	269.62	839.57	12.06
1994	54.72	30.81	27.91	22.42	54.27	139.42	346.51	611.44	377.14	471.18	173.36	55.02	197.02	611.44	22.42
1995	39.07	22.20	14.90	25.42	63.11	114.48	296.21	524.82	477.63	471.18	173.36	55.02	189.78	524.82	14.90
1996	167.55	167.55	119.59	63.80	157.58	455.68	629.41	1113.24	456.52	284.88	103.45	63.72	315.25	1113.24	63.72
1997	47.25	41.81	25.25	59.52	73.46	230.78	383.93	489.15	350.38	376.84	402.74	198.79	223.32	489.15	25.25
1998	92.46	52.89	55.23	34.47	64.72	117.89	505.73	1004.54	745.09	586.34	248.07	92.69	300.01	1004.54	34.47
1999	54.72	30.81	27.91	22.42	54.27	139.42	346.51	611.44	377.14	471.18	173.36	55.02	197.02	611.44	22.42
2000	39.07	22.20	14.90	25.42	63.11	114.48	296.21	524.82	477.63	471.18	173.36	55.02	189.78	524.82	14.90
2001	40.56	24.95	31.14	28.32	67.59	250.46	554.80	723.61	569.81	327.03	135.98	55.02	234.11	723.61	24.95
2002	40.56	24.95	31.14	28.32	20.74	91.58	276.61	401.18	332.79	87.66	31.12	24.49	115.93	401.18	20.74
2003	16.50	8.82	13.02	16.97	8.61	36.62	233.03	473.98	426.34	184.88	50.45	29.10	124.86	473.98	8.61
2004	45.38	57.21	67.88	79.73	89.11	137.31	282.31	373.63	356.64	356.88	127.41	78.37	170.99	373.63	45.38
2005	65.53	56.54	56.53	41.90	78.11	96.05	262.04	475.01	472.31	286.10	106.98	78.37	172.96	475.01	41.90
2006	54.72	30.81	27.91	22.42	54.27	139.42	346.51	611.44	377.14	471.18	173.36	55.02	197.02	611.44	22.42
2007	12.06	16.14	8.63	8.94	25.87	80.42	298.42	960.99	568.56	309.24	310.68	167.55	230.62	960.99	8.63
2008	12.06	17.76	13.63	54.31	117.20	257.55	530.14	839.57	624.50	417.13	269.97	81.64	269.62	839.57	12.06
2009	54.72	30.81	27.91	22.42	54.27	139.42	346.51	611.44	377.14	471.18	173.36	55.02	197.02	611.44	22.42
2010	39.07	22.20	14.90	25.42	63.11	114.48	296.21	524.82	477.63	471.18	173.36	55.02	189.78	524.82	14.90
2011	167.55	167.55	119.59	63.80	157.58	455.68	629.41	1113.24	456.52	284.88	103.45	63.72	315.25	1113.24	63.72
2012	47.25	41.81	25.25	59.52	73.46	230.78	383.93	489.15	350.38	376.84	402.74	198.79	223.32	489.15	25.25
2013	92.46	52.89	55.23	34.47	64.72	117.89	505.73	1004.54	745.09	586.34	248.07	92.69	300.01	1004.54	34.47
2014	40.56	24.95	31.14	28.32	67.59	250.46	554.80	723.61	569.81	327.03	135.98	55.02	234.11	723.61	24.95
2015	40.56	24.95	31.14	28.32	20.74	91.58	276.61	401.18	332.79	87.66	31.12	24.49	115.93	401.18	20.74
2016	16.50	8.82	13.02	16.97	8.61	36.62	233.03	473.98	426.34	184.88	50.45	29.10	124.86	473.98	8.61

2017	45.38	57.21	67.88	79.73	89.11	137.31	282.31	373.63	356.64	356.88	127.41	78.37	170.99	373.63	45.38
2018	65.53	56.54	56.53	41.90	78.11	96.05	262.04	475.01	472.31	286.10	106.98	78.37	172.96	475.01	41.90

Appendix 7: SWAT weather Gen

Month	Jan	Feb	Mar	Apr	May	Jun	Jul	Aug	Sep	Oct	Nov	Dec
Station	TMPMX	TMPMX	TMPMX	TMPMX	TMPMX	TMPMX	TMPMX	TMPMX	TMPMX	TMPMX	TMPMX	TMPMX
Jinka	32.05	31.79	30.06	28.39	27.88	27.43	28.48	29.97	29.37	30.19	30.47	31.18
Hossan	23.91	24.75	24.44	23.22	22.97	21.09	19.71	19.98	21.32	22.32	23.37	23.81
Jimm	28.85	29.69	28.89	27.1	26.29	25.78	25.38	25.91	26.7	26.77	27.22	28.03
Sewula	28.85	29.69	28.89	27.1	26.29	25.78	25.38	25.91	26.7	26.77	27.22	28.03
Teppi	31.51	32.78	32.08	30.34	29.27	28.14	27.34	27.62	28.71	29.57	30.17	30.92
Wolikite	26.87	27.42	25.75	24.6	22.76	21.55	22.48	23.76	25.11	25.75	26.43	26.6
W/Sodo	27.7	27.81	26.48	24.73	23.31	21.79	22.37	23.89	24.71	26.38	26.66	26.94
Station	TMPMN	TMPMN	TMPMN	TMPMN	TMPMN	TMPMN	TMPMN	TMPMN	TMPMN	TMPMN	TMPMN	TMPMN
Jinka	16.8	17.67	18.26	18.16	17.97	17.8	17.98	17.92	17.45	16.35	15.69	15.9
Hossan	9.65	10.62	10.77	11.57	10.97	10.97	10.63	10.89	10.86	10.18	10.12	9.3
Jimm	14.8	15.68	16.62	16.96	16.64	16.06	15.81	15.96	16.37	16.28	14.72	14.27
Sewula	14.8	15.68	16.62	16.96	16.64	16.06	15.81	15.96	16.37	16.28	14.72	14.27
Teppi	14.05	14.34	16	16.43	16.35	15.85	15.78	15.83	15.59	15.17	14.26	13.73
Wolikite	13.13	13.28	12.65	12.24	12.17	12.1	11.63	11.7	11.93	12.41	12.88	12.93
W/Sodo	14.28	15.1	15.06	14.69	14.46	13.83	13.68	13.78	13.79	14.27	14.32	14.02
Station	TMPSTD MX1	TMPSTD MX2	TMPSTD MX3	TMPSTD MX4	TMPSTD MX5	TMPSTD MX6	TMPSTD MX7	TMPSTD MX8	TMPSTD MX9	TMPSTD MX10	TMPSTD MX11	TMPSTD MX12
Jinka	3.55	3.65	3.21	2.29	1.83	2.16	2.13	2.07	2.24	2.19	2.7	3.25
Hossan	1.7	1.78	2.66	1.96	2.08	1.77	2.12	1.83	1.49	1.8	1.33	1.4
Jimm	2.13	2.42	2.21	2.02	1.67	1.77	1.65	1.71	2.31	1.66	1.74	2.06

Sewula	2.13	2.42	2.21	2.02	1.67	1.77	1.65	1.71	2.31	1.66	1.74	2.06
Teppi	2.14	2.15	2.48	2.29	1.76	1.69	1.88	1.82	1.8	1.9	1.96	2.14
Wolikite	1.97	2.02	2.67	3	2.22	1.93	2.38	1.99	1.35	1.31	1.6	1.8
W/Sodo	1.98	2.2	2.17	1.53	1.53	1.67	1.65	1.57	1.84	1.39	1.39	1.68
Station	TMPSTD MN1	TMPSTD MN2	TMPSTD MN3	TMPSTD MN4	TMPSTD MN5	TMPSTD MN6	TMPSTD MN7	TMPSTD MN8	TMPSTD MN9	TMPSTD MN10	TMPSTD MN11	TMPSTD MN12
Jinka	2.63	2.85	1.76	1.34	1.43	1.6	1.53	1.83	1.49	2.3	2.27	2.71
Hossan	2.62	2.97	2.9	2.12	2.93	1.77	2.1	1.58	1.45	1.9	2	2.54
Jimm	1.77	1.81	1.59	1.24	1.96	2.31	1.27	1.79	1.45	1.87	2.72	2.2
Sewula	1.77	1.81	1.59	1.24	1.96	2.31	1.27	1.79	1.45	1.87	2.72	2.2
Teppi	2.23	2.17	1.96	1.75	1.59	2.13	1.37	1.49	1.44	2.03	1.91	2.31
Wolikite	2.79	1.96	1.78	1.94	1.66	1.76	2.02	2.76	1.97	2.75	2.25	3.45
W/ Sodo	1.88	1.93	1.74	1.27	1.17	1.16	1.14	1.33	1.5	1.53	1.67	2.06
Station	PCPMM	PCPMM	PCPMM	PCPMM	PCPMM	PCPMM	PCPMM	PCPMM	PCPMM	PCPMM	PCPMM	PCPMM
Jinka	30.65	36.98	46.23	133.26	127.14	50.21	39.74	33.63	56.67	98.46	46.71	34.56
Hossan	32.17	55.96	107.99	153.46	146.21	116.86	153.94	172.33	149.32	70.02	15.38	28.72
Jimm	37.37	36.86	87.67	136.34	176.79	220.44	215.27	205.83	185.95	123.49	46.96	44.55
Sewula	57.9	44.97	117.88	177.04	165.99	93.41	101.12	84.66	98.77	144.54	108.46	75
Teppi	33.29	51.31	119.91	164.24	187.12	164.21	196.8	200.3	171.94	114.46	73.68	54.22
Wolikite	44.3	67.55	83.55	120.22	222.45	252.53	235.82	113.69	31.75	6.81	11.97	19.63
W/ Sodo	33.18	41.16	73.55	152.88	181.61	125.49	165.87	165.8	90.31	91.87	46.23	36.52
Station	PCPSTD	PCPSTD	PCPSTD	PCPSTD	PCPSTD	PCPSTD	PCPSTD	PCPSTD	PCPSTD	PCPSTD	PCPSTD	PCPSTD

Jinka	3.7	5.52	3.85	8.68	8.63	5.49	4.21	4.4	4.86	7.27	5.06	4.43
Hossan	3.89	5.53	7.69	9.14	9.44	6.1	7	8	7.72	7.11	2.81	5
Jimm	4.32	3.39	5.55	8.33	8.91	9.06	9.44	8.56	8.71	8	5.94	4.67
Sewula	5.35	5.32	7.26	9.05	10.2	7.72	8.08	7.14	7.36	8.75	8.05	6.54
Teppi	3.42	4.83	7.25	8.54	9.81	8.31	9.86	9.83	8.85	7.02	5.68	4.76
Wolikite	4.3	6.13	6.43	6.97	9.79	9.76	9.47	6.71	4.42	1.65	2.19	3.12
W/ Sodo	4.01	5.61	5.48	9.29	11.25	9.05	9.55	9.51	6.18	6.46	6.12	4.54
Station	PCPSKW 1	PCPSKW 2	PCPSKW 3	PCPSKW 4	PCPSKW 5	PCPSKW 6	PCPSKW 7	PCPSKW 8	PCPSKW 9	PCPSKW1 0	PCPSKW1 1	PCPSKW1 2
Jinka	5.12	7.51	3.96	2.79	3.2	5.78	4.95	7.24	4.6	3.99	4.71	6.12
Hossan	5.23	4.17	3.47	2.65	4.86	2.24	2.16	2.79	3	5.89	7.73	7.8
Jimm	7.77	4.3	2.94	2.97	2.3	1.56	2.08	2.04	2.13	2.75	5.37	4.79
Sewula	4.35	6.21	3.23	2.16	2.75	4.21	4.54	4.59	4.21	3.43	3.78	3.91
Teppi	4.4	3.62	2.84	2.27	3.08	2.29	2.58	2.22	2.34	2.67	3.56	3.9
Wolikite	4.1	3.72	4.57	2.66	2.34	2.14	1.9	2.76	5.34	11.28	6.92	7.15
W/Sodo	6.73	6.96	4.29	2.67	3.12	3.62	2.79	2.78	3.55	3.66	6.24	6.19
Station	PR_W1	PR_W1	PR_W1	PR_W1	PR_W1	PR_W1	PR_W1	PR_W1	PR_W1	PR_W1	PR_W1	PR_W1
Jinka	0.11	0.17	0.26	0.36	0.32	0.21	0.2	0.21	0.31	0.29	0.17	0.08
Hossan	0.09	0.15	0.28	0.29	0.32	0.48	0.68	0.6	0.53	0.1	0.04	0.06
Jimm	0.17	0.22	0.33	0.39	0.43	0.71	0.82	0.75	0.62	0.23	0.13	0.12
Sewula	0.15	0.17	0.34	0.54	0.34	0.23	0.23	0.23	0.3	0.39	0.23	0.13
Teppi	0.16	0.23	0.36	0.55	0.52	0.61	0.65	0.66	0.63	0.3	0.26	0.18
Wolikite	0.13	0.2	0.23	0.32	0.62	0.88	0.61	0.23	0.07	0.03	0.04	0.08

W/ Sodo	0.14	0.18	0.34	0.46	0.41	0.42	0.49	0.5	0.49	0.26	0.13	0.1
Station	PR_W2	PR_W2	PR_W2	PR_W2	PR_W2	PR_W2	PR_W2	PR_W2	PR_W2	PR_W2	PR_W2	PR_W2
Jinka	0.5	0.51	0.55	0.69	0.64	0.49	0.55	0.48	0.59	0.68	0.53	0.6
Hossan	0.52	0.64	0.6	0.73	0.7	0.68	0.73	0.78	0.73	0.62	0.48	0.47
Jimm	0.51	0.59	0.66	0.73	0.77	0.79	0.83	0.86	0.77	0.69	0.5	0.55
Sewula	0.5	0.45	0.59	0.68	0.62	0.53	0.55	0.56	0.6	0.66	0.61	0.59
Teppi	0.42	0.48	0.64	0.69	0.72	0.7	0.73	0.73	0.73	0.64	0.58	0.47
Wolikite	0.53	0.55	0.59	0.71	0.8	0.87	0.83	0.75	0.43	0.33	0.44	0.4
W/Sodo	0.47	0.5	0.61	0.71	0.7	0.64	0.73	0.7	0.66	0.69	0.42	0.57
Station	PCPD	PCPD	PCPD	PCPD	PCPD	PCPD	PCPD	PCPD	PCPD	PCPD	PCPD	PCPD
Jinka	5.57	7	11.29	15.86	15.1	8.33	9.43	8.67	13.14	14.95	7.95	5.67
Hossan	4.9	8	12.57	15.62	15.57	18.05	21.95	22.76	20.24	7.57	2.19	2.62
Jimm	7.67	9.48	15.38	17.67	19.71	23.57	25.29	26.19	22.29	13.76	6.05	6.76
Sewula	7.33	6.29	14.1	18.38	15.14	9.86	10.52	10.57	12.48	16.62	11.33	8.05
Teppi	6.86	8.24	15.52	18.95	19.62	20.33	21.76	22.1	21	14.57	11	8.05
Wolikite	7.1	8.24	11.57	14.81	23.48	25.95	24.57	15.38	3.76	1.43	1.86	3.24
W/ Sodo	6.43	7	14.57	18.1	18.19	16.1	20	19.57	17.48	14.48	5.62	5.9
Station	SOLAR	SOLAR	SOLAR	SOLAR	SOLAR	SOLAR	SOLAR	SOLAR	SOLAR	SOLAR	SOLAR	SOLAR
Jinka	20.33	21.64	23.05	22.16	21.35	19.97	19.99	18.87	17.78	18.02	19.45	19.23
Hossan	21.07	21.83	21.55	20.44	20.18	18	16.67	16.86	18.31	20.76	21.6	21.13
Jimm	17.04	18.05	19.35	20.26	18.55	18.77	18.76	19.4	20.24	19.79	18.25	16.9
Sewula	19.29	20.66	21.47	19.22	19	18.05	17.38	18.7	20	18.92	18.14	19.27

Teppi	16.7	17.89	19.15	20.3	18.71	18.37	19.17	20.15	20.84	19.84	18.01	16.62
Wolikite	17.48	18.93	19.92	19.66	19.18	19.19	19.35	19.66	19.96	19.84	18.49	17.46
W/Sodo	18.85	19.03	18.79	19.49	19.59	17.9	19.33	20.86	20.8	21	19.9	18.52
Station	WND	WND	WND	WND	WND	WND	WND	WND	WND	WNDA	WNDA	WNDA
Jinka	0.61	0.67	0.76	0.73	0.74	0.82	0.81	0.86	0.8	0.6	0.5	0.56
Hossan	1.56	1.66	1.64	1.62	1.37	1.42	1.51	1.45	1.15	1.58	1.68	1.66
Jimm	0.42	0.49	0.54	0.52	0.48	0.45	0.44	0.4	0.41	0.4	0.35	0.36
Sewula	0.95	1.1	1.05	0.97	0.89	0.77	0.76	0.94	1.11	0.91	0.81	0.84
Teppi	1.56	1.66	1.64	1.62	1.37	1.42	1.51	1.45	1.15	1.58	1.68	1.66
Wolikite	3.99	3.87	3.11	2.79	1.92	1.15	1.04	0.99	1.23	2.67	4.07	4.58
W/Sodo	0.38	0.45	0.53	0.5	0.43	0.37	0.34	0.35	0.39	0.37	0.37	0.36

Appendix 8: SWAT model Soil

	SNAM	NLAYERS	HYDGRP	SOL_ZMX	SOL_Z1	SOL_BD1	SOL_AWC1	SOL_K1	SOL_CBN1	CLAY1	SILT1	SAND1	SOL_ALB1	USLE_K1	SOL_EC1
1	eucam	2	B	1800	210	1.45	0.22	38.4	1.2	11	67	22	0.13	0.3	0.13
2	chrlu	3	B	900	600	1.5	0.2	33.63	1.63	21	33	46	0	0.3	0.11
3	eunit	1	A	1000	100	1.62	150	360	0.58	8	12	80	0.32	0.16	0.1
4	euflu	3	C	2422	181	1.1	0.11	4.34	1.47	60.6	23.3	16.1	0.09	0.2	0.07
5	chrve	3	B	900	200	1.45	0.19	30	0.5	25	31	44	0.13	0.3	0.09
6	pelve	2	B	50	30	1.35	0.1	65.68	1.9	50	23	27	0.14	0.25	0.12
7	dyfluv	3	A	1200	500	1.44	0.19	287.3	1.8	35	38	27	0.13	0.21	0.09
8	chroca	3	A	1500	900	1.43	0.2	7.15	1.8	33	55	12	0.13	0.21	0.14
9	lepto	3	A	1500	900	1.43	0.2	7.15	1.8	33	55	12	0.13	0.21	0.14
10	calxer	1	C	1250	120	1.1	0.12	6.23	1.9	55	30	15	0.17	0.21	0
11	calfl	1	A	1000	100	1.68	75	180	3.27	5	21	74	0.23	0.13	0.1
12	verlu	3	C	200	30	0	0	18	3.2	25	35	40	0.23	0.13	0.1
13	vitan	3	C	200	20	0	0	20	1.3	20	24	56	0.23	0.13	0.1
13	chroca	4	B	1651	177.8	1.15	0.16	200	2.33	7.5	27.2	65.3	0.01	0.17	0
	SNAM	NLAYERS	HYDGRP	SOL_ZMX	SOL_Z2	SOL_BD2	SOL_AWC2	SOL_K2	SOL_CBN2	CLAY2	SILT2	SAND2	SOL_ALB2	USLE_K2	SOL_EC2
1	eucam	2	B	1800	260	1.46	0.21	37.2	0.3	14	66	20	0.13	0.3	0.1
2	chrlu	3	B	900	850	1.46	0.18	39.86	1.1	13	46	41	0	0.34	0.11
3	eunit	1	A	1000	0	0	0	0	0	0	0	0	0	0	0
4	euflu	3	C	2422	363.3	1.27	0.11	4.54	1.37	60.6	18.6	20.8	0.09	0.2	0.04
5	chrve	3	B	900	600	1.37	0.09	5.52	0.22	44	23	33	0.13	0.11	0.04

6	pelve	2	B	50	50	1.19	0.09	4.98	1.6	67.8	27	5.2	0.06	0	0.4
7	dyfluv	3	A	1200	800	1.4	0.07	0.14	0.58	75	17.8	7.42	0.23	0	0.8
8	chroca	3	A	1500	1200	1.3	0.17	0.8	0.75	48.7	25.3	80.8	0.06	0	0.08
9	lepto	3	A	1500	1200	1.3	0.17	0.8	0.75	48.7	25.3	80.8	0.06	0	0.08
10	calxer	1	C	1250	450	1.19	0.09	4.98	1.6	67.8	27	5.2	0.17	0.2	0
11	calfl	1	A	1000	0	0	0	0	0	0	0	0	0	0	0
12	verlu	3	C	200	10	1.3	0	0	0	0	0	0	0	0	0
13	vitan	3	C	200	80	1.2	0	0	0	0	0	0	0	0	0
13	chroca	4	B	1651	533.4	1.15	0.13	250	1.45	5	34.4	60.5	0.01	0.1	0

	SNAM	NLAYERS	HYDGRP	SOL_ZMX	SOL_Z3	SOL_BD3	SOL_AWC3	SOL_K3	SOL_CBN3	CLAY3	SILT3	SAND3	ROCK3	SOL_ALB3	USLE_K3
1	eucam	2	B	1800	460	1.45	0.2	34.8	0.21	19	59	22	0	0.13	0.3
2	chrlu	3	B	900	900	1.45	0.06	0.9	0.66	73.6	18.5	8.6	0	0	0
3	eunit	1	A	1000	0	0	0	0	0	0	0	0	0	0	0
4	euflu	3	C	2422	847.8	1.28	0.1	5.16	1.41	19	59	22	0	0.09	0.2
5	chrve	3	B	900	900	1.42	0.15	10.56	0.21	35	35	30	0	0.13	0.28
6	pelve	2	B	50	0	0	0	0	0.73	64.5	16.5	27.7	0	0	0
7	dyfluv	3	A	1200	1200	1.55	0.02	0.8	0.19	75	17.5	7.42	0	0	0
8	chroca	3	A	1500	1500	1.35	0.16	0.9	0.15	34.3	22	8.7	0	0	0
9	lepto	3	A	1500	1500	1.35	0.16	0.9	0.15	34.3	22	8.7	0	0	0
10	calxer	1	C	1250	700	1.14	0.2	9.34	1.7	30	60	10	0	0.17	0.3
11	calfl	1	A	1000	0	0	0	0	0	0	0	0	0	0	0
12	verlu	3	C	200	200	0	0	0	0	0	0	0	0	0	0
13	vitan	3	C	200	200	0	0	0	0	0	0	0	0	0	0

13	chroca	4	B	1651	685.8	1.3	0.09	400	0.73	1.5	16.5	81.9	27.62	0.06	0.1

Appendix 9: Seasonal rainfall, wet and dry season trend across the area

No	STAIONS	Long	Lat	Elev	Bega	Belg	Kiremt	Max	Min	Annual	Mean	Sdv	CV
1	Areka	37.42	7.04	1750	232.44	123.36	187.82	229.74	28.88	1504.27	1198.27	37.59	0.31
2	Asendabo	37.23	7.77	2400	130.80	355.96	685.72	196.52	18.83	1172.49	1837.56	67.77	0.37
3	Baco	37.19	9.19	1650	107.79	75.49	219.84	263.87	9.19	1308.65	1320.74	40.21	0.30
4	Bonga	36.23	7.22	1650	334.02	577.13	761.77	209.15	49.68	1672.92	1320.74	40.21	0.30
5	Chida	36.78	7.17	1640	271.81	582.95	622.61	194.49	41.5	1477.36	1227.63	38.03	0.31
6	Chira	36.18	7.13	1500	316.17	565.84	947.69	253.83	48.33	1829.70	1367.52	77.70	0.57
7	EJAJI	37.14	9.00	1900	135.19	76.55	175.16	255.29	11.64	1320.75	1305.02	47.81	0.37
8	Indibir	36.44	5.14	397	151.30	58.18	41.10	250.72	13.55	466.20	1559.64	48.81	0.31
9	Hossaina	37.87	7.55	2200	148.64	418.34	614.18	184.39	17.42	1181.14	1504.27	59.36	0.39
10	Jimma	36.83	7.67	1725	229.47	447.45	820.43	215.89	34.41	1497.35	1768.23	54.20	0.31
11	Jinka	36.63	5.80	1480	364.93	488.38	377.25	171.03	47.11	1230.54	1415.26	76.46	0.54
12	L.Genet	36.95	8.10	1690	284.96	469.31	1085.49	294.04	25.2	1839.76	1178.81	76.97	0.65
13	Sekoru	37.40	7.92	1896	139.05	377.53	830.49	225.15	15.59	1347.07	1689.74	50.84	0.30
14	Tep	35.15	5.59	1540	315.14	135.72	224.73	213.89	42.69	1609.29	1236.53	37.71	0.30
15	W.Soddo	37.72	6.83	2100	212.85	479.39	700.65	208.79	29.45	1392.88	1637.16	74.06	0.45
16	Welliso	37.98	8.55	2000	71.12	252.95	863.57	278.72	6.47	1187.66	1308.65	84.74	0.65
17	Wolkite	37.75	8.27	1500	103.93	328.94	861.36	282.56	10.8	1294.23	1288.01	49.52	0.38

Appendix 10: The standard deviation and coefficient of variation rainfall data.

No	STAIONS	Long	Lat	Elev	Bega	Belg	Kiremt	Max	Min	Annual	Mean	Sdv	CV
1	Areka	37.42	7.04	1750	232.44	123.36	187.82	229.74	28.88	1504.27	1198.27	37.59	0.31
2	Asendabo	37.23	7.77	2400	130.80	355.96	685.72	196.52	18.83	1172.49	1837.56	67.77	0.37
3	Baco	37.19	9.19	1650	107.79	75.49	219.84	263.87	9.19	1308.65	1320.74	40.21	0.30
4	Bonga	36.23	7.22	1650	334.02	577.13	761.77	209.15	49.68	1672.92	1320.74	40.21	0.30
5	Chida	36.78	7.17	1640	271.81	582.95	622.61	194.49	41.5	1477.36	1227.63	38.03	0.31
6	Chira	36.18	7.13	1500	316.17	565.84	947.69	253.83	48.33	1829.70	1367.52	77.70	0.57
7	EJAJI	37.14	9.00	1900	135.19	76.55	175.16	255.29	11.64	1320.75	1305.02	47.81	0.37
8	Indibir	36.44	5.14	397	151.30	58.18	41.10	250.72	13.55	466.20	1559.64	48.81	0.31
9	Hossaina	37.87	7.55	2200	148.64	418.34	614.18	184.39	17.42	1181.14	1504.27	59.36	0.39
10	Jimma	36.83	7.67	1725	229.47	447.45	820.43	215.89	34.41	1497.35	1768.23	54.20	0.31
11	Jinka	36.63	5.80	1480	364.93	488.38	377.25	171.03	47.11	1230.54	1415.26	76.46	0.54
12	L.Genet	36.95	8.10	1690	284.96	469.31	1085.49	294.04	25.2	1839.76	1178.81	76.97	0.65
13	Sekoru	37.40	7.92	1896	139.05	377.53	830.49	225.15	15.59	1347.07	1689.74	50.84	0.30
14	Tep	35.15	5.59	1540	315.14	135.72	224.73	213.89	42.69	1609.29	1236.53	37.71	0.30
15	W.Soddo	37.72	6.83	2100	212.85	479.39	700.65	208.79	29.45	1392.88	1637.16	74.06	0.45
16	Welliso	37.98	8.55	2000	71.12	252.95	863.57	278.72	6.47	1187.66	1308.65	84.74	0.65
17	Wolkite	37.75	8.27	1500	103.93	328.94	861.36	282.56	10.8	1294.23	1288.01	49.52	0.38

List of Publications

1. Chaemiso, S. E., Kartha, S. A., & Pingale, S. M. (2021). “Effect of land use/land cover changes on surface water availability in the Omo-Gibe basin, Ethiopia”. *Hydrological Sciences Journal*, Taylor and Francis, 66(13), 1936-1962 (Peer-Reviewed Journal)

2. Chaemiso, S. E., Kartha, S. A. (2019). The Impact of Precipitation and Evaporation on Stream flow under the Response of Climate Change Using Hydrological and Climate Model. Case study in Upper Omo Gibe Basin, Ethiopia. 19th Symposium on Sustainable Water Resources Development (ISSWRD19), Arba Minch Water Technology Institute (AWTI). (Conference Paper presented)